QUANTUM ENGINEERING, INC.
2104 EAST VILLA STREET
PASADENA, CALIFORNIA

AREA CODE 213
PHONE 795-9701
681-6617

PRELIMINARY EXAMINATION OF PROBLEMS IN COMMUNICATING WITH AN ION-ROCKET-DRIVEN INTERPLANETARY SPACECRAFT BY MEANS OF 2.1- TO 2.3-GHz RADIO SIGNALS

George I. Cohn

October 1966

"This work was performed for the Jet Propulsion Laboratory, California Institute of Technology, sponsored by the National Aeronautics and Space Administration under Contract NAS7-100."

PRELIMINARY EXAMINATION OF PROBLEMS IN COMMUNICATING WITH AN ION-ROCKET-DRIVEN INTERPLANETARY SPACECRAFT BY MEANS OF 2.1- TO 2.3-GHz RADIO SIGNALS

George I. Cohn

October 1966

"This work was performed for the Jet Propulsion Laboratory, California Institute of Technology, sponsored by the National Aeronautics and Space Administration under Contract NAS7-100."

Under P.O. Numbers: AX-405 8 73
AX 4-315834

Prepared with the assistance of:

Harold Tornhiem, Ph.D.
Peggy Kirk
Mary Deratany
Gary Wood
Albert Tajaden
Manuel Fernandez
Jon Bostrom

PREFACE

The use of ion rockets for space propulsion poses the problem of possible interference with communications to and from the space-craft. The investigation reported on here was primarily carried out in 1964. The initial orientation of the investigation was towards a broad generalized approach that would quantitatively provide the magnitude of the effects on the communication channel as a function of the ion rocket properties and the ion rocket disposition. So as to gain closure of this investigation and issue a report within the alloted support, a great deal of truncation on various lines of inquiry had to be made. Because of Quantum Engineering, Inc's. basic interest in this area of activity, part of the support was provided by company funds. A great deal of significant work remains for further investi-gation.

The many useful practical suggestions and technical inputs given by Gerald S. Levy and others of the Jet Propulsion Laboratory staff during the course of the investigation are gratefully acknowledged.

TABLE OF CONTENTS

LIST OF APPENDICES

LIST OF APPENDICES (Continued)

LIST OF APPENDICES (Continued)

LIST OF FIGURES

LIST OF FIGURES (Continued)

LIST OF FIGURES (continued)

CHAPTER I: INTRODUCTION

1.1 Objective

The ion exhaust beam of an ion-rocket-propelled spacecraft may cause communication problems due to:

1. Signal attenuation,
2. Signal distortion,
3. Radio noise generation.

A preliminary assessment of the attenuation, distortion, and noise generation is presented here. This information is needed to help answer such questions as:

1. For what ranges of ion rocket engine parameters, and under what circumstances, are communication difficulties produced?
2. Is it necessary to orient the spacecraft and antenna system so that signal rays do not pass through the ion exhaust beam?
3. Is it necessary to turn off the ion rocket for various time intervals to facilitate communication?
4. Can reasonable modifications be made in the design of the ion rocket so that the ion exhaust beam does not present objectionable effects?

The most desirable solution would be an ion rocket engine design which did not produce objectionable effects in the communication system. Then it would not be necessary to provide an orientation-control subsystem to keep signal rays from passing through objectionable portions of the ion exhaust beam or to turn off the ion rocket engine for various time intervals in order to facilitate communication. However, this presupposes that such an ion rocket design would not have to sacrifice any significant fraction of its desirable performance characteristics as a thrustor. Should the design changes required to mitigate communication problems compromise the thrustor characteristics, a future more comprehensive investigation could optimize the trade-offs for the overall mission objective.

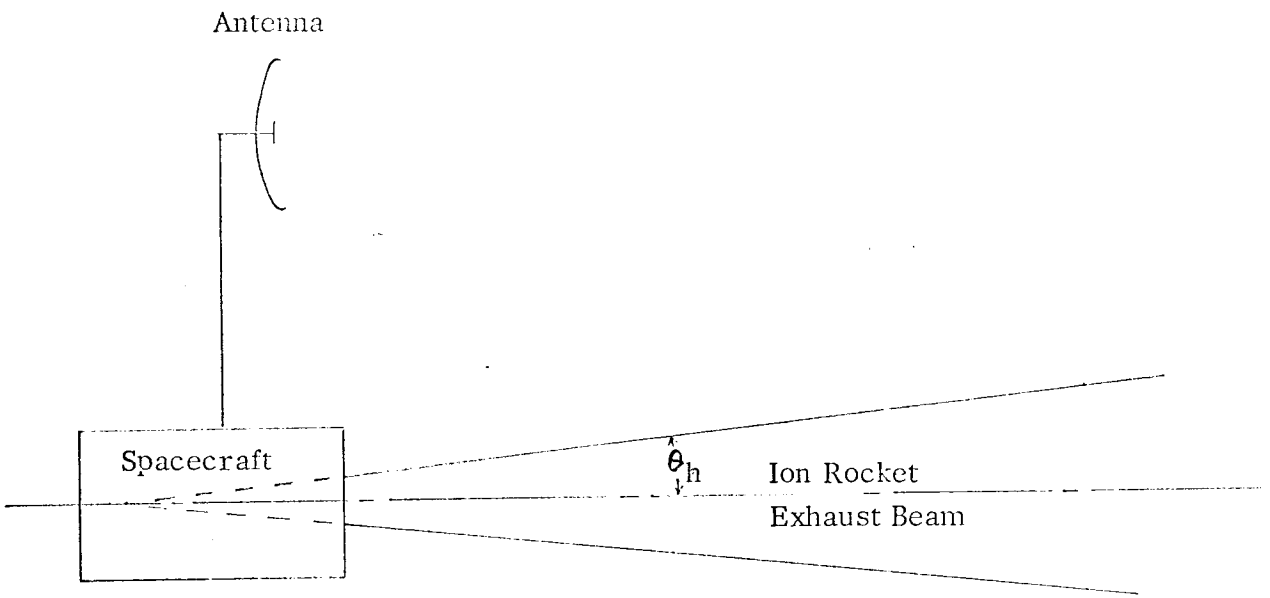

Rig. 1.1 Conical Approximation to Ion Rocket Exhaust Beam

1.2 Preliminary Ion Exhaust Beam Model

Problem assessment requires the quantitative investigation of a methematical model. Formulation of mathematical models requires anticipation of the system's qualitative nature in sufficient detail. For quantitative determination of the attenuation, distortion and noise effects, it is necessary to know the properties of the spacecraft, the ion rocket exhaust and the communication system. Where these characteristics are insufficiently specified or known, it is necessary to make preliminary assumptions.

This investigation requires a knowledge of both the ion exhaust beam and the antenna beam characteristics. In comparison with characteristics of the ion rocket exhaust beam, antenna beam characteristics are relatively well known. Studies of plasma produced by ion engines have been primarily concerned with:

1. plasmas in the ion engine interior, which provide better understanding of the functioning of the ion engine (Refs. 1, 2, 3 and 4),
2. the macroscopic neutralization process which takes place in a relatively short distance from the ion rocket engine (Refs. 5, 6, 7 and 9).

These studies have not been extensively concerned with the determination of the properties of the ion exhaust beam after it has progressed any considerable distance from the ion rocket engine. Experimental studies in laboratory vacuum chambers are limited to a relatively short section of the ion rocket exhaust immediately following the ion rocket engine.

In the present preliminary analysis, the ion exhaust beam is approximated by:

1. a cone with a small half-angle (depicted in Fig. 1.1),
2. an ion distribution which is homogeneous over a cross section perpendicular to the axis of symmetry,
3. negligible ion-electron recombination.

Fig. 1.2 Report Organization

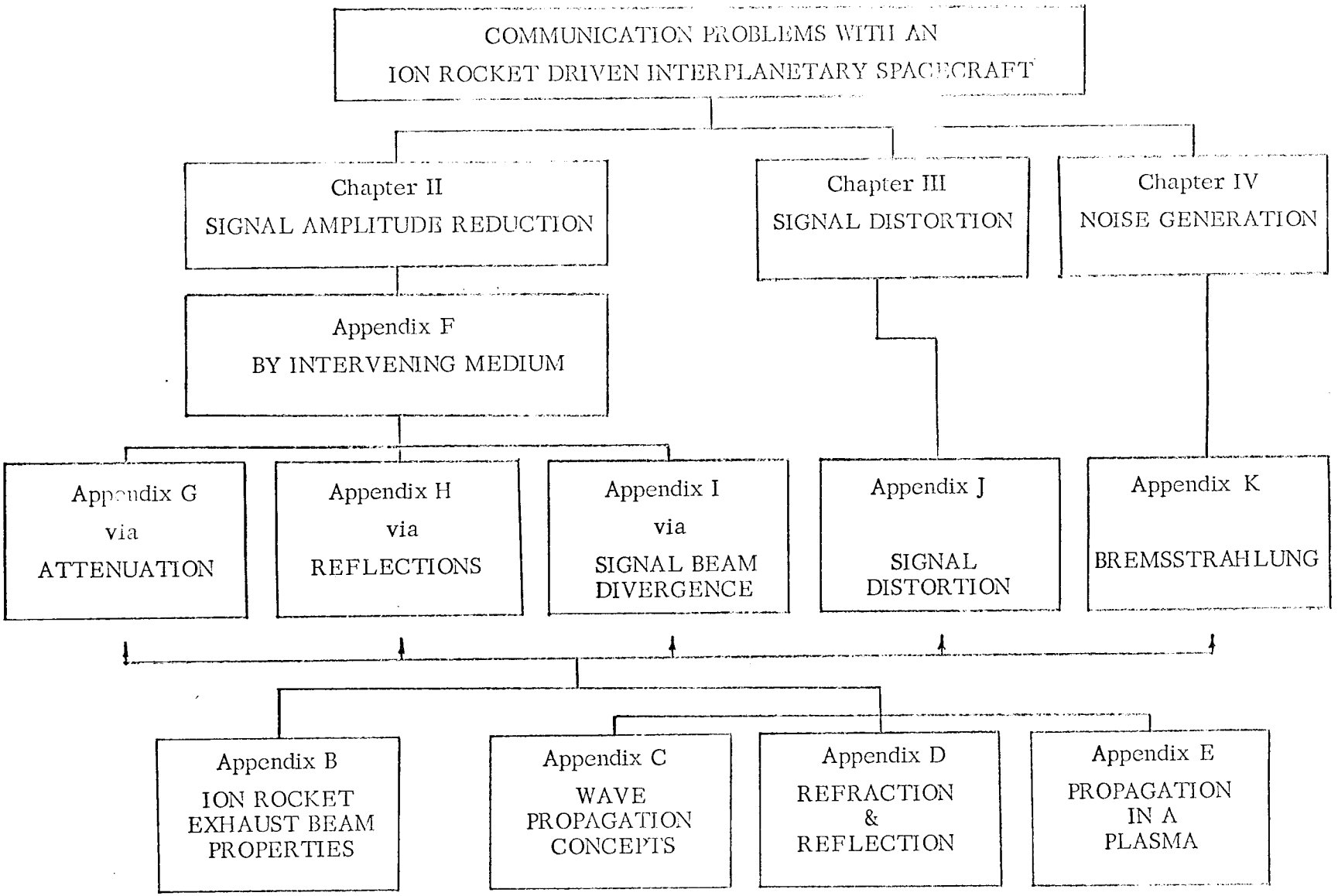

Deviations from this semihomogeneous conical model of the ion exhaust beam which may cause significant changes in the results are:

1. inhomogeneities in the beam, which may change the signal losses, the signal distortion and the noise generation,
2. diffusion of the plasma from the main part of the ion exhaust beam, which engulf the antenna.

1.3 Report Organization

The results are summarized in the chapters. The body of work is presented in the appendices. Each appendix deals with one selected topic or subject area. Required background material on the ion beams, propagation and plasma is given in appendices B, C, D and E. The report organization is summarized in Fig. 1.2. Two additional appendices A and L present notations and references.

CHAPTER II: SIGNAL STRENGTH REDUCTION BY THE ION EXHAUST BEAM

2.1 Introduction

A plasma scatters and usually attenuates electromagnetic waves. Under certain conditions, the plasma can also amplify (negatively attenuate) electromagnetic waves. In general, it is necessary to consider together the effects of attenuation and scattering. Conventional boundary-value-problem techniques are adequate for analyzing a few simple cases. An integral equation approach is required for the general case. A much simpler approach is provided by geometrical optics, if the radii of curvature and other dimensions involved are large compared with the wavelength. A preliminary assessment of the applicability of the geometrical optics ray concept can be made by comparing the ion exhaust beam radius with the signal wavelenth. The beam radius, b, normalized with respect to λ, the signal wavelength, is expressed as

$$\xrightarrow[\lambda = 13.7\text{cm}]{\text{B-66}} (1) \quad \frac{b}{\lambda} = \frac{502}{I_{sp}\sqrt{\frac{P_b}{i_b}}}$$

where

$$\xrightarrow{\text{sym def}} (2) \left\{ \begin{matrix} P_b \\ i_b \\ I_{sp} \end{matrix} \right\} = \text{the ion exhaust beam} \left\{ \begin{matrix} \text{power} \\ \text{ion current density} \\ \text{specific impulse} \end{matrix} \right\} .$$

Here, a wavelength of 13.7 cm has been used. Since the frequency band of interest (2.1 to 2.3 Gc) is small, the use of the mean wavelength in Eq. (1) gives a result which adequately represents the entire band. Fig. 2.1 depicts the ion exhaust beam exit radius dependence on specific impulse for various power levels and current densities. Entering the curves at the point specified by

* The arrow bookkeeping notation at the left of the equation numbers is explained in Appendix A.

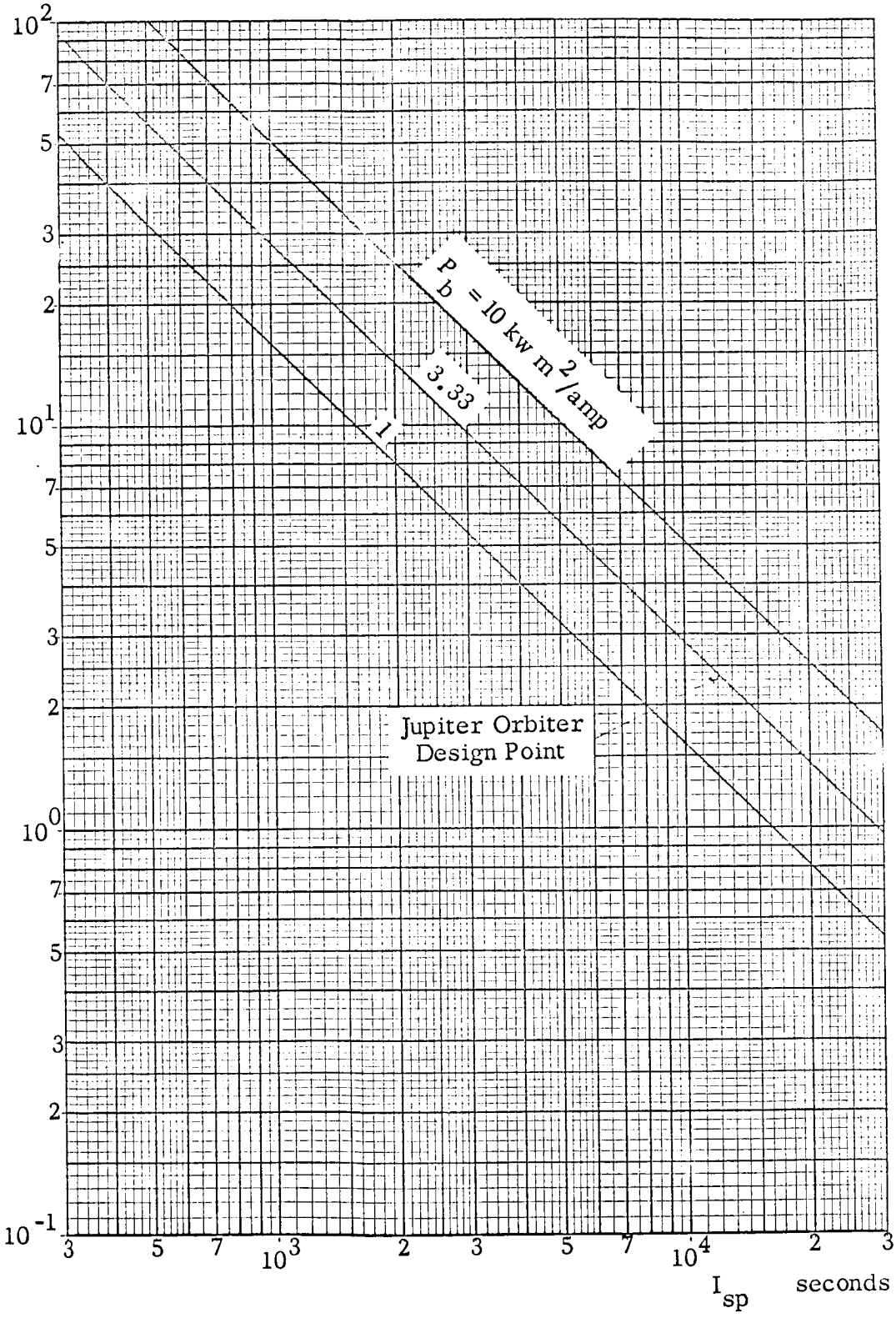

Fig. 2.1 Ion Exhaust Beam Radius at Exit Plane (normalized with Respect to Wavelength) as a Function of Specific Impulse and Power

Jupiter Orbiter example * $\rightarrow$ (3) $\begin{Bmatrix} P_b \\ i_b \\ I_{sp} \end{Bmatrix} = \begin{Bmatrix} 500\ \text{KW} \\ 15\ \text{ma/cm}^2 \\ 12{,}000\ \text{sec.} \end{Bmatrix}$

gives a beam radius to 2.4 wavelengths at the ion rocket exhaust plane. Thus for ion engines needed for distant interplanetary missions, Fig. 2.1 shows that the beam diameter at the exhaust plane is large compared with the wavelength; hence, the ray approximation is fairly good. The ray approximation becomes better at greater distances from the ion rocket because of the ion beam expansion. For sufficiently large ion rocket engines, the ion exhaust beam will probably be a cluster of beams, rather than a single uniform circular beam. For large ion rockets, the individual beams in the cluster will probably have a fine structure, consisting of an array of smaller circular beams or of hollow concentric beams. As the ion beams recede from the rocket engine, they merge together, giving a more homogeneous beam. In this preliminary investigation, the entire ion exhaust beam is considered as uniform over each circular cross section.

2.2 Ray Theory Approximation

The size of the ion exhaust beam diameter, compared with the signal wavelength, indicates that ray theory can be used for a good first approximation. In terms of ray theory the reduction in signal strength caused by the presence of the ion exhaust beam between the transmitter and receiver antennas is caused by:

1. absorption during transit through the plasma
2. interface reflections
3. change in signal beam cross section due to refraction
4. signal beam divergence.

---

* Private communication from D. J. Kerrisk.

The absorption losses which reduce the signal strength are caused by the collision between the plasma particles, and by incoherent scattering. In the geometrical optics approach, the coherent scattering is accounted for by means of reflections and refractions.

The power reflected at each interface is considered as lost in the first approximation. Successive reflections can cause part of the reflected power to be recombined with the main signal beam. However, phase interference effects may weaken, as well as strengthen, the signal beam.

The cross-section area of a signal beam changes upon refraction through an oblique interface. The change in signal beam cross section alters the signal strength density (Poynting's vector). This change is an increase for propagation into a region of lower refraction index, and a decrease for propagation into a region of higher refractive index.

The ion exhaust beam surface curvature and the spatial variation of refractive index cause the rays passing through the ion exhaust beam to diverge. This divergence reduces the signal intensity and, hence, reduces the signal strength with distance. In the geometrical optics approach, the divergence due to diffraction is neglected.

The ray theory becomes cumbersome when it is necessary to include the multiple internal reflections, giving multiple-signal beams, which must be added to obtain the total fields. If the plasma is sufficiently tenuous, the rays produced by higher-order reflections are sufficiently weak and, hence, can be neglected. In this case, the ray theory need only include a single ray. However, if many rays must be added, it may be easier to treat the problem by another method. Inclusion of more than one reflection, in order to obtain a reasonable accuracy, may be required first (if at all) in the section having the greatest density, which

is the section of the ion exhaust beam immediately adjacent to the ion rocket engine.

The effect of the ion exhaust beam on the transmitted signal strength

$\xrightarrow{\text{sym def}}$ (4) p = the power intensity

is expressed in terms of

$\xrightarrow{\text{sym def}}$ (5) $\left\{ \begin{matrix} T_A \\ T_P \end{matrix} \right\}$ = the power transmission factor through $\left\{ \begin{matrix} \text{the beam interior} \\ \text{an interface} \end{matrix} \right\}$

$\xrightarrow{\text{sym def}}$ (6) T_S = the signal beam convergence ratio

and

$\xrightarrow{\text{sym def}}$ (7) G = the antenna gain

by

$\xrightarrow{\text{F-25}}$ (8) $\frac{p_o}{p_i} = T_A T_{P_o} T_{P_i} T_S \frac{G(\theta_i, \varphi_i)}{G(\theta_o, \varphi_o)}$

where

$\xrightarrow{\text{sym def}}$ (9) $\left\{ \begin{matrix} \theta \\ \varphi \end{matrix} \right\}$ = the signal ray $\left\{ \begin{matrix} \text{polar} \\ \text{azimuth} \end{matrix} \right\}$ angles

and

$\xrightarrow{\text{sym def}}$ (10) $\left\{ \begin{matrix} i \\ o \end{matrix} \right\}$ designates $\left\{ \begin{matrix} \text{input} \\ \text{output} \end{matrix} \right\}$.

Each of the factors in (8) which relates the signal intensity with the ion exhaust beam interposed to the signal intensity without the ion exhaust beam interposed, accounts for a separately computed affect. Each of these are individually examined in the next several sections.

2.3 Attenuation Transmission Factor

The power lost by the signal beam traversing the interior of the ion rocket exhaust beam is accounted for by the attenuation transmission factor

$$\xrightarrow[G\text{-}4]{G\text{-}9} (11) \quad T_A = \exp\left(-2\int_{\ell_1}^{\ell_2} \alpha d\ell\right) = e^{-2A}$$

where α is the attenuation factor. Appendix G treats the problem more generally, but for the special case in which the signal ray passes perpendicularly through the ion exhaust beam,

$$\xrightarrow{G\text{-}103} (12) \quad 2A_\perp = \frac{943\sqrt{i_b P_b}}{I_{sp}^3\sqrt{1 - 10.7\,\frac{i_b}{I_{sp}}}}$$

For the Jupiter Orbiter example the attenuation is only about 7.6×10^{-4} db. Consequently, the attenuation due to electron collisions is completely negligible for ion rockets anticipated in the near future. However, it must be specifically noted that, if the ratio of specific impulse to ion emission current density becomes too low (which is equivalent to the condition in which plasma resonant frequency is not sufficiently below the signal frequency), or if the signal frequency is lowered too close to the plasma frequency, the attenuation can reach large values.

For the specific case in which the signal ray enters the ion exhaust beam cone and does not exit through the conical surface, the attenuation is related to that for the perpendicularly traversing signal ray by

$$\xrightarrow{\text{G-92}} (13) \quad A_{||S} = \frac{A_{\perp S}}{6 \sin \theta_h} \quad .$$

The subscript S designates that the signal frequency is sufficiently above the plasma resonant frequency that the index of refraction of the ion exhaust beam can be approximated by unity. If the beam half-angle is greater than 9.6 deg. then $A_{\perp S}$ is greater than $A_{||S}$. The ion rocket beam divergence angle remains to be determined in terms of the ion rocket parameters and the distance from the ion rocket.

2.4 Interface Power Transmission Factor

The signal ray loses power by reflection upon entering, as well as upon leaving, the ion exhaust beam. The power transmission factor is related to the reflection coefficient by

$$\xrightarrow[\text{conservation}]{\text{D-80, energy}} (14) \quad T_p = 1 - \Gamma_p \quad .$$

The transmission loss per reflection, in db, is given by

$$\xrightarrow{14} (15) \quad T_{Pdb} = 8.7 \ln (1 - \Gamma_p) \, .$$

As shown by Figs. D.3 and D.4, the power transmission coefficient and hence the reflection coefficient are slowly varying functions of the incidence angle, except near the critical angle. Consequently the losses due to reflections can be exemplified by the normal incidence case, except near the critical angle

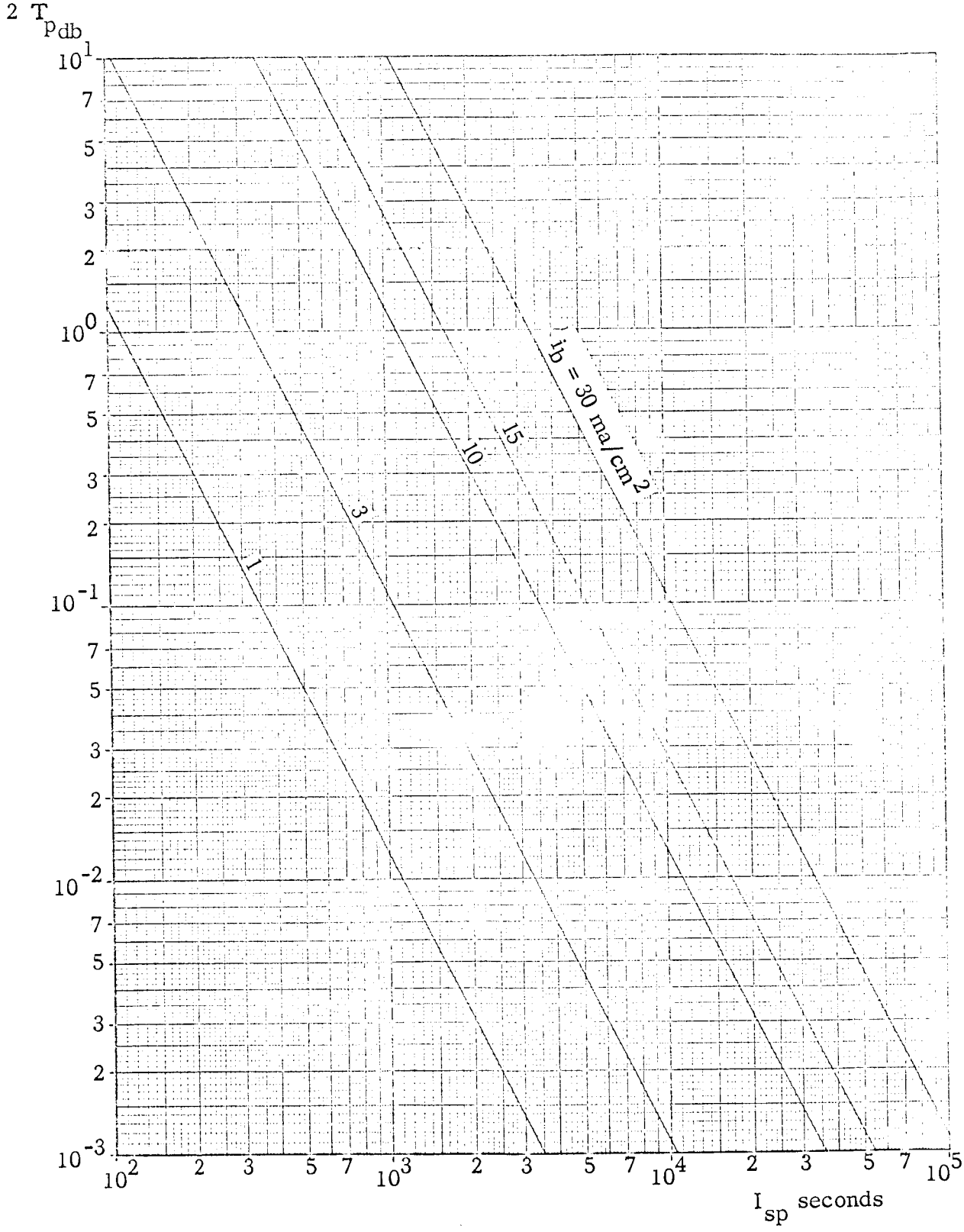

Fig. 2.2 Signal attenuation due to reflections for the elementary ion exhaust beam model.

which will be considered separately. For normal incidence, the power reflection coefficient is given by

$$\xrightarrow{\text{H-16}} (16) \qquad \Gamma_P = 7.08 \frac{i_b^2}{I_{sp}^2}$$

for the cases of interest. Since the power reflection coefficient is small compared to unity for the cases of interest, the first term in the expansion

$$\xrightarrow{\text{RE3(607)}} (17) \qquad \ell n\, x = x - \frac{x^2}{2} + \frac{x^3}{3} - \cdots \qquad x^2 < 1 \;\&\; x = 1$$

can be used to simplify the expression for the power transmission loss to

$$\xrightarrow[17,16]{15} (18) \qquad T_{Pdb} = -61.6 \frac{i_b^2}{I_{sp}^2} \quad .$$

Twice this amount is graphically depicted in Fig. 2.2. The Jupiter orbiter design parameters with the simplified ion exhaust beam model, gives an attenuation due to reflection of only 0.02 db. Although this loss is not serious, a practical ion rocket exhaust beam will have a complex internal structure which may increase the loss due to reflections by an order of magnitude or more. For large reflections, Eq. (18) is not valid because of the approximations involved. The loss due to reflections is many orders of magnitude greater than that due to electron collision in the region of interest if the signal frequency is sufficiently above the plasma frequency.

For nonnormal incidence, the power transmission factor decreases with incidence angle for transverse electric polarization, but may increase at first for transverse magnetic polarization. However, as the incidence angle approaches the critical angle, the power transmission factor rapidly drops to zero. At and beyond the critical angle, the signal ray does not penetrate the ion exhaust beam.

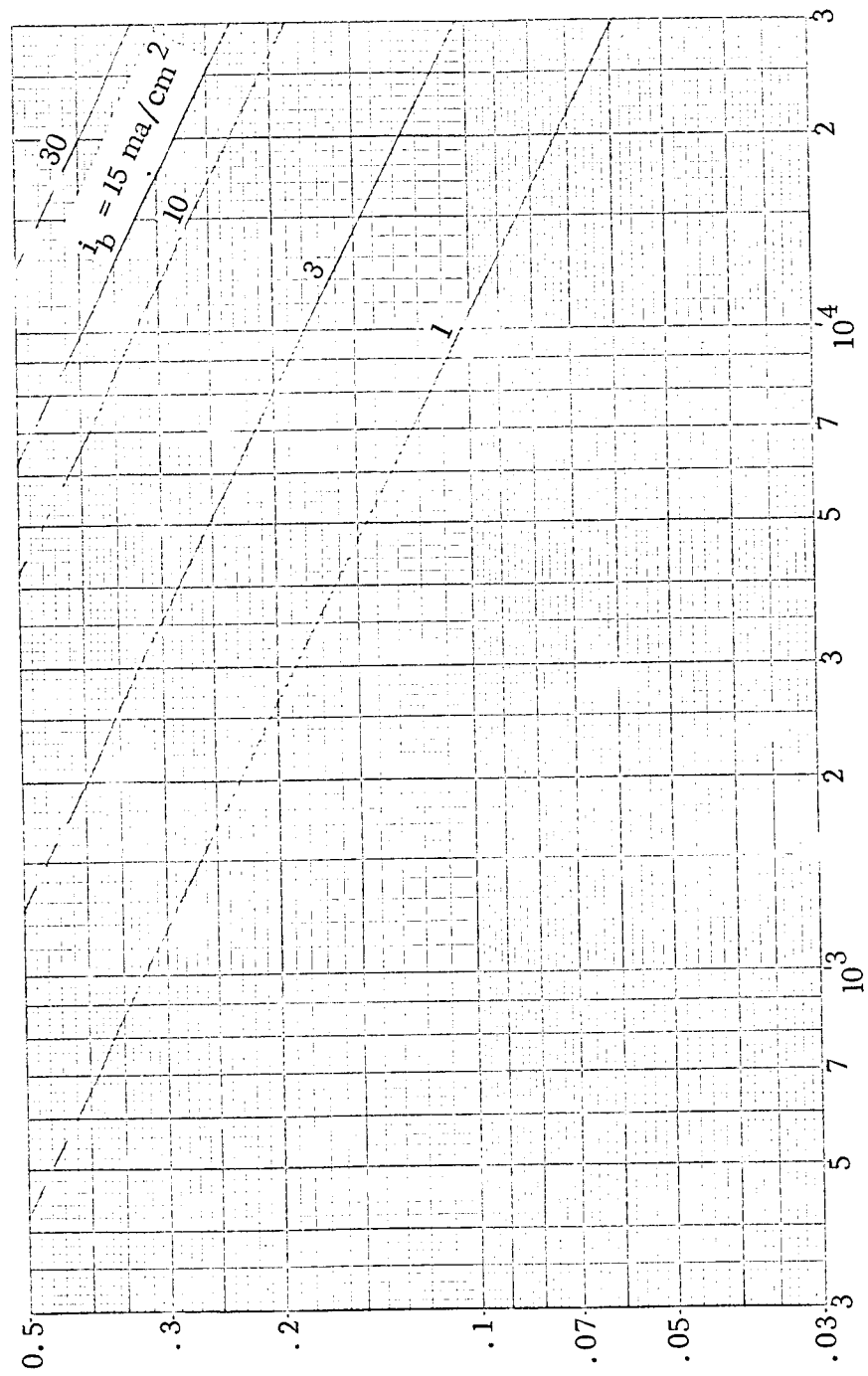

Fig. 2.3 Angular Plasma Frequency and $\theta_{BR} - \theta_h$ versus I_{sp} and i_b

As a result, there is a solid angle within which the signal ray is completely blocked by the ion exhaust beam. The magnitude of this solid angle indicates the seriousness of this effect. The maximum angular range (in the plane containing the ion exhaust beam axis of symmetry) over which the signal rays are blocked is given by

$$\xrightarrow{\text{H-37}} (19) \quad \theta_{BR} = \theta_h + \frac{\omega_p}{\omega} \text{ radians} \quad .$$

The difference between the maximum blocking angle and the ion exhaust beam half-angle is the normalized plasma frequency which, in terms of the ion rocket parameters, is expressed by

$$\xrightarrow{\text{H-39}} (20) \quad \theta_{BR} - \theta_h = \frac{\omega_p}{\omega} = 3.26\sqrt{\frac{i_b}{I_{sp}}} \quad .$$

This relationship is shown graphically in Fig. 2.3.

The fraction of the ion exhaust which blocks the signal rays in the plane perpendicular to the axis of symmetry is given by

$$\xrightarrow{\text{H-24}} (21) \quad \frac{b_{BR}}{b} = 5.31\frac{i_b}{I_{sp}}$$

The geometrical interpretation of the fraction and a graph of its behavior are given in Fig. 2.4. For an actual spacecraft configuration, the total solid angle within which signals are blocked also depends on the location of the antenna, and remains to be determined.

The solid angle over which reflections significantly reduce the signal ray power is only a little larger than the solid angle over which the signal ray is entirely blocked. Fig. 2.5 depicts an approximate three dimensional view of the blocked region caused by the ion exhaust beam. If this solid angle is so large that diffraction effects will not adequately fill the hole in the antenna pattern caused

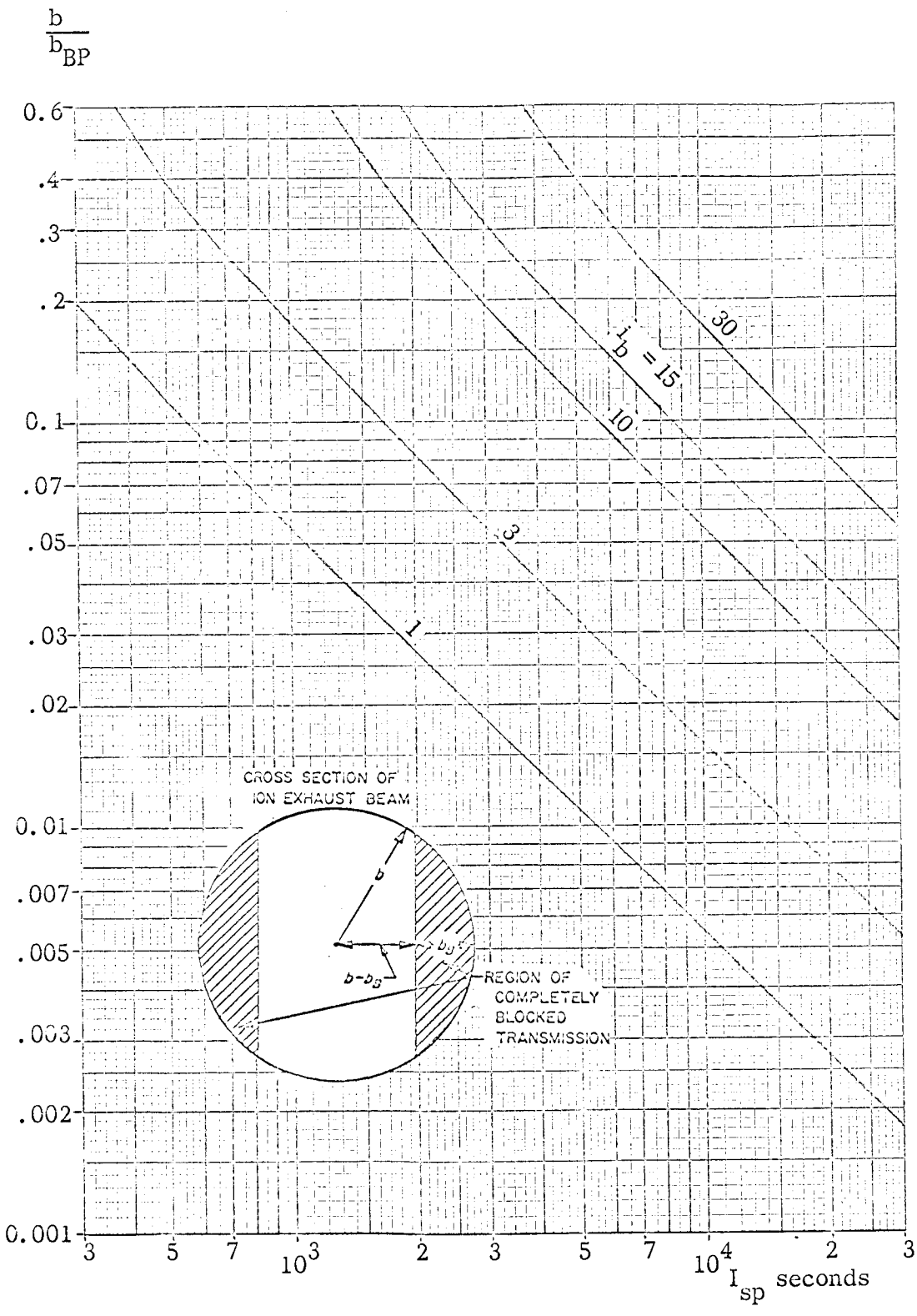

Fig. 2.4 Fraction of Ion Exhaust Beam which Completely Blocks Plane Wave Perpendicular to Axis of Symmetry

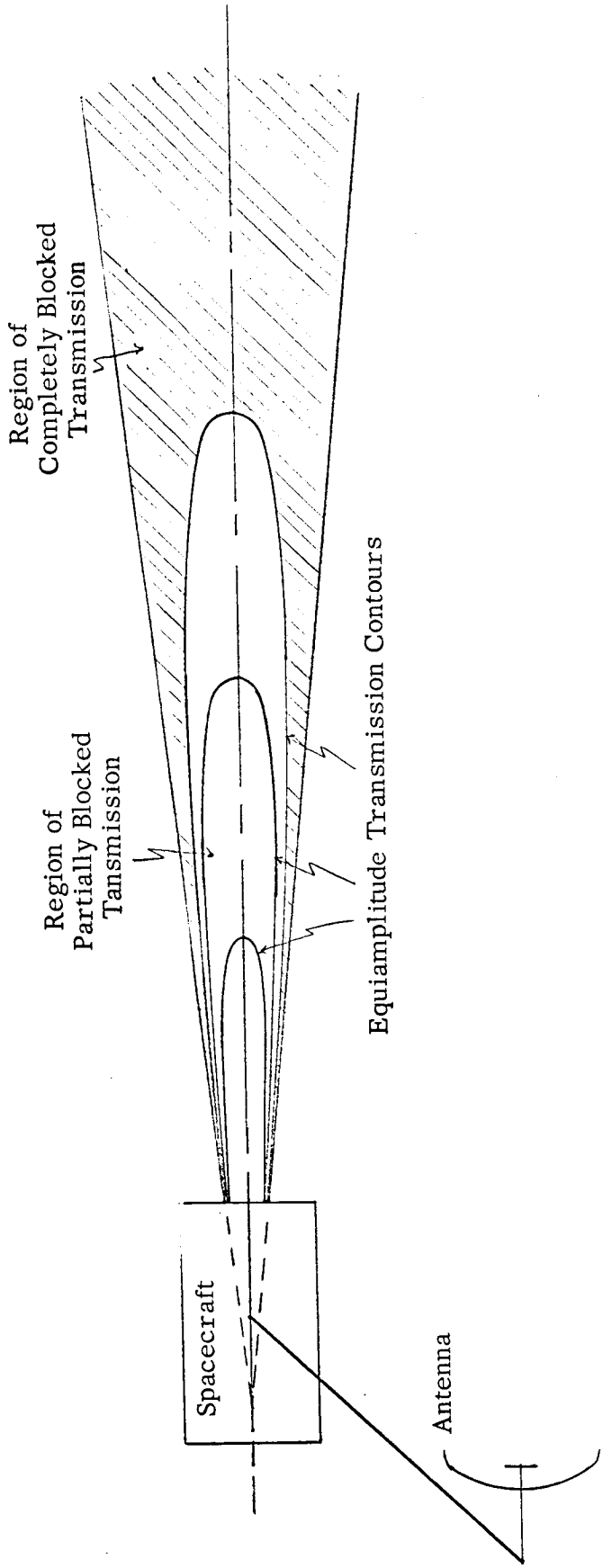

Fig. 2.5 Pictogram of Transmission Blockage Caused by the Ion Rocket Exhaust Beam

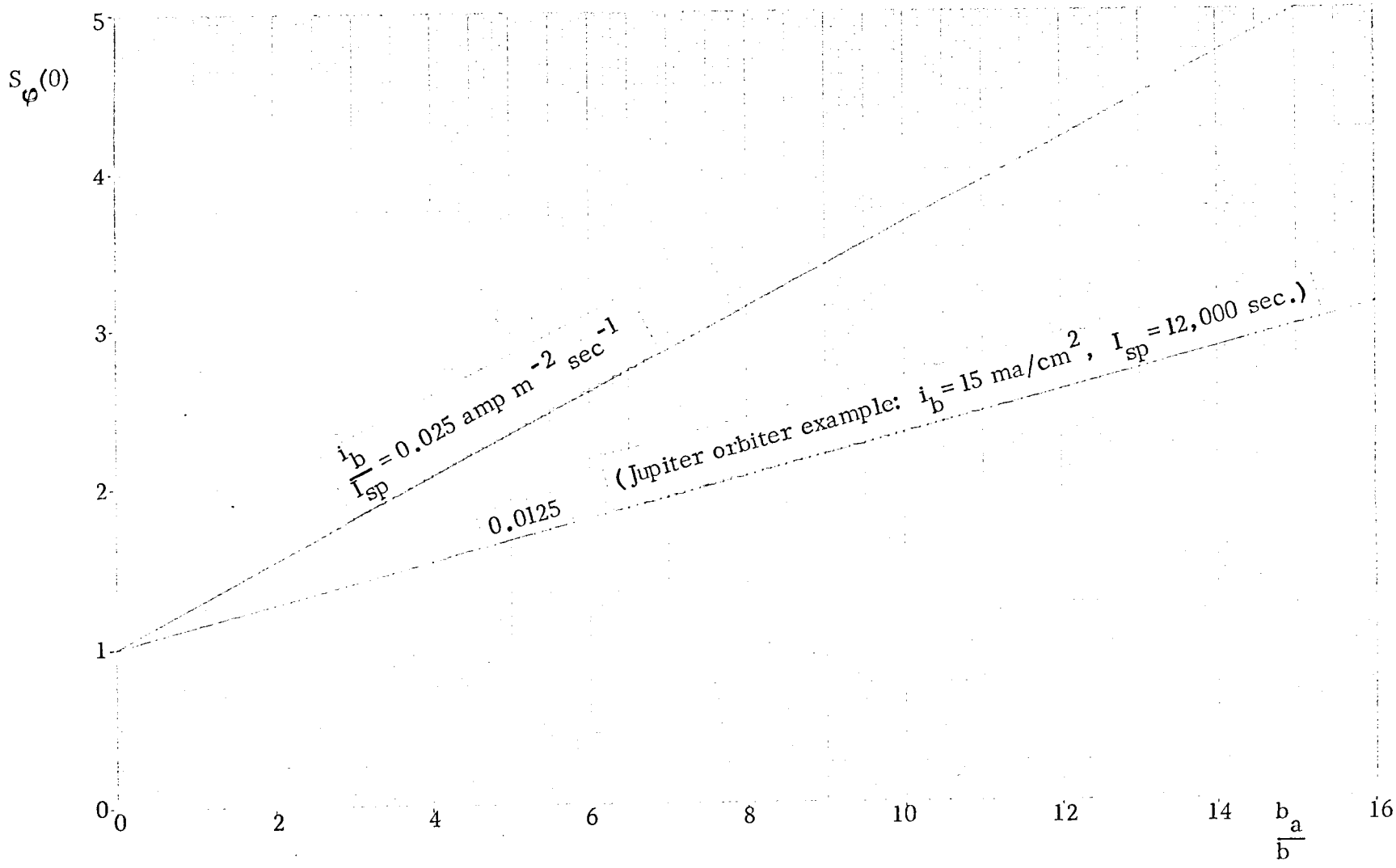

Fig. 2.6 Minimum Transverse Spreading Factor for Signal Rays in a Plane Perpendicular to the Ion Exhaust Beam Axis

by reflections, then it will be necessary to orient the spacecraft and antenna system so that the signal beam and the ion exhaust beam do not intersect.

2.5 Signal Reduction due to Beam Spreading

The signal ray also loses power intensity by the defocusing effect of the ion rocket exhaust beam. The special case for which the signal rays are in the plane perpendicular to the ion exhaust beam axis of symmetry is given by

$$\xrightarrow[I\text{-}24]{I\text{-}37, I\text{-}1, I\text{-}3} (22) \quad S_\varphi = \frac{1}{T_{S\varphi}} = 1 + 2\frac{b_a}{b}\left[\frac{b_a - b\cos\varphi}{\sqrt{n^2(b_a^2 - 2bb_a\cos\varphi + b^2) - b_a^2\sin^2\theta}} - \frac{b_a - b\cos\varphi}{b_a\cos\varphi - b}\right] .$$

The special case for the signal ray passing through the axis

$$\xrightarrow{I\text{-}38} (23) \quad S_\varphi(0) = 1 + 2\frac{b_a}{b}\left(\frac{1}{n} - 1\right)$$

for ion exhaust beams of interest

$$\xrightarrow{I\text{-}40} (24) \quad S_\varphi(0) = 1 = 10.62\frac{b_a i_b}{b I_{sp}}$$

is plotted in Fig. 2.6. These curves show a power intensity decrease of 2 to 3 db (and more) in the region of interest. This is a serious loss, particularly considering that these curves represent only lower bounds.

CHAPTER III: SIGNAL DISTORTION

3.1 Introduction

The probability of errors being introduced into the transmitted information increases as the ratio of distortion level to signal level increases. Signal distortion results whenever the transmission channel causes the different frequency components of the signal to have different relative amplitudes and/or different relative phases. The distortion can be caused by extensive properties of the transmission channel which cause mulitpathing: i.e., signal rays arriving at the receiver from different directions. The distortion can also be caused by the intensive properties of the medium, determined by the particle densities and collision frequencies, which cause the different frequency components to propagate with different phase velocities and different attenuation factors. Only the latter cause is investigated here.

3.2 Phase Distortion Index

The analytical formulation of distortion is given in Appendix J. For relatively narrow-band signals, amplitude distortion is likely to be small compared with phase distortion. A phase distortion index is defined in terms of the Taylor expansion remainder after the linear term of the transfer function phase characteristic by

$$\xrightarrow{\text{J-51}} (1) \quad \Psi_D = \frac{f_o^2}{B^2} R_2 \underline{/T(\omega)}$$

where

$$\xrightarrow{\text{sym def}} (2) \left\{ \begin{matrix} f_o \\ B \end{matrix} \right\} = \text{the signal} \left\{ \begin{matrix} \text{carrier frequency} \\ \text{bandwidth} \end{matrix} \right\} .$$

Small phase distortion requires that the inequality

J-53 → (3) $|\Psi_D| << \frac{f_o^2}{B^2}$

be satisfied.

3.3 Distortion Index for a Ray Perpendicular to the Ion Exhaust Beam Axis

A preliminary and representative estimate of the range of conditions over which phase distortion is negligible is obtained for the case of the signal ray passing through, and perpendicular to, the ion exhaust beam axis. For this case, the phase distortion factor is expressed by

J-65 → (4) $$\Psi_D = -\frac{\pi L}{4\lambda_o} \frac{f_p^2 f_o^{-2}}{(1 - f_p^2 f_o^{-2})^{3/2}}$$

where

sym def → (5) L = signal path length through plasma.

For ion engines that appear likely to be built in the next decade this reduces to

J-68 → (6) $$\Psi_D = -\frac{\pi b}{2\lambda_o} \frac{f_p^2}{f_o^2} \quad .$$

In terms of the ion exhaust beam properties this is

J-69 → (7) $$\Psi_D = \frac{1.82 \times 10^{12}}{f_o} \frac{\sqrt{P_b i_b}}{I_{sp}^2} \quad .$$

Using the center frequency for the specified frequency band gives

J-70 → (8) $$\Psi_D = -830 \frac{\sqrt{P_b i_b}}{I_{sp}^2}$$

Consequently, the maximum value for the phase distortion index for the Jupiter orbiter examples is given by

$$\xrightarrow{\text{J-72}} (9) \quad \Psi_D = 0.5 \quad .$$

The minimum carrier frequency to the bandwidth ratio for consideration is

$$\xrightarrow{\text{J-73}} (10) \quad \frac{f_o}{B} = 11 \quad .$$

Consequently, the inequality, (3), is more than satisfied thereby making distortion insignificant for the next generation of comtemplated ion engines.

CHAPTER IV: NOISE GENERATION IN AN ION ROCKET EXHAUST BEAM

4.1 Introduction

The basic source of noise in the ion rocket exhaust beam plasma is the radiation from electrons accelerated by the positive ions. This process is called bremsstrahlung. Since the collision interactions of the electrons and ions are random, the bremsstrahlung radiation is incoherent, and hence is noise. The noise energy generated by bremsstrahlung can be greatly increased by:

1. Up-conversion through various nonlinear process which can occur in the plasma
2. Amplification via growing-wave phenomena, which can also occur in a variety of modes in the plasma.

These processes may produce sizable fluctuations on a scale which is large compared to the charged particle nearest neighbor spacing but small compared to the dimensions of the ion exhaust beam. The noise radiation from these small scale fluctuations may be substantially greater than the basic bremsstrahlung radiation. Consequently, even if the noise directly generated (in the band of interest) by bremsstrahlung were completely negligible, the possible growing-wave, up-conversion and intermediate scale fluctuation processes may cause an objectionable amount of noise to be present, and hence should be investigated.

4.2 Spectral Power Generated by Bremsstrahlung per Unit Length of the Ion Exhaust Beam

A preliminary estimate of

$$\xrightarrow{\text{sym def}} (1) \quad P_{1f} = \text{the spectral power generated per unit length of the ion exhaust beam}$$

is given in terms of the estimated ion exhaust beam cross section area and the estimated spectral power generated per unit volume by

addition → (2) $P_{1f} = A_b p_f$.

In terms of the ion beam cross section area,

B-60 → (3) $A_b = \pi b^2$,

and the noise power generated per unit volume for the frequency range of interest,

K-164 → (4) $p_f = 2.84 \times 10^{-52} \frac{n^2}{V_\infty} \ell n\, 3.5 \times 10^3\, V_\infty$,

the noise power per unit length of ion exhaust beam is given by

2, 3, 4 → (5) $P_{1f} = 8.92 \times 10^{-52} \frac{n^2 b^2}{V_\infty} \ell n\, 3.5 \times 10^3\, V_\infty$ watts/Hz/unit length.

Expressing the radius and ion density in terms of beam power, current density and specific impulse gives

B-55, B-66 → (6) $n^2 b^2 = 1.873 \times 10^{39} \frac{P_b i_b}{I_{sp}^4}$.

Consequently, the noise generated per unit length by bremsstrahlung is given by

5, 6 → (7) $P_{1f} = \frac{1.67 \times 10^{-12}\, P_b i_b}{V_\infty\, I_{sp}^4} \ell n\, 3.5 \times 10^3\, V_\infty$.

A range of relative electron energies from 1 ev to 0.1 ev is taken in order to give a numerical indication of the dependence on this parameter,

7 → (8) $P_{1f} = \begin{Bmatrix} 9.77 \\ 1.36 \end{Bmatrix} \times 10^{-11} \frac{P_b i_b}{I_{sp}^4}$ watts/Hz/unit length, $\begin{matrix} V_\infty \\ \begin{Bmatrix} 0.1 \\ 1.0 \end{Bmatrix} \end{matrix}$.

This is graphed as a function of ion current density for the Jupiter orbiter example

$$\xrightarrow{2\text{-}3} (9) \quad \frac{P_b}{I_{sp}^4} = 2.41 \times 10^{-11} \text{ watts-sec.}^{-4}$$

and another example having one third the specific impulse

P_b = 500 kw

I_{sp} = 4,000 sec.

$$\xrightarrow{} (10) \quad \frac{P_b}{I_{sp}^4} = 1.95 \times 10^{-9} \text{ watts-sec.}^{-4} \quad .$$

Thus

$$\xrightarrow[9,10]{8} (11) \quad P_{1f} = \begin{matrix} & \overset{V_\infty}{\overbrace{\begin{matrix} 0.1 & 1.0 \end{matrix}}} & \\ \left\{ \begin{matrix} 191 & 26.5 \\ 2.35 & 0.328 \end{matrix} \right. & \times 10^{-21} \, i_b \text{ w/Hz/unit length} & \left\{ \begin{matrix} \overset{I_{sp}\text{sec}}{} \\ 4,000 \\ 12,000 \end{matrix} \right. \end{matrix} \quad .$$

This is graphed in Fig. 4.1.

4.3 Comparison with Thermal Noise

In order to obtain some appreciation for the significance of the noise power generated by bremsstrahlung, a comparison is made with available spectral noise power from a resistance

$$\xrightarrow{R4\text{-}1:259} (12) \quad P_{fANR} = kT = 1.38 \times 10^{-23} T \text{ w/Hz} \quad .$$

The temperature that a resistance must have to give a specified spectral power is, hence,

$$\xrightarrow{12} (13) \quad T = 7.25 \times 10^{22} P_f \quad {}^{o}K \quad .$$

A temperature scale based on this relationship is placed on the right-hand ordinate of the graph in Fig. 4.1. For the Jupiter orbiter example, an ion exhaust beam having a specific impulse of 12,000 sec., a power of 500 kw, a current density of 15 ma/cm^2, and

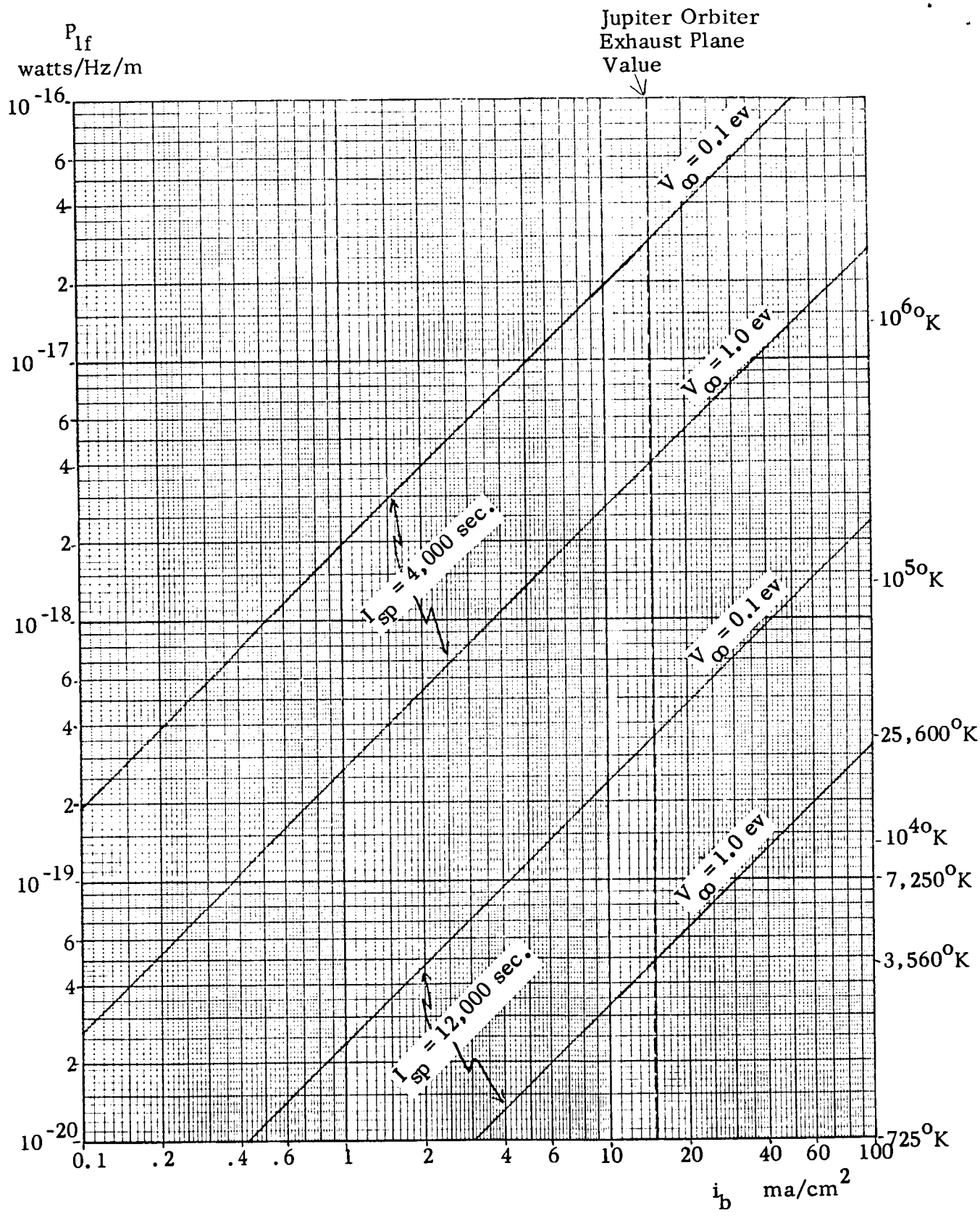

Fig. 4.1 Bremsstrahlung Spectral Power Per Unit Length Generated in a 500 KW Ion Rocket Exhaust Beam

relative electron kinetic energy with respect to the ions of 0.1 ev would produce 3.5×10^{-19} w/Hz/m of ion exhaust beam. If all this power were absorbed by a receiver, it would be the same as that supplied by a matched resistance at 25,600 ^{o}K. If the relative electron kinetic energy were 1ev, the noise generation would reduce to 5×10^{-20} w/Hz/m, which corresponds to a resistance temperature of 3,560 ^{o}K. This effective temperature is large. If this temperature were low, the bremsstrahlung alone would not be of significance. But since it is not, it is necessary to determine the actual amount of noise power accepted by the receiving antenna. Note that the bremsstrahlung noise power density generated per unit length of beam varies with position, hence decreases with increasing distance from the spacecraft. Note also that the presence of up-conversion, amplification via growing waves, and intermediate scale fluctuations could increase the noise level by many orders of magnitude. As a consequence, further work is required before an adequate assessment can be made of the noise power generated by the ion exhaust beam.

4.4 Comparison with Black Body Radiation

Black body radiation provides another comparative index. For the long wavelength of interest the spectral power radiated per unit area of black body surface is given by

Rayleigh-Jeans Law $\rightarrow$ (14) $\quad dR_\lambda = \dfrac{2\pi ckT}{\lambda^4} d\lambda \quad$ watts m^{-2} .

In terms of this

sym def $\rightarrow$ (15) $\quad W_f =$ the spectral power emittance (power/unit area/Hz)

is given by

14, 15 $\rightarrow$ (16) $\quad W_f = \dfrac{dP_\lambda}{df} = \dfrac{2\pi ckT}{\lambda^4} \left|\dfrac{d\lambda}{df}\right| \quad$ watts m^{-2} Hz^{-1} .

Using

$$\xrightarrow{\text{C-124}} (17) \quad \left|\frac{d\lambda}{df}\right| = \frac{c}{f^2}$$

gives

$$\xrightarrow[17]{16} (18) \quad W_f = \frac{2\pi kT}{\lambda^2} \text{ watts m}^{-2} \text{ Hz}^{-1} .$$

Using the wavelength at the center frequency in the band of interest gives

$$\xrightarrow[\lambda = 0.1363\,\text{m}, 12]{18} (19) \quad W_f = 338kT = 4.67 \times 10^{-21} T \text{ watts/Hz/m}^2 .$$

Comparing this with the available spectral power from a resistance shows that the area required to deliver the same power at the same temperature,

$$\xrightarrow{12, 15} (20) \quad A = \frac{P_{fANR}}{W_f} \text{ m}^2 ,$$

is given by

$$\xrightarrow[19, 12]{20} (21) \quad A = \frac{1}{338} = 2.96 \times 10^{-3} \text{ m}^2 = 29.6 \text{ cm}^2 .$$

The spectral power that would be radiated by a cylindrical black body of unit length is given by

$$\xrightarrow{15} (22) \quad P_{Blf} = 2\pi b W_f .$$

For the Jupiter orbiter example the radius at the exhaust plane is given by

$$\xrightarrow[2\text{-}3]{\text{B-66}} (23) \quad b_r = 0.31\,\text{m} .$$

Consequently,

$$\xrightarrow[22]{21} (24) \quad P_{B1f} = 1.95 W_f$$

and hence

$$\xrightarrow[19]{24} (25) \quad P_{B1f} = 9.11 \times 10^{-21} T \quad \text{watts/m}^2\text{/Hz} \quad .$$

In this case, the equivalent black body temperature required to radiate a specified spectral power is given by

$$\xrightarrow{25} (26) \quad T = 1.1 \times 10^{20} P_f$$

and is approximately two and a half orders of magnitude less that the temperature given by (13). Consequently the bremsstrahlung noise radiation from the ion exhaust beam for the Jupiter orbiter example is of the same order as that from a black body at a temperature of 100 ^{o}K.

4.5 Comments

The analysis of bremsstrahlung in the literature, which presents readily usable results, rests on approximations which lead to improper integration at both the upper and lower limits. The more exact treatment presented here eliminates the singularity at the upper limit without resorting to any cutoff mechanism including those provided by a more detailed knowledge of the plasma behavior. The singularity at the lower limit is eliminated by considering the extended structure of the electron as a quantum mechanical wavepacket. This approach gives a lower limit more directly determined by the electrons momentum rather than by its energy, as is usually done in the literature. As a consequence the noise radiation appears to be substantially larger under some circumstances of interest here. While comparisons of bremsstrahlung

generated noise power in the ion exhaust beam, with noise from a

1. resistor
2. black body

may appear somewhat arbitrary, it does provide a relative orientation. If the bremsstrahlung generated noise is insignificant by comparison it can be neglected; however, the converse statement cannot be made.

If the noise due to bremsstrahlung is significant, then its directional properties and polarization become important and should be examined since the communication signal is affected according to its polarization and the antenna pattern orientation. These properties are a consequence of the streaming motion.

CHAPTER V: CONCLUDING REMARKS

5.1 Results

The results obtained are considered preliminary because of their partial coverage of the subject, and tentative because of the approximations involved. Under the conditions considered, the principal results may be summarized as follows:

1. The signal loss via attenuation in the ion rocket exhaust beam (due to electron-ion collisions) is negligible for contemplated ion rocket engines, provided that the signal frequency is sufficiently above the plasma frequency. This is the case with 2.1- to 2.3- Gc frequency band and the chosen design parameters for the Jupiter craft.
2. For the semihomogeneous ion exhaust beam model, the signal ray losses for normal incidence are several orders of magnitude above the electron collision losses in the parameter ranges of interest, but are still sufficiently small to be neglected. However, the ion exhaust beam internal structure for practical ion rockets may cause reflection (or scattering) losses which are one or more orders of magnitude larger. For nonnormal incidence, the signal rays encounter a solid angle or area within the ion exhaust beam which completely blocks transmission.
3. The reduction in signal power intensity due to spreading of the signal beam which passes through the ion rocket exhaust beam has a lower bound of a few decibels at the exit plane of its Jupiter craft example.
4. Distortion is negligible with the signal frequency substantially above the plasma resonant frequency for normal operation, and for the case in which the signal ray is perpendicular to, and passes through, the axis of symmetry of the ion rocket exhaust beam. Any other case of signal ray orientation is not expected to make distortion significant.

5. The bremsstrahlung noise power generated per unit length of ion exhaust beam may be significant in the frequency band of interest. To verify this result, the analysis must be pursued in greater detail. Up-conversion, amplification processes and intermediate scale fluctuations may increase the noise level by many orders magnitude and thereby present a serious noise problem.

5.2 Operational Recommendations

1. Orient the spacecraft and antenna system so that signal ray directions of interest do not pass through the dead blockage region or the strong divergence region of the ion exhaust beam.
2. Program ion-rocket off-time for communication use if gross attenuation and noise generation cannot be adequately mitigated without significant degradation of the ion rocket propulsion capability.

5.3 General Recommendations for Further Work

1. Design critical experiments to verify predictions.
2. Determine a more realistic model for the ion rocket exhaust beam by including the effects of diffusion and recombinations.
3. Using the more realistic ion exhaust beam model, particularly the alteration of sharp boundaries to diffuse boundaries, determine the effect on the signal strength reduction.
4. Determine the added reflection and scattering losses due to multiple emitter design of the ion rocket engine.
5. Improve the bremsstrahlung noise generation analysis and take into account the radiation pattern and polarization characteristics caused by the anisotropic velocity distribution.
6. Determine the amount of noise generated by nonlinear up-conversion, growing wave amplification and intermediate scale fluctuation processes.

7. Determine the extent of the antenna detuning by the proximity of the ion exhaust beam, particularly by the diffusion of plasma into the near field region at the antenna.
8. Determine the effect of diffusion from the ion exhaust beam on the antenna breakdown properties.

APPENDIX A: NOTATION

A.1 Development-Tracking Notation

A special notation scheme is employed to increase the ease with which mathematical developments can be followed and, simultaneously, to simplify the process of committing them to written form with adequate detail. Arrows are placed to the left of each equation number to serve as a bookkeeping aid for the equation derivation. The information above each arrow designates the principal source or sources from which the equation originates. The information below the arrow refers to auxiliary sources of information or special conditions substituted into the primary sources in order to obtain the equation. Examples of the equation bookkeeping scheme, where the principal information source is one or more other equations, are given in Table A1.

Examples of the arrow bookkeeping scheme, where the principal source of information is not another equation, are given in Table A2.

In each Section (or Appendix), the equations are independently numbered, starting from (1). Equations in the same Section (or Appendix) are referred to by number only, whereas the numbers of equations in a different Section (or Appendix) are preceded by the Section number (or Appendix letter). This is exemplified in Table A3.

Table A1. Bookkeeping scheme when principal sources for equations are in same Section

Example	Meaning
9 → (12); 10, 11	(12) is obtained by using (10) and (11) in (9)
1 + 8 → (9)	(9) is obtained by adding (1) and (8)
17 ÷ 9 → (31)	(31) is obtained by dividing (17) by (9)
9 → (12); 10/11	(12) is obtained by substituting (11) into (10) and that result into (9)
19 → (41); $y = 3$	(41) is obtained by substituting $y = 3$ into (19)
8 → (26); $a << b$	(26) is obtained from (8) if $a << b$
12 → (27); 17, 19	Part one of (27) is obtained by substituting (17) into (12) and Part two of (27) is obtained by substituting (19) into (12)

Material from other documents or papers are indicated as in Table A4.

Table A3. Bookkeeping scheme when source equations are in other Sections

Example	Meaning
9 → (12)	(12) is obtained from Eq. (9) in the same Section (or Appendix)
III-9 → (12)	(12) is obtained from Eq. (9) in Section III
F-9 → (12)	(12) is obtained from Eq. (9) in Appendix F

Table A2. Bookkeeping scheme when sources are not equations

Example	Meaning
Fig 1 → (3)	(3) is obtained from the information in Fig. 1
Table 3 → (12)	(12) is obtained from the information in Table 3
causality → (2)	(2) is a basic cause-and-effect relationship
name → (5)	(5) is _____'s (name) law or equation
14 analog → (72)	(72) is obtained by a development analogous to the way in which (14) is obtained
sym def → (4)	(4) is a symbol definition
phys def → (6)	(6) is a physical definition
geom def → (8)	(8) is a geometrical definition
con def → (7)	(7) is a conceptual definition
identity → (9)	(9) is an identity
linearity → (13)	(13) is obtained by linear superposition of component parts

Table A4. Bookkeeping scheme when sources are in other documents

Example	Meaning
Ref 3:132 → (12)	(12) is obtained from page 132 of Ref. 3
Ref 5(6–73) → (8)	(8) is obtained from Eq. (6–73) of Ref. 5

A.2 Physical Constants

		Quantity	Name
RA2:591 → (1)	ϵ_v	$= 8.8552 \times 10^{-12}$ farads/m $\simeq \frac{1}{36\pi} \times 10^{-9}$ farads/m	vacuum capacity
RA2:591 → (2)	μ_v	$= 4\pi \times 10^{-7}$ henries/m $\simeq 1.2566 \times 10^{-6}$ henries/m	vacuum inductivity
RA2:591 → (3)	c	$= 2.9978 \times 10^{8}$ m/sec	vacuum speed of light
RA2:591 → (4)	e	$= 1.6020 \times 10^{-19}$ coulombs $= 4.8028 \times 10^{-10}$ esu	electron charge
RA1:7-3 → (5)	m_e	$= 9.1085 \times 10^{-31}$ kg	electron mass
4 − 5 → (6)	$\frac{e}{m_e}$	$= 1.7594 \times 10^{11}$ coulombs/kg	charge/mass ratio
RA1:7-3 → (7)	M_1	$= 1.6598 \times 10^{-27}$ kg	mass of particle with atomic weight one
RA1:7-3 → (8)	m_p	$= 1.6724 \times 10^{-27}$ kg	proton mass
14 − 5 → (9)	m_p/m_e	$= 1,836$	proton to electron mass
RA3:F-81 → (10) Lat 50°	g	$= 9.8107$ m/sec^2 $= 32.187$ ft/sec^2	acceleration of gravity
RA1:7-3 → (11)	h	$= 6.6251 \times 10^{-34}$ joules-sec $= 4.1355 \times 10^{-15}$ ev-sec $= 6.6251 \times 10^{-27}$ erg-sec	Planck's constant
RA1:7-3 → (12)	k	$= 1.3805 \times 10^{-23}$ joules/deg $= 8.6170 \times 10^{-5}$ ev/deg $= 1.3805 \times 10^{-16}$ erg/deg	Boltzmann's constant
RA1:7-3 → (13)	σ	$= 5.6697 \times 10^{-12}$ w/cm^2(deg K)^4	Stephan-Boltzmann constant
RA1:7-3 → (14)	N_A	$= 6.0248 \times 10^{23}$ molecules(g-mole)	Avogadro's number

A.3 Set Notation

Highly repetitive expressions which have a similar structure can be expressed with a substantial savings of reading, writing and abstracting time by the use of set brackets, $\{\ \}$. For example:

Set Notation		Long Hand Notation
$\{x_i\}\quad 1 \le i \le N$	$\longleftrightarrow$	$x_1, x_2, x_3, x_4, \ldots, x_n, \ldots x_N$
$\begin{Bmatrix} n \\ \varkappa \end{Bmatrix} = \sqrt{\begin{Bmatrix} 1 \\ -1 \end{Bmatrix} x + \sqrt{x^2+y^2}}$	$\longleftrightarrow$	$n = \sqrt{x+\sqrt{x^2+y^2}}$ $\varkappa = \sqrt{-x+\sqrt{x^2+y^2}}$
$\begin{Bmatrix} i \\ r \end{Bmatrix}$ = the angle of $\begin{Bmatrix} \text{incidence} \\ \text{refraction} \end{Bmatrix}$	$\longleftrightarrow$	i = the angle of incidence r = the angle of refraction

A.4 Matrix Notation

If the members of a set can be specified by an address, they can be illustrated as a table. Sometimes it is convenient to omit (but understand) the lines which compartmentalize the table into sections designated by the various addresses. Varying degrees of this are illustrated by

$$\left|\begin{array}{c|c} A_{11} & A_{12} \\ \hline A_{21} & A_{22} \\ \hline A_{31} & A_{32} \end{array}\right| = \begin{bmatrix} A_{11} & A_{12} \\ A_{21} & A_{22} \\ A_{31} & A_{32} \end{bmatrix} = \left[\begin{matrix} A_{11} & A_{12} \\ A_{21} & A_{22} \\ A_{31} & A_{32} \end{matrix}\right] = \left\|\begin{matrix} A_{11} & A_{12} \\ A_{21} & A_{22} \\ A_{31} & A_{32} \end{matrix}\right\| = \begin{pmatrix} A_{11} & A_{12} \\ A_{21} & A_{22} \\ A_{31} & A_{33} \end{pmatrix} = \left\lceil\begin{matrix} A_{11} & A_{12} \\ A_{21} & A_{22} \\ A_{31} & A_{32} \end{matrix}\right\rceil .$$

Corresponding shorthand notation is given by

$$\text{table of A} = \boxed{A_{ij}} = \left[A_{ij}\right] = \|A_{ij}\| = (A_{ij}) = \left\lceil A_{ij} \right\rceil = \underline{\underline{A}} .$$

A table is a matrix and the commonly used notations are the third, fourth and fifth illustrated above. These commonly used notations are unfortunate from the standpoint that the

same type of bracket symbols also have other meanings. The last notation on the right is advantageous because it has the greatest degree of consistency with the fundamental principles which govern choise of notation:

1. parsimony
2. clarity
3. neatness
4. minimum usage for other purposes
5. flexibility for generalization.

For example,

table of f(x,y) =

x \ y	.03	1.2
1	31	26
1.5	3.7	0.7
2	0.2	-18

=

	y	
1	31	26
1.5	3.7	0.8
2	0.2	-18
x		

$= \left[f(x_1 y) \right]_x^y = \underline{f(x,y)}$

A.5 Vector and Dyad Notation

Bold face or Clarendon type utilized in books, for representing vectors are not practicably available for handwritten or typed material. The many notations such as bars, arrows, asterisks, etc., which may be placed over or under a symbol to to designate that the symbol is to represent a vector are all unsatisfactory because of the multiplicity of different meanings for such symbols. A much neater and ambiguity-free notation for the representation of printed or typed vector symbols is a vertical stroke integrated into the symbol to make it appear as a single symbol, instead of a combination of two symbols, and also make it simulate a bold face symbol, for example:

$\mathfrak{a}\ \mathfrak{b}\ \mathfrak{c}\ \mathfrak{d}\ \mathfrak{e}\ \mathfrak{f}\ \mathfrak{h}\ \mathfrak{i}\ \mathfrak{j}\ \mathfrak{k}\ \mathfrak{l}\ \mathfrak{m}\ \mathfrak{n}\ \mathfrak{o}\ \mathfrak{p}\ \mathfrak{q}\ \mathfrak{r}\ \mathfrak{s}\ \mathfrak{t}\ \mathfrak{u}\ \mathfrak{v}\ \mathfrak{w}\ \mathfrak{x}\ \mathfrak{y}\ \mathfrak{z}$

$\mathfrak{A}\ \mathfrak{B}\ \mathfrak{C}\ \mathfrak{D}\ \mathfrak{E}\ \mathfrak{F}\ \mathfrak{G}\ \mathfrak{H}\ \mathfrak{I}\ \mathfrak{J}\ \mathfrak{K}\ \mathfrak{L}\ \mathfrak{M}\ \mathfrak{N}\ \mathfrak{O}\ \mathfrak{P}\ \mathfrak{Q}\ \mathfrak{R}\ \mathfrak{S}\ \mathfrak{T}\ \mathfrak{U}\ \mathfrak{V}\ \mathfrak{W}\ \mathfrak{X}\ \mathfrak{Y}\ \mathfrak{Z}$

The major exception to this notation form, the unit vectors, are designated by a unit body symbol and with the approprate subscript. For example

$$\mathfrak{b} = b_x \mathfrak{l}_x + b_y \mathfrak{l}_y + b_z \mathfrak{l}_z = b_r \mathfrak{l}_r + b_\theta \mathfrak{l}_\theta + b_\varphi \mathfrak{l}_\varphi .$$

Dyads are written the same as vectors but with two dots inside the bold parts. Unit dyads are designated by a unit symbol with two subscripts.

example $\mathfrak{E} = \sum_{i=1}^{3} \sum_{j=1}^{3} \mathfrak{l}_{ij} \epsilon_{ij}$

A.6 Operator Symbols on the Body-Symbol Level

$\int$	integral	$\lvert\ \rvert$	absolute value
$\sum$	sum	$\lvert\ \rvert$	determinant
d	differential	$\langle\ \rangle$	average
∂	partial derivative	$\angle$	angle
∂_α	partial derivative with respect to α	$\sqrt[n]{\ }$	nth root
Δ	difference, deviation	$\mathcal{R}$	real part
∇	del	$\mathcal{I}$	imaginary part
$\cdot$	dot product	R_n	remainder after nth term
x	cross product	$>$	greater than
$\approx$	approximate	$>>$	much greater than
/	not		
$\div$ or /	divide by		

A.7 Symbols Placed over the Body Symbol

$\dot{}$	derivative with respect to time	$\frown$	maximum value
$\bar{}$	average	$\smile$	minimum vlaue
$\tilde{}$	transform	$\vee$	complex quantity

A.8 Superscript Symbols

$^{-1}$	functional or operator inverse	1	first order or degree
*	complex conjugate	2	second order or degree
'	derivative with respect to the argument	E	E wave
o	degree	H	H wave

A.9 Subscript Symbols

$\wedge$	value giving maximum
$\vee$	value giving minimum
$\parallel$	parallel
$\perp$	perpendicular
1	per unit
1	region-1, part-1, term-1
2	region-1, part-2, term-2
a	antenna
A	attenuation
b	beam
B	blocked
c	collision
c	critical
d	delay
d	double
D	Debye
D	distortion
e	electron
E	electric field
h	half
H	magnetic field
i	ion
i	incident
i	input
K	kinetic
m	material
n	neutral particle
o	output
p	plasma
P	potential
P	power
r	relative
r	refracted
r	radial component
R	reflected
R	reception
s	species
S	surface
S	special
S	spreading
sp	specific
T	transmission
v	vacuum
x	x-component
y	y-component
z	z-component
θ	θ-component
π	power density
ρ	ρ-component
φ	φ-component
Ω	solid angle

A.10 Latin Body Symbols

a	distance from antenna	m	meter
A	area	m	particle mass
A	attenuation	M	mass
b	collision parameter	n	refractive index
b	beam radius	n	number density
B	bandwidth	N	number
B	normalized radial distance	p	power intensity(scalar)
B	magnetic flux density (scalar)	$\mathbb{P}$	power intensity(vector)
$\mathbb{B}$	magnetic flux density (vector)	$\mathbb{P}$	particle momentum
c	speed of light	P	power
D	electric flux density (scalar)	q	particle charge
$\mathbb{D}$	electric flux density (vector	Q	charge
e	electron's charge	r	radial coordinate
E	electric field intensity (scalar)	r	refraction angle
$\mathbb{E}$	electric field intensity (vector)	r	radius
f	frequency	$\mathbb{r}$	position vector
f	function	R	radial distance
F	any field function or component	R	remainder
g	free fall acceleration	R	normalized ratio
G	antenna or radiator gain	S	spreading factor
h	Planck's constant	S	surface area
H	magnetic field intensity (scalr)	$\mathbb{S}$	surface vector
$\mathbb{H}$	magnetic field intensity (vector)	t	tangent
i	incidence angle	t	time
i	current density (scalar)	T	time interval, period
$\mathbb{i}$	current density (vector)	T	transfer function
I	current	T	thrust
I	impulse	T	temperature
j	$\sqrt{-1}$	T	transmission coefficient
j	particle flux density	u	speed
J	particle flux	$\mathbb{u}$	velocity
k	Boltzmann constant	v	phase speed
K	normalized ion beam parameter	V	voltage
ℓ	angular momentum	V	energy in electron volts
ℓ	length	W	energy
L	length	W	weight
$\mathbb{L}$	length vector		

Latin Body Symbols (Cont.)

x	rectangular coordinate	Z	charge number
y	rectangular coordinate	$\mathbb{Z}$	characteristic impedance
z	rectangular coordinate	$\mathfrak{z}$	normalized z-coordinate

A.11 Greek Body Symbols

α	attenuation factor	ν	collision frequency
$\boldsymbol{\alpha}$	attenuation factor vector	ξ	normalized collision parameter
β	phase factor	π	power density scalar
$\boldsymbol{\beta}$	phase factor vector	$\boldsymbol{\pi}$	Poynting's vector
γ	Euler constant (0.5772)	π	3.14159 ...
Γ	reflection coefficient	ρ	charge density
δ	deflection angle	ρ	cylindrical radial coordinate
Δ	incremental change	$\boldsymbol{\rho}$	cylindrical radial vector
ϵ	capacitivity	σ	conductivity
ζ	normalized z-coordinate	σ	collision cross section
η	normalized y-coordinate	τ	time constant
θ	polar coorcinate	φ	aximuth corrdinate
$\varkappa$	absorption index	χ	susceptibility
λ	wavelength	ψ	phase coordinate
Λ	volume	Ψ	distortion index
μ	permeability	ω	angular frequency
		Ω	solid angle

A.12 Composite Symbols

Composite symbols are defined in the text where first introduced. Because of the large number of them and their restricted usage they are not redefined here, with the exception of the more universal of the composite symbols which are listed below. In general however their meaning can be directly obtained from that of the body symbol together with the sub and super scripts given in the previous sections.

amp	ampere	I_ν	1st type order ν modified Bessel function
cm	centimeter	K_g	kilogram
Cs	cesium	K_ν	2nd type order ν modified Bessel function
Hz	Hertz		
I_{sp}	specific impulse		

APPENDIX B: ION ROCKET EXHAUST BEAM PROPERTIES

B.1 Introduction

Propulsion device characteristics normally considered by the ion rocket designer are: specific impulse, thrust, power, beam voltage and beam current. Not all of these are independent nor are they always specified.

Communication with an ion rocket driven spacecraft can be affected by the densities and collision frequencies of the constituent particles of the ion exhaust beam; hence, it is necessary to know these quantities to predict the effects of the ion exhaust beam on communications. For some purposes it is also necessary to know the distribution functions for the constituent particles.

The objective of this appendix is to provide simple formulae and charts which give the needed information in terms of more readily available information.

B.2 Mechanical Variables

The flight time is primarily determined by (Ref. B.1)

sym def* (1) T = thrust

and the terminal mass is primarily determined by (Ref. B.1)

sym def (2) I_{sp} = Specific (weight) Impulse.

These two quantities are the most direct measure of the thrustors propulsion capability.

B.3 Specific Impulse

The total momentum ejected is called

* See Appendix A for an explanation of the arrows and associated notation to the left of the equation numbers.

sym def → (3) $I = \text{Impulse}$.

In terms of

sym def → (4) $M = \text{the total mass ejected}$

and

sym def → (5) $u = \text{the ejection speed}$

the momentum ejected is given by

phys def → (6) $I = Mu$.

In terms of

sym def → (7) $W = \text{the ejected weight,}$

the specific impulse is given by

phys def → (8) $I_{sp} = \frac{I}{W}$.

The ejected weight is related to the ejected mass by

Newton → (9) $W = Mg$,

where

sym def → (10) $g = \text{the free fall acceleration.}$

Consequently, the specific impulse is related to the ejection speed by

8, 6, 9 → (11) $I_{sp} = \frac{u}{g}$.

The specific impulse can also be expressed in terms of

$\xrightarrow{\text{sym def}}$ (12) $\dot{I}$ = the impulse per unit time

divided by

$\xrightarrow{\text{sym def}}$ (13) $\dot{W}$ = the weight ejection rate

thus,

$\xrightarrow{8}$ (14) $I_{sp} = \frac{\dot{I}}{\dot{W}}$.

B.4 Thrust

The thrust is force resulting from mass ejection, i.e. the momentum ejected per unit time. In terms of ejection speed and

$\xrightarrow{\text{sym def}}$ (15) $\dot{M}$ = the mass ejection rate

the thrust is given by

$\xrightarrow{\text{phys def}}$ (16) $T = \dot{M}u$.

If u is in meters per second and M in kilograms per second, then the thrust T is in newtons.

The thrust in kilograms in terms of the thrust in newtons is given by

$\xrightarrow{1\,kg = g\,newtons}$ (17) $T_{Kg} = \frac{1}{g} T_{newtons}$,

consequently

$\xrightarrow[16]{17}$ (18) $T_{Kg} = \dot{M}\frac{u}{g}$.

The thrust in kilograms is related to the specific impulse by

$$\xrightarrow[11]{18} (19) \quad T_{Kg} = \dot{M} I_{sp} \quad .$$

Since the impulse imparted per unit time,

$$\xrightarrow{6} (20) \quad I = \dot{M} u \quad ,$$

is the thrust

$$\xrightarrow[20]{16} (21) \quad T = \dot{I} \quad ,$$

the specific impulse can also be expressed as the thrust per weight of material ejected per unit time

$$\xrightarrow[21]{14} (22) \quad I_{sp} = \frac{T}{\dot{W}} \quad .$$

B.5 Electrical Variables

The electrical variables

$$\xrightarrow{\text{sym def}} (23) \quad V_b = \text{the beam voltage}$$

and

$$\xrightarrow{\text{sym def}} (24) \quad I_b = \text{the beam ion current}$$

are more closely related to the particle densities and collision frequencies required for analysis of communication problems than are the specific impulse and thrust.

B.6 Beam Voltage in Terms of Specific Impulse

For the ion velocity ranges of interest,

sym def → (25) W_K = the particle kinetic energy

is given with sufficient accuracy by the nonrelativistic approximation,

phys def → (26) $W_K = \frac{1}{2} m_i u^2$,

where

sym def → (27) m_i = ion mass

and the speed of the ions with respect to the spacecraft is the mass ejection speed. During acceleration,

sym def → (28) W_P = the potential energy given up by the ions

is given by

phys def → (29) $W_P = q_i V_b$

where

sym def → (30) q_i = the ion charge.

Since the potential energy is converted into kinetic energy during the acceleration process,

energy conservation → (31) $W_K = W_P$.

Consequently,

$$\xrightarrow[26,29]{31} (32) \quad u = \sqrt{\frac{2q_i V_b}{m_i}} \quad .$$

The specific impulse in terms of the beam voltage is consequently

$$\xrightarrow[32]{11} (33) \quad I_{sp} = \frac{1}{g}\sqrt{\frac{2q_i V_b}{m_i}} \quad .$$

For singly ionized cesium ions,

$$\xrightarrow[\text{Cs A\#} = 132.9]{\text{A-7}} (34) \quad m_{Cs} = 2.21 \times 10^{-25} \text{ Kg} \quad ;$$

hence, the specific impulse for a cesium beam is

$$\xrightarrow[34,\text{A-4},\text{A-10}]{33} (35) \quad I_{sp} = 123 \sqrt{V_b} \text{ sec.}$$

The voltage required to produce a desired specific impulse is consequently

$$\xrightarrow{35} (36) \quad V_b = 6.63 \times 10^{-5} I_{sp}^2 \text{ volts} \quad .$$

B.7 Beam Current in Terms of Thrust and Specific Impulse

In terms of the ion charge and

$$\xrightarrow{\text{sym def}} (37) \quad J_i = \text{the ion flux}$$

$$\xrightarrow{\text{con def}} (38) \quad J_i = \text{the number of ions ejected per second,}$$

the beam current is given by

$$\xrightarrow{\text{phys def}} (39) \quad I_b = q_i J_i \quad .$$

The mass ejection rate in terms of the ion mass and ion flux can be expressed by

$$\xrightarrow{\text{phys def}} (40) \quad \dot{M} = m_i J_i \quad .$$

The beam current in terms of the mass ejection rate is consequently given by

$$\xrightarrow[40]{39} (41) \quad I_b = \frac{q_i}{m_i} \dot{M} \quad .$$

Expressing the beam current in terms of thrust and specific impulse gives

$$\xrightarrow[19]{41} (42) \quad I_b = \frac{q_i}{m_i} \frac{T_{Kg}}{I_{sp}} \quad .$$

For singly ionized cesium ions, the beam current is

$$\xrightarrow[A\text{-}4,34]{42} (43) \quad I_b = 7.26 \times 10^5 \frac{T_{Kg}}{I_{sp}} \quad .$$

For graphical conversion from mechanical to electrical units, it is more convenient to use

$$\xrightarrow{43} (44) \quad T_{Kg} = 1.377 \times 10^{-6} I_b I_{sp} \quad .$$

A chart for conversion between mechanical and electrical properties is given in Fig. B.1.

B.8 Beam Power

A frequently specified quantity is

$$\xrightarrow{\text{sym def}} (45) \quad P_b = \text{the beam power.}$$

In terms of electrical quantities, the beam power is given by

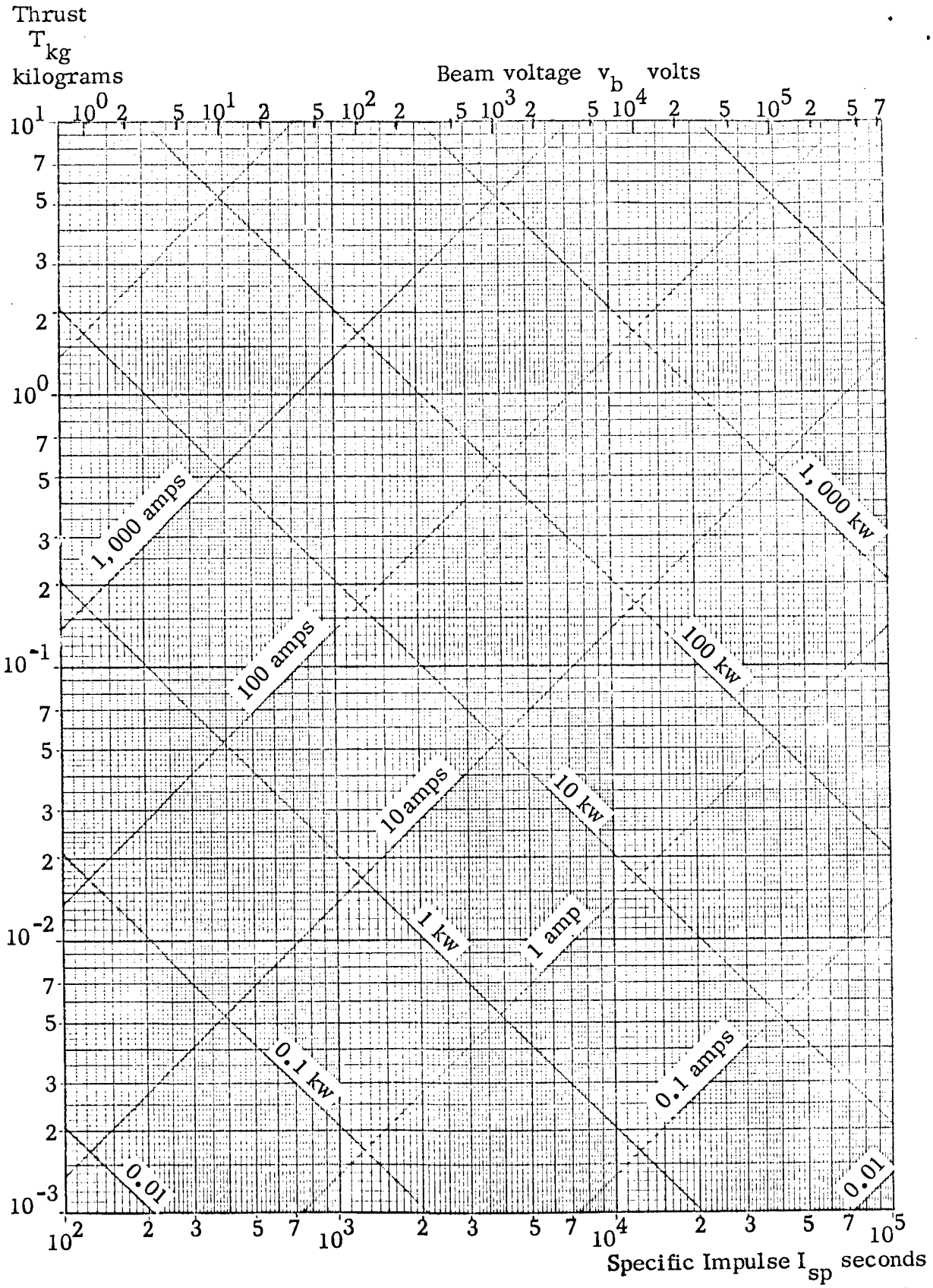

Fig. B.1 Chart for conversion between mechanical and electrical characteristics of an ion rocket.

phys def (46) $P_b = V_b I_b$.

In terms of mechanical quantities the beam power is given by

phys def (47) $P_b = \frac{1}{2} M u^2$

and hence also by

47, 11, 18 (48) $P_b = \frac{g^2}{2} T_{Kg} I_{sp}$.

Expressing the coefficient numerically gives

48, A-10 (49) $P_b = 48.1\ T_{Kg} I_{sp}$.

For plotting, it is more convenient to express this in the form,

49 (50) $T_{Kg} = \frac{2.08 \times 10^{-2} P_b}{I_{sp}}$.

These constant power curves are also incorporated in Fig. B.1.

Fig. B.1 allows conversion from any two independent ion exhaust beam parameters to the other ion exhaust beam parameters. For example, a 100KW ion beam with a specific impulse of 10,000 seconds has a thrust of 210 grams, a beam current of 14 amperes and a beam voltage of 700 volts.

B.9 Ion Density

The cesium ion density in the exhaust beam is primarily determined by the

sym def (51) i_b = the ion current density in the exhaust beam.

The current densities obtainable from porous tungsten surfaces are plotted in

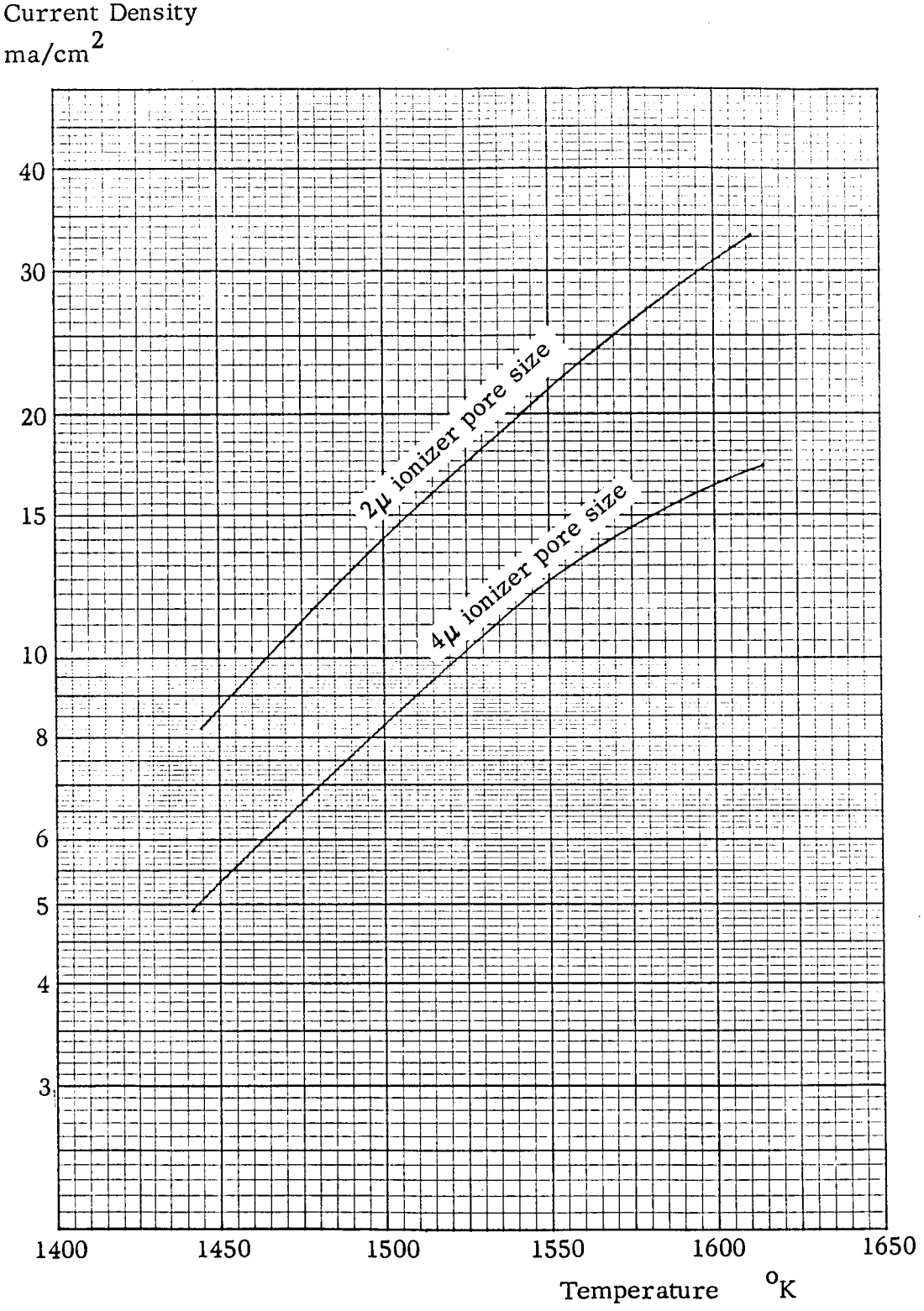

Fig. B.2 Emission Current Density vs Temperature.
(Reproduced from Fig. 25 in Ref. B.2.)

Fig. B.2 (Fig. 25 in Ref. B.2) against temperature for various pore sizes. Reference B.2 specifies 15 ma/cm^2 as a reasonable value for the Jupiter craft ion rocket design.

The current density is related to

$\xrightarrow{\text{sym def}}$ (52) n_i = the ion density

by

$\xrightarrow[\text{E-12}]{\text{E-13}}$ (53) $i_b = q_i n_i u$.

Consequently, the ion density in terms of the ion current density and specific impulse is given by

$\xrightarrow[11]{53}$ (54) $n_i = \dfrac{i_b}{q_i g I_{sp}}$;

hence,

$\xrightarrow[\text{A-4, A-10}]{54}$ (55) $n_i = 6.36 \times 10^{17} \dfrac{i_b}{I_{sp}}$ ions per m^3 .

The ion density is plotted against specific impulse for various current densities in Fig. B.3. Since the ion beam is essentially neutral, the electron density is the same as the ion density; hence the plasma resonant frequency is given by

$\xrightarrow[55]{\text{E-56}}$ (56) $f_p = 7.16 \times 10^9 \sqrt{\dfrac{i_b}{I_{sp}}}$ Hz .

For the following current densities

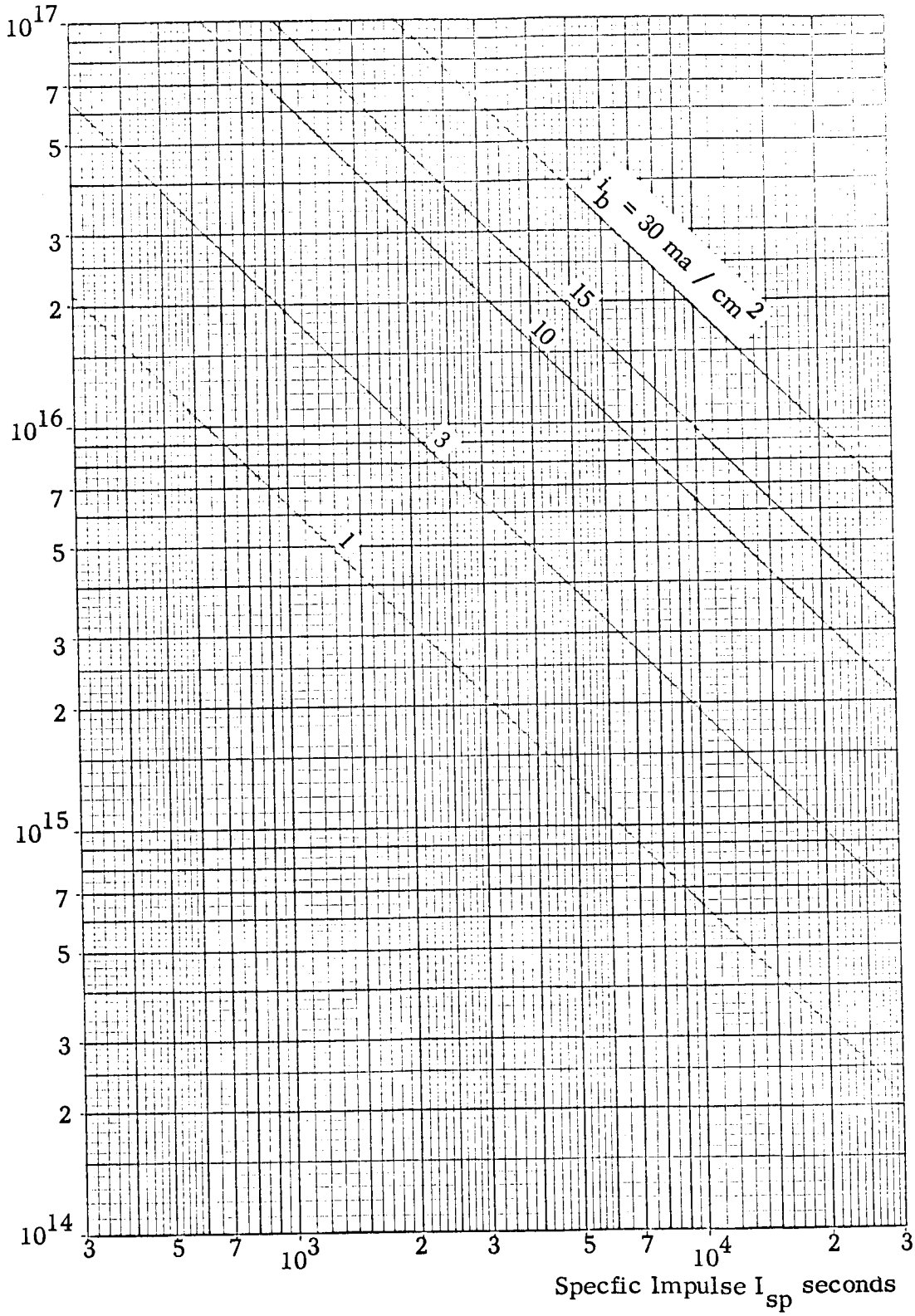

Fig. B.3 Ion density in the ion rocket exhaust beam

choice → (57)

$1\ ma = 10^{-3}\ amp$

$1\ cm^2 = 10^{-4}\ m^2$

i_b ma/cm^2	i_b amp/m^2	$\sqrt{i_b}$
1	10	3.16
3	30	5.47
10	100	10
15	150	12.25
30	300	17.32

the plasma frequency is given by

56 / 57 → (58)

$$f_p = \begin{Bmatrix} 2.27 \\ 3.92 \\ 7.17 \\ 8.77 \\ 12.4 \end{Bmatrix} \frac{10^{10}}{\sqrt{I_{sp}}} \quad \text{Hz} \quad \begin{Bmatrix} i_b\ \text{ma/cm}^2 \\ 1 \\ 3 \\ 10 \\ 15 \\ 30 \end{Bmatrix}$$

This is graphed in Fig. B.4. The two horizontal dashed lines bound the signal band of interest.

As an example of the use of Fig. B.3, consider the design values of 12,000 seconds specific impulse and 15 ma/cm^2 current density for the Jupiter orbiter spacecrapt; Fig. B.3 gives an ion density of 8×10^{15} ions per m^3 and Fig. B.4 gives a plasma frequency of 805 Mc.

As the ion exhaust beam recedes from the spacecraft, the divergence of the beam reduces the current density and, hence, the ion density. The way in which the density depends on distance is in part determined by the total size of the ion beam.

B.10 Ion Exhaust Beam Radius

The ion exhaust beam radius can be obtained from the total current, the current density and the assumed distribution over the exhaust beam cross section. Considerations here are limited to circular beams with a uniform distribution over the cross section. The emission ion current density depends on the emitter temperature and design. The ion current density downstream depends on the

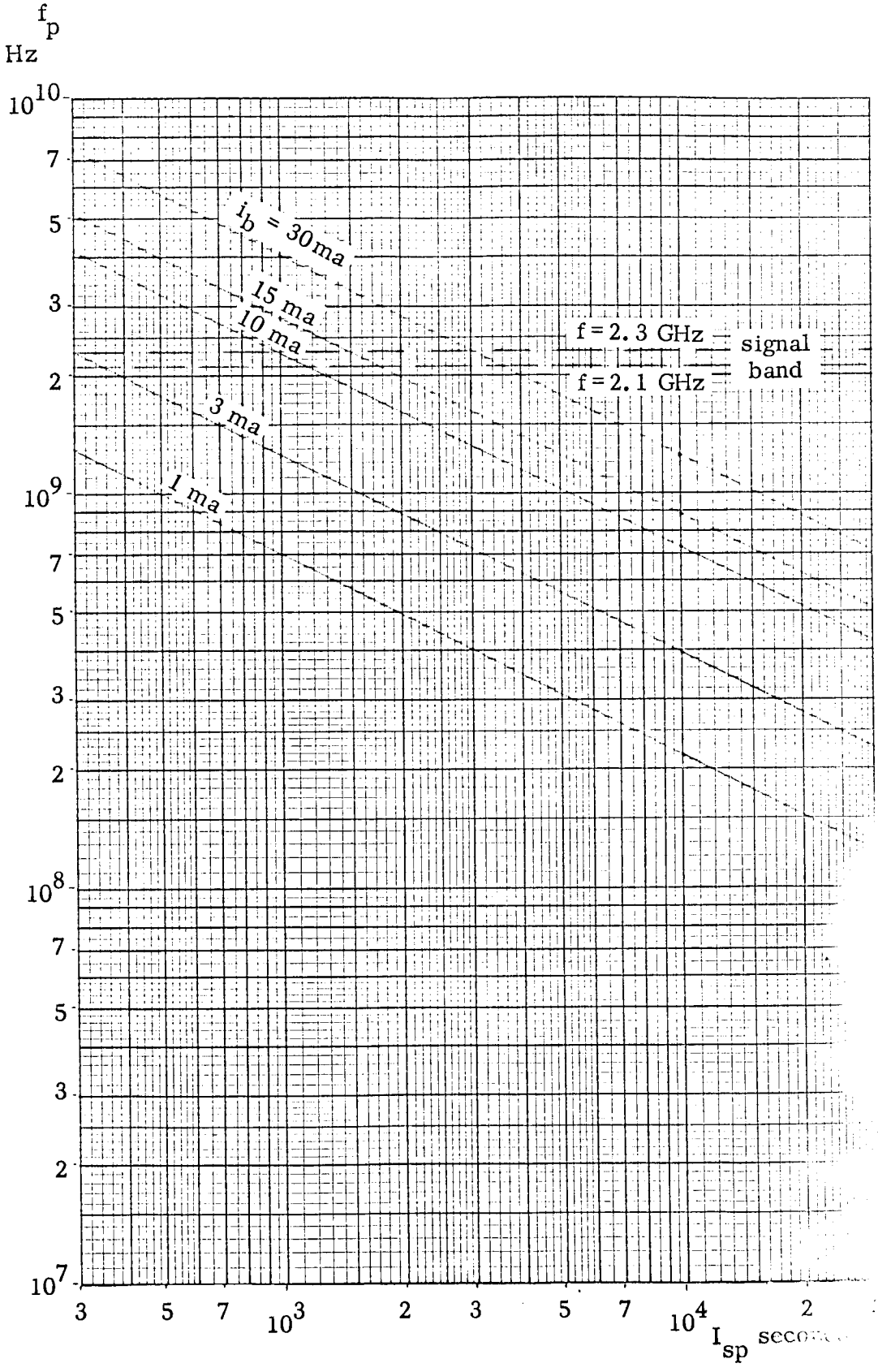

Fig. B.4 Plasma frequency in the ion exhaust beam

emission current density, the ion exhaust beam divergence angle and the ion current. In terms of

sym def → (59) A_b = the ion exhaust beam cross section area perpendicular to the axis of symmetry,

the ion exhaust beam radius is given by

geometry → (60) $b = \sqrt{\frac{A_b}{\pi}}$.

If the current density is uniform over the beam cross section, the cross section area is given by

def of i_b → (61) $A_b = \frac{I_b}{i_b}$,

hence the exhaust beam radius can be expressed by

60, 61 → (62) $b = \sqrt{\frac{I_b}{\pi i_b}}$.

It is desirable to express the ion exhaust beam radius in terms of power and specific impulse. The ion beam current can be expressed by

46 → (63) $I_b = \frac{P_b}{V_b}$

and hence by

63, 33 → (64) $I_b = \frac{2q_i P_b}{m_i g^2 I_{sp}^2}$.

The ion exhaust beam diameter can thus be expressed by

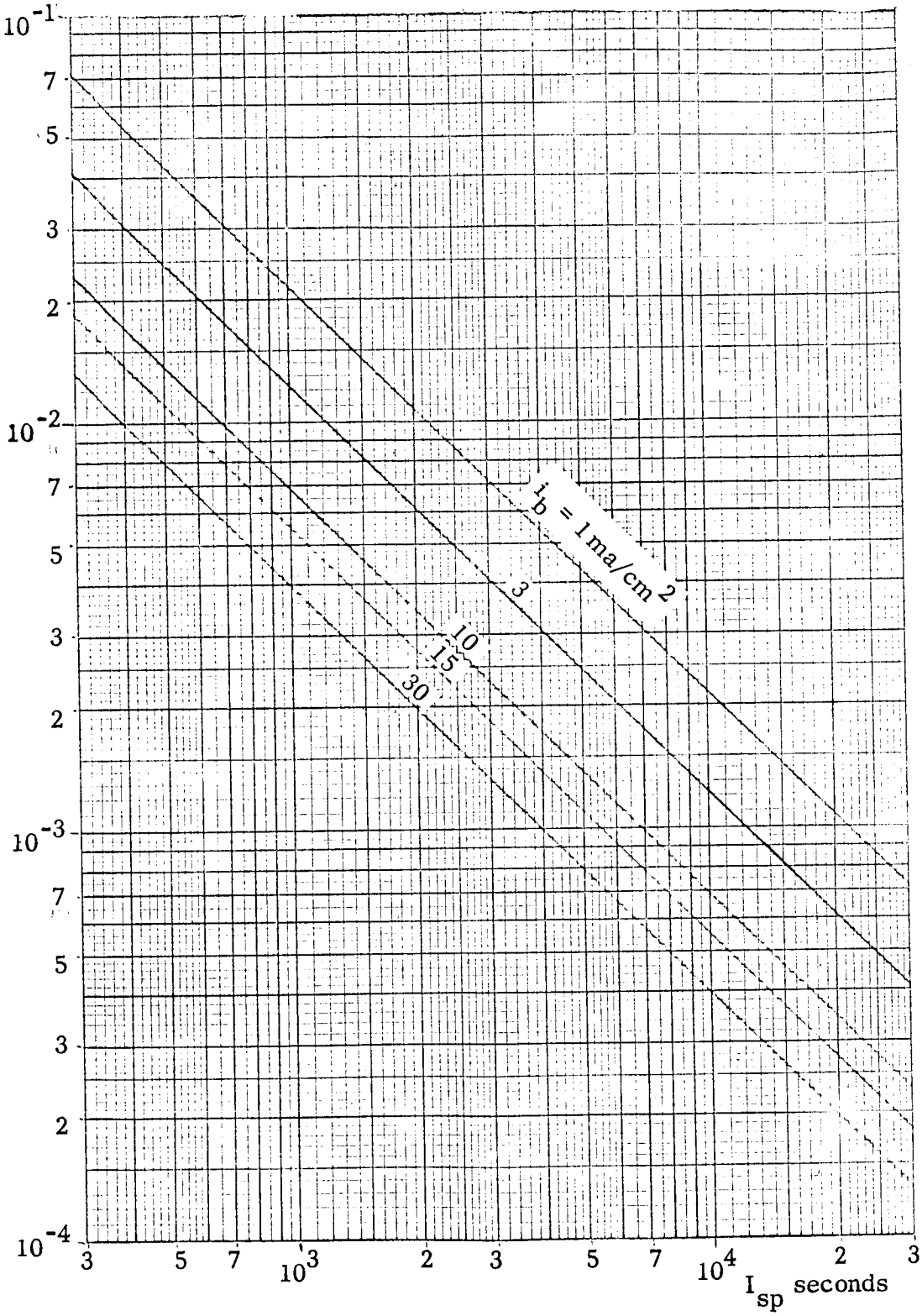

Fig. B.5 Ion rocket exhaust beam radius per $\sqrt{\text{watt}}$

$$\xrightarrow[64]{62} (65) \quad b = \frac{1}{g I_{sp}} \sqrt{\frac{2 q_i P_b}{\pi m_i i_b}} \quad .$$

Evaluating the numerical constants gives

$$\xrightarrow[34,\ A\text{-}4,\ A\text{-}10]{65} (66) \quad \frac{b}{\sqrt{P_b}} = \frac{68.0}{I_{sp} \sqrt{i_b}} \quad \text{meters per square root watt.}$$

$$\xrightarrow{66} (67) \quad \frac{b}{\sqrt{P_b}} = \begin{Bmatrix} 21.5 \\ 12.4 \\ 6.80 \\ 5.55 \\ 3.93 \end{Bmatrix} \frac{1}{I_{sp}} \quad \text{m per } \sqrt{\text{watt}} \quad \begin{Bmatrix} i_b \text{ ma/cm}^2 \\ 1 \\ 3 \\ 10 \\ 15 \\ 30 \end{Bmatrix} \quad .$$

This is graphed in Fig. B.5. With the Jupiter orbiter spacecraft as an example, entering the 15 ma/cm^2 current density curve at the absicissa value of 12,000 seconds gives the radius per square root watt of 0.46 mm. Hence the radius in the exit plane of a half megawatt ion rocket is 32.5 cm which is a diameter of 65 cm or 2.13 ft.

B.11 Variation of Ion Exhaust Beam Radius with Distance

The ion exhaust beam in this investigation is represented by a conical model with

$$\xrightarrow{\text{sym def}} (68) \quad \theta_h = \text{the half cone angle.}$$

Consequently the ion exhaust beam radius varies as

$$\xrightarrow{\text{Fig. 1.1}} (69) \quad b = z \tan \theta_h$$

where

$$\xrightarrow{\text{sym def}} (70) \quad z = \text{distance along the symmetry axis from the conical beam virtual point source.}$$

$z_r = z_d - z_r$

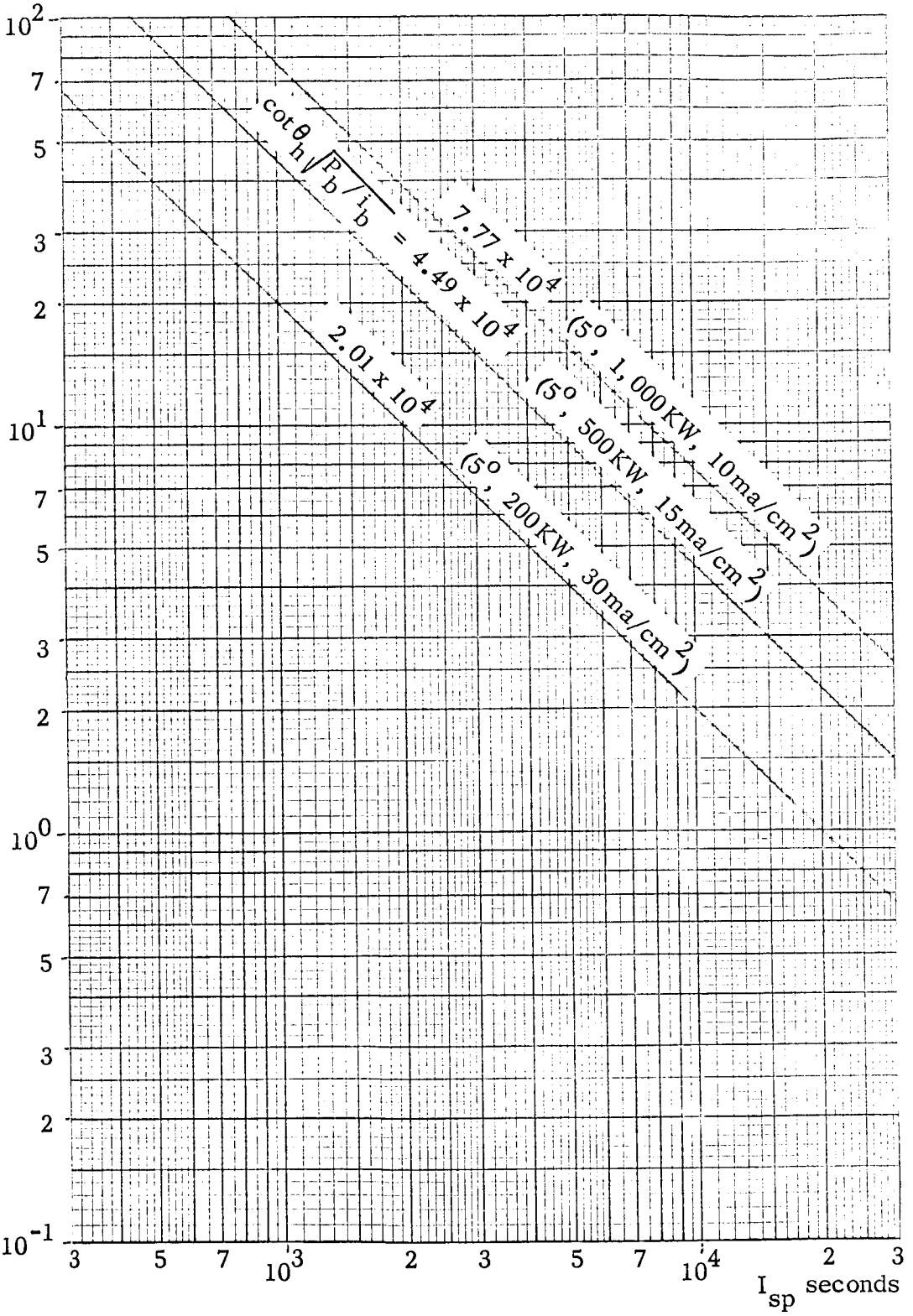

Fig. B.6 Distance over which ion exhaust beam doubles its initial value; also the distance of the virtual point source from the exit plane source.

The position of the virtual point source depends on

$\xrightarrow{\text{sym def}}$(71) b_r = the radius of the ion exhaust beam at the real source (ion rocket exit plane)

$\xrightarrow{\text{sym def}}$(72) z_r = the distance of the real source from the virtual source

and the half cone angle according to

$\xrightarrow[71,72]{69}$(73) $z_r = b_r \cot \theta_h$.

In terms of

$\xrightarrow{70,72}$(74) $z - z_r$ = the distance from the real source of the beam,

the beam radius is given by

$\xrightarrow{63}$(75) $b = \left[(z - z_r) + z_r\right] \tan \theta_h$

and hence

$\xrightarrow[73]{75}$(76) $b = b_r + (z - z_r) \tan \theta_h$.

The number of parameters involved makes it awkward to provide a generalized plot.

Some insight is provided by considering

$\xrightarrow{\text{sym def}}$(77) z_d = the distance required to double the beamwidth,

which is given by

$\xrightarrow[b = 2b_r]{76}$(78) $z_d - z_r = b_r \cot \theta_h$.

Hence

$$\xrightarrow[66]{78} (79) \quad z_d - z_r = \frac{68.0 \cot \theta_h}{I_{sp}} \sqrt{\frac{P_b}{i_{br}}} \quad .$$

For small angles this becomes

$$\xrightarrow{79} (80) \quad z_d - z_r = \frac{68.0}{\theta_h I_{sp}} \sqrt{\frac{P_b}{i_{br}}} \quad .$$

Expressing the half beam angle in degrees gives

$$\xrightarrow{80} (81) \quad z_d - z_r = \frac{3900}{\theta_h^o I_{sp}} \sqrt{\frac{P_b}{i_{br}}} \quad .$$

This is graphed in Fig. B.6. Using the Jupiter orbiter spacecraft ion engine design as an example, together with the assumption of a five degree beam half angle, gives distance of 3.75 meters for the beam to double its diameter.

B.12 Collision Frequency

In the ion exhaust beam,

$$\xrightarrow{\text{sym def}} (82) \quad \nu_e = \text{the electron collision frequency}$$

is a function of position because it is a function of the particle densities and velocities which in turn are functions of position. In terms of

$$\xrightarrow{\text{sym def}} (83) \quad \left\{ \begin{matrix} \nu_{ei} \\ \nu_{en} \\ \nu_{ee} \end{matrix} \right\} = \text{the collision frequency of electrons with} \left\{ \begin{matrix} \text{ions} \\ \text{neutrals} \\ \text{electrons} \end{matrix} \right\} ,$$

the total collision frequency is given by

$$\xrightarrow{83} (84) \quad \nu_e = \nu_{ei} + \nu_{en} + \nu_{ee}$$

In terms of

$$\xrightarrow{\text{sym def}} (85) \left\{ \begin{matrix} \langle u_{ei} \rangle \\ \langle u_{en} \rangle \\ \langle u_{ee} \rangle \end{matrix} \right\} = \text{the average relative electron speed with respect to the} \left\{ \begin{matrix} \text{ions} \\ \text{neutrals} \\ \text{electrons} \end{matrix} \right\},$$

$$\xrightarrow{\text{sym def}} (86) \left\{ \begin{matrix} \sigma_{ei} \\ \sigma_{en} \\ \sigma_{ee} \end{matrix} \right\} = \text{the electron collision cross section with respect to} \left\{ \begin{matrix} \text{ions} \\ \text{neutrals} \\ \text{electrons} \end{matrix} \right\}$$

and

$$\xrightarrow{\text{sym def}} (87) \left\{ \begin{matrix} n_i \\ n_n \\ n_e \end{matrix} \right\} = \text{the density of} \left\{ \begin{matrix} \text{ions} \\ \text{neutrals} \\ \text{electrons} \end{matrix} \right\},$$

the collision frequencies are given by

$$\xrightarrow{\text{kinetics}} (88) \left| \begin{matrix} \nu_{ei} \\ \nu_{en} \\ \nu_{ee} \end{matrix} \right| = \left| \begin{matrix} \langle u_{ei} \rangle & n_i \sigma_{ei} \\ \langle u_{en} \rangle & n_n \sigma_{en} \\ \langle u_{ee} \rangle & n_e \sigma_{ee} \end{matrix} \right| .$$

For the initial determination of attenuation, the average relative electron velocity is assumed to be independent of position. This assumption is not valid in the section of the ion exhaust beam immediately adjacent to the ion rocket engine where the neutralization process is taking place and where strong plasma oscillations are present. Consequently it may also not be true over a substantial portion of the ion exhaust beam.

The density of cesium ions is large compared to the density of neutral atoms

$$\xrightarrow[\text{condition}]{\text{operating}} (89) \quad n_i >> n_n$$

and the collision cross section of electrons with ions is large compared to that of

electrons with neutrals

interaction laws $\xrightarrow{\quad}$ (90) $\sigma_{ei} >> \sigma_{en}$.

Consequently

$\xrightarrow[89,90]{88_{1,2}}$ (91) $\nu_{en} << \nu_{ei}$,

and collision between electrons and neutrals can be neglected.

The electron-electron collision frequency is also neglected in this first approximation. The validity of this approximation needs further investigation but is essentially based on the relative collective behavior of the electrons induced by the electromagnetic wave, with respect to that of the ions. The electromagnetic wave produces a collective oscillation of the electrons with respect to the ions. The dominant collisions which tend to disrupt the electrons collective oscillations are those between the electrons and the ions rather than between the electrons. Hence the electron-electron collisions are relatively unimportant, since

collective behavior $\xrightarrow{\quad}$ (92) $\nu_{ee} << \nu_{ei}$,

from the point of view of their effectiveness in contributing to the attenuation. Consequently the total electron collision frequency is approximated adequately by

$\xrightarrow[91,92]{84}$ (93) $\nu_e = \nu_{ei}$.

The motion of the electrons with respect to the ions has both a thermal component and a drift component, each of which varies with distance from the spacecraft. The neutralization process normally injects electrons into the ion exhaust beam with a velocity relative to the spacecraft that is lower than that of the ions. The ions sub-

sequently accelerate the electrons and thereby reduce their relative drift velocity difference as their distance from the spacecraft increases. This acceleration process can also generate plasma oscillations of substantial amplitude. It is necessary to determine the amplitude of these plasma oscillations and their rate of growth and decay with distance in order to determine their contribution to u_{ei} . It also is necessary to know the way in which the electron temperature varies with the position in the ion exhaust beam to obtain the random thermal contributions to u_{ei} . Examination of these considerations are left for a later investigation.

An approximate upper bound for the average initial relative velocity of the electrons with respect to the ions is provided by the velocity of the ion beam, and a lower bound is provided by the random thermal speed of the emitted electron:

$$\xrightarrow[\text{approximation}]{\text{kinetics}} (94) \quad u_{et} \leq \langle u_{ei} \rangle \leq u_i \quad .$$

This may be used to obtain upper and lower bounds for the attenuation. If the attenuation upper bound is sufficiently small, the problem need not be pursued further.

The conventional coulomb scattering cross section between charged particles is infinite. This singularity is avoided by using

$$\xrightarrow{\text{sym def}} (95) \quad r_D = \text{the Debye radius}$$

$$\xrightarrow{\text{RB.3 (8.5)}} (96) \quad r_D = \sqrt{\frac{\epsilon_v kT}{n_e e^2}} \quad .$$

Evaluating the physical constants gives

$$\xrightarrow[\text{A-1, A-4, A-10}]{96} (97) \quad r_D = 69.0 \sqrt{\frac{T}{n_e}} \text{ meters} \quad .$$

Using the Debye radius as a cut off for the potential of the ion in order to give a finite scattering cross section, gives

$$\xrightarrow{\text{RB.3(8.17)}} (98) \quad \sigma_{ei} = A \ln 9N_D \quad ,$$

where

$$\xrightarrow{\text{sym def}} (99) \quad N_D = \text{the number of electrons in a Debye sphere,}$$

$$\xrightarrow{\text{phys def}} (100) \quad N_D = \frac{4}{3}\pi r_D^3 n_e \quad .$$

Hence

$$\xrightarrow[97]{100} (101) \quad N_D = 1.378 \times 10^6 \frac{T^{3/2}}{\sqrt{n_e}} \quad .$$

In equation (98),

$$\xrightarrow{\text{RB.3(8.17)}} (102) \quad A = \frac{1}{\pi}\left(\frac{e^2}{2\epsilon_v m_e u_{ei}^2}\right)^2 \quad m^2 \quad .$$

It is more convenient to express the energy in this equation in terms of electron volts, viz.,

$$\xrightarrow{102} (103) \quad A = \frac{1}{\pi}\left(\frac{e}{4\epsilon_v V_{ei}}\right)^2 \quad .$$

Evaluating the physical constants gives

$$\xrightarrow[\text{A-1, A-4}]{103} (104) \quad A = \frac{6.53 \times 10^{-18}}{V_{ei}^2} \quad m^2 \quad .$$

The cross section is relatively insensitive to the electron density and temperature,

as described above, since these variables only appear in the logarithm. Hence it will suffice here to compute the logarithm factor for a nominal value of temperature and electron density. Using

$$\xrightarrow{\text{Fig. B.3}} (105) \quad T = 1550^{\circ}K$$

and

$$\xrightarrow{\text{Fig. B.4}} (106) \quad n_e = 10^{16} \text{ electrons/m}^2$$

gives

$$\xrightarrow[105,106]{101} (107) \quad N_D = 841 \text{ electrons} \quad .$$

Hence

$$\xrightarrow{107} (108) \quad \ln 9N_D = 8.93$$

and

$$\xrightarrow[104,108]{98} (109) \quad \sigma_{ei} = \frac{5.83 \times 10^{-17}}{V_{ei}^2} \text{ m}^2 = \frac{5.83 \times 10^{-13}}{V_{ei}^2} \text{ cm}^2 \quad .$$

Comparison of this electron-ion cross section with the electron-neutral atom cross sections of alkali metals gives

$$\xrightarrow{109;\text{RB.4, Fig. 9}} (110) \quad \sigma_{ei} \approx 10\sigma_{en} \quad ,$$

thereby supporting (90).

It is convenient to express the speed entering the collision frequency expression in terms of the corresponding energy in electron volts relative to the ions,

$$\xrightarrow[i \rightarrow e]{32} (111) \quad u_{ei} = \sqrt{\frac{2e V_{ei}}{m_e}} \quad .$$

Evaluating the physical constants gives

$$\xrightarrow[A\text{-}4,\, A\text{-}5]{111} (112) \quad u_{ei} = 5.93 \times 10^5 \sqrt{V_{ei}} \quad \text{m/sec.} \quad .$$

Thus the collision frequency can be expressed by

$$\xrightarrow[109,\, 112]{88} (113) \quad \nu_{ei} = \frac{3.45 \times 10^{-11}}{V_{ei}^{3/2}} \, n_i \quad .$$

Since an objective of this preliminary investigation is to obtain a reasonably close upper bound for the attenuation, the largest reasonable collision frequency should be used. The largest reasonable collision frequency is obtained by using the smallest reasonable relative kinetic energy. As a first step, consider the thermal kinetic energy which is a lower bound (94). For this case, it is more convenient to express the formula in terms of temperature. Using

$$\xrightarrow{\text{kinetics}} (114) \quad eV = kT$$

gives

$$\xrightarrow[A\text{-}4,\, A\text{-}12]{114} (115) \quad V = 8.62 \times 10^{-5} \, T \quad ,$$

and hence

$$\xrightarrow[115]{113} (116) \quad \nu_{ei} = 4.31 \times 10^{-5} \, \frac{n_i}{T^{3/2}} \quad .$$

Using the nominal temperature of the contact ionization surface gives

$$\xrightarrow[105]{116} (117) \quad \nu_{ei} = 7.07 \times 10^{-10} \, n_i \quad .$$

It is interesting to note that the ratio of collision frequency to plasma resonant frequency is

$$\xrightarrow{117 \div E\text{-}56} (118) \quad \frac{\nu_{ei}}{f_p} = 7.88 \times 10^{-11} \sqrt{n_i} \quad .$$

For the Jupiter orbiter spacecraft design point, the largest ion density encountered is that at the exit plane is

$$\xrightarrow[\text{J-orbiter}]{\text{Fig. B.3}} (119) \quad n_{ir} = 8 \times 10^{15}$$

hence

$$\xrightarrow[119]{118} (120) \quad \frac{\nu_{ei}}{f_{pr}} = 7.05 \times 10^{-3} \quad .$$

In practice, the mean ejection velocity of the neutralizing electrons would not be equal to that of the ions. Even if their ejection velocities were matched to as low as one electron volt the collision frequency would be

$$\xrightarrow[V_{ei}=1]{113} (121) \quad \nu_{ei} = 3.45 \times 10^{-11} \, n_i$$

in which case

$$\xrightarrow{121 \div E\ 56} (122) \quad \frac{\nu_{ei}}{f_p} = 3.84 \times 10^{-12} \sqrt{n_i}$$

and hence

$$\xrightarrow[119]{122} (123) \quad \frac{\nu_{ei}}{f_{pr}} = 3.44 \times 10^{-4} \quad .$$

Thus the ratio of collision frequency to plasma resonance frequency varies by an order of magnitude with only a small change of conditions ($\sim$ 1 ev). For the case in which the electron exhaust velocity is not matched to that of the ions the electron temperature gradually increases with distance due to collision relaxation. The entire question of collision frequency needs to be examined in greater detail.

APPENDIX C: WAVE PROPAGATION CONCEPTS

C.1 Power Density

The manner in which

$\xrightarrow{\text{sym def}}$ (1) P = the propagating power

is distributed over a surface through which it passes or impinges upon is designated by

$\xrightarrow{\text{sym def}}$ (2) π = the power density.

The direction of propagation is designated by

$\xrightarrow{\text{sym def}}$ (3) 1_{π} = the unit vector in the propagation direction.

Thus the vector power density (Poynting's vector) is represented by

$\xrightarrow{\text{vector def}}$ (4) $\vec{\pi} = 1_{\pi}\pi$.

The power density is defined in terms of

$\xrightarrow{\text{sym def}}$ (5) dP_S = the differential power

propagating through

$\xrightarrow{\text{sym def}}$ (6) $d\$$ = a differential surface

by

---

* The arrow bookkeeping notation to the left of the equation number and other notation conventions employed are explained in Appendix A.

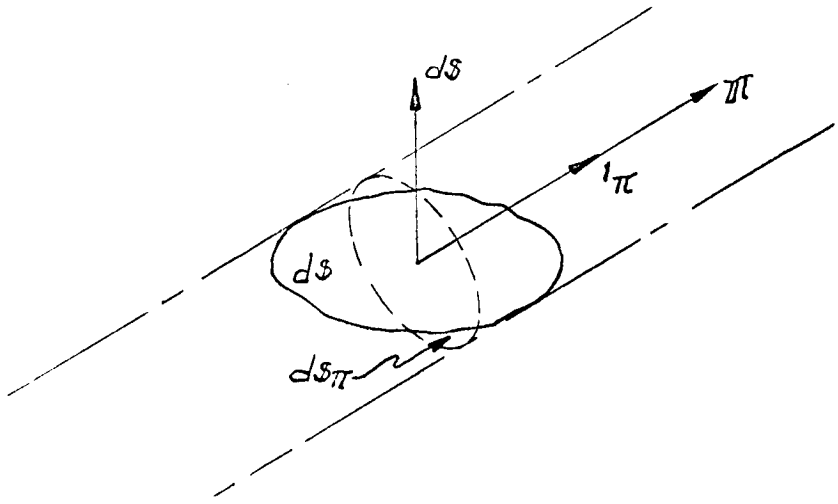

Fig. C.1 Propagation through a Differential Surface.

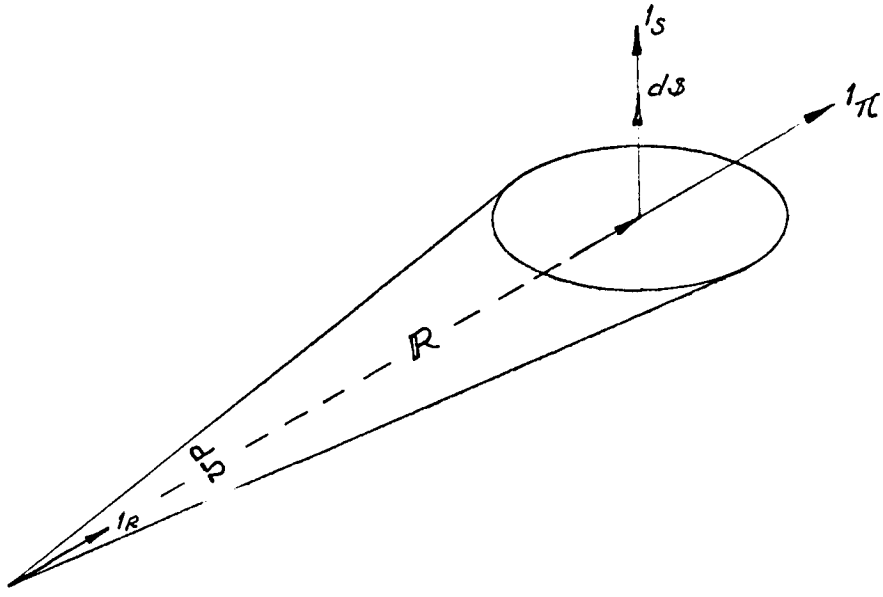

Fig. C.2 Differential Solid Angle, Capped by a Differential Surface, Bounding a Differential Power from a Point Source.

$$\xrightarrow{\text{phys def}} (7) \quad \pi = \frac{dP_S}{dS_\pi} ,$$

where

$$\xrightarrow{\text{sym def}} (8) \quad dS_\pi = \text{the component of differential surface } d\$ \text{ which the direction of propagation is normal to, depicted in Fig. C.1,}$$

i.e.

$$\xrightarrow{\text{math def}} (9) \quad dS_\pi = 1_\pi \cdot d\$.$$

The differential power through the differential surface can thus be expressed in the form,

$$\xrightarrow{7} (10) \quad dP_S = \pi dS_\pi ,$$

or

$$\xrightarrow[9/4]{10} (11) \quad dP_S = \boldsymbol{\pi} \cdot d\$.$$

C.2 Power Intensity

The manner in which the propagating power emitted from a source is distributed over a solid angle within which it propagates is designated by

$$\xrightarrow{\text{sym def}} (12) \quad p = \text{the power intensity} .$$

The vector power intensity is designated by

$$\xrightarrow[12,2]{\text{vector def}} (13) \quad \mathbb{P} = 1_\pi p .$$

The power intensity is defined in terms of

$\xrightarrow{\text{sym def}}$ (14) dP_Ω = the differential power

propagating within

$\xrightarrow{\text{sym def}}$ (15) $d\Omega$ = a differential solid angle

by

$\xrightarrow{\text{phys def}}$ (16) $p = \frac{dP_\Omega}{d\Omega}$.

The differential power within the differential solid angle can be expressed in the form

$\xrightarrow{16}$ (17) $dP_\Omega = pd\Omega$.

C.3 Relationship Between Power Intensity and Density

The relationship between power intensity and density radiated from a source can be obtained by taking the differential surface element through which the differential power is propagating, as the cap of the differential solid angle within which the differential power is propagating, as depicted in Fig. C.2. In this case,

$\xrightarrow{\text{Fig. C.2}}$ (18) $dP_S = dP_\Omega$.

Consequently,

$\xrightarrow[17, 11]{18}$ (19) $\mathcal{P} \cdot d\$ = pd\Omega$.

The differential solid angle is given in terms of

$\xrightarrow{\text{sym def}}$ (20) 1_R = the unit vector in the radial direction from the source

and

$$\xrightarrow{\text{sym def}} (21) \quad R = \text{the radial distance from the source}$$

by

$$\xrightarrow{\text{Fig. C.2}} (22) \quad d\Omega = \frac{1_R \cdot d\$}{R^2} .$$

However, the direction of propagation is the radial direction,

$$\xrightarrow{\substack{\text{source} \\ \text{location}}} (23) \quad 1_R = 1_\pi .$$

Consequently,

$$\xrightarrow[23]{22} (24) \quad d\Omega = \frac{1_\pi \cdot d\$}{R^2} .$$

Therefore,

$$\xrightarrow[24/13]{19} (25) \quad \pi \cdot d\$ = \frac{\mathbb{P} \cdot d\$}{R^2} .$$

Since the direction of the differential surface capping the differential solid angle is completely arbitrary,

$$\xrightarrow{25} (26) \quad \pi = \frac{\mathbb{P}}{R^2} .$$

C.4 Radiator Gain

An isotropic radiator distributes the power uniformly over the 4π steradian solid angle surrounding it; consequently, the power intensity issuing from an

isotropic radiator is given by

$$\xrightarrow[\text{radiator}]{\text{isotropic}} (27) \quad p = \frac{P}{4\pi} \ .$$

If the transmitted power is not uniformly distributed over the surrounding solid angle, the average radiated power intensity is

$$\xrightarrow{\text{con def}} (28) \quad \langle p \rangle = \frac{P}{4\pi} \ .$$

The dependence of the power intensity on direction,

$$\xrightarrow{\text{sym def}} (29) \quad G = \text{the radiator gain,}$$

is given by

$$\xrightarrow{\text{con def}} (30) \quad G = \frac{p}{\langle p \rangle} \ .$$

The power intensity can be expressed in terms of the power and the radiator gain function by

$$\xrightarrow[28]{30} (31) \quad p = \frac{G}{4\pi} P \ .$$

For an isotropic radiator

$$\xrightarrow{\text{isotropy}} (32) \quad \langle p \rangle = p \ ;$$

consequently, the gain is given by

$$\xrightarrow[32]{30} (33) \quad G\Big|_{\text{radiator}}^{\text{isotropic}} = 1 \ .$$

C.5 Waves

Any variable representing a physical quantity of a wave designated by

$\xrightarrow{\text{sym def}}$ (34) F = any scalar field or component of a wave

is a function

$\xrightarrow{\text{sym def}}$ (35) $\left\{ \begin{matrix} t \\ \\ \mathbf{r} \end{matrix} \right\}$ = the $\left\{ \begin{matrix} \text{time} \\ \\ \text{position vector} \end{matrix} \right\}$

and hence can be expressed in the form

$\xrightarrow{\text{causality}}$ (36) $F = F(t, \mathbf{r})$.

An elementary wave is one for which the field properties do not vary over surfaces which are orthogonal to

$\xrightarrow{\text{sym def}}$ (37) 1_β = the unit vector in the wave propagation direction.

The scalar position coordinate,

$\xrightarrow{\text{sym def}}$ (38) r_β = the distance along the normal to the wave surface,

is given in terms of the position vector and the propagation direction unit vector by

$\xrightarrow{37, 38}$ (39) $r_\beta = 1_\beta \cdot \mathbf{r}$.

Since the fields of elementary waves do not vary over the wave surface, only the normal coordinate to the wave surface need appear in the function argument,

$$\xrightarrow[\text{elementary wave}]{36} (40) \quad F = F(t, r_\beta) \quad .$$

The manner in which a spatial field distribution changes with time qualifies the field as a wave. A well defined (traveling) wave has a spatial shape which is invariant with time and whose position changes with time. A change in shape with time is called distortion. The basic wave propagation concepts are more easily defined for distrotionless waves and then generalized to waves with varying wave shapes. If the shape of the wave is preserved as it moves, the wave shape can be expressed in terms of a single coordinate,

$$\xrightarrow{\text{sym def}} (41) \quad \psi = \text{the wave phase in a coordinate reference frame synchronized with the wave.}$$

In the synchronous coordinate reference frame, the field function is just

$$\xrightarrow[\text{invariant wave shape}]{40} (42) \quad F = F(\psi) \quad .$$

If the field quantity can be expressed in this form, it represents a single wave.

C.6 Phase Factor

The wave phase is related to both the time and space coordinates by

$$\xrightarrow{\text{causality}} (43) \quad \psi = \psi(t, r_\beta) \quad .$$

For a wave moving with a constant speed, the transformation is linear, that is,

$$\xrightarrow[\text{linearity}]{43} (44) \quad \psi = \omega t - \beta r_\beta + \psi_o \quad ,$$

where the transformation coefficients ω and β represent

$$\xrightarrow{\text{con def}} (45) \quad \left\{ \begin{matrix} \omega \\ \beta \end{matrix} \right\} = \text{the phase change per unit} \left\{ \begin{matrix} \text{time} \\ \text{length} \end{matrix} \right\} .$$

The phase coordinate of an invariant waveform does not change with time or position. Consequently, the minus sign in (44) is required for a positively traveling wave since both the time and position coordinates are increasing together. A positive sign would be required to keep the phase invariant for a wave propagating in the negative direction since time is increasing and the position coordinate is decreasing. The coefficients depend on the phase coordinate units and on the wave shape.

The phase depends on the position vector and the wave surface orientation, that is,

$$\xrightarrow[39]{45} (46) \quad \psi = \omega t - \beta 1_\beta \cdot \mathbf{r} + \psi_o .$$

Hence, it is convenient to define a vector phase change per unit length whose direction is that in which the phase change takes place,

$$\xrightarrow{\text{sym def}} (47) \quad \boldsymbol{\beta} = 1_\beta \beta .$$

The phase coordinate can now be expressed by

$$\xrightarrow[47]{46} (48) \quad \psi = \omega t - \boldsymbol{\beta} \cdot \mathbf{r} + \psi_o .$$

C.7 Phase Velocity

The rate at which the phase changes with time at any arbitrarily moving point is given by

$$\xrightarrow{44} (49) \quad \frac{d\psi}{dt} = \omega - \beta \frac{dr_\beta}{dt} ,$$

where the speed of the moving point is

$$\xrightarrow{\text{kinematics}} (50) \quad u = \frac{dr_\beta}{dt} .$$

The speed of the moving point is related to the observed rate of phase change by

$$\xrightarrow[49]{50} (51) \quad u = \frac{\omega - \dot{\psi}}{\beta} .$$

The speed of a wave is the speed of the points comprising the wave. Since each point is specified by its phase, the speed of the wave is called

$$\xrightarrow{\text{sym def}} (52) \quad v = \text{the phase velocity.}$$

(Usage has established the term, phase velocity, rather than the more appropriate term, phase speed.) The phase velocity is thus the speed of a point which is synchronized with the wave,

$$\xrightarrow{\text{phys def}} (53) \quad v = u\Big|_{\dot{\psi} = 0} ,$$

since it is the speed with which the phase at that point in the wave moves. The phase speed is consequently

$$\xrightarrow[51]{53} (54) \quad v = \frac{\omega}{\beta} .$$

If the speed of each phase point is the same, the wave shape moves without distortion; otherwise, the shape of the wave changes as it propagates.

C.8 Monochromatic Waves

A monochromatic wave consists of a single frequency sinusoidal waveform for which

convention

$$\xrightarrow{\text{def}} (55) \quad 1 \text{ cycle} = 2\pi \text{ radians},$$

where

$$\xrightarrow{\text{sym def}} (56) \quad \left\{\begin{matrix} T \\ \lambda \end{matrix}\right\} = \text{a cycle in } \left\{\begin{matrix} \text{time} \\ \text{space} \end{matrix}\right\} \text{ at a fixed } \left\{\begin{matrix} \text{point in space} \\ \text{instant of time} \end{matrix}\right\} .$$

Cycles in time and space are called by special names:

$$\xrightarrow{\text{name def}} (57) \quad \left\{\begin{matrix} T \\ \\ \lambda \end{matrix}\right\} = \text{the } \left\{\begin{matrix} \text{period} \\ \\ \text{wavelength} \end{matrix}\right\} .$$

At a fixed $\left\{\begin{matrix} \text{point in space} \\ \text{instant of time} \end{matrix}\right\}$ the change in the phase variable is given by

$$\xrightarrow{44} (58) \quad \left|\begin{matrix} \Delta\psi|_{r_\beta = \text{const}} \\ \Delta\psi|_{t = \text{const}} \end{matrix}\right| = \left|\begin{matrix} \omega\Delta t \\ -\beta\Delta r_\beta \end{matrix}\right| .$$

For a one cycle of change

$$\xrightarrow[\Delta t = T,\ \Delta r_\beta = \lambda]{58} (59) \quad \left|\begin{matrix} \Delta\psi|_{r_\beta = \text{const}} \\ \Delta\psi|_{t = \text{const}} \end{matrix}\right| = \left|\begin{matrix} \omega T \\ -\beta\lambda \end{matrix}\right| ,$$

and since the phase changes by 2π radians in one cycle,

$$\xrightarrow{55} (60) \quad \left|\begin{matrix} \Delta\psi|_{r_\beta = \text{const}} \\ \Delta\psi|_{t = \text{const}} \end{matrix}\right| = \left|\begin{matrix} 2\pi \\ -2\pi \end{matrix}\right|$$

the phase coefficients and cycle values are related by

$$\xrightarrow{59=60} (61) \quad \left|\begin{matrix} 2\pi \\ 2\pi \end{matrix}\right| = \left|\begin{matrix} \omega T \\ \beta\lambda \end{matrix}\right| .$$

Consequently, the phase densities, ω and β, are related to cycle values by

$$\xrightarrow{61} (62) \quad \left|\begin{matrix}\omega \\ \\ \beta\end{matrix}\right| = 2\pi \left|\begin{matrix}\frac{1}{T} \\ \\ \frac{1}{\lambda}\end{matrix}\right| ,$$

which are usually taken as the starting definitions for

$$\xrightarrow{\text{name def}} (63) \quad \left\{\begin{matrix}\omega \\ \\ \beta\end{matrix}\right\} = \text{the} \left\{\begin{matrix}\text{angular frequency} \\ \\ \text{phase factor}\end{matrix}\right\} .$$

Closely allied quantities are

$$\xrightarrow{\text{sym def}} (64) \quad \left\{\begin{matrix}f \\ \\ n_\lambda\end{matrix}\right\} = \text{the} \left\{\begin{matrix}\text{frequency} \\ \\ \text{wave number}\end{matrix}\right\} ,$$

which are

$$\xrightarrow{\text{con def}} (65) \quad \left\{\begin{matrix}f \\ \\ n_\lambda\end{matrix}\right\} = \text{the number of cycles per unit} \left\{\begin{matrix}\text{time} \\ \\ \text{length}\end{matrix}\right\} ,$$

and hence,

$$\xrightarrow{65} (66) \quad \left|\begin{matrix}f \\ \\ n_\lambda\end{matrix}\right| = \left|\begin{matrix}\frac{1}{T} \\ \\ \frac{1}{\lambda}\end{matrix}\right| .$$

Consequently,

$$\xrightarrow[66]{62} (67) \quad \left|\begin{matrix}\omega \\ \\ \beta\end{matrix}\right| = 2\pi \left|\begin{matrix}f \\ \\ n_\lambda\end{matrix}\right| .$$

The phase velocity of a monochromatic wave in terms of frequency and wavelength,

$\xrightarrow[62_2,67_1]{54}$ (68) $v = f\lambda$,

now follows as a logical consequence of the kinematic description of wave propagation instead of as an independently postulated fact.

Since a monochromatic wave function is sinusoidal,

$\xrightarrow{42}$ (69) $F(\psi) = F_o \begin{Bmatrix} \sin \\ \cos \end{Bmatrix} \psi$,

phasor representation,

$\xrightarrow{69}$ (70) $\overset{v}{F} = F_o e^{j\psi}$,

can be used. The circumflex over the complex phasor symbol will be omitted (but understood) except where there is a possibility of an ambiguous meaning. Thus, all components of such waves can be represented in the form,

$\xrightarrow[48]{70}$ (71) $F = F_o e^{j(\omega t - \beta \cdot \mathbb{r})}$,

where the constant reference phase, ψ_o, is absorbed in the coefficient.

C.9 Attenuation

If the wave amplitude decrease with distance is proportional to its magnitude

$\xrightarrow[\text{attenuation}]{\text{simple}}$ (72) $\left(\frac{dF}{dr}\right)_\alpha = -\alpha F$

the proportionality factor is called

$\xrightarrow{\text{sym def}}$ (73) α = the attenuation factor

if

sym def → (74) r_α = the direction in which the maximum rate of decrease takes place .

With attenuation, the field components vary with distance according to the more general form,

71,72 → (75) $F = F_o e^{-\alpha r_\alpha} e^{j(\omega t - \beta \cdot r)}$.

It is convenient to introduce the vector attenuation factor,

sym def
analog 47 → (76) $\alpha = 1_\alpha \alpha$,

just as it was convenient to introduce the vector phase factor. The field component can now be more compactly expressed in the form,

75
76/78 → (77) $F = F_o e^{j(\omega t - \check{\beta} \cdot r)}$

by use of the complex phase factor,

sym def → (78) $\check{\beta} = \beta - j\alpha$.

For homogeneous waves α and β have the same direction.

For a monochromatic plane wave, all the partial differential field equations can be reduced to algebraic equations by noting that

78 → (79) $\begin{vmatrix} \partial_t \\ \nabla \end{vmatrix} \longrightarrow \begin{vmatrix} j\omega \\ -j\check{\beta} \end{vmatrix}$.

C.10 Electromagnetic Fields

The electromagnetic fields,

sym def → (80) $\begin{Bmatrix} \mathbb{E} \\ \mathbb{H} \end{Bmatrix}$ = the $\begin{Bmatrix} \text{electric} \\ \text{magnetic} \end{Bmatrix}$ field intensity

and

$$\xrightarrow{\text{sym def}} (81) \begin{Bmatrix} \mathbb{D} \\ \mathbb{B} \end{Bmatrix} = \text{the} \begin{Bmatrix} \text{electric} \\ \text{magnetic} \end{Bmatrix} \text{flux density} \quad ,$$

and the sources of these fields,

$$\xrightarrow{\text{sym def}} (82) \begin{Bmatrix} \mathbb{i} \\ \rho \end{Bmatrix} = \text{the} \begin{Bmatrix} \text{current} \\ \text{charge} \end{Bmatrix} \text{density,}$$

are interrelated by Maxwell's equations,

$$\xrightarrow{\text{Faraday, Gauss}} (83) \begin{bmatrix} \nabla\times & \partial_t \\ 0 & \nabla\cdot \end{bmatrix} \begin{bmatrix} \mathbb{E} \\ \mathbb{B} \end{bmatrix} = \begin{bmatrix} 0 \\ 0 \end{bmatrix}$$

and

$$\xrightarrow{\text{Ampere, Maxwell, Gauss}} (84) \begin{bmatrix} \nabla\times & -\partial_t \\ 0 & \nabla\cdot \end{bmatrix} \begin{bmatrix} \mathbb{H} \\ \mathbb{D} \end{bmatrix} = \begin{bmatrix} \mathbb{i} \\ \rho \end{bmatrix} ,$$

and by the constitutive parameters,

$$\xrightarrow{\text{sym def}} (85) \begin{Bmatrix} \epsilon \\ \mu \\ \sigma \end{Bmatrix} = \text{the scalar} \begin{Bmatrix} \text{capacitivity} \\ \text{inductivity} \\ \text{conductivity} \end{Bmatrix}$$

via the constitutive relations,

$$\xrightarrow{\text{isotropic constitution}} (86) \begin{bmatrix} \mathbb{D} \\ \mathbb{B} \\ \mathbb{i} \end{bmatrix} = \begin{bmatrix} \epsilon\mathbb{E} \\ \mu\mathbb{H} \\ \sigma\mathbb{E} \end{bmatrix} ,$$

for isotropic media. The charge and current densities may be subsumed in the

in the constitutive parameters.

C-11 Monochromatic Electromagnetic Waves

A single monochromatic wave solution exists only for a linear system. If the constitutive parameters representing the medium are linear (i.e., independent of the field strengths),the field partial differential equations can be reduced directly to the algebraic equations.

$$\xrightarrow[79]{83} (87) \quad \begin{vmatrix} -\check{\beta}x & \omega \\ 0 & \check{\beta}\cdot \end{vmatrix} \begin{vmatrix} \mathbb{E} \\ \mathbb{B} \end{vmatrix} = \begin{vmatrix} 0 \\ 0 \end{vmatrix}$$

and

$$\xrightarrow[79]{84} (88) \quad \begin{vmatrix} \check{\beta}x & \omega \\ 0 & \check{\beta}\cdot \end{vmatrix} \begin{vmatrix} \mathbb{H} \\ \mathbb{D} \end{vmatrix} = j \begin{vmatrix} \mathbb{J} \\ \rho \end{vmatrix}$$

Reducing the number of field variables by the constitutive relations for isotropic media and restricting considerations to neutral media,

$$\xrightarrow{\text{condition}} (89) \quad \rho = 0 \ ,$$

gives

$$\xrightarrow[87_1, 88_1]{} (90) \quad \begin{vmatrix} \check{\beta}x & -\omega\mu \\ -j(\sigma + j\omega\epsilon) & \check{\beta}x \end{vmatrix} \begin{vmatrix} \mathbb{E} \\ \mathbb{H} \end{vmatrix} = \begin{vmatrix} 0 \\ 0 \end{vmatrix}$$

and

$$\xrightarrow{87_2, 88_2} (91) \quad \check{\beta} \begin{vmatrix} \mathbb{E} \\ \\ \mathbb{H} \end{vmatrix} = \begin{vmatrix} 0 \\ \\ 0 \end{vmatrix} .$$

The vector phase factor is perpendicular to both the electric and magnetic field intensities, shown by (91). The electric and magnetic field intensities are perpendicular to each other, shown by (90). Therefore,

$$\xrightarrow{90, 91} (92)$$

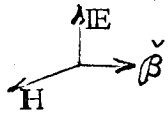

The equation for the electric field alone is

$$\xrightarrow{90} (93) \quad \check{\beta} \times (\check{\beta} \times \mathbb{E}) = j\omega\mu(\sigma + j\omega\epsilon)\,\mathbb{E} .$$

Expanding the triple cross product gives

$$\xrightarrow{93} (94) \quad (\check{\beta}\cdot\mathbb{E})\,\check{\beta} - \check{\beta}^2\,\mathbb{E} = j\omega\mu(\sigma + j\omega\epsilon)\,\mathbb{E} .$$

Since the complex phase factor is perpendicular to the electric field intensity,

$$\xrightarrow[91_1]{94} (95) \quad \left[\check{\beta}^2 + j\omega\mu(\sigma + j\omega\epsilon)\right]\mathbb{E} = 0 .$$

Since the electric field intensity is not identically zero, the complex phase factor is given by

$$\xrightarrow{95} (96) \quad \check{\beta}^2 = -j\omega\mu(\sigma + j\omega\epsilon) .$$

C.12 Phase and Attenuation Factors in a Lossy Medium

Expressing the complex phase factor in terms of the phase factor and the attenuation factor,

$$\xrightarrow[47,74]{77} (97) \quad \check{\beta} = \beta - j\alpha \quad ,$$

gives

$$\xrightarrow[97]{96} (98) \quad \beta^2 - \alpha^2 - 2j\alpha\beta = -j\omega\mu(\sigma + j\omega\epsilon).$$

Equating real and imaginary parts gives

$$\xrightarrow{\mathcal{R}\,98} (99) \quad \beta^2 - \alpha^2 = \omega^2\mu\epsilon$$

and

$$\xrightarrow{\mathcal{I}\,98} (100) \quad 2\alpha\beta = \omega\mu\sigma \quad .$$

Separating variables,

$$\xrightarrow{100} (101) \quad \alpha = \frac{\omega\mu\sigma}{2\beta} \quad ,$$

gives

$$\xrightarrow[101]{99} (102) \quad \beta^4 - \omega\mu\epsilon\beta^2 - \frac{1}{4}\omega^2\mu^2\sigma^2 = 0 \quad .$$

Consequently,

$$\xrightarrow{102} (103) \quad \beta^2 = \frac{\omega^2\mu\epsilon \pm \sqrt{\omega^4\mu^2\epsilon^2 + \omega^2\mu^2\sigma^2}}{2} \quad .$$

A more convenient form is

$$\xrightarrow{103} (104) \quad \beta^2 = \omega^2\mu\epsilon\,\frac{1 \pm \sqrt{1 + \dfrac{\sigma^2}{\omega^2\epsilon^2}}}{2} \quad .$$

Since β is a real quantity, β^2 must be a positive quantity; consequently, the minus sign is extraneous; hence,

$$\xrightarrow[\text{- extraneous}]{104} (105) \quad \beta^2 = \omega^2\mu\epsilon \frac{1+\sqrt{1+\frac{\sigma^2}{\omega^2\epsilon^2}}}{2} \quad .$$

Hence,

$$\xrightarrow{105} (106) \quad \beta = \pm \omega\sqrt{\frac{\mu\epsilon}{2}} \sqrt{1+\sqrt{1+\frac{\sigma^2}{\omega^2\epsilon^2}}} \quad .$$

The plus sign is for positively traveling waves and the minus sign for negatively traveling waves. The attenuation is given by

$$\xrightarrow[106]{101} (107) \quad \alpha = \pm \sigma\sqrt{\frac{\mu}{2\epsilon}} \frac{1}{\sqrt{1+\sqrt{1+\frac{\sigma^2}{\omega^2\epsilon^2}}}}$$

The attenuation may also be expressed in the form

$$\xrightarrow{107} (108) \quad \alpha = \pm \omega\sqrt{\frac{\mu\epsilon}{2}} \sqrt{-1+\sqrt{1+\frac{\sigma^2}{\omega^2\epsilon^2}}} \quad .$$

The phase velocity is given by

$$\xrightarrow[106]{54} (109) \quad v = \pm \frac{1}{\sqrt{\frac{\mu\epsilon}{2}} \sqrt{1+\sqrt{1+\frac{\sigma^2}{\omega^2\epsilon^2}}}}$$

$$= \pm \frac{\omega}{\sigma}\sqrt{\frac{2\epsilon}{\mu}} \sqrt{-1+\sqrt{1+\frac{\sigma^2}{\omega^2\epsilon^2}}} \quad .$$

From here on, the $\pm$ signs will be dropped, but it will be understood that a + sign is used for a positively traveling wave and a - sign for a negatively traveling wave.

An important approximation can be made when the displacement current is large compared to the conduction current, which is the case if the frequency is sufficiently high or the conductivity sufficiently low,

$$i_D^2 >> i_C^2 \xrightarrow{\quad} (110) \quad \sigma^2 << \omega^2\epsilon^2 \quad .$$

If this condition holds, an accurate approximation for the phase factor, attenuation factor and phase speed is obtained by the first terms in

$$\xrightarrow{R2(5.3)} (111) \quad \sqrt{1 + \frac{\sigma^2}{\omega^2\epsilon^2}} = 1 + \frac{\sigma^2}{2\omega^2\epsilon^2} - \frac{1}{8}\left(\frac{\sigma^2}{\omega^2\epsilon^2}\right)^2 + \cdots$$

Thus,

$$\xrightarrow[111]{106} (112) \quad \beta = \omega\sqrt{\mu\epsilon}\sqrt{1 + \frac{\sigma^2}{4\omega^2\epsilon^2}} \quad ,$$

$$\xrightarrow[110]{108} (113) \quad \alpha = \frac{\sigma}{2}\sqrt{\frac{\mu}{\epsilon}}\sqrt{1 - \frac{\sigma^2}{4\omega^2\epsilon^2}} \quad ,$$

and

$$\xrightarrow{109} (114) \quad v = \frac{1}{\sqrt{\mu\epsilon}\sqrt{1 + \frac{\sigma^2}{4\omega^2\epsilon^2}}} \quad .$$

The same current density inequality allows the approximations to be simplified to

$$\xrightarrow{112} (115) \quad \beta = \omega\sqrt{\mu\epsilon}\left[1 + \frac{\sigma^2}{8\omega^2\epsilon^2}\right] \quad ,$$

$$\xrightarrow{113} (116) \quad \alpha = \frac{\sigma}{2}\sqrt{\frac{\mu}{\epsilon}}\left[1 - \frac{\sigma^2}{8\omega^2\epsilon^2}\right] \quad ,$$

and

$$\xrightarrow{114} (117) \quad v = \frac{1}{\sqrt{\mu\epsilon}}\left[1 - \frac{\sigma^2}{8\omega^2\epsilon^2}\right] ,$$

and still further simplified to

$$\xrightarrow{115} (118) \quad \beta = \omega\sqrt{\mu\epsilon} ,$$

$$\xrightarrow{116} (119) \quad \alpha = \frac{\sigma}{2}\sqrt{\frac{\mu}{\epsilon}} ,$$

and

$$\xrightarrow{117} (120) \quad v = \frac{1}{\sqrt{\mu\epsilon}} .$$

The phase velocity of an electromagnetic wave in vacuum is represented by a special symbol,

$$\xrightarrow{\text{sym def}} (121) \quad c = v\Big|_{\text{vacuum}} = v_v = \text{the speed of light in vacuum.}$$

Using the subscript v to designate a quantity in vacuum gives

$$\xrightarrow{54, 121} (122) \quad c = \frac{\omega}{\beta_v}$$

and

$$\xrightarrow{120, 121} (123) \quad c = \frac{1}{\sqrt{\mu_v\epsilon_v}}$$

and

$$\xrightarrow[121]{68} (124) \quad c = f\lambda_v .$$

Normalizing the phase velocity with respect to the vacuum value gives

$$\xrightarrow{120 \div 123} (125) \quad \frac{v}{c} = \sqrt{\frac{\mu_v \epsilon_v}{\mu \epsilon}} \ .$$

It is convenient to introduce

$$\xrightarrow{\text{sym def}} (126) \quad \left\{ \begin{matrix} \epsilon_r \\ \mu_r \end{matrix} \right\} = \text{the relative} \left\{ \begin{matrix} \text{capacitivity} \\ \text{inductivity} \end{matrix} \right\} = \left\{ \begin{matrix} \text{dielectric constant} \\ \text{permeability} \end{matrix} \right\}$$

which are

$$\xrightarrow{\text{con def}} (127) \quad \left| \begin{matrix} \epsilon_r \\ \mu_r \end{matrix} \right| = \left| \begin{matrix} \epsilon/\epsilon_v \\ \mu/\mu_v \end{matrix} \right| \ .$$

The wave phase speed in terms of its vacuum value, is given by

$$\xrightarrow[127]{125} (128) \quad v = \frac{c}{\sqrt{\mu_r \epsilon_r}} \ .$$

Convenient formula are

$$\xrightarrow[128]{120} (129) \quad \sqrt{\mu \epsilon} = \frac{1}{c} \sqrt{\mu_r \epsilon_r}$$

and

$$\xrightarrow[129/122]{118} (130) \quad \beta = \beta_v \sqrt{\mu_r \epsilon_r} \ .$$

C.13 Characteristic Impedance

An important property of the medium in which a monochromatic wave is propagating is

$$\xrightarrow{\text{sym def}} (131) \quad \mathbb{Z} = \text{the characteristic impedance} \ ,$$

which is defined similarly to circuit impedance by

$$\xrightarrow{\text{con def}} (132) \quad \mathbb{Z} = \frac{E}{H} \quad .$$

For a plane monochromatic wave,

$$\xrightarrow{90} (133) \quad \mathbb{Z} = \frac{\omega\mu}{\check{\beta}} = \frac{\check{\beta}}{\omega\epsilon - j\sigma} \quad .$$

Using

$$\xrightarrow{96} (134) \quad \beta = \sqrt{-j\omega\mu(\sigma + j\omega\epsilon)}$$

gives

$$\xrightarrow[134]{133} (135) \quad \mathbb{Z} = \sqrt{\frac{j\omega\mu}{\sigma + j\omega\epsilon}} \quad .$$

For conduction currents which are small compared to displacement currents, it is more convenient to reexpress the complex phase factor and the characteristic impedance in the form,

$$\xrightarrow{134} (136) \quad \check{\beta} = \omega\sqrt{\mu\epsilon}\sqrt{1 - j\frac{\sigma}{\omega\epsilon}}$$

and

$$\xrightarrow{135} (137) \quad \mathbb{Z} = \sqrt{\frac{\mu}{\epsilon}} \frac{1}{\sqrt{1 - j\frac{\sigma}{\omega\epsilon}}} \quad .$$

If the conduction current is sufficiently smaller than the displacement current, all but the first two terms in the expansion of the reciprocal square root can be neglected to give

$$\xrightarrow{137} (138) \quad \mathbb{Z} = \sqrt{\frac{\mu}{\epsilon}} \left[1 + j\frac{\sigma}{2\omega\epsilon}\right] .$$

For a lossless medium, the characteristic impedance reduces to

$$\xrightarrow[\sigma = 0]{135} (139) \quad \mathbb{Z} = \sqrt{\frac{\mu}{\epsilon}} .$$

APPENDIX D: REFRACTION AND REFLECTION

D.1 Introduction

The ray theory of propagation provides a sufficiently accurate description of a wide variety of propagation phenomena. This combined with its simplicity makes it a handy tool for the investigation of various devices and natural phenomena. The objective of this section is to provide a collation of concepts and formulae needed for ray theory analysis.

D.2 Snell's Law

The normal to the interface between two materials and a ray passing obliquely through the interface all lie in a single plane. Snell's law relates the angles

$$\xrightarrow{\text{sym def}^*}(1)\quad \left\{\begin{matrix}\theta_1\\ \theta_2\end{matrix}\right\} = \text{the angle between interface normal and ray in region } \left\{\begin{matrix}1\\ 2\end{matrix}\right\}$$

via

$$\xrightarrow{\text{Snell's Law}}(2)\quad n_1 \sin\theta_1 = n_2 \sin\theta_2 ,$$

where the coefficients multiplying the sine function are called

$$\xrightarrow{\text{sym def}}(3)\quad \left\{\begin{matrix}n_1\\ n_2\end{matrix}\right\} = \text{refractive index of material in region } \left\{\begin{matrix}1\\ 2\end{matrix}\right\} .$$

Ray bending at an interface is depicted in Fig. D.1,

---

* The arrow bookkeeping notation to the left of the equation number and other specialized notation is explained in Appendix A.

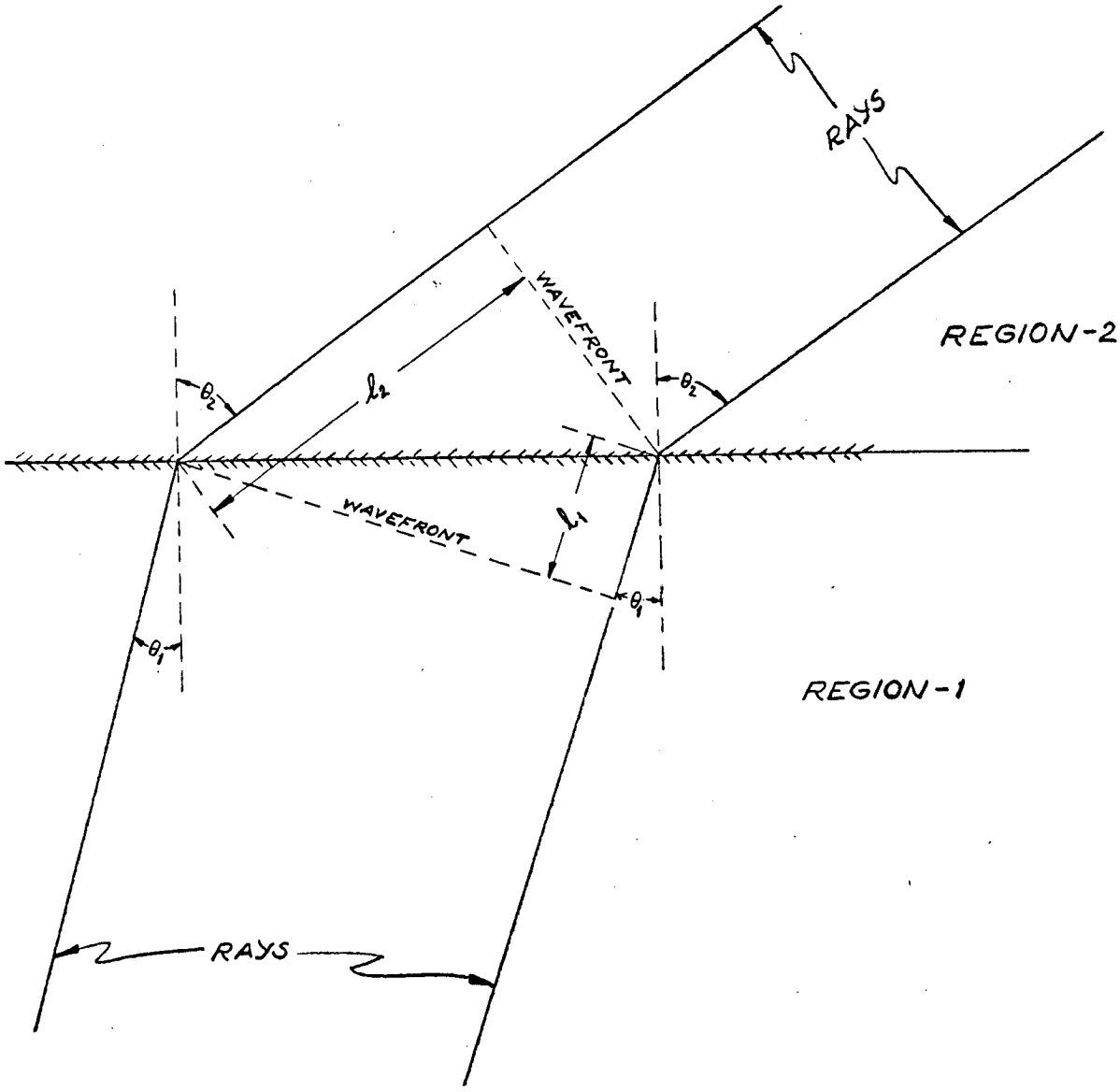

Fig. D.1 Ray Bending at an Interface

Snell's law gives the ratio of the refractive indices,

$$\xrightarrow{2} (4) \quad \frac{n_2}{n_1} = \frac{\sin\theta_1}{\sin\theta_2} \quad .$$

In particular, if a ray passes through an interface between any material and vacuum, then

$$\xrightarrow{4} (5) \quad \frac{n_m}{n_v} = \frac{\sin\theta_v}{\sin\theta_m} \quad ,$$

where

$$\xrightarrow{\text{sym def}} (6) \quad \left\{ \begin{matrix} \theta_m \\ \\ \theta_v \end{matrix} \right\} = \text{angle between interface normal and ray in} \left\{ \begin{matrix} \text{material} \\ \\ \text{vacuum} \end{matrix} \right\}$$

and

$$\xrightarrow{\text{sym def}} (7) \quad \left\{ \begin{matrix} n_m \\ \\ n_v \end{matrix} \right\} = \text{refractive index of} \left\{ \begin{matrix} \text{material} \\ \\ \text{vacuum} \end{matrix} \right\} \quad .$$

By the arbitrary definition of the refractive index of vacuum as unity,

$$\xrightarrow{\text{reference def}} (8) \quad n_v = 1 \, ,$$

the relative refractive index of the material with respect to vacuum becomes the refractive index of the material; thus, the refractive index of a material is given by

$$\xrightarrow[8]{5} (9) \quad n_m = \frac{\sin\theta_v}{\sin\theta_m} \quad .$$

If only a single material is involved, the subscript on the refractive index can be omitted without ambiguity.

Snell's law given above is independent of the direction in which the rays pass through the interface. The literature frequently designates which part of a ray is the incident portion and which part is the refracted portion and thereby makes the detailed expression of Snell's law dependent on the direction of propagation. Designating

$$\xrightarrow{\text{sym def}}(10)\quad \begin{Bmatrix} i \\ \\ r \end{Bmatrix} = \text{the angle between interface normal and} \begin{Bmatrix} \text{incident} \\ \\ \text{refracted} \end{Bmatrix} \text{ray}$$

gives for a ray passing from a material into vacuum

$$\xrightarrow[\text{mat}\longrightarrow\text{vac}]{10}(11)\quad \left[\begin{matrix} \theta_m \\ \\ \theta_v \end{matrix}\right. = \left[\begin{matrix} i \\ \\ r \end{matrix}\right. .$$

In this case, Snell's law is

$$\xrightarrow[\text{mat}\longrightarrow\text{vac}]{9/11}(12)\quad n = \frac{\sin r}{\sin i} .$$

On the other hand, for a ray passing from vacuum into a material,

$$\xrightarrow[\text{vac}\longrightarrow\text{mat}]{10}(13)\quad \left[\begin{matrix} \theta_m \\ \\ \theta_v \end{matrix}\right. = \left[\begin{matrix} r \\ \\ i \end{matrix}\right. .$$

In this case, Snell's law is

$$\xrightarrow[\text{vac}\longrightarrow\text{mat}]{9/13}(14)\quad \frac{1}{n} = \frac{\sin r}{\sin i} .$$

D.3 Refractive Index in Terms of Wave Speeds

The refractive index can be expressed in terms of the phase speed of the wave.

Let

$\xrightarrow{\text{sym def}}$(15) T = time required for the wavefront to propagate between the two positions depicted in Fig. D.1

and

$\xrightarrow{\text{sym def}}$(16) $\left\{\begin{matrix} v_1 \\ v_2 \end{matrix}\right\}$ = the wave phase speed in region $\left\{\begin{matrix} 1 \\ 2 \end{matrix}\right\}$

and

$\xrightarrow{\text{sym def Fig. D.1}}$(17) $\left\{\begin{matrix} \ell_1 \\ \ell_2 \end{matrix}\right\}$ = the distance traversed by the wavefront $\left\{\begin{matrix} \text{right} \\ \text{left} \end{matrix}\right\}$ end.

These distances are related to the speeds and transit time by

kinematics, Fig. D.1 $\xrightarrow{\quad}$(18) $\begin{vmatrix} \ell_1 \\ \ell_2 \end{vmatrix} = T \begin{vmatrix} v_1 \\ v_2 \end{vmatrix}$

and are related to each other by

Fig. D.1 $\xrightarrow{\quad}$(19) $\dfrac{\ell_2}{\sin \theta_2} = \dfrac{\ell_1}{\sin \theta_1}$.

Consequently, the ray angles and phase speeds are related by

$\xrightarrow[18]{19}$(20) $\dfrac{\sin \theta_1}{\sin \theta_2} = \dfrac{v_1}{v_2}$.

The refractive indices in terms of wave speeds is consequently given by

$$\xrightarrow[20]{4} (21) \quad \frac{n_2}{n_1} = \frac{v_1}{v_2} \quad .$$

Specializing one region to vacuum

$$\xrightarrow{\text{reg.1} \leftrightarrow \text{vac}} (22) \quad v_1 = c$$

and dropping the subscript on the other give the refractive index in terms of the phase speeds,

$$\xrightarrow[22,8]{21} (23) \quad n = \frac{c}{v} \quad .$$

The refractive index can also be expressed in terms of

$$\xrightarrow{\text{sym def}} (24) \quad \left\{ \begin{matrix} \lambda \\ \\ \lambda_v \end{matrix} \right\} = \text{the wave length in the} \left\{ \begin{matrix} \text{material} \\ \\ \text{vacuum} \end{matrix} \right\}$$

by means of

$$\xrightarrow{22,C\text{-}68} (25) \quad \left| \begin{matrix} \lambda \\ \\ \lambda_v \end{matrix} \right| = \frac{1}{f} \left| \begin{matrix} v \\ \\ c \end{matrix} \right| \quad .$$

Thus,

$$\xrightarrow[25]{23} (26) \quad n = \frac{\lambda_v}{\lambda} \quad .$$

The refractive index can be expressed in terms of the phase factors by

$$\xrightarrow{C\text{-}61_2} (27) \quad \left| \begin{matrix} \beta \\ \\ \beta_v \end{matrix} \right| = 2\pi \left| \begin{matrix} 1/\lambda \\ \\ 1/\lambda_v \end{matrix} \right| \quad .$$

Thus,

$$\xrightarrow[27]{26} (28) \quad n = \frac{\beta}{\beta_v} \quad .$$

D.4 Refractive Index in Terms of Constitutive Parameters

In the previous section the refractive index was expressed in terms of electromagnetic field state variables. However, in linear media, the refractive index is a constitutive parameter that depends only on the medium properties and not on the strength of the wave propagating in the medium. Since the phase speed depends on the constitutive parameters,

$$\xrightarrow{\text{sym def}} (29) \quad \begin{Bmatrix} \epsilon \\ \mu \\ \sigma \end{Bmatrix} = \begin{Bmatrix} \text{capacitivity} \\ \text{inductivity} \\ \text{conductivity} \end{Bmatrix}$$

according to

$$\xrightarrow[C\text{-}129]{C\text{-}109} (30) \quad v = \frac{c}{\sqrt{1+\sqrt{1+\dfrac{\sigma^2}{\omega^2\epsilon^2}}}} \sqrt{\frac{2}{\mu_r\epsilon_r}} \quad ,$$

the index of refraction is given by

$$\xrightarrow[30]{23} (31) \quad n = \sqrt{\frac{\mu_r\epsilon_r}{2}} \sqrt{1+\sqrt{1+\frac{\sigma^2}{\omega^2\epsilon^2}}} \quad .$$

For the case of small conductivity, the phase speed is

$$\xrightarrow[C\text{-}129]{C\text{-}117} (32) \quad v = \frac{c}{\sqrt{\mu_r\epsilon_r}} \left[1 - \frac{\sigma^2}{8\omega^2\epsilon^2}\right] \quad ,$$

and hence,

$$\xrightarrow[32]{23} (33) \quad n = \sqrt{\mu_r\epsilon_r} \left[1 + \frac{\sigma^2}{8\omega^2\epsilon^2}\right] \quad .$$

If the losses can be neglected completely,

$$\xrightarrow{33} (34) \quad n = \sqrt{\mu_r \epsilon_r} \quad .$$

D. 5 Absorption Index

The lossy nature of a substance causes the field intensity to decrease exponentially according to

$$\xrightarrow{C\text{-}75} (35) \quad F = F_o e^{-\alpha x} \quad ,$$

where

$$\xrightarrow{\text{sym def}} (36) \quad \alpha = \text{the attenuation factor.}$$

The corresponding normalized factor giving the attenuation on a per free space radian basis,

$$\xrightarrow{\text{phys def}} (37) \quad \varkappa = \frac{\alpha}{2\pi/\lambda_v} \quad ,$$

is called

$$\xrightarrow{\text{sym def}} (38) \quad \varkappa = \text{the absorption index} \quad .$$

This is more compactly given by

$$\xrightarrow[27_2]{37} (39) \quad \varkappa = \frac{\alpha}{\beta_v} \quad .$$

Expressing the attenuation factor in terms of the constitutive parameters gives

$$\xrightarrow[C\text{-}129, C\text{-}122]{C\text{-}108} (40) \quad \alpha = \beta_v \sqrt{\frac{\mu_r \epsilon_r}{2}} \sqrt{-1 + \sqrt{1 + \frac{\sigma^2}{\omega^2 \epsilon^2}}} \quad .$$

Consequently, the absorption index in terms of the constitutive parameters is given by

$$\xrightarrow[40]{39} (41) \quad \varkappa = \sqrt{\frac{\mu_r \epsilon_r}{2}} \sqrt{-1 + \sqrt{1 + \frac{\sigma^2}{\omega^2 \epsilon^2}}} \quad .$$

For the case of small conductivity,

$$\xrightarrow{C\text{-}119} (42) \quad \alpha = \frac{\sigma}{2}\sqrt{\frac{\mu}{\epsilon}} \quad .$$

Consequently,

$$\xrightarrow[C\text{-}118/C\text{-}127]{39} (43) \quad \varkappa = \frac{\sigma}{2\omega\epsilon_v}\sqrt{\frac{\mu_r}{\epsilon_r}} \quad .$$

D.6 The Complex Refractive Index

The complex refractive index is the same generalization of the refractive index as the complex phase factor is of the phase factor; consequently,

$$\xrightarrow{28} (44) \quad \breve{n} = \frac{\breve{\beta}}{\beta_v} \quad .$$

Expressing the complex phase factor in terms of the phase factor and attenuation factor,

$$\xrightarrow{C\text{-}97} (45) \quad \breve{\beta} = \beta - j\alpha \quad ,$$

gives

$$\xrightarrow[45]{44} (46) \quad \breve{n} = \frac{\beta}{\beta_v} - j\frac{\alpha}{\beta_v} \quad .$$

In terms of the refractive and absorption indices,

$$\xrightarrow[28,39]{46} (47) \quad \breve{n} = n - j\varkappa \quad .$$

The complex refractive index in terms of the constitutive parameters is given by

$$n = \sqrt{\mu_r \epsilon_r}\sqrt{1 - j\frac{\sigma}{\omega\epsilon}} \quad (42)$$

44
C-118, C-122
C-136

D.7 Fresnel Equations

The electric and magnetic fields in the refracted, reflected, and incident rays on the two sides of an interface are related by the interface boundary conditions. Relatively simple relationships between the field components can be obtained by resolving an arbitrarily polarized incident wave into two orthogonally polarized waves:

phys def (49) { E / H } - wave = wave with polarization plane { parallel / perpendicular } to ray plane

where

geom def (50) { ray / polarization } plane = plane which is parallel to the ray and { interface normal / electric field } .

A large number of entities enter the following considerations. A number of superscripts and subscripts are utilized with a substantial mnemonic content to minimize the strain on the memory. The following table summarizes the usage

sym def → (51)

SYMBOL	SYMBOL POSITION		
	BODY	SUPERSCRIPT	SUBSCRIPT
E	electric field intensity	an E-wave	for an electric field
H	magnetic field intensity	an H-wave	for a magnetic field
i	angle of incidence		for the medium containing the incident ray, or for the incident ray
r	angle of refraction		for the medium containing the refracted ray, or for the refracted ray
R			for the reflected ray

If the permeability of the media on both sides of the interface are the same, the electric fields for the E-wave are related by

Fresnel → (52)
$$\begin{vmatrix} E_r^E \\ \\ E_R^E \end{vmatrix} = E_i^E \begin{vmatrix} \dfrac{2 \sin r \cos i}{\sin(i+r)\cos(i-r)} \\ \\ \dfrac{\tan(i-r)}{\tan(i+r)} \end{vmatrix} ,$$

and the electric fields for H-wave are related by

Fresnel → (53)
$$\begin{vmatrix} E_r^H \\ \\ E_R^H \end{vmatrix} = \frac{E_i^H}{\sin(i+r)} \begin{vmatrix} 2 \sin r \cos i \\ \\ -\sin(i-r) \end{vmatrix} .$$

The magnetic fields can be obtained from the electric fields by using

con def → (54) $\mathcal{Z} = \dfrac{E}{H}$,

which in terms of the constitutive parameter is given by

C = 134
C = 135
C = 136
→ (55)
$$\mathcal{Z} = \sqrt{\frac{\mu}{\epsilon}} \begin{cases} \left[1 - j\dfrac{\sigma}{\omega\epsilon}\right]^{-\frac{1}{2}} & \text{any loss} \\ \left[1 + j\dfrac{\sigma}{2\omega\epsilon}\right] & \text{low loss} \\ 1 & \text{no loss} \end{cases} .$$

Analysing reflection and refraction phenomena is facilitated by using normalized ratios called reflection and transmission coefficients, which are dependent only (for linear media) on the properties of the media at the interface and on the ray direction. These coefficients are designated by

$$\xrightarrow{\text{sym def}} (56) \quad \left\{ \begin{matrix} \Gamma \\ \\ T \end{matrix} \right\} = \left\{ \begin{matrix} \text{reflection} \\ \\ \text{transmission} \end{matrix} \right\} \text{ coefficients .}$$

There are many varieties of such coefficients. These are described in the following sections.

D.8 Field Intensity Transmission and Reflection Coefficients

The electric field intensity reflection and transmission coefficients are given by

$$\xrightarrow{\text{con def}} (57) \quad \left| \begin{matrix} \Gamma_E \\ \\ T_E \end{matrix} \right| = \frac{1}{E_i} \left| \begin{matrix} E_R \\ \\ E_r \end{matrix} \right| .$$

The magnetic field intensity reflection and transmission coefficients are given by

$$\xrightarrow{\text{con def}} (58) \quad \left| \begin{matrix} \Gamma_H \\ \\ T_E \end{matrix} \right| = \frac{1}{H_i} \left| \begin{matrix} E_R \\ \\ H_r \end{matrix} \right| .$$

The reflection and transmission coefficients are different for E-waves and H-waves; this is designated by the appropriate superscripts. For E-waves,

$$\xrightarrow[52]{57} (59) \quad \left| \begin{matrix} \Gamma_E^E \\ \\ T_E^E \end{matrix} \right| = \left| \begin{matrix} \dfrac{\tan(i-r)}{\tan(i+r)} \\ \\ \dfrac{2 \sin r \cos i}{\sin(i+r)\cos(i-r)} \end{matrix} \right| ,$$

and for H-waves,

$$\xrightarrow[53]{58} (60) \quad \begin{vmatrix} \Gamma_E^H \\ T_E^H \end{vmatrix} = \frac{1}{\sin(i+r)} \begin{vmatrix} -\sin(i-r) \\ 2 \sin r \cos i \end{vmatrix} .$$

The magnetic field reflection and transmission coefficients in terms of the electric fields are given by

$$\xrightarrow[54]{58} (61) \quad \begin{vmatrix} \Gamma_H \\ T_H \end{vmatrix} = \frac{Z_i}{E_i} \begin{vmatrix} E_R Z_i^{-1} \\ E_r \mathbb{Z}_r^{-1} \end{vmatrix} .$$

Consequently,

$$\xrightarrow[57,53]{61} (62) \quad \begin{vmatrix} \Gamma_H \\ T_H \end{vmatrix} = \begin{vmatrix} \Gamma_E \\ T_E \frac{\mathbb{Z}_i}{\mathbb{Z}_r} \end{vmatrix} .$$

If the losses are sufficiently low,

$$\xrightarrow{55} (63) \quad \frac{Z_i}{Z_r} = \sqrt{\frac{\mu_i \epsilon_r}{\epsilon_i \mu_r}}$$

and

$$\xrightarrow{34} (64) \quad \frac{n_r}{n_i} = \sqrt{\frac{\mu_r \epsilon_r}{\epsilon_i \mu_i}} .$$

For most cases of the interest, the permeabilities are the same in both regions; hence,

$$\xrightarrow[\mu_i = \mu_r]{63,64} (65) \quad \frac{\mathbb{Z}_i}{\mathbb{Z}_r} = \frac{n_r}{n_i} .$$

The relationship between the electric field and magnetic field transmission coefficients for this can thus be expressed by

$$\xrightarrow[65]{62} (66) \quad T_H = \frac{n_r}{n_i} T_E \ .$$

Using the relative refractive index expressed in terms of the ray angles,

$$\xrightarrow[\theta_1 = i, \theta_2 = r]{4} (67) \quad \frac{n_r}{n_i} = \frac{\sin i}{\sin r} \ ,$$

gives

$$\xrightarrow[67]{66} (68) \quad T_H = \frac{\sin i}{\sin r} T_E \ .$$

Consequently, the magnetic field transmission coefficients for both types of plane polarized waves are given by

$$\xrightarrow[59_2, 60_2]{68} (69) \quad \begin{vmatrix} T_H^E \\ T_H^H \end{vmatrix} = \frac{\sin 2i}{\sin(i+r)} \begin{vmatrix} \frac{1}{\cos(i-r)} \\ 1 \end{vmatrix} \ .$$

D.9 Power Density Transmission and Reflection Coefficients

The reflection and transmission coefficients for

$$\xrightarrow{\text{sym def}} (70) \quad \pi = \text{the power density (Poynting vector magnitude),}$$

which for elementary plane waves is given by

$$\xrightarrow{\text{phys def}} (71) \quad \pi = EH \ ,$$

are defined by

$$\xrightarrow{\text{con def}} (72) \quad \begin{vmatrix} \Gamma_\pi \\ T_\pi \end{vmatrix} = \frac{1}{\pi_i} \begin{vmatrix} \pi_R \\ \pi_r \end{vmatrix} \ .$$

Consequently, the power density coefficients are simply related to the field intensity coefficients. Using

$$\xrightarrow[71]{72} (73) \quad \begin{vmatrix} \overline{\Gamma_\pi} \\ \\ T_\pi \end{vmatrix} = \frac{1}{E_i H_i} \begin{vmatrix} \overline{E_R H_R} \\ \\ E_r H_r \end{vmatrix}$$

gives

$$\xrightarrow[57,58]{73} (74) \quad \begin{vmatrix} \overline{\Gamma_\pi} \\ \\ T_\pi \end{vmatrix} = \begin{vmatrix} \overline{\Gamma_E \Gamma_H} \\ \\ T_E T_H \end{vmatrix} .$$

The power density coefficients can be put in the alternate forms,

$$\xrightarrow[62]{74} (75) \quad \begin{vmatrix} \overline{\Gamma_\pi} \\ \\ T_\pi \end{vmatrix} = \begin{vmatrix} \overline{\Gamma_E^2} \\ \\ \frac{Z_i}{Z_r} T_E^2 \end{vmatrix} ,$$

or for the special case $\mu_r = \mu_i$,

$$\xrightarrow[66 \text{ or } 68]{75_2} (76) \quad T_\pi = \frac{n_r}{n_i} T_E^2 = \frac{\sin i}{\sin r} T_E^2 .$$

D.10 Power Transmission and Reflection Coefficients

The reflection and transmission coefficients for

$$\xrightarrow{\text{sym def}} (77) \quad P = \text{the power in a beam}$$

are given by

$$\xrightarrow{\text{con def}} (78) \quad \begin{vmatrix} \overline{\Gamma_P} \\ \\ T_P \end{vmatrix} = \frac{1}{P_i} \begin{vmatrix} \overline{P_R} \\ \\ P_r \end{vmatrix}$$

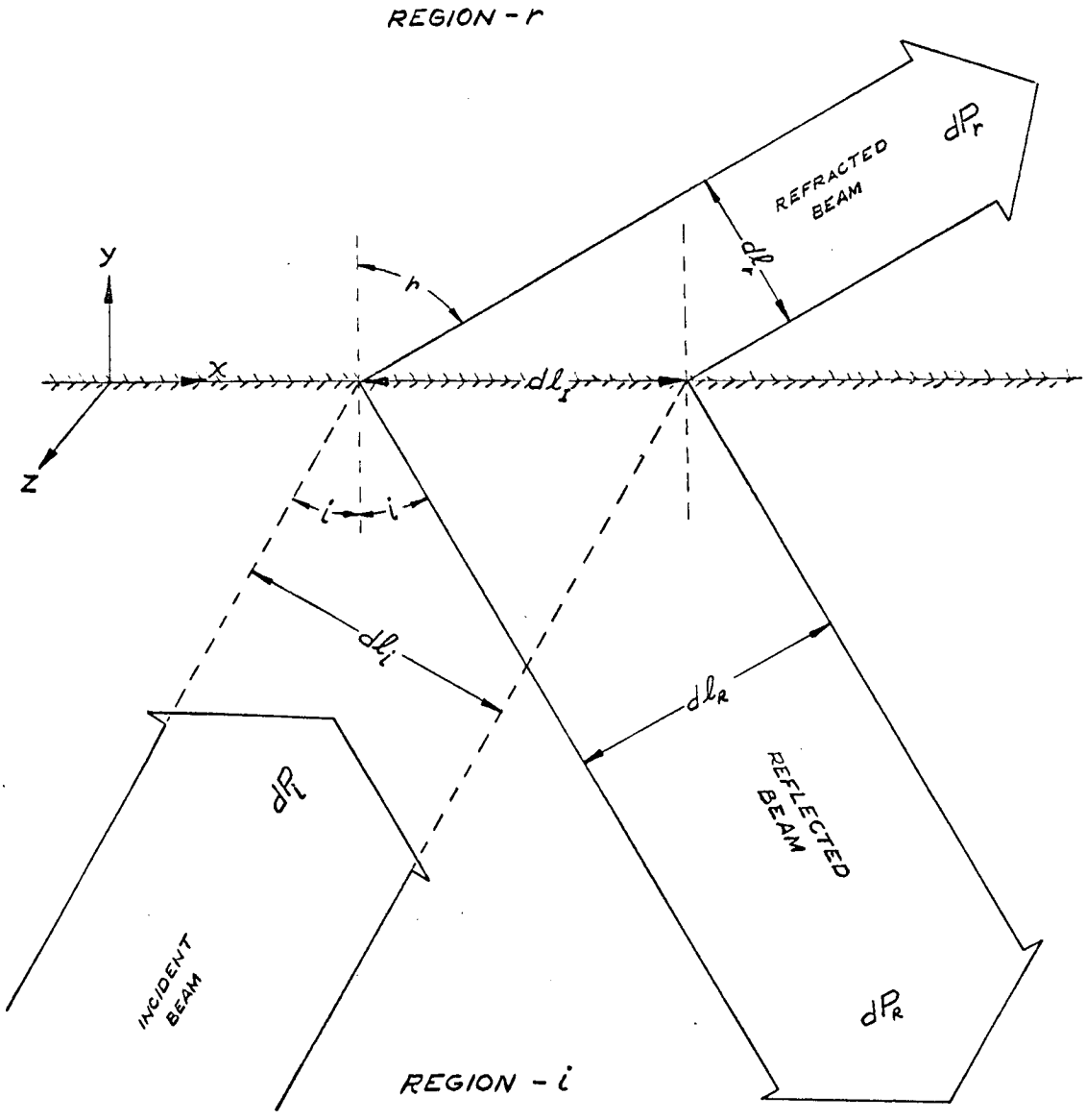

Fig. D. 2 Reflection and Refraction at an Interface.

for the case in which the interface conditions are uniform over the beam cross section. The reflection and transmission coefficients are properties of the interface structure which may vary with position; hence, the definitions should be made in terms of

$\xrightarrow{\text{sym def}}$ (79) dP = the differential power in an electromagnetic beam of differential cross section area.

For this case,

$$\xrightarrow{\text{con def}} (80) \quad \begin{vmatrix} \Gamma_P \\ T_P \end{vmatrix} = \frac{1}{dP_i} \begin{vmatrix} dP_R \\ dP_r \end{vmatrix},$$

where the differential beams are as depicted in Fig. D.2.

The power coefficients are directly related to the power density coefficients. Using

$$\xrightarrow{\text{Fig. D.2}} (81) \quad \begin{vmatrix} dP_i \\ dP_R \\ dP_r \end{vmatrix} = \begin{vmatrix} \pi_i d\ell_i \\ \pi_R d\ell_R \\ \pi_r d\ell_r \end{vmatrix} dz$$

gives

$$\xrightarrow[81]{80} (82) \quad \begin{vmatrix} \Gamma_P \\ T_P \end{vmatrix} = \frac{1}{\pi_i d\ell_i} \begin{vmatrix} \pi_R d\ell_R \\ \pi_r d\ell_r \end{vmatrix}.$$

Using the expressions relating the differential lengths,

$$\xrightarrow{\text{Fig. D.2}} (83) \quad \begin{vmatrix} d\ell_i \\ d\ell_R \\ d\ell_r \end{vmatrix} = d\ell_s \begin{vmatrix} \cos i \\ \cos i \\ \cos r \end{vmatrix},$$

gives the power reflection and transmission coefficients in terms of the power density reflection and transmission coefficients,

$$\xrightarrow[72,83]{82} (84) \quad \begin{vmatrix} \Gamma_P \\ T_P \end{vmatrix} = \begin{vmatrix} \Gamma_\pi \\ \frac{\cos r}{\cos i}\, T_\pi \end{vmatrix} .$$

Hence, the power reflection and transmission coefficients in terms of the electric field reflection and transmission coefficients are given by

$$\xrightarrow[75]{84} (85) \quad \begin{vmatrix} \Gamma_P \\ T_P \end{vmatrix} = \begin{vmatrix} \Gamma_E^2 \\ \frac{Z_i \cos r}{Z_r \cos i}\, T_E^2 \end{vmatrix} .$$

For the $\mu_i = \mu_r$ case,

$$\xrightarrow[76]{84_2} (86) \quad T_P = \frac{\tan i}{\tan r}\, T_E^2 .$$

Expressing this in terms of the sine angles gives

$$\xrightarrow{86} (87) \quad T_P = \frac{\sin i}{\sin r} \sqrt{\frac{1 - \sin^2 r}{1 - \sin^2 i}}\, T_E^2 .$$

Expressing this in terms of the refractive indices gives

$$\xrightarrow[4,\ r \leftrightarrow 2]{87\ \ i \leftrightarrow 1} (88) \quad T_P = \sqrt{\frac{n_r^2 n_i^{-2} - \sin^2 i}{1 - \sin^2 i}}\, T_E^2 .$$

The power transmission curves are graphed in Fig. D.3 for H-waves and in Fig. D.4 for E-waves. These curves have several interesting features:

1. For incidence angles less than but not too close to the critical angle the transmission factors vary relatively little with incidence angle.
   As the incidence angle closely approaches the critical angle the power transmission factor rapidly drops to zero.
2. The transmission factor decreases monotonically with increasing incidence

angle for H-waves; whereas for E-waves the transmission factor first increases with the incidence angle until it reaches a maximum of unity and thereafter monotonically decreases with incidence angle. Consequently, if it is desired transmit as large a fraction of the electromagnetic wave as possible, the E-wave polarization should be employed.

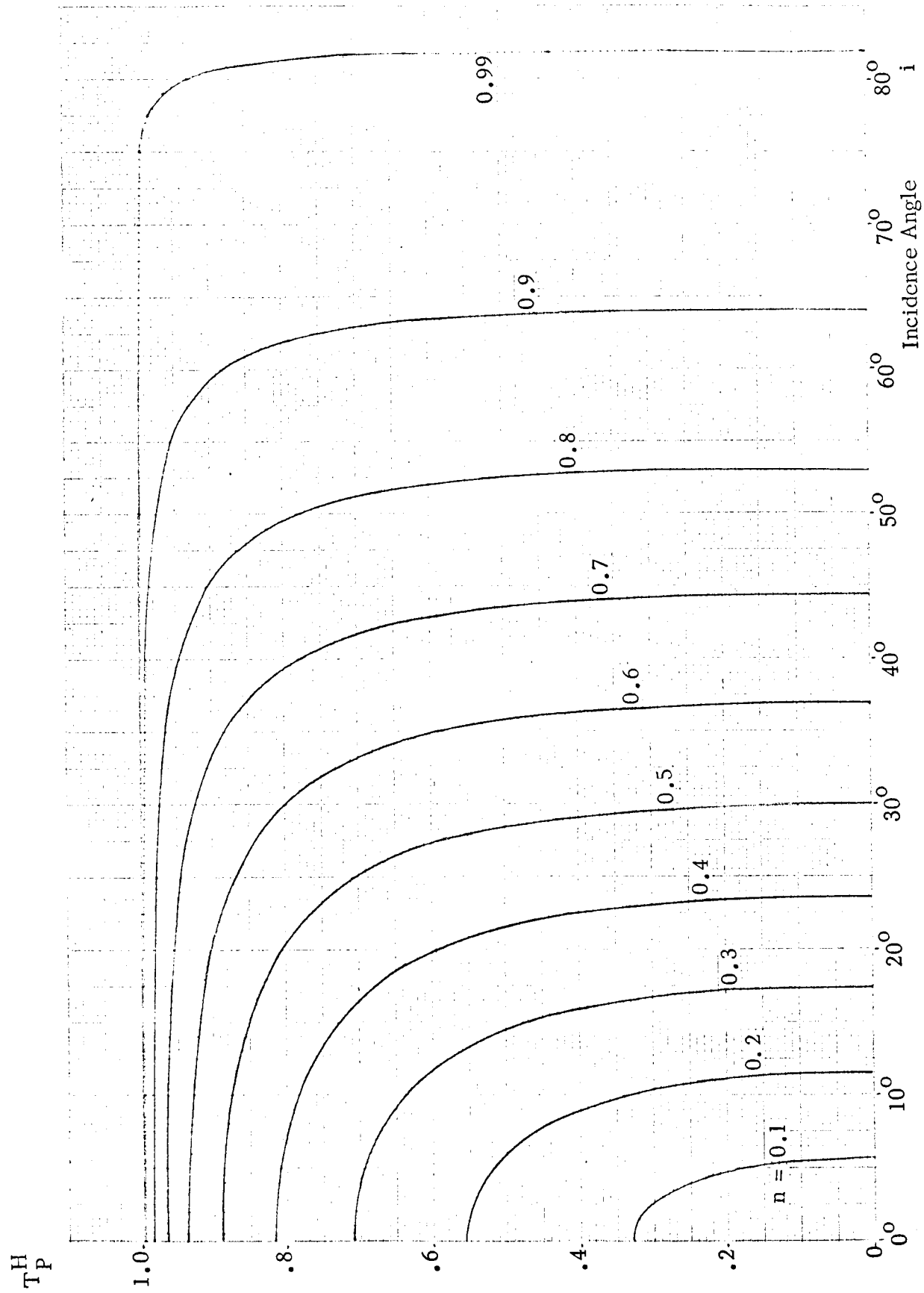

Fig. D.3 Power transmission coefficient versus incidence angle for TE polarization (H-waves)

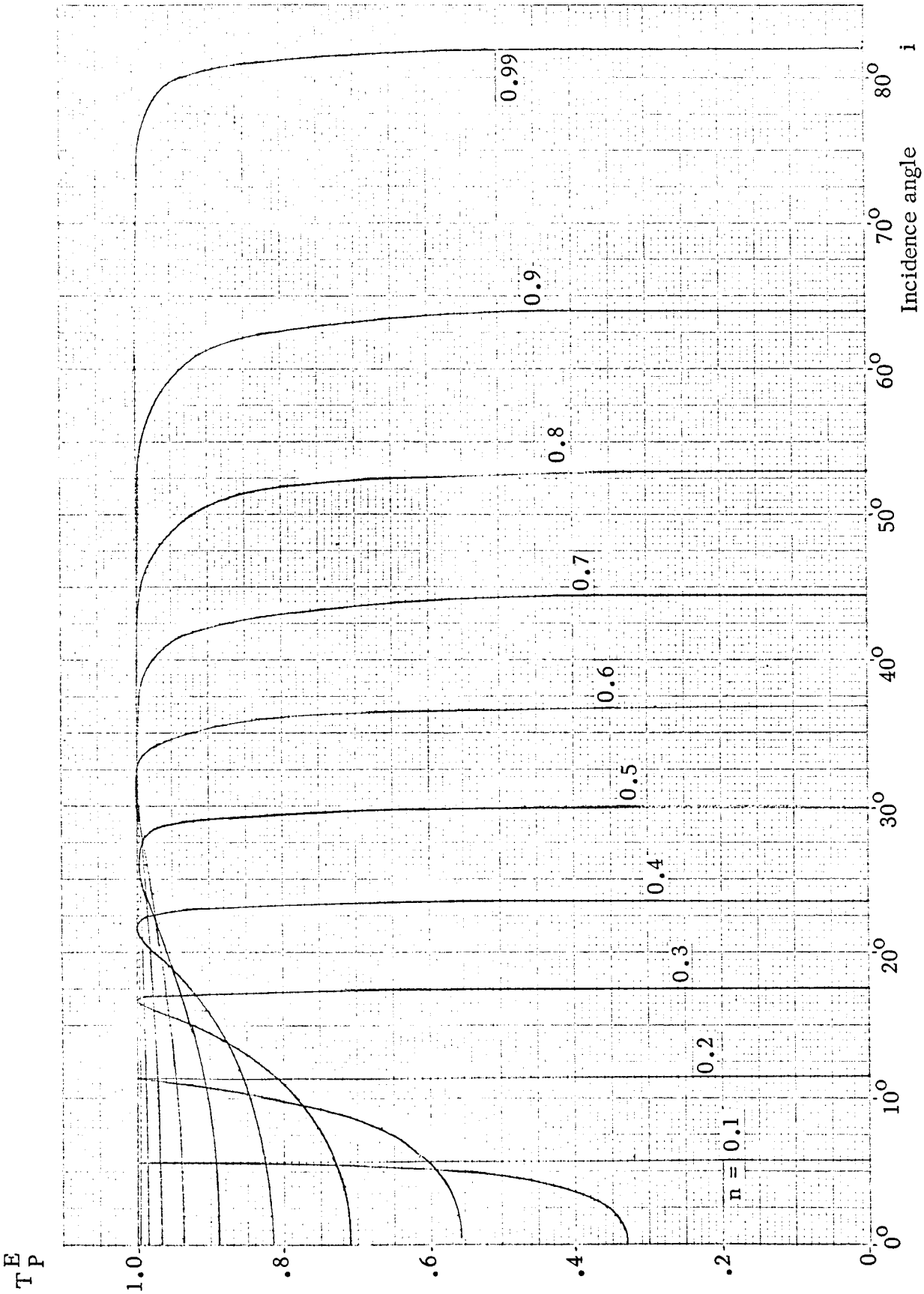

Fig. D.4 Power transmission coefficient versus incidence angle for TM polarization (E-waves)

APPENDIX E: PROPAGATION IN A PLASMA

E.1 Introduction

The basic concepts of propagation were treated in Appendix C. The effect of the charges were subsumed in the constitutive parameters and the propagation formulae were given in terms of the constitutive parameters. If the charged particle densities and their collision frequencies are specified instead of the constitutive parameters, it is generally more convenient to have the propagation formulae in terms of the particle densities and collision frequencies, or at least have the constitutive parameters expressed in terms of these quantities

E.2 Field Equations

A plasma is an aggregate of charges in free space. Consequently the constitutive parameters for free space,

$$\xrightarrow[\text{A-1, A-2}]{\text{sym def, vacuum}} (1) \quad \begin{vmatrix} \epsilon \\ \mu \\ \sigma \end{vmatrix} = \begin{vmatrix} \epsilon_v \\ \mu_v \\ 0 \end{vmatrix} = \begin{vmatrix} 8.855 \times 10^{-12} \text{ farad/m} \\ 4\pi \times 10^{-7} \text{ henries/m} \\ 0 \end{vmatrix} \approx \begin{vmatrix} \frac{1}{36\pi} \times 10^{-9} \text{ f/m} \\ 1.257 \times 10^{-6} \text{ h/m} \\ 0 \end{vmatrix},$$

must be used in the field equations. The constitutive equations for free space reduce to

$$\xrightarrow[1]{\text{C-86}} (2) \quad \begin{vmatrix} \mathbb{D} \\ \mathbb{B} \end{vmatrix} = \begin{vmatrix} \epsilon_v \mathbb{E} \\ \mu_v \mathbb{H} \end{vmatrix}.$$

The description of phenomena in terms of the constituent particles in a vacuum requires that the charge and current densities be the total charge and current densities since there is no subsumption of these in the vacuum constitutive parameters.

The field sources must now be specified on the basis of individual species,

$$\xrightarrow{\text{sym def}} (3) \quad \begin{Bmatrix} \vec{i}_s \\ \rho_s \end{Bmatrix} = \text{the species-s} \begin{Bmatrix} \text{current} \\ \text{charge} \end{Bmatrix} \text{density} \quad ,$$

in order to facilitate the analytic derivation. The total field source densities are

$$\xrightarrow{\text{superposition}} (4) \quad \begin{vmatrix} \vec{i} \\ \rho \end{vmatrix} = \sum_s \begin{vmatrix} \vec{i}_s \\ \rho_s \end{vmatrix}$$

Maxwell's equations can now be expressed in the form

$$\xrightarrow[2_2]{\text{C-83}} (5) \quad \begin{vmatrix} \nabla \times & \mu_v \partial_t \\ 0 & \nabla \cdot \end{vmatrix} \begin{vmatrix} \mathbb{E} \\ \mathbb{H} \end{vmatrix} = \begin{vmatrix} 0 \\ 0 \end{vmatrix}$$

and

$$\xrightarrow[2_1, 4]{\text{C-84}} (6) \quad \begin{vmatrix} \epsilon_v \nabla & 0 \\ -\epsilon_v \partial_t & \nabla \times \end{vmatrix} \begin{vmatrix} \mathbb{E} \\ \mathbb{H} \end{vmatrix} = \sum_s \begin{vmatrix} \rho_s \\ \vec{i}_s \end{vmatrix}$$

E.3 Field Sources

The particles comprising a species are defined by their characteristics and behavior

$$\xrightarrow{\text{sym def}} (7) \quad \begin{Bmatrix} m_s \\ q_s \\ u_s \\ n_s \\ \nu_s \end{Bmatrix} = \text{the species-s particle} \begin{Bmatrix} \text{mass} \\ \text{charge} \\ \text{velocity} \\ \text{density} \\ \text{collision frequency} \end{Bmatrix}$$

Formulation of a meaningful number density requires the formulation of

$\xrightarrow{\text{sym def}}$ (8) Λ_s = an intermediate size volume element

that satisfies the double inequality

$\xrightarrow[\text{requirements}]{\text{macro-density}}$ (9) spacing between neighboring particles $\ll$ dimensions of Λ_s $\ll$ wavelength and structural dimensions .

A meaningful number density is then given in terms of

$\xrightarrow{\text{sym def}}$ (10) N_s = the number of species-s particles in Λ_s

by

$\xrightarrow{\text{phys def}}$ (11) $n_s = \dfrac{N_s}{\Lambda_s}$

This type of density is called a macro-density. If the intermediate size volume dimensions are smaller than the average spacing between nearest neighbor particles but larger than the size of the particles themselves, then the density fluctuates between zero and the value corresponding to one particle (occasionally several particles) depending on whether or not a particle (or several particles) is in the volume. If the volume dimensions become smaller, the fluctuations become larger. In the limit, as the dimensions go to zero, the density fluctuates between zero and infinity. This type of density, micro-density, is not useful in the development of continuum analysis for an aggregate of discrete particles.

The charge density for each species is given by

$\xrightarrow{\text{phys def}}$ (12) $\rho_s = q_s n_s$,

and the current density for each species is given by

$$\xrightarrow{\text{phys def}} (13) \quad \vec{i}_s = \rho_s \vec{u}_s \ .$$

There are two species of interest,

$$\xrightarrow{\text{symm def}} (14) \quad \begin{Bmatrix} e \\ i \end{Bmatrix} \text{ for } \begin{Bmatrix} \text{electrons} \\ \text{ions} \end{Bmatrix}$$

if there is only one type of heavy ion. Consequently

$$\xrightarrow{4, 14} (15) \quad \begin{vmatrix} \rho \\ \vec{i} \end{vmatrix} = \begin{vmatrix} \rho_i + \rho_e \\ \vec{i}_i + \vec{i}_e \end{vmatrix} \ .$$

Since

$$\xrightarrow{\text{phys def}} (16) \quad \begin{vmatrix} q_e \\ q_i \end{vmatrix} = \begin{vmatrix} -e \\ e \end{vmatrix}$$

the source densities are given by

$$\xrightarrow[12, 13, 16]{15} (17) \quad \begin{vmatrix} \rho \\ \vec{i} \end{vmatrix} = \begin{vmatrix} n_i - n_e \\ n_i \vec{u}_i - n_e \vec{u}_e \end{vmatrix} \ .$$

In a neutral plasma,

$$\xrightarrow{\text{neutrality}} (18) \quad n_i = n_e \ ,$$

and hence the source densities reduce to

$$\xrightarrow[18]{17} (19) \quad \begin{vmatrix} \rho \\ \vec{i} \end{vmatrix} = n_e e \begin{vmatrix} 0 \\ \vec{u}_i - \vec{u}_e \end{vmatrix}$$

Since the ions are very heavy compared to the electrons their responses to a given field will be small

$$\xrightarrow{m_i >> m_e} (20) \quad |u_i| << |u_e| \quad .$$

With this approximation the source densities reduce to

$$\xrightarrow[20]{19} (21) \quad \begin{vmatrix} \rho \\ \\ \mathbb{i} \end{vmatrix} = \begin{vmatrix} 0 \\ \\ -en_e u_e \end{vmatrix}$$

E.4 Force Equation

The force on a species-s charged particle moving in an electric and a magnetic field is given by

$$\xrightarrow[\text{Lorentz}]{\text{Newton,}} (22) \quad \frac{dm_s u_s}{dt} = q_s(\mathbb{E} + u_s \times \mathbb{B}) \quad .$$

The electric and magnetic fields fluctuate strongly along a path through the aggregate of charged particles. This is due to the great increase in field strengths of each individual particle as the path approaches it. In the treatment of a macroscopic aggregate of particles on a continium basis, it is convenient to work with the macro-averages of quantities (i.e. averages over the volume element Λ_s defined in equation (9) rather than the highly fluctuation micro-averages between the charged particles. While Maxwell's equations for the macro-averaged fields are the same as those for the microscale fields this is not so for the force equations. The reason for this resides in the manner in which the macro-averages are obtained. The macro-average for the microscale fields is obtained by integrating over the entire volume, Λ_s, and consequently the highly fluctuating portion of the fields of the individual particles average to zero. The macro-average of the highly fluctuating

microscale forces on the charged particles does not average out to zero because the average is taken over the particle trajectories within the volume element Λ_s and not over the entire volume of Λ_s. The highly fluctuating portion of the microscale forces are the collision forces between the particles.

The mass of species-s particles in the cell Λ_s is given by

$\xrightarrow{7_1, 10}$ (23) $M_s = N_s m_s$,

and the charge of species-s particles in the cell Λ_s is given by

$\xrightarrow{7_2, 10}$ (24) $Q_s = N_s q_s$.

The momentum transferred to the species-s particles in Λ_s by collisions (micro-scale interaction forces),

$\xrightarrow{\text{sym def}}$ (25) $\mathbb{F}_c$ = the averaged force exerted by collisions ,

is expressed as a separate term in the force equation for the aggregate of species-s particles in the cell, thus,

$\xrightarrow[(22)]{\text{macro-average}}$ (26) $\dfrac{dM_s u_s}{dt} = Q_s(\mathbb{E} + u \times \mathbb{B}) + \mathbb{F}_c$,

where the electric and magnetic field are now the macro-averages. In terms of

$\xrightarrow{\text{sym def}}$ (27) $\mathbb{P}_{s1}$ = the momentum gained per unit collision

and

$\xrightarrow{\text{sym def}}$ (28) ν_s = the number of unit collisions per unit time,

the collision force exerted on the aggregate of species-s particles in Λ_s is given by

Newton addition $\longrightarrow$ (29) $\quad \mathbb{F}_c = N_s \nu_s \mathbb{P}_{s1}$.

By definition, a unit collision is one that brings a particle with the macro-average velocity to rest. Hence, the momentum loss is the momentum just prior to collision. The momentum gained per unit collision is consequently given by

phys def $\longrightarrow$ (30) $\quad \mathbb{P}_{s1} = -m_s u_s$.

Consequently

29, 30 $\longrightarrow$ (31) $\quad \mathbb{F}_c = -N_s \nu_s m_s u_s$,

and hence the equation of motion for the species-s contents of Λ_s is given by

26, 31 $\longrightarrow$ (32) $\quad \frac{dM_s u_s}{dt} = Q_s(\mathbb{E} + u_s \times \mathbb{B}) - N_s \nu_s m_s u_s$.

An effective equation of motion for an individual particle is given by dividing through by the number of particles

(32) $\div N_s$, 23, 24 $\longrightarrow$ (33) $\quad \frac{dm_s u_s}{dt} + \nu_s m_s u_s = q_s(\mathbb{E} + u_s \times \mathbb{B})$.

While this equation now appears to be for each individual particle of species-s, it really is for the average particle of the combined aggregate of species-s particles in the small volume cell over which the macro-average was taken. Consequently, the range of validity is greater than the equation per se implies. If this equation of motion were for one particle only, its validity would depend on the collision frequency being large compared to the signal frequency. However this equation

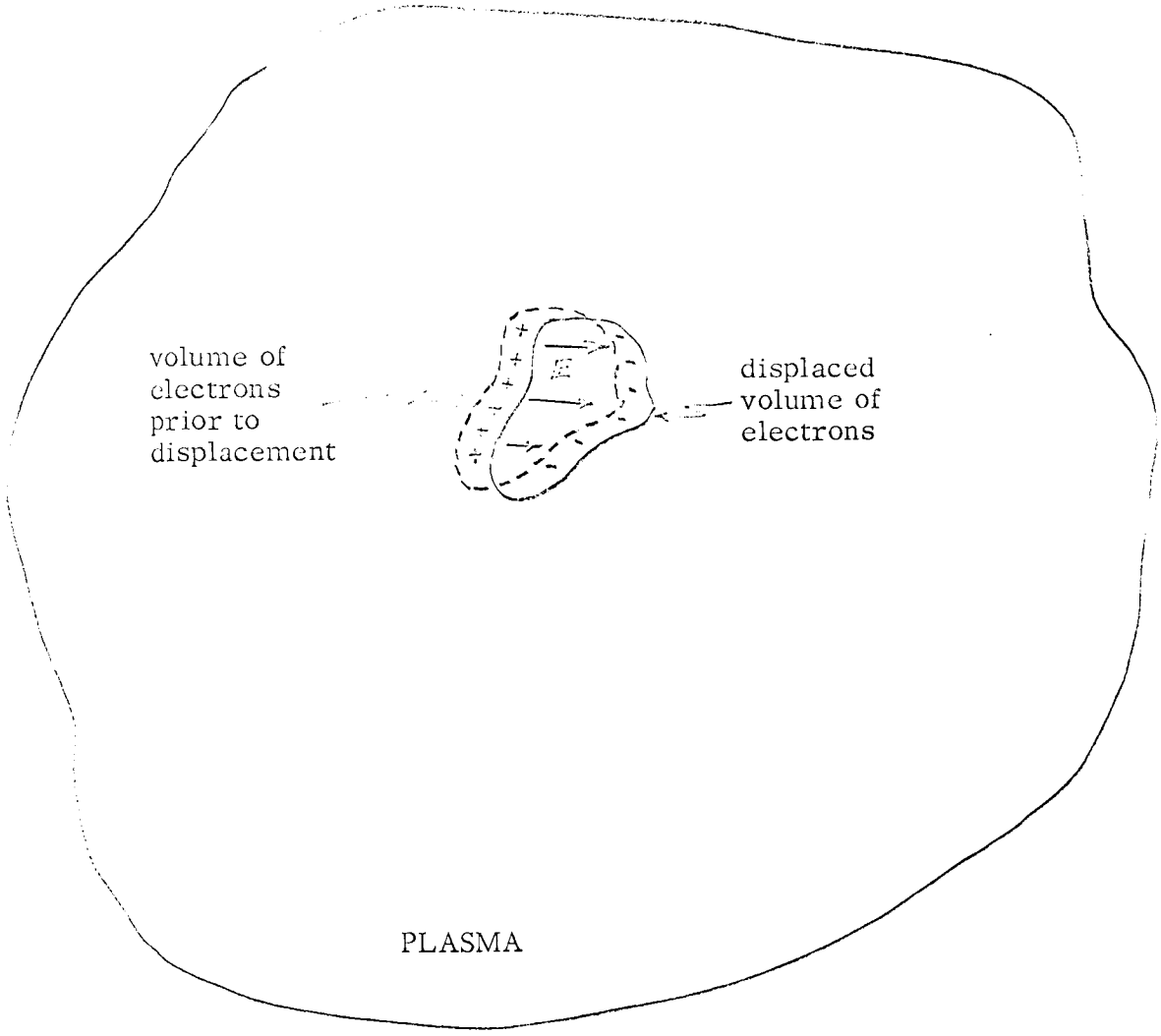

Fig. E.1 Originally Neutral Plasma with a Displaced Volume of Electrons.

is also valid for collision frequencies that are small compared to the signal frequency since the large number of particles in the cell makes the collisions per cell per unit time sufficiently large.

Initial considerations are restricted to the cases for which there is no superimposed fluid motion and for which the induced oscillatory flow is small,

$$\xrightarrow[\text{fluid motion}]{\text{negligible}} (34) \quad \frac{d}{dt} \longrightarrow \partial_t \quad ,$$

and for which there is no significant applied magnetic field, so that

$$\xrightarrow[\text{non relativistic case}]{\text{negligible applied field}} (35) \quad |\mathbf{u} \times \mathbb{B}| \ll |\mathbb{E}| \quad .$$

Under these conditions, the species equation of motion reduces to*

$$\xrightarrow[34,35]{33} (36) \quad m_s \partial_t \mathbf{u}_s + \nu_s m_s \mathbf{u}_s = q_s \mathbb{E}$$

E.5 Plasma Frequency

If a volume of electrons is displaced from its neutral position, as depicted in Fig. E.1, the plasma is no longer neutral. If the electron density in the plasma were originally uniform, such a displacement would produce two regions of charge. If the electron density was originally nonuniform there would now be a net charge density over the entire displaced volume as well as over its original position. The separated charges produce an electric field which exerts a restoring force that tends to pull them back to their original position. When the displaced volume of charges reaches its original position, the momentum acquired in the process

---

* A more general case, including fluid motion, magnetic fields and compressibility, is given in Reference F-1.

causes an overshoot. As a consequence of the restoring forces and the momentum, the displaced charges oscillate back and forth about the neutral position. For the collisionless case the frequency of oscillation is called

$\xrightarrow{\text{sym def}}$ (37) f_p = the plasma frequency.

If collisions are present, the resonant plasma frequency is lower than the plasma frequency.

The plasma frequency can be obtained from the equation of motion. The ion mass is so large compared to the electron mass that ion motion can be neglected. In this case only the equation of motion for the electrons need be considered,

$\xrightarrow[16_1, \nu=0]{36}$ (38) $m_e \partial_t \mathbf{u}_e = -e\mathbb{E}$.

Gauss' law for this case is

$\xrightarrow{6_1}$ (39) $\epsilon_v \nabla \cdot \mathbb{E} = e(n_i - n_e)$.

The remaining field equation needed (Maxwell's generalization of Ampere's Law) is

$\xrightarrow{6_2}$ (40) $\nabla \times \mathbf{H} = \epsilon_v \partial_t \mathbb{E} + \mathbf{i}$.

Since the magnetic field does not have a significant effect on the current, even though the current creates a magnetic field, it is more convenient to eliminate the magnetic field from this field equation. Using

$\xrightarrow[\text{identity}]{\text{vector}}$ (41) $\nabla \cdot \nabla \times (\text{any vector}) = 0$

gives

$$\xrightarrow{40,41} (42) \quad 0 = \epsilon_v \partial_t \nabla\cdot\mathbb{E} + \nabla\cdot\hat{\mathbb{i}} \quad .$$

Since the ion motion is negligible, the current density is that of the electrons only, hence

$$\xrightarrow[21_1]{42} (43) \quad \epsilon_v \partial_t \nabla\cdot\mathbb{E} = e n_e \nabla\cdot u_e \quad .$$

Removing n_e from inside the del operator restricts the results to the case for a negligible spatial variation of electron density over the displaced region. It is more convenient to express the equation in terms of

$$\xrightarrow{\text{sym def}} (44) \quad n_1 = \text{the deviation of the electron number density from the neutrality value}$$

which is

$$\xrightarrow{\text{phys def}} (45) \quad n_1 = n_e - n_i$$

In terms of this, Gauss' law becomes

$$\xrightarrow[45]{39} (46) \quad \epsilon_v \nabla\cdot\mathbb{E} = -e n_1$$

and the Maxwell-Ampere law becomes

$$\xrightarrow[46]{43} (47) \quad \partial_t n_1 = -n_e \nabla\cdot u_e \quad .$$

Converting the equation of motion to facilitate elimination of the electric field intensity and electron velocity gives

$$\xrightarrow{38} (48) \quad m_e \partial_t \nabla\cdot u_e = -e \nabla\cdot\mathbb{E} \quad .$$

Therefore

$$\xrightarrow[46,47]{48} (49) \quad -\frac{m_e}{n_e}\partial_t^2 n_1 = \frac{e^2}{\epsilon_v} n_1$$

or

$$\xrightarrow{49} (50) \quad \partial_t^2 n_1 + \frac{e^2 n_e}{\epsilon_v m_e} n_1 = 0$$

This is the harmonic motion equation whose solution is

$$\xrightarrow{50} (51) \quad n_1 = \hat{n}_1 \cos\left(\sqrt{\frac{e^2 n_e}{\epsilon_v m_e}}\, t + \phi\right) ,$$

where the two constants of integration are

$$\xrightarrow{\text{sym def}} (52) \quad \hat{n}_1 = \text{the peak value of } n_1$$

and

$$\xrightarrow{\text{sym def}} (53) \quad \phi = \text{the oscillation phase at } t=0 \ .$$

The angular frequency of the plasma charge displacement is given by

$$\xrightarrow{51} (54) \quad \omega_p = \sqrt{\frac{e^2 n_e}{\epsilon_v m_e}}$$

and the plasma frequency by

$$\xrightarrow{54} (55) \quad f_p = \frac{1}{2\pi}\sqrt{\frac{e^2 n_e}{\epsilon_v m_e}} \quad \text{Hz} \ .$$

Evaluating the constants gives

$$\xrightarrow[A-1,A-2]{55} (56) \quad f_1 = 8.978\sqrt{n_e} \ \text{Hz} \approx 9\sqrt{n_e} \ \text{Hz}$$

E.6 Propagation in a Plasma

A great variety of waves can propagate in a plasma[E-2]. Only elementary plane electromagnetic waves are considered here, hence

$$\xrightarrow{C\text{-}79} (57) \quad \begin{vmatrix} \partial_t \\ \nabla \end{vmatrix} \longrightarrow \begin{vmatrix} j\omega \\ -j\beta \end{vmatrix} .$$

Consequently the field equation reduces to

$$\xrightarrow[21_1,57]{5_1,6_2} (58) \quad \begin{vmatrix} \beta \times & -\omega\mu_v \\ \omega\epsilon_v & \end{vmatrix} \begin{vmatrix} \mathbb{E} \\ \mathbb{H} \end{vmatrix} = \begin{vmatrix} 0 \\ -jen_e u_e \end{vmatrix}$$

and

$$\xrightarrow[21_1,57]{5_2,6_2} (59) \quad \check{\beta}\cdot \begin{vmatrix} \mathbb{E} \\ \mathbb{H} \end{vmatrix} = \begin{vmatrix} 0 \\ 0 \end{vmatrix} ,$$

and the equation of motion reduces to

$$\xrightarrow{36} (60) \quad (j\omega + \nu) m_e u_e = -e\mathbb{E} .$$

Eliminating the velocity field and the magnetic field gives

$$\xrightarrow[58_1,60]{58_2} (61) \quad \check{\beta} \times \frac{\check{\beta} \times \mathbb{E}}{\omega\mu_v} + \omega\epsilon_v \mathbb{E} = -jen_e \frac{-e\mathbb{E}}{m_e(\nu + j\omega)} .$$

Expanding the triple vector product and multiplying through by $\omega\mu_v$ gives

$$\xrightarrow{61} (62) \quad \check{\beta}\cdot\mathbb{E}\check{\beta} - \check{\beta}^2\mathbb{E} + \left(\omega^2\mu_v\epsilon_v - \frac{e^2 n_e \omega\mu_v}{m_e(\omega - j\nu)}\right)\mathbb{E} = 0 .$$

Consequently,

$$\xrightarrow[59_1]{67} (63) \quad \left[\check{\beta}^2 - \omega^2\mu_v\epsilon_v + \frac{e^2 n_e \omega \mu_v}{m_e(\omega - j\nu)}\right] \mathbb{E} = 0 \quad .$$

Since only fields which are not identically zero are of interest, it is necessary that

$$\xrightarrow{63} (64) \quad \check{\beta}^2 - \omega^2\mu_v\epsilon_v + \frac{e^2 n_e \omega \mu_v}{m_e(\omega - j\nu)} = 0 \quad .$$

The complex phase propagation factor is consequently given by

$$\xrightarrow{64} (65) \quad \check{\beta}^2 = \omega^2\mu_v\epsilon_v \left[1 - \frac{e^2 n_e}{\omega\epsilon_v m_e(\omega - j\nu)}\right] \quad .$$

It is convenient to express this in terms of the vacuum phase factor

$$\xrightarrow[C-123]{C-122} (66) \quad \beta_v = \omega\sqrt{\mu_v\epsilon_v}$$

and the plasma frequency, thus

$$\xrightarrow[66,54]{65} (67) \quad \check{\beta}^2 = \beta_v^2\left[1 - \frac{\omega_p^2}{\omega(\omega - j\nu)}\right] \quad .$$

Expressing this in terms of the real phase and attenuation factors, and rationalizing the right hand side gives

$$\xrightarrow[C-77]{67} (68) \quad \beta^2 - \alpha^2 - 2j\beta\alpha = \beta_v^2\left[1 - \frac{\omega_p^2}{\omega}\,\frac{\omega + j\nu}{\omega^2 + \nu^2}\right]$$

Consequently the phase and attenuation factors can be obtained by solving

$$\xrightarrow{68} (69) \quad \begin{vmatrix} \beta^2 - \alpha^2 \\ \\ 2\beta\alpha \end{vmatrix} = \beta_v^2 \begin{vmatrix} 1 - \dfrac{\omega_p^2}{\omega^2+\nu^2} \\ \\ \dfrac{\nu}{\omega}\dfrac{\omega_p^2}{\omega^2+\nu^2} \end{vmatrix}$$

It is convenient to utilize the refractive and extinction indices,

$$\xrightarrow{D\text{-}28, D\text{-}39} (70) \quad \begin{vmatrix} n \\ \\ \varkappa \end{vmatrix} = \frac{1}{\beta_v} \begin{vmatrix} \beta \\ \\ \alpha \end{vmatrix}$$

since they are the phase and attenuation factors normalized with respect to the vacuum phase factor value. Also using

$$\xrightarrow{\text{sym def}} (71) \quad R = \frac{\omega_p^2}{\omega^2 + \nu^2}$$

gives the equations for the normalized phase and attenuation factors as

$$\xrightarrow[70,61]{69} (72) \quad \begin{vmatrix} n^2 - \varkappa^2 \\ \\ 2n\varkappa \end{vmatrix} = \begin{vmatrix} 1-R \\ \\ \dfrac{\nu}{\omega}R \end{vmatrix}$$

Using

$$\xrightarrow{72_2} (73) \quad \varkappa = \frac{\nu R}{2\omega n}$$

to eliminate $\varkappa$ gives

$$\xrightarrow[73]{72_1} (74) \quad n^2 - \left(\frac{\nu R}{2\omega n}\right)^2 = 1 - R$$

Hence the quadratic equation for n^2 is

$$\xrightarrow{74} (75) \quad n^4 - (1-R)n^2 - \left(\frac{\nu R}{2\omega}\right)^2 = 0 \quad .$$

Solving gives

$$\xrightarrow{75} (76) \quad n^2 = \frac{1-R}{2} \pm \sqrt{\left(\frac{1-R}{2}\right)^2 + \left(\frac{\nu R}{2\omega}\right)^2} \quad .$$

Since the phase factor is a real quantity, its square must be a positive number. Consequently the negative sign in front of the square root is extraneous, hence

$$\xrightarrow[n^2 \geq 0]{76} (77) \quad n^2 = \frac{1-R}{2} + \sqrt{\left(\frac{1-R}{2}\right)^2 + \left(\frac{\nu R}{2\omega}\right)^2} \quad .$$

Consequently

$$\xrightarrow{77} (78) \quad n = \pm \frac{1}{\sqrt{2}} \sqrt{1-R+\sqrt{\left(1-R\right)^2 + \left(\frac{\nu}{\omega}R\right)^2}}$$

The plus and minus signs in front of the root are for positively and negatively traveling waves respectively, and hereafter are omitted, but are to be understood. The normalized attenuation factor, the extinction index, is given by

$$\xrightarrow[78]{73} (79) \quad \varkappa = \frac{\nu R}{\sqrt{2}\,\omega\sqrt{1-R+\sqrt{\left(1-R\right)^2+\left(\frac{\nu}{\omega}R\right)^2}}}$$

Rearranging gives

$$\xrightarrow{79} (80) \quad \varkappa = \frac{1}{\sqrt{2}}\sqrt{-1+R+\sqrt{\left(1-R\right)^2+\left(\frac{\nu}{\omega}R\right)^2}}$$

It is convenient to combine the refractive and extinction coefficient formulae into a single formula

$$\xrightarrow{78,80} (81) \quad \begin{Bmatrix} n \\ \\ \varkappa \end{Bmatrix} = \frac{1}{\sqrt{2}} \sqrt{(1-R)\begin{Bmatrix} 1 \\ -1 \end{Bmatrix} + \sqrt{(1-R)^2 + \left(\frac{\nu}{\omega} R\right)^2}}$$

Removing the abbreviated symbols gives

$$\xrightarrow[70,71]{81} (82) \quad \begin{Bmatrix} \beta \\ \\ \alpha \end{Bmatrix} = \frac{\beta_v}{\sqrt{2}} \sqrt{\left(1 - \frac{\omega_p^2}{\omega^2+\nu^2}\right)\begin{Bmatrix} 1 \\ -1 \end{Bmatrix} + \sqrt{\left(1 - \frac{\omega_p^2}{\omega^2+\nu^2}\right)^2 + \left(\frac{\nu}{\omega} \frac{\omega_p^2}{\omega^2+\nu^2}\right)^2}}$$

It is frequently convenient to normalize the plasma and collision frequencies with respect to the signal frequency or angular frequency, thus

$$\xrightarrow{\text{sym def}} (83) \quad \begin{vmatrix} \nu_p \\ \\ \nu_c \end{vmatrix} = \frac{1}{\omega} \begin{vmatrix} \omega_p \\ \\ \nu \end{vmatrix} .$$

In terms of the normalized frequencies

$$\xrightarrow[83]{82} (84) \quad \begin{Bmatrix} \beta \\ \\ \alpha \end{Bmatrix} = \frac{\beta_v}{\sqrt{2}} \sqrt{\left(1 - \frac{\nu_p^2}{1+\nu_c^2}\right)\begin{Bmatrix} 1 \\ -1 \end{Bmatrix} + \sqrt{\left(1 - \frac{\nu_p^2}{1+\nu_c^2}\right) + \frac{\nu_c \nu_p^2}{1+\nu_c^2}}}$$

or

$$\xrightarrow{84} (85) \quad \begin{Bmatrix} \beta \\ \\ \alpha \end{Bmatrix} = \frac{\beta_v}{\sqrt{2}} \sqrt{\frac{\left(1+\nu_c^2-\nu_p^2\right)\begin{Bmatrix} 1 \\ -1 \end{Bmatrix} + \sqrt{\left(1+\nu_c^2-\nu_p^2\right)^2 + \left(\nu_c \nu_p^2\right)^2}}{1+\nu_c^2}}$$

or

$$\xrightarrow{85} (86) \quad \begin{Bmatrix} \beta \\ \\ \alpha \end{Bmatrix} = \frac{\beta_v}{\sqrt{2}} \sqrt{\frac{\left(1-\nu_p^2+\nu_c^2\right)\begin{Bmatrix} 1 \\ -1 \end{Bmatrix} + \sqrt{1+\nu_c^2}\sqrt{\left(1-\nu_p^2\right)^2 + \nu_c^2}}{1+\nu_c^2}}$$

or

$$\xrightarrow{86} (87) \quad \begin{Bmatrix} \beta \\ \alpha \end{Bmatrix} = \frac{\beta_v}{\sqrt{2}} \sqrt{\left(1 - \frac{\nu_p^2}{1+\nu_c^2}\right) \begin{Bmatrix} 1 \\ -1 \end{Bmatrix} + \sqrt{1 - \frac{2-\nu_p^2}{1+\nu_c^2}\nu_p^2}} \quad .$$

The most convenient form to use depends on the parameter range. The refractive index is graphed in Fig. E. 2 and E. 3 for different parameter ranges. It is more convenient to have the attenuation in db per free space wavelength than in terms of the extinction index in nepers per radian, hence

$$\xrightarrow[1 \text{ neper}=8.7 \text{ db}]{70_2} (88) \quad \alpha\lambda_v = 2\pi\varkappa \times 8.7 = 54\varkappa \text{ db per } \lambda_v$$

is plotted in Figs. E. 4 and E. 5.

E. 7 Phase Factor Minimum

The smallest value of the refractive index,

$$\xrightarrow{84} (89) \quad n = \frac{1}{\sqrt{2}} \sqrt{1 - \frac{\nu_p^2}{1+\nu_c^2} + \sqrt{\left(1 - \frac{\nu_p^2}{1+\nu_c^2}\right)^2 + \left(\frac{\nu_c \nu_p^2}{1+\nu_c^2}\right)^2}} \quad ,$$

occurs when the quantity under the square root is a minimum. The value of ν_p for which n is a minimum is obtainable from

$$\xrightarrow{\text{calculus, } 89} (90) \quad \frac{d}{d\nu_p} \left[1 - \frac{\nu_p^2}{1+\nu_c^2} + \sqrt{\left(1 - \frac{\nu_p^2}{1+\nu_c^2}\right)^2 + \left(\frac{\nu_c \nu_p^2}{1+\nu_c^2}\right)^2} \right] = 0 \quad .$$

This development is simplified by using

$$\xrightarrow{\text{sym def}} (91) \quad x = \frac{\nu_p^2}{1+\nu_c^2} \quad ,$$

in which case,

$$\xrightarrow{\frac{90}{91}} (92) \quad \frac{d}{dx}\left[1 - x + \sqrt{(1-x)^2 + \nu_c^2 x^2}\right] = 0 \quad .$$

Differentiating gives

$$\xrightarrow{92} (93) \quad -1 + \tfrac{1}{2}\frac{2(1-x)(-1) + 2\nu_c^2 x}{\sqrt{(1-x)^2 + \nu_c^2 x^2}} = 0 \quad .$$

Simplifying gives

$$\xrightarrow{93} (94) \quad -(1-x) + \nu_c^2 = \sqrt{(1-x)^2 + \nu_c^2 x^2} \quad .$$

Squaring gives

$$\xrightarrow{94} (95) \quad (1-x)^2 - 2(1-x)\nu_c^2 x + \nu_c^4 x^2 = (1-x)^2 + \nu_c^2 x^2 \quad .$$

Simplifying gives

$$\xrightarrow{95} (96) \quad -2(1-x) + \nu_c^2 x = x \quad .$$

Therefore

$$\xrightarrow{96} (97) \quad x_v = \frac{2}{1+\nu_c^2} \quad .$$

Consequently

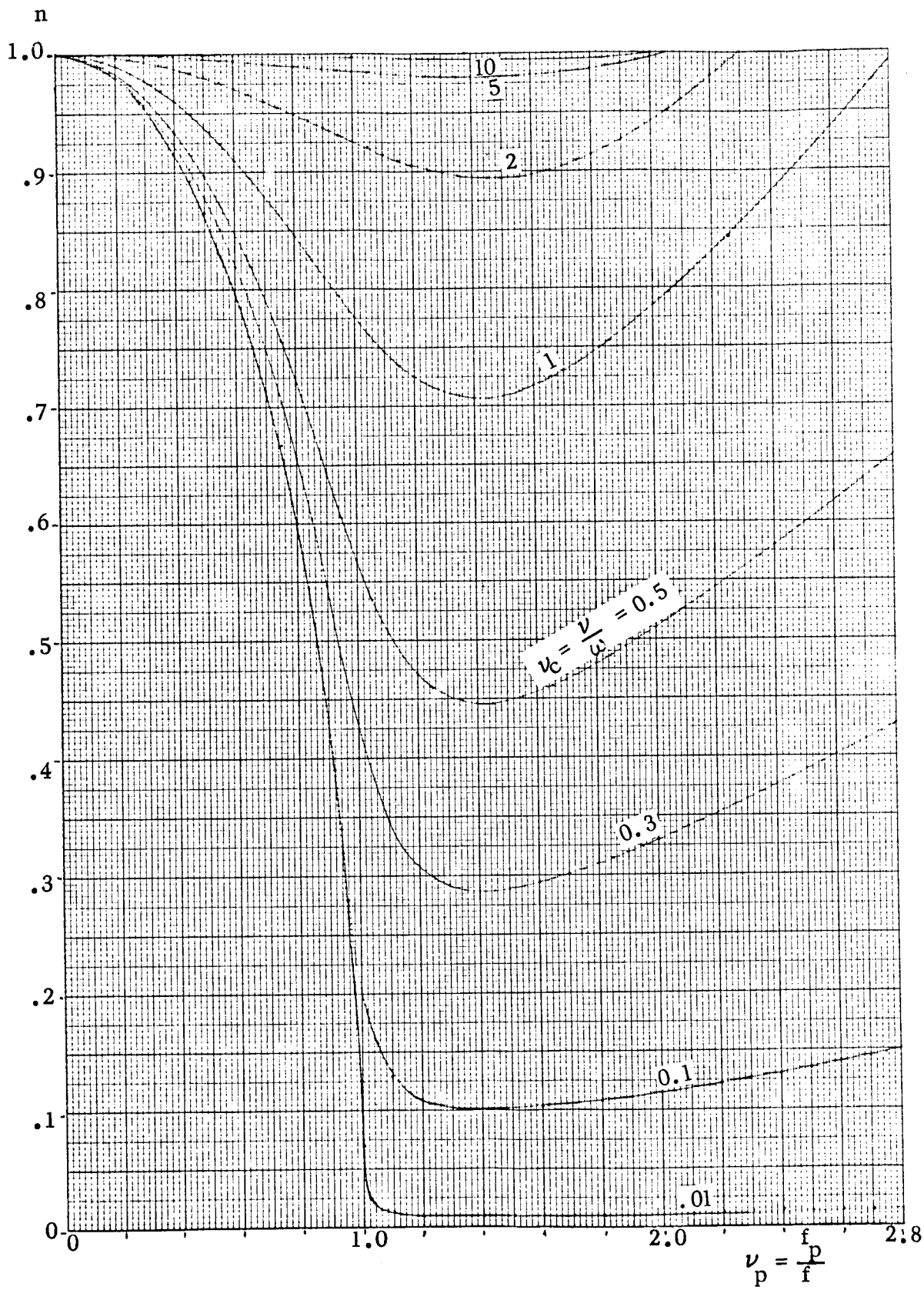

Fig. E.2 Refractive index, n, as a function of the normalized plasma frequency, ν_p, for various normalized collision frequencies, ν_c.

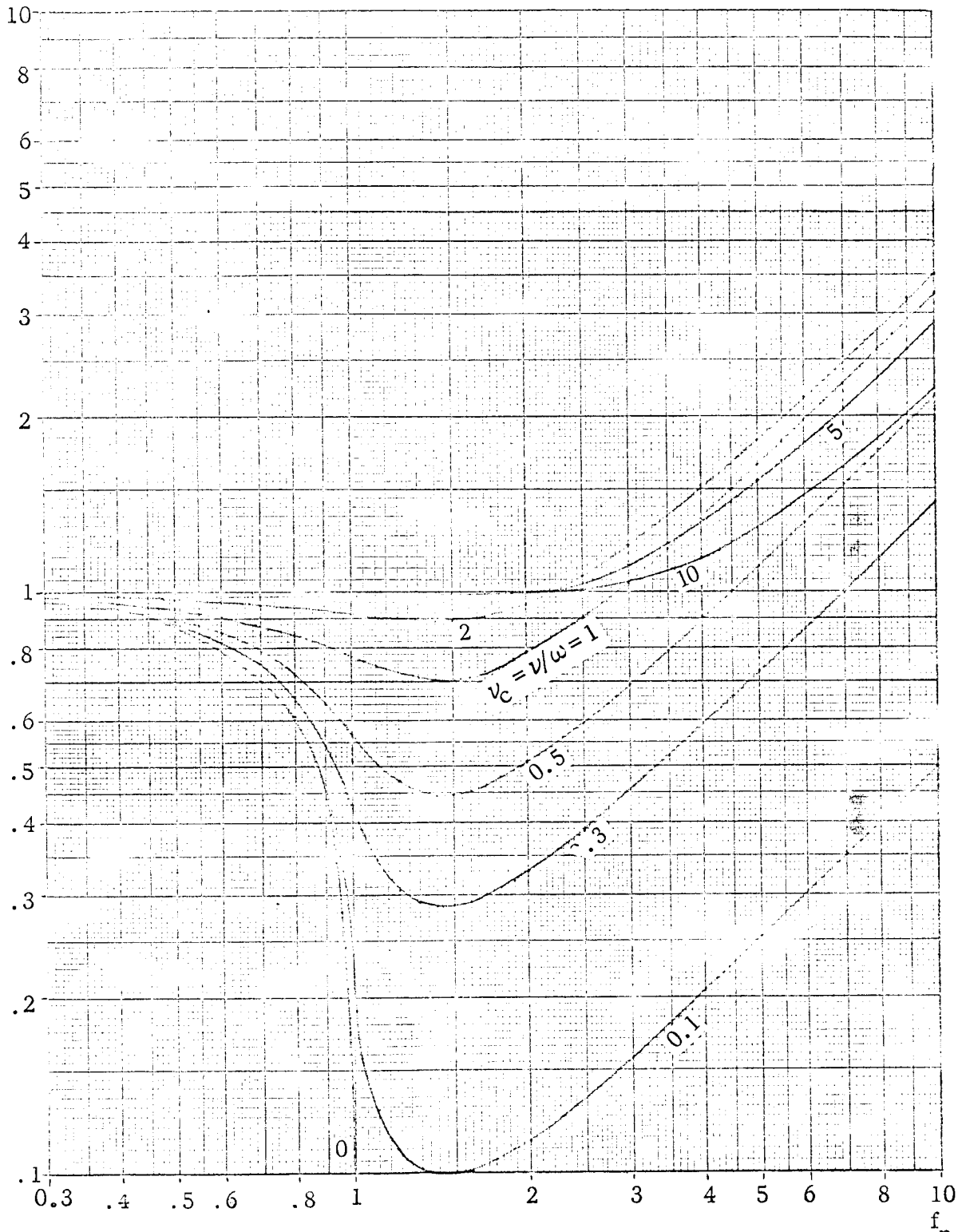

Fig. E.3 Refractive index, n, as a function of the normalized plasma frequency, ν_p, for various normalized collision frequencies, ν_c.

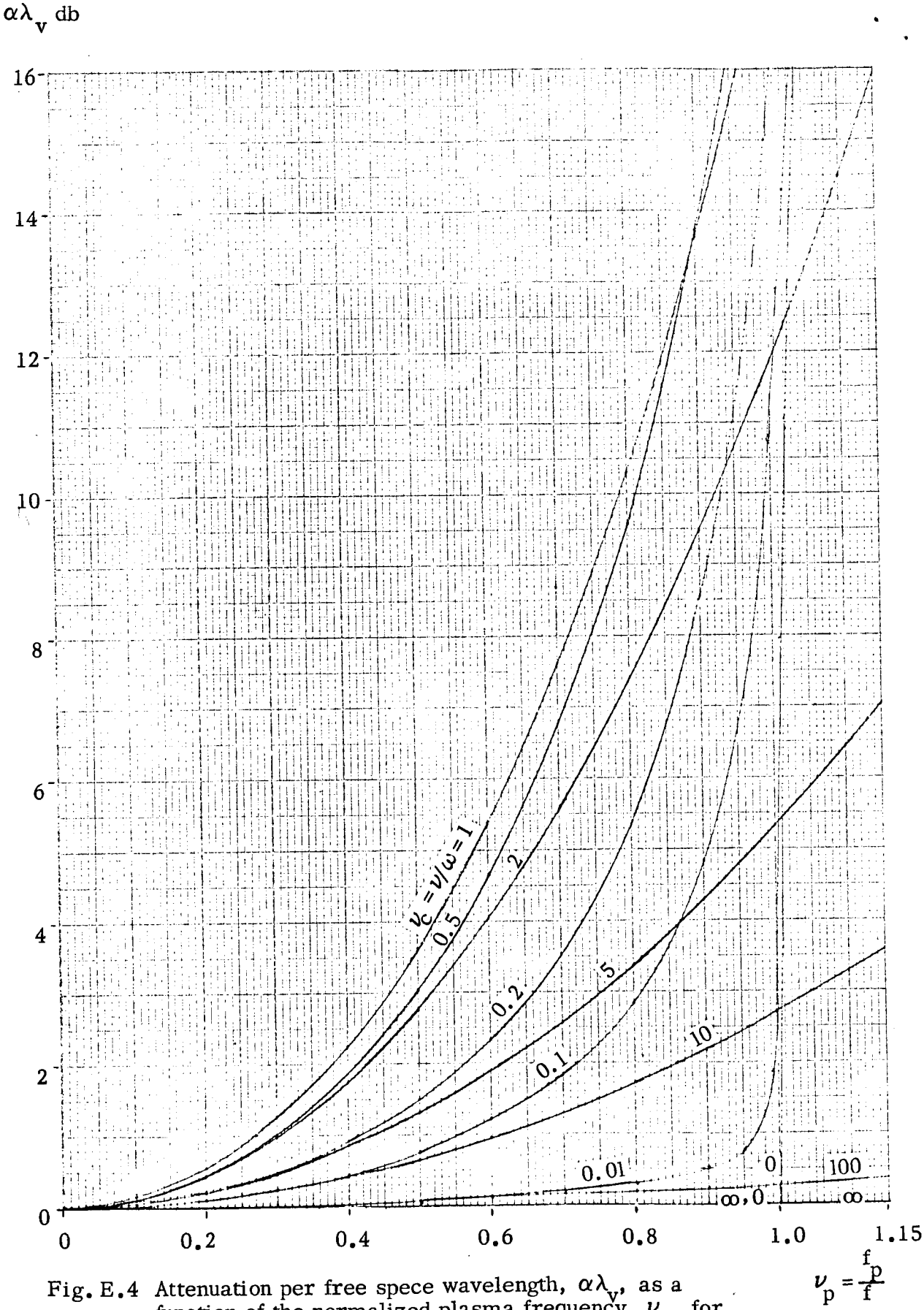

Fig. E.4 Attenuation per free spece wavelength, $\alpha\lambda_v$, as a function of the normalized plasma frequency, ν_p, for various normalized collision frequencies ν_c.

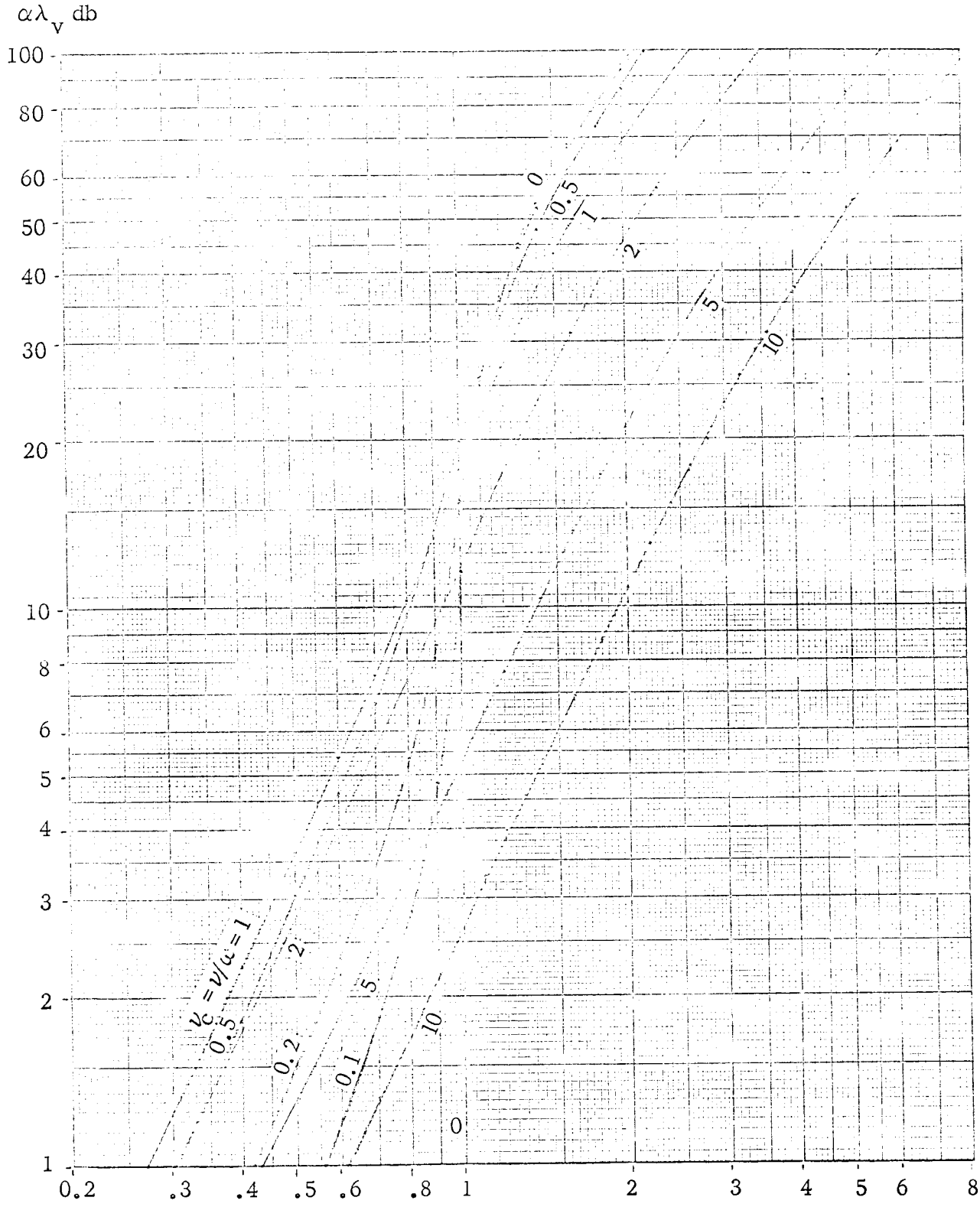

Fig. E.5 Attenuation per free space wavelength, $\alpha\lambda_v$, as a function of the normalized plasma frequency, ν_p, for various normalized collision frequencies ν_c.

$$\nu_p = \frac{f_p}{f}$$

$$\xrightarrow{91,97} (98) \quad \nu_{pv}^2 = 2 \ ,$$

and

$$\xrightarrow{98} (99) \quad \nu_{pv} = \sqrt{2} = 1.414$$

The minimum value of refractive index is given by

$$\xrightarrow[98]{89} (100) \quad n = \frac{1}{\sqrt{2}} \sqrt{1 - \frac{2}{1+\nu_c^2} + \sqrt{\left(1 - \frac{2}{1+\nu_c^2}\right)^2 + \left(\frac{2\nu_c}{1+\nu_c^2}\right)^2}}$$

$$= \frac{1}{\sqrt{2}} \sqrt{\frac{\nu_c^2 - 1}{\nu_c^2 + 1} + \sqrt{\frac{\left(\nu_c^2 - 1\right)^2 + 4\nu_c^2}{\left(\nu_c^2 + 1\right)^2}}}$$

and hence

$$\xrightarrow{100} (101) \quad \breve{n} = \frac{\nu_c}{\sqrt{\nu_c^2 + 1}}$$

An approximation for the refractive index in the vicinity of its minimum value is given by using

$$\xrightarrow{\text{sym def}} (102) \quad \Delta\nu_p = \nu_p - \sqrt{2}$$

where

$$\xrightarrow{\text{restriction}} (103) \quad |\Delta\nu_p| << \nu_p$$

It should be noted that terms through the square must be retained but higher power

terms can be dropped. Consequently the expression for the refractive index can be expressed in the form

$$\xrightarrow[102]{87_1} (104) \quad n = \frac{1}{\sqrt{2}} \sqrt{1 - \frac{2+2\sqrt{2}\,\Delta\nu_p+(\Delta\nu_p)^2}{1+\nu_c^2} + \sqrt{1+\frac{2\sqrt{2}+\Delta\nu_p}{1+\nu_c^2}\Delta\nu_p\left[2+2\sqrt{2}\,\Delta\nu_p\right]}}$$

Simplifying and retaining terms only through the square in $\Delta\nu_p$ under the inner root gives

$$\xrightarrow{104} (105) \quad n = \frac{1}{\sqrt{2}} \sqrt{1 - \frac{2+2\sqrt{2}\,\Delta\nu_p+(\Delta\nu_p)^2}{1+\nu_c^2} + \sqrt{1+2\frac{2\sqrt{2}+5\,\Delta\nu_p}{1+\nu_c^2}\Delta\nu_p}} \quad .$$

Using

$$\xrightarrow{RE3(5.3)} (106) \quad \sqrt{1+x} = 1+\frac{1}{2}x-\frac{1}{8}x^2+\frac{1}{16}x^3 - \cdots$$

to expand the inner root and dropping terms beyond the second power in $\Delta\nu_p$ gives

$$\xrightarrow{105,106} (107) \quad n = \frac{1}{\sqrt{2}} \sqrt{1 - \frac{2+2\sqrt{2}\,\Delta\nu_p+(\Delta\nu_p)^2}{1+\nu_c^2} + 1 + \frac{2\sqrt{2}+5\,\Delta\nu_p}{1+\nu_c^2}\Delta\nu_p - \left(\frac{2\Delta\nu_p}{1+\nu_c^2}\right)^2} \quad .$$

Collecting terms and simplifying give

$$\xrightarrow{107} (108) \quad n = \sqrt{1 - \frac{1}{1+\nu_c^2} + 2\frac{(\Delta\nu_p)^2}{1+\nu_c^2}\left(1-\frac{1}{1+\nu_c^2}\right)}$$

and hence

$$\xrightarrow{108} (109) \quad n = \frac{\nu_c}{\sqrt{1+\nu_c^2}} \sqrt{1+2\frac{(\Delta\nu_p)^2}{1+\nu_c^2}}$$

Expanding the root and keeping terms only through the second $\Delta\nu_p$ gives

$$\xrightarrow[101]{109,106} (110) \quad n = \breve{n}\left[1+\frac{(\Delta\nu_p)^2}{1+\nu_c^2}\right] .$$

E.8 Approximation for Small Plasma Frequencies

For small plasma frequencies,

$$\xrightarrow{\text{condition}} (111) \quad \nu_p^2 << 1 ,$$

the normalized phase and attenuation factors can be approximated by

$$\xrightarrow[111]{87,106} (112) \quad \begin{Bmatrix} n \\ \\ \varkappa \end{Bmatrix} = \frac{1}{\sqrt{2}}\sqrt{\left(1-\frac{\nu_p^2}{1+\nu_2^2}\right)\begin{Bmatrix} 1 \\ -1 \end{Bmatrix} + 1\ \frac{1-\frac{1}{2}\nu_p^2}{1+\nu_c^2}\,\nu_p^2} .$$

Hence

$$\xrightarrow{112} (113) \quad \begin{Bmatrix} n \\ \\ \varkappa \end{Bmatrix} = \frac{1}{\sqrt{2}}\sqrt{\begin{Bmatrix} 2-\frac{\nu_p^2}{1+\nu_c^2}(2-\frac{1}{2}\nu_p^2) \\ \\ \frac{\frac{1}{2}\nu_p^4}{1+\nu_c^2} \end{Bmatrix}}$$

Consequently,

$$\xrightarrow{113} (114) \quad \begin{bmatrix} n \\ \\ \varkappa \end{bmatrix} = \begin{bmatrix} \sqrt{1-\frac{1-\frac{1}{4}\nu_p^2}{1+\nu_c^2}\nu_p^2} \\ \\ \frac{\frac{1}{2}\nu_p^2}{\sqrt{1+\nu_c^2}} \end{bmatrix}$$

Simplifying, retaining terms only through the second power in ν_p, gives

$$\xrightarrow[106]{114} (115) \quad \begin{Bmatrix} n \\ \\ \varkappa \end{Bmatrix} = \begin{Bmatrix} \sqrt{1 - \frac{1}{2}\frac{\nu_p^2}{1+\nu_c^2}} \\ \\ \frac{1}{2}\frac{\nu_p^2}{\sqrt{1+\nu_c^2}} \end{Bmatrix} .$$

It is more convenient to use the attenuation in db per vacuum wavelength

$$\xrightarrow[115_2]{88} (116) \quad \alpha\lambda_v = \frac{8.7\pi\nu_p^2}{\sqrt{1+\nu_c^2}} = \frac{27.3\nu_p^2}{\sqrt{1+\nu_c^2}} \text{ db per vacuum wavelength} .$$

E.9 Approximation for Large Plasma Frequency

For large plasma frequencies

$$\xrightarrow{\text{condition}} (117) \quad \nu_p^2 >> 1+\nu_c^2 ,$$

the phase and attenuation factors can be approximated by

$$\xrightarrow[117]{87} (118) \quad \begin{Bmatrix} n \\ \\ \varkappa \end{Bmatrix} = \frac{!}{\sqrt{2}}\sqrt{\frac{\nu_p^2}{1+\nu_c^2}\begin{Bmatrix} 1 \\ \\ -1 \end{Bmatrix} + \frac{\nu_p^2}{\sqrt{1+\nu_c^2}}}$$

Simplifying gives

$$\xrightarrow{118} (119) \quad \begin{Bmatrix} n \\ \\ \varkappa \end{Bmatrix} = \frac{\nu_p}{\sqrt{2}\sqrt{1+\nu_c^2}}\sqrt{\sqrt{1+\nu_c^2} + \begin{Bmatrix} 1 \\ \\ -1 \end{Bmatrix}}$$

E.10 Approximation for Small Collision Frequency

For small collision frequency compared to the signal frequency

condition → (120) $\nu_c \equiv \frac{\nu}{\omega} << 1$

It is convenient to use approximations for the phase and attenuation factors, or their normalized values, the refractive and extinction coefficients. These are readily obtainable from

72 → (121)

	$R < 1$	$R > 1$
n	$\sqrt{1 - R + \varkappa^2}$	$\frac{\nu}{\omega} \frac{R}{2\varkappa}$
$\varkappa$	$\frac{\nu}{\omega} \frac{R}{2n}$	$\sqrt{R - 1 + n^2}$

Using

120, 121 / $R \not\approx 1$ → (122)

$R < 1$	$R > 1$
$\varkappa^2 << 1 - R$	$n^2 << R - 1$

gives

121 / 122 → (123)

	$R \not\approx 1$	
	$R < 1$	$R > 1$
n	$\sqrt{1 - R}$	$\frac{\nu}{\omega} \frac{R}{2\varkappa}$
$\varkappa$	$\frac{\nu}{\omega} \frac{R}{2n}$	$\sqrt{R - 1}$

Expressing without the abbreviations gives

$$\omega^2+\nu^2 \not\approx \omega_p^2$$

$\omega^2+\nu > \omega_p^2$	$\omega^2+\nu^2 < \omega_p^2$
$\sqrt{1-\frac{\omega_p^2}{\omega+\nu^2}}$	$\frac{\nu}{2\varkappa\omega}\frac{\omega_p^2}{\omega^2+\nu^2}$
$\frac{\nu}{2n\omega}\frac{\omega_p^2}{\omega^2+\nu^2}$	$\sqrt{\frac{\omega_p^2}{\omega^2+\nu^2}-1}$

$$\xrightarrow[71,70]{123} \xrightarrow{\text{(124)}} \begin{vmatrix} \beta \\ \\ \alpha \end{vmatrix} = \beta_v$$

Reducing further gives

$$\omega \not\approx \omega_p$$

$\omega > \omega_p$	$\omega < \omega_p$
$\sqrt{1-\frac{\omega_p^2}{\omega^2}}$	$\frac{\nu\omega_p^2}{2\varkappa\omega^3}$
$\frac{\nu\omega_p^2}{2n\omega^3}$	$\sqrt{\frac{\omega_p^2}{\omega^2}-1}$

$$\xrightarrow[120]{124} \xrightarrow{\text{(125)}} \begin{vmatrix} \beta \\ \\ \alpha \end{vmatrix} = \beta_v$$

E.11 Approximation for Large Collision Frequency

For large collision frequency compared to the signal frequency

$$\xrightarrow{\text{condition}} \xrightarrow{\text{(126)}} \frac{\nu}{\omega} >> 1$$

the parameter R becomes

$$\xrightarrow[126]{71} \xrightarrow{\text{(127)}} R = \frac{\omega_p^2}{\nu^2} ;$$

hence the propagation parameters become

$$\xrightarrow{72} \xrightarrow{\text{(128)}} \begin{vmatrix} n^2-\varkappa^2 \\ \\ 2n\varkappa \end{vmatrix} = \begin{vmatrix} 1-\frac{\omega_p^2}{\nu^2} \\ \\ \frac{\omega_p^2}{\omega\nu} \end{vmatrix}$$

Using

$$\xrightarrow[\omega_p \not\approx \nu]{126,128} (129)$$

$\nu > \omega_p$	$\nu < \omega_p$
$\chi^2 << 1 \quad \frac{\omega_p^2}{\nu^2}$	$n^2 << \frac{\omega_p^2}{\nu^2} - 1$

gives

$$\xrightarrow[129]{128} (130) \qquad \begin{vmatrix} n \\ \chi \end{vmatrix} =$$

	$\nu \not\approx \omega_p$	
	$\nu > \omega_p$	$\nu < \omega_p$
	$\sqrt{1 - \frac{\omega_p^2}{\nu^2}}$	$\frac{\omega_p^2}{2\chi\omega\nu}$
	$\frac{\omega_p^2}{2n\omega\nu}$	$\sqrt{\frac{\omega_p^2}{\nu^2} - 1}$

APPENDIX F: SIGNAL STRENGTH ALTERATION CAUSED BY AN INTERVENING MEDIUM

F.1 Introduction

The strength of a signal ray traversing an intervening medium is modified by the following factors:

1. losses due to reflections,
2. signal beam cross section alteration due to refraction at interface, and in inhomogeneous media,
3. absorption due to collisions and incoherent scattering,
4. signal beam divergence alterations due to interface curvature.

The intervening medium of interest is the ion rocket exhaust beam.

F.2 Interface Transmission Effects

Transmission through an interface alters the signal strength because:

1. reflection produces losses and
2. refraction alters the signal beam cross section.

Fig. F.1 illustrates a differential signal beam passing out of the ion exhaust beam.

In terms of

sym def, Fig. F.1 → (1) $d\Omega_o$ = the differential output signal beam solid angle

and

sym def, Fig. F.1 → (2) dP_o = the differential output signal beam power

the expression for

sym def → (3) p_o = the output signal power intensity

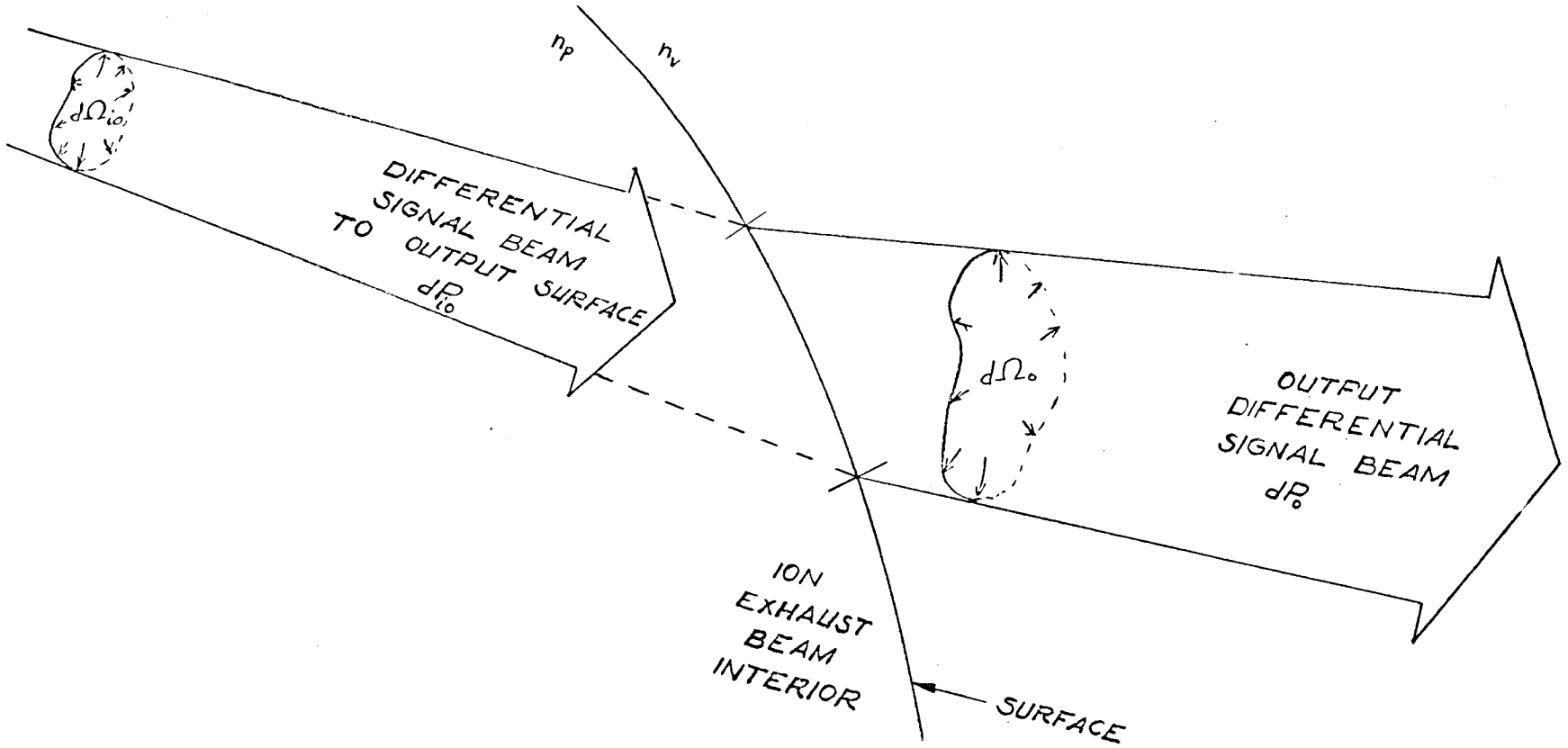

Fig. F.1 Signal Beam Emerging from the Ion Exhaust Beam, as Viewed in the Ray Plane.

is given by

C-16, Fig. F.1 → (4) $p_o = \frac{dP_o}{d\Omega_o}$.

In terms of

sym def → (5) T_{P_o} = the power transmission coefficient at the output surface

and

sym def → (6) dP_{io} = the incident differential signal power on the interior side of the output surface

the power in the differential output signal beam is given by

D-80$_2$ → (7) $dP_o = T_{P_o} dP_{io}$.

Fig. F.2 illustrates a differential signal beam passing into the ion exhaust beam. In terms of

sym def → (8) T_{P_i} = the power transmission coefficient at the input surface

and

sym def → (9) dP_i = the differential input signal power

the expression for

sym def → (10) dP_{oi} = the differential power in the refracted beam

is

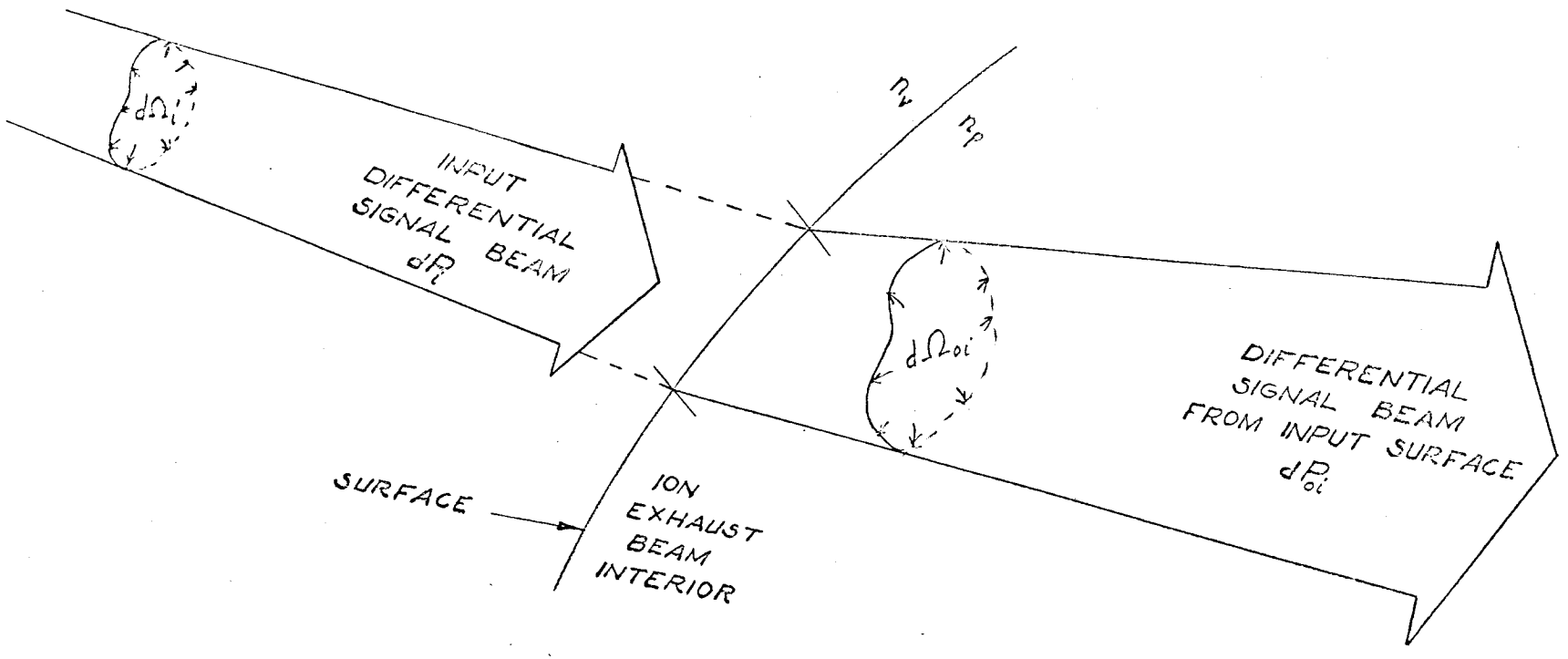

Fig. F.2 Signal Beam Entering the Ion Exhaust Beam, as Viewed in the Ray Plane.

$$dP_{oi} = T_{P_i} dP_i \quad . \tag{11}$$

F.3 Interior Transmission Losses

Collision absorption and scattering attenuate the signal beam traversing the ion exhaust beam interior. The signal beams, interior to the ion exhaust beam, depicted in Figs. F.1 and F.2 are different ends of the same signal beam; consequently, the differential power at the input side of the output surface is related to the differential power at the output side of the input surface by

beam continuity

$$dP_{io} = T_A dP_{oi} \tag{12}$$

where

sym def

$$T_A = \text{the transmission factor through the ion exhaust beam interior for the differential signal beam power.} \tag{13}$$

Figures F.1 and F.2 depict the rays inside the ion exhaust beam to be straight lines. For the model being analyzed, this is correct only if the rays lie in a plane perpendicular to the ion exhaust beam symmetry axis. Since the plasma density varies with position, the index of refraction varies with position; hence, the rays are generally curved. However, the ray paths are approximated by straight lines in the preliminary analysis in this report.

F.4 Power Transmission Through the Ion Exhaust Beam

The differential output power can now be related to the differential input power. Using

12
11

$$dP_{io} = T_A T_{P_i} dP_i \tag{14}$$

gives

$$\xrightarrow[14]{7} (15) \quad dP_o = T_{P_o} T_A T_{P_i} dP_i \quad .$$

F.5 Power Intensity Alteration by the Ion Exhaust Beam

Of basic interest is the reduction in signal intensity due to the ion exhaust beam. The signal intensity in the output beam can be expressed by

$$\xrightarrow[15]{4} (16) \quad p_o = T_{P_o} T_A T_{P_i} \frac{dP_i}{d\Omega_o} \quad .$$

The signal intensity in the input beam is

$$\xrightarrow{\text{C-16, Fig. F.2}} (17) \quad p_i = \frac{dP_i}{d\Omega_i} \quad .$$

Consequently

$$\xrightarrow[17]{16} (18) \quad p_o = T_{P_o} T_A T_{P_i} \frac{d\Omega_i}{d\Omega_o} p_i \quad .$$

In terms of

$$\xrightarrow{\text{sym def}} (19) \quad T_S = \text{the signal beam spreading factor,}$$

$$\xrightarrow{\text{con def}} (20) \quad T_S = \frac{d\Omega_i}{d\Omega_o} \quad .$$

The effect of the ion exhaust beam can be expressed by

$$\xrightarrow[20]{18} (21) \quad \frac{p_o}{p_i} = T_A T_{P_o} T_{P_i} T_S \quad .$$

F.6 Effect of the Antenna Pattern

Since the signal ray direction exiting the ion exhaust beam differs from its direction before entering the ion exhaust beam, and since the antenna gain generally depends on the direction, the signal power intensity ratio that would be observed in a given direction by switching the ion exhaust beam on and off is not that given by (21). The antenna gain variation with angle must be taken into account in order to give the observed ratio. This is done by expressing the signal power intensities with directional arguments,

$$\xrightarrow{21} (22) \quad p_o(\theta_o, \varphi_o) = T_A T_{P_o} T_{P_i} T_S p_i(\theta_i, \varphi_i) \quad .$$

The comparison should be made with the power intensity which would be received in the absence of the ion beam, thus

$$\xrightarrow{22} (23) \quad \frac{p_o(\theta_o, \varphi_o)}{p_i(\theta_o, \varphi_o)} = T_A T_{P_o} T_{P_i} T_S \frac{p_i(\theta_i, \varphi_i)}{p_i(\theta_o, \varphi_o)} \quad .$$

Using the antenna gain function

$$\xrightarrow{C\text{-}30} (24) \quad G(\theta, \varphi) = \frac{p_i(\theta, \varphi)}{\langle p_i \rangle}$$

gives the signal intensity variation factor caused by the ion exhaust beam

$$\xrightarrow[24]{23} (25) \quad \frac{p_o}{p_i} = T_A T_{P_o} T_{P_i} T_S \frac{G(\theta_i, \varphi_i)}{G(\theta_o, \varphi_o)} \quad .$$

APPENDIX G: SIGNAL ATTENUATION IN THE ION EXHAUST BEAM

G.1 Introduction

A signal ray transversing the interior of the ion exhaust beam is depicted in Fig. G.1. Within the ion exhaust beam, collisions and scattering produce

$\xrightarrow{\text{sym def}}$ (1) A = signal attenuation.

In terms of

$\xrightarrow{\text{sym def}}$ (2) α = the attenuation factor

$\xrightarrow{\text{phys def}}$ (3) $\alpha = \frac{dA}{d\ell}$,

the signal attenuation is given by

$\xrightarrow{3}$ (4) $A = \int_{\ell_1}^{\ell_2} \alpha(\ell)\, d\ell$.

Electromagnetic theory gives the attenuation factor more directly than the attenuation, whereas measurement gives the attenuation more directly than the attenuation factor.

The electric and magnetic field intensities of the output and input signal rays are related via

$\xrightarrow{4,\,C\text{-}75}$ (5) $\begin{vmatrix} E_{out} \\ H_{out} \end{vmatrix} = e^{-A} \begin{vmatrix} E_{in} \\ H_{in} \end{vmatrix}$.

The power in a signal beam depends on the product of the electric and magnetic field intensities; hence

$\xrightarrow{(5)}$ (6) $P_{out} = P_{in} e^{-2A}$.

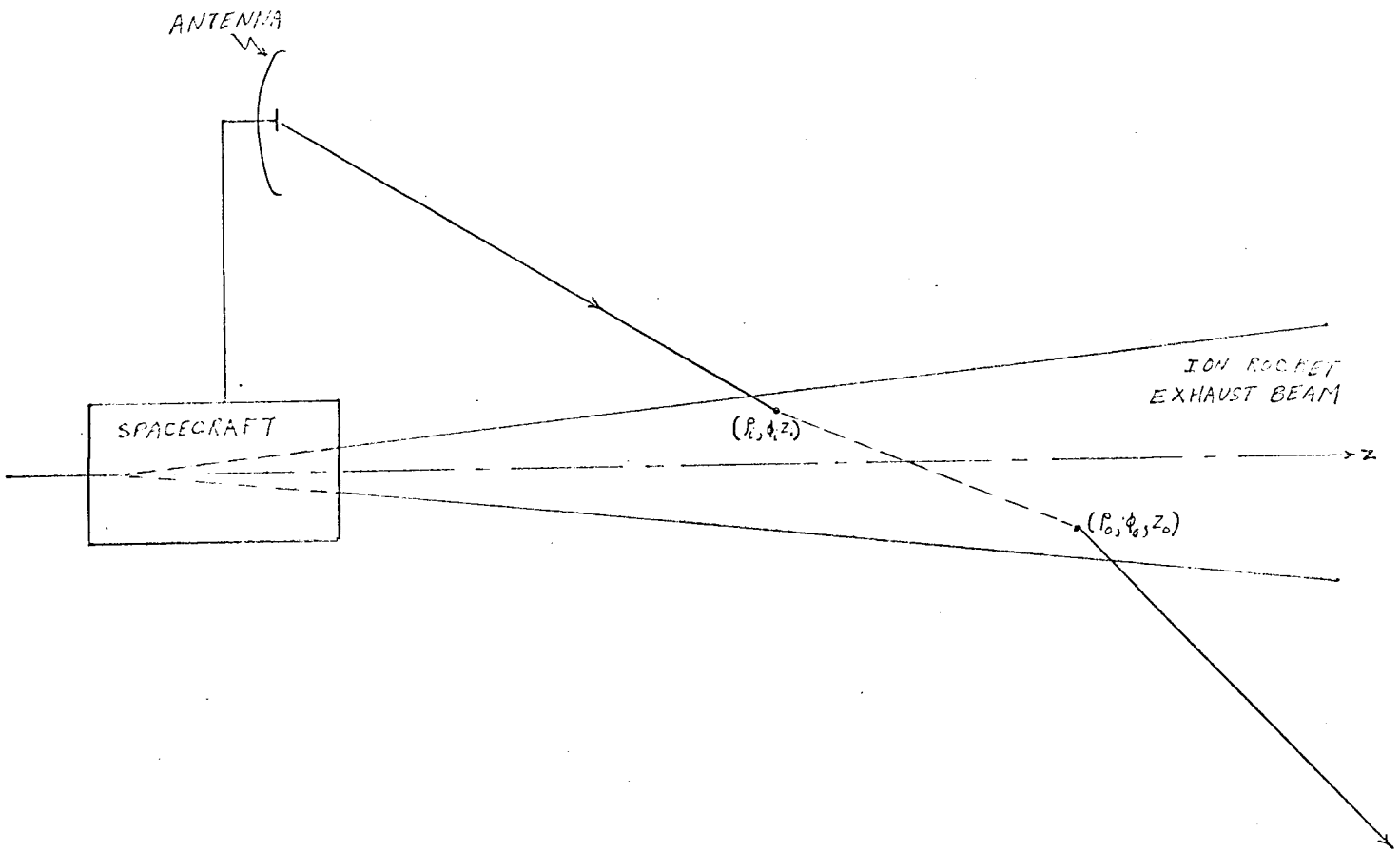

Fig. G.1 Signal Ray Path Through Ion Rocket Exhaust Beam

Consequently,

$$\xrightarrow{\text{sym def}} (7) \quad T = \text{the power transfer function}$$

$$\xrightarrow{\text{con def}} (8) \quad T = \frac{P_{out}}{P_{in}}$$

that accounts for the attenuation is given by

$$\xrightarrow{(8)} (9) \quad T_A = e^{-2A} \quad .$$

The attenuation can be obtained from (4). The path of integration, the signal ray curve, can be specified by the ray entry point into the ion exhaust beam and by the ray direction prior to entry. An alternate specification is by the entry into and exit points from the ion exhaust beam.

If the signal path within the ion exhaust beam is perpendicular to the ion beam axis, the attentuation factor does not vary along the internal path portion in the model under consideration. In this case,

$$\xrightarrow{(4)} (10) \quad A = \alpha L$$

where

$$\xrightarrow{\text{sym def}} (11) \quad L = \text{the length of the propagation path within the ion exhaust beam.}$$

G.2 Attenuation Factor Dependence on Position

The explicit functional dependence of α on position is required before the integral for the attenuation can be evaluated. Solution for the general conditions of propagation is beyond the scope of this preliminary investigation. Fortunately, the Jupiter orbiter ion rocket driven spacecraft with the proposed ion rockets has a maximum plasma

frequency of

Sec. B-9 (12) $\widehat{f}_p = 805$ MHz

at the exhaust plane of the ion rocket. Consequently the maximum plasma frequency normalized with respect to the signal frequency of 2.2 GHz is approximately

12 (13) $\frac{\widehat{f}_p}{f} = \frac{0.805}{2.2} = 0.368$.

As shown in section B-12, the collision frequency is sufficiently small compared to the signal frequency for the attenuation factor approximation,

E-130$_2$ / 70$_1$, C-122 (14) $$\alpha = \frac{\frac{\nu}{2c}\frac{\omega_p^2}{\omega^2}}{\sqrt{1 - \frac{\omega_p^2}{\omega^2}}} ,$$

to be accurate. The validity of the above formula also depends on small gradients of ω_p and ν in comparison with the electric and magnetic field gradients.

It is convenient to represent the collision frequency and plasma angular frequency in terms of their values at a reference position, which is taken at

sym def (15) z_r = the ion rocket engine exhaust surface.

Thus,

E-54 (16) $$\omega_p = \omega_{pr}\sqrt{\frac{n_e}{n_{er}}}$$

and

B-88 (17) $$\nu = \nu_r \frac{n_e}{n_{er}} .$$

With the origin at the apex of the cone used to approximate the envelope of the ion exhaust beam, the electron density varies with position according to

$$\xrightarrow{\text{electron conservation}} (18) \quad n_e = n_{er} \frac{z_r^2}{z^2}$$

if recombination of electrons and cesium ions is neglected and the plasma density is taken as uniform over a cross section of the cone perpendicular to the z-axis. This formula also neglects the effects of plasma oscillations and fluctuations.

It is generally convenient to normalize quantities with respect to their values at the ion rocket exit plane, z_r. The ion exhaust beam radius at z_r, is given by

$$\xrightarrow{\text{Fig.G.1}} (19) \quad b_r = z_r \tan\theta_h \quad .$$

The angular plasma resonant frequency and the collision frequency are related to position by

$$\xrightarrow[18]{16} (20) \quad \omega_p = \omega_{pr} \frac{z_r}{z}$$

and

$$\xrightarrow[18]{17} (21) \quad \nu = \nu_r \frac{z_r^2}{z^2} \quad .$$

The functional dependence of the attenuation on position is thus

$$\xrightarrow[20,21]{14} (22) \quad \alpha = \frac{\frac{\nu_r}{2c}\left(\frac{\omega_{pr}}{\omega}\frac{z_r^2}{z^2}\right)^2}{\sqrt{1-\left(\frac{\omega_{pr}}{\omega}\frac{z_r}{z}\right)^2}}$$

and thereby gives the explicit dependence of the integrand of (4) on the position.

G.3 Propagation Path Differential Length

The differential path length in the attenuation integral, (4), must also be expressed in terms of the common integration parameter, z, in order to evaluate the integral. In terms of

$$\xrightarrow{\text{sym def}} (23) \left\{ \begin{matrix} x_i, y_i, z_i \\ \\ x_o, y_o, z_o \end{matrix} \right\} = \text{the} \left\{ \begin{matrix} \text{input} \\ \\ \text{output} \end{matrix} \right\} \text{point cartesian coordinates}$$

and

$$\xrightarrow{\text{sym def}} (24) \quad 1_x, 1_y, 1_z = \text{the cartesian unit vectors,}$$

the expression for

$$\xrightarrow{\text{sym def}} (25) \quad \mathbb{L}_{io} = \text{the distance vector from the input point to the output point}$$

is given by

$$\xrightarrow{\text{Fig.G.1}} (26) \quad \mathbb{L}_{io} = 1_x(x_o - x_i) + 1_y(y_o - y_i) + 1_z(z_o - z_i) \quad .$$

If the curvature of the propagation path within the ion exhaust beam is negligible, the distance vector from the input point to any point (x, y, z) on the propagation path is

$$\xrightarrow{\text{Fig.G.1}} (27) \quad \mathbb{L} = 1_x(x - x_i) + 1_y(y - y_i) + 1_z(z - z_i) \quad .$$

The differential length vector is

$$\xrightarrow{27} (28) \quad d\mathbb{L} = 1_x dx + 1_y dy + 1_z dz \quad .$$

The distance between the input and output points is

$$\xrightarrow{26} (29) \quad L_{io} = \sqrt{(x_o - x_i)^2 + (y_o - y_i)^2 + (z_o - z_i)^2} \quad .$$

For the straight line propagation path approximation,

$$\xrightarrow[\text{vector def}]{\text{unit}} (30) \quad l_L = \frac{\mathbb{L}_{io}}{L_{io}} \quad ;$$

hence, the unit vector along the interior ray path is

$$\xrightarrow[26,29]{30} (31) \quad l_L = l_x \frac{x_o - x_i}{L_{io}} + l_y \frac{y_o - y_i}{L_{io}} + l_z \frac{z_o - z_i}{L_{io}} \quad .$$

The scalar differential length along the ray path is

$$\xrightarrow{\text{identity}} (32) \quad dL = l_L \, d\mathbb{L} \quad ;$$

hence

$$\xrightarrow[28,31]{32} (33) \quad dL = \frac{x_o - x_i}{L_{io}} dx + \frac{y_o - y_i}{L_{io}} dy + \frac{z_o - z_i}{L_{io}} dz \quad .$$

The equation of the straight line ray is

$$\xrightarrow{\text{geometry}} (34) \quad \frac{x - x_i}{x_o - x_i} = \frac{y - y_i}{y_o - y_i} = \frac{z - z_i}{z_o - z_i} \quad .$$

The coordinate differentials are consequently related by

$$\xrightarrow{34} (35) \quad \frac{dx}{x_o - x_i} = \frac{dy}{y_o - y_i} = \frac{dz}{z_o - z_i} \quad .$$

Eliminating the transverse coordinate differential, dx and dy, from the expression for the differential path length gives

$$\xrightarrow[35]{33} (36) \quad dL = \frac{x_o - x_i}{L_{io}} \frac{x_o - x_i}{z_o - z_i} dz + \frac{y_o - y_i}{L_{io}} \frac{y_o - y_i}{z_o - z_i} dz + \frac{z_o - z_i}{L_{io}} dz \quad .$$

This simplifies to

$$\xrightarrow[29]{36} (37) \quad dL = \frac{L_{io}}{z_o - z_i} dz \quad .$$

G.4 Attenuation Integral Evaluation

The attenuation integral can now be expressed as

$$\xrightarrow[22,37]{4} (38) \quad A = \frac{L_{io}}{z_o - z_i} \frac{\nu_r \omega_{pr}^2 z_r^4}{2c\omega^2} \int_{z_i}^{z_o} \frac{dz}{z^4 \sqrt{1 - \left(\frac{\omega_{pr} z_r}{\omega} \frac{z_r}{z}\right)^2}} \quad .$$

Integration is simplified by using the normalized parameter

$$\xrightarrow{\text{sym def}} (39) \quad \zeta = \frac{\omega z}{\omega_{pr} z_r} \quad .$$

The integration differential is

$$\xrightarrow{39} (40) \quad d\zeta = \frac{\omega}{\omega_{pr} z_r} dz$$

and the integration limits are

$$\xrightarrow{39} (41) \quad \zeta_{i,o} = \frac{\omega z_{i,o}}{\omega_{pr} z_r} \quad .$$

Hence, the attenuation integral can be expressed by

$$\xrightarrow[39,40,41]{38} (42) \quad A = \frac{L_{io}}{\zeta_o - \zeta_i} \frac{\nu_r \omega^2}{2c\omega_{pr}^2} \int_{\zeta_i}^{\zeta_o} \frac{d\zeta}{\zeta^4 \sqrt{1 - \zeta^{-2}}} \quad .$$

Using

$$\xrightarrow{\text{RE3(283.01)}}(43)\quad \int \frac{2\zeta}{\zeta^3\sqrt{\zeta^2-1}} = \frac{1}{2\zeta^2}\sqrt{\zeta^2-1} + \tfrac{1}{2}\cos^{-1}\frac{1}{\zeta}$$

gives

$$\xrightarrow{42,43}(44)\quad A = \frac{L_{io}}{z_o - z_i}\frac{\nu_r z_r \omega}{4c\omega_{pr}}\left[\frac{\sqrt{1-\zeta_o^{-2}}}{\zeta_o}\sqrt{1-\zeta_o^{-2}} + \cos^{-1}\frac{1}{\zeta_o} - \cos^{-1}\frac{1}{\zeta_i}\right]$$

for the attenuation of the signal ray passing through the ion exhaust beam.

G.5 Attenuation of Signal Rays Passing Through Axis of Symmetry

The worst possible conditions which might exist are of special interest. The class of propagation paths having the largest attenuationare those for which the signal ray passes through the z-axis. Should the attenuation along these paths be insignificant, this problem could be dismissed, otherwise it would be necessary to determine the results for all paths in order to determine the effective attenuation of a signal beam.

Because of the circular cylindrical symmetry of the ion exhaust beam, it is appropriate to use circular cylindrical coordinates. These are related to rectangular coordinates via

$$\xrightarrow{\text{Fig. G.1}}(45)\quad \begin{bmatrix} x \\ y \\ z \end{bmatrix} = \begin{bmatrix} \rho\cos\varphi \\ \rho\sin\varphi \\ z \end{bmatrix} .$$

Since the attenuation of a signal ray lying in a φ - constant plane is independent of the φ - angle, it is convenient to choose the coordinate of the ray entrance point into the ion exhaust beam such that

$$\xrightarrow[\varphi_1 = \pi/2]{45} (46) \quad \begin{bmatrix} x_i \\ y_i \end{bmatrix} = \begin{bmatrix} 0 \\ \rho_i \end{bmatrix} .$$

With this choice and the ray passing through the z-axis, the ray exit point from the ion exhaust beam is given by

$$\xrightarrow[45, 46]{\text{Fig. G.1}} (47) \quad \begin{bmatrix} x_o \\ y_o \end{bmatrix} = \begin{bmatrix} 0 \\ -\rho_i - (z_o - z_i) \tan\theta_h \end{bmatrix} .$$

Hence

$$\xrightarrow[46, 47]{29} (48) \quad \frac{L_{io}}{z_o - z_i} = \sqrt{1 + \left(\frac{2\rho_i}{z_o - z_i} + \tan\theta_h\right)^2} .$$

The attenuation can now be expressed by

$$\xrightarrow[48]{44} (49) \quad A = \frac{\nu_r z_r \omega}{4c\,\omega_{pr}} \sqrt{1 + \left(\frac{2\rho_i}{z_o - z_i} + \tan\theta_h\right)^2} \left[\frac{\sqrt{1 - \zeta_o^{-2}}}{\zeta_o} - \frac{\sqrt{1 - \zeta_i^{-2}}}{\zeta_i} + \cos^{-1}\frac{1}{\zeta_o} - \cos^{-1}\frac{1}{\zeta_i} \right] .$$

To check the above equation, two special cases are separately derived: one for which the signal ray is parallel to the z-axis, $A_{||}$, and the other for which the signal ray is perpendicular to the z-axis, $A_{\perp}$.

G.6 Attenuation of Signal Rays Parallel to the Axis of Symmetry

For the signal ray parallel to the symmetry axis the total attenuation is given by

$$\xrightarrow{4} (50) \quad A_{||} = \int_{z_i}^{z_o} \alpha(z)\,dz .$$

Hence

$$\xrightarrow[22]{50} (51) \quad A_{\parallel} = \frac{\nu_r \omega_{pr}^2 z_r^4}{2c\omega^2} \int_{z_i}^{z_o} \frac{dz}{z^4 \sqrt{1 - \left(\frac{\omega_{pr}}{\omega} \frac{z_r}{z}\right)^2}} \quad .$$

This checks (38) with $L_{io} = z_o - z_i$ and hence integrates to (44) with this change.

G.7 Attenuation of Signal Rays Perpendicular to the Axis of Symmetry

The attenuation factor does not vary over a path which is perpendicular to the axis of symmetry; hence

$$\xrightarrow{4} (52) \quad A_{\perp} = \alpha(z) L_{\perp} \quad .$$

The length of the internal path perpendicular to, and through, the z-axis is given by

$$\xrightarrow{\text{Fig. G.1}} (53) \quad L_{\perp} = 2z \tan\theta_h \quad .$$

Consequently

$$\xrightarrow[22,\,53]{52} (54) \quad A_{\perp} = \frac{\nu_r \omega_{pr}^2 z_r^4 \tan\theta_h}{c\omega^2 z^3 \sqrt{1 - \left(\frac{\omega_{pr}}{\omega} \frac{z_r}{z}\right)^2}} \quad .$$

In terms of the normalized parameter ζ this is

$$\xrightarrow[39]{54} (55) \quad A_{\perp} = \frac{\nu_r \omega_{zr} \tan\theta_h}{c\omega_{pr} \zeta^2 \sqrt{\zeta^2 - 1}} \quad .$$

The reduction of (48) to the transverse case involves the evaluation of the indeterminate form

$$\xrightarrow[z_o \to z_i]{49} (56) \quad A_\perp = \frac{\nu_r \omega^2}{4c\omega_{pr}^2} \lim_{z \to z_i} \sqrt{(z_o - z_i)^2 + \left[2\rho_i + (z_o - z_i)\tan\theta_h\right]^2} \cdot$$

$$\times \lim_{\zeta_o \to \zeta_i} \left[\frac{\sqrt{\frac{\zeta_o^2 - 1}{\zeta_o^2}} - \sqrt{\frac{\zeta_i^2 - 1}{\zeta_i^2}} + \cos^{-1}\frac{1}{\zeta_o} - \cos^{-1}\frac{1}{\zeta_i}}{\zeta_o - \zeta_i} \right]$$

The first limit factor is trivial. Using the limit definition of the derivatives to evaluate the second limit factor gives

$$\xrightarrow{56} (57) \quad A_\perp = \frac{\nu_r \omega^2 \rho_i}{2c\omega_{pr}^2} \frac{d}{d\zeta} \left[\frac{\sqrt{\zeta^2 - 1}}{\zeta^2} + \cos^{-1}\frac{1}{\zeta} \right] .$$

Using signal ray path length, which is the ion exhaust beam diameter for this case

$$\xrightarrow{\text{Fig. G.1}} (58) \quad L_\perp = 2\rho_i$$

and differentiating gives

$$\xrightarrow[57]{56} (59) \quad A = \frac{\nu_r \omega^2 L_\perp}{4c\omega_{pr}^2} \left[-\frac{2}{\zeta^3}\sqrt{\zeta^2 - 1} + \frac{1}{2\zeta^2} \frac{2\zeta}{\sqrt{\zeta^2 - 1}} - \frac{1}{\sqrt{1 - \zeta^{-2}}}\left(-\frac{1}{\zeta^2}\right) \right] .$$

This simplifies to

$$\xrightarrow{59} (60) \quad A_\perp = \frac{\nu_r \omega^2 L_\perp}{2c\omega_{pr}^2 \zeta^3 \sqrt{\zeta^2 - 1}} .$$

Hence the attenuation of a signal ray passing through and perpendicular to the ion exhaust beam axis is given by

$$\xrightarrow[53]{60} (61) \quad A_\perp = \frac{\nu_r \omega z_r \tan\theta_h}{c\omega_{pr} \zeta^2 \sqrt{\zeta^2 - 1}} .$$

This checks (55), thereby validating (49) for the transverse ray case, and hence its likelihood for the more general case.

G.8 Case for Signal Frequency Substantially above Plasma Frequency

If the signal frequency is larger (3 times or more) than the plasma frequency, the attenuation formula simplifies to

$$\xrightarrow[\omega^2 >> \omega_{po}^2]{38} (62) \quad A_S = \frac{\nu_r \omega^2_{pr} z_r^4 L_{io}}{2c\omega^2(z_o - z_i)} \int_{z_i}^{z_o} \frac{dz}{z^4} \quad .$$

This is true for most cases of immediate interest according to (13). Integrating gives

$$\xrightarrow{62} (63) \quad A_S = \frac{\nu_r \omega^2_{pr} z_r^4 L_{io}}{6c\omega^2(z_o - z_i)} \left(\frac{1}{z_i^3} - \frac{1}{z_o^3}\right) \quad .$$

Expressing in terms of the normalized ζ coordinate gives

$$\xrightarrow[39]{63} (64) \quad A_S = \frac{\nu_r \omega^2 L_{io}}{6c\omega^2_{pr}(\zeta_o - \zeta_i)} \left(\frac{1}{\zeta_i^3} - \frac{1}{\zeta_o^3}\right) \quad .$$

This can be checked against the more general expression (43) by using

$$\xrightarrow{\text{RE3 (5.3)}} (65) \quad \sqrt{1 - x} = 1 - \tfrac{1}{2}x - \frac{1}{8}x^2 - \frac{1}{16}x^3 - \frac{5}{128}x^4 - \cdots$$

and

$$\xrightarrow{\text{RE3 (502)}} (66) \quad \cos^{-1}x = \frac{\pi}{2} - x - \frac{1}{6}x^3 - \frac{3}{40}x^5 \ \ldots\ldots \quad .$$

Thus the expansion for the attenuation is given by

$$\xrightarrow[39, 65, 66]{43} (67) \quad A = \frac{\nu_r \omega^2 L_{io}}{4c\omega^2_{pr}(\zeta_o - \zeta_i)} \left[\frac{1}{\zeta}\left(1 - \frac{1}{2\zeta^2} - \frac{1}{2\zeta^2} - \frac{1}{8\zeta^4} - \ldots\right) + \frac{\pi}{2} - \frac{1}{\zeta} - \frac{1}{6\zeta^3} - \cdots\right]_{\zeta_i}^{\zeta_o}$$

Simplifying gives

$$\xrightarrow{67}(68) \quad A = \frac{\nu_r \omega_{pr}^2 L_{io}}{4c\omega_{pr}^2(\zeta_o - \zeta_i)} \left[\frac{\pi}{2} - \frac{2}{3\zeta^3} - \frac{1}{5\zeta^5} - \cdots\right]\Bigg|_{\zeta_i}^{\zeta_o} .$$

Inserting the limits gives

$$\xrightarrow{68}(69) \quad A = \frac{\nu_r \omega^2 L_{io}}{6c\omega_{pr}^2(\zeta_o - \zeta_i)} \left[\frac{1}{\zeta_i^3} - \frac{1}{\zeta_o^3} + \frac{3}{10\zeta_i^5} - \frac{3}{10\zeta_o^5} + \cdots\right] .$$

This checks the approximation given by (64).

G.9 Preparation of Attanuation Expressions for Graphing

The normalized parameter ζ introduced in (38) to facilitate integration, is not convenient for comparison of attenuation caused by different ion rocket exhaust beams because the normalizing factor z_r varies from case to case. The divergence angle, the plasma frequency, and the initial beam radius differ for various cases; hence these quantities should not be implicitly contained in the normalized distance. The frequency range of interest is

$$\xrightarrow{\text{Chap. I}}(70) \quad 2.1 \text{ GHz} \leq f \leq 2.3 \text{ GHz} .$$

The corresponding wavelength range is

$$\xrightarrow{70}(71) \quad 14.28 \geq \lambda \geq 13.04 \text{ cm} .$$

Since the frequency range is relatively narrow, it would be satisfactory to normalize the distance with respect to the wavelength (or some suitable multiple of the wavelength) of the center frequency. The center frequency is

$$\xrightarrow{70}(72) \quad f_o = 2.2 \text{ GHz} ,$$

and hence, the center frequency wavelength is

$$\xrightarrow{72} (73) \quad \lambda_o = 13.63 \text{ cm} \quad .$$

More generally, normalization can be made for any frequency in the range; for example, the distance can be normalized directly with the signal wavelength

$$\xrightarrow{\text{sym def}} (74) \quad \delta = \frac{z}{\lambda} \quad .$$

As long as the parameters do not vary radically with the frequency, this normalization is not likely to be misleading. The previous normalized distance in terms of the new normalized distance is given by

$$\xrightarrow[74]{39} (75) \quad \zeta = \frac{\omega \lambda \delta}{\omega_{pr} z_r} \quad .$$

It is more convenient to express this by the form,

$$\xrightarrow{75} (76) \quad \zeta = K\delta \quad ,$$

where K is the dimensionless ratio

$$\xrightarrow{\text{sym def}} (77) \quad K = \frac{\omega \lambda}{\omega_{pr} z_r} \quad .$$

Since the initial beam radius b_r and the beam divergence half angle θ_h are specified more directly than the ion exhaust beam exit plane coordinate z_r, it is more appropriate to eliminate z_r, to give

$$\xrightarrow[C\text{-}124,19]{77} (78) \quad K = \frac{c}{f_{pr} b_r} \tan\theta_h \quad .$$

In terms of the particle density

$$\xrightarrow[E\text{-}55,\,A\text{-}3]{78} (79) \quad K = \frac{3.34 \times 10^7 \tan\theta_h}{b_r \sqrt{n_{er}}} \quad .$$

In terms of the normalized distance δ, the attenuation through the ion exhaust beam is given by

$$\xrightarrow[19,76]{49} (80) \quad A = \frac{\omega \nu_r b_r \cot\theta_h}{4c\omega_{pr}} \sqrt{1 + \left(\frac{2r_i}{\delta_o - \delta_i} + \tan\theta_h\right)^2} \left[\frac{\sqrt{K^2\delta_o^2 - 1}}{K^2\delta_o^2} \right.$$

$$\left. - \frac{\sqrt{K^2\delta_i^2 - 1}}{K^2\delta_i^2} + \cos^{-1}\frac{1}{K\delta_o} - \cos^{-1}\frac{1}{K\delta_i} \right]$$

where

$$\xrightarrow{\text{sym def}} (81) \quad r_i = \frac{\rho_i}{\lambda} \quad .$$

The special cases are

$$\xrightarrow[19,76]{55} (82) \quad A_\perp = \frac{\nu_r b_r \omega}{c\omega_{pr} K^2 \delta^2 \sqrt{K^2\delta^2 - 1}}$$

and

$$\xrightarrow[76,78]{64} (83) \quad A_S = \frac{\nu_r b_r \omega \frac{L_{io}}{\lambda} \cot\theta_h}{6c\omega_{pr}(\delta_o - \delta_i)K^3} \left(\frac{1}{\delta_i^3} - \frac{1}{\delta_o^3}\right) \quad .$$

It is convenient to introduce the dimensionless factor

$$\xrightarrow{\text{sym def}} (84) \quad B = \frac{\nu_r \omega b_r}{c\omega_{pr}} = \frac{\nu_r}{f_{pr}} \frac{b_r}{\lambda} \quad .$$

In terms of this factor the attenuation formulae are

$$\xrightarrow[84]{80} (85) \quad A = \frac{B}{4} \cot\theta_h \sqrt{1 + \left(\frac{2r_i}{\delta_o - \delta_i} + \tan\theta_h\right)^2} \left[\frac{\sqrt{K^2\delta_o^2 - 1}}{K^2\delta_o^2}\right.$$

$$\left. - \frac{\sqrt{K^2\delta_i^2 - 1}}{K^2\delta_i^2} + \cos^{-1}\frac{1}{K\delta_o} - \cos^{-1}\frac{1}{K\delta_i}\right]$$

and

$$\xrightarrow[84]{82} (86) \quad A_\perp = \frac{B}{K^2\delta^2\sqrt{K^2\delta^2 - 1}}$$

and

$$\xrightarrow[84]{83} (87) \quad A_S = \frac{B\,\frac{L_{io}}{\lambda}\cot\theta_h}{6(\delta_o - \delta_i)K^3}\left(\frac{1}{\delta_i^3} - \frac{1}{\delta_o^3}\right) .$$

Using

$$\xrightarrow[74,81]{48} (88) \quad \frac{L_{io}}{\lambda(\delta_o - \delta_i)} = \sqrt{1 + \left(\frac{2r_i}{\delta_o - \delta_i} + \tan\theta_h\right)^2}$$

gives

$$\xrightarrow[88]{87} (89) \quad A_S = \frac{B\cot\theta_h}{6K^3}\sqrt{1 + \left(\frac{2r_i}{\delta_o - \delta_i} + \tan\theta_h\right)^2}\left(\frac{1}{\delta_i^3} - \frac{1}{\delta_o^3}\right) .$$

G.10 Transverse vs. Parallel Path Attenuations

A special case of interest is that for which the signal ray enters but does not leave the ion exhaust beam cone:

$$\xrightarrow[\delta_o \to \infty]{89} (90) \quad A_{||S} = \frac{B}{6\sin\theta_h K^3\delta^3} .$$

For the special case for which the signal frequency is sufficiently above the plasma resonant frequency,

$$\xrightarrow[\omega^2 >> \omega_{p,77}^2]{86} (91) \quad A_{\perp S} = \frac{B}{K^3 \delta^3} \quad .$$

Consequently,

$$\xrightarrow[91]{90} (92) \quad A_{\| S} = \frac{A_{\perp S}}{6 \sin\theta_h} \quad .$$

The two cases are equal if

$$\xrightarrow[A_{\| S} = A_S]{92} (93) \quad \theta_h = \sin^{-1} \frac{1}{6} = 9.6^o \quad .$$

Consequently

$$\xrightarrow{92,93} (94) \quad A_{\| S} > A_{\perp S} \quad \text{if} \quad \theta_h < 9.6^o \quad ,$$

and

$$\xrightarrow{92,93} (95) \quad A_{\| S} < A_{\perp S} \quad \text{if} \quad \theta_h > 9.6^o \quad .$$

It is expected that under conditions of interest for most ion exhaust beams the divergence angle will be less than 9.6^o. However, this point should be investigated.

G.11 Transverse Attenuation Case

If an upper bound on the collision frequency is considered to be provided by a one electron volt speed differential between the electrons and ions, then in terms of the ion exhaust beam parameter, the collision frequency to plasma frequency ratio

$$\xrightarrow[B-55]{B-122} (96) \quad \frac{\nu_r}{f_{pr}} = 3.06 \times 10^{-3} \sqrt{\frac{i_b}{I_{sp}}} \quad .$$

It should be noted here that the collision frequency utilized is that determined by a drift velocity of the electrons with respect to the ions which is many times the mean thermal speed of the electrons. If thermal equilibrium existed between the electrons and ions, with the electron's temperature being that of the emitter, then the collision frequency would be more than an order of magnitude larger, compare (B-118) and (B-122), in which case the signal ray attenuation within the ion exhaust beam would be very significant. The parameter B for the case considered is consequently given by

$$\xrightarrow[96,2\text{-}1]{84} (97) \quad B = 1.54 \sqrt{\frac{P_b}{I_{sp}^3}} \quad .$$

The parameter K is given by

$$\xrightarrow[B\text{-}55,2\text{-}1,73]{79} (98) \quad K = 6.12 \times 10^{-4} \tan\theta_h \frac{I_{sp}^{3/2}}{\sqrt{P_b}} \quad .$$

The normalized distance is

$$\xrightarrow[B\text{-}69]{74} (99) \quad \delta = \frac{b}{\lambda} \cot\theta_h$$

consequently,

$$\xrightarrow{98 \times 99} (100) \quad K_\delta = \frac{6.12 \times 10^{-4} b I_{sp}^{3/2}}{\lambda \sqrt{P_b}} \quad .$$

Expressing the ion exhaust beam radius in terms of other ion exhaust beam parameter and using the wavelength for the center frequency give

$$\xrightarrow[73,B\text{-}66]{100} (101) \quad K_\delta = 0.305 \sqrt{\frac{I_{sp}}{i_b}} \quad .$$

Hence the attenuation of a signal ray which is perpendicular to and passes through the ion exhaust beam axis is given by

$$\xrightarrow[97,101]{86} (102) \quad A_{\perp} = \frac{54.3\sqrt{i_b^3 P_b}}{I_{sp}^3\sqrt{1 - 10.7 i_b/I_{sp}}}$$

Converting from nepers to dbs gives

$$\xrightarrow[\substack{1 \text{ neper} = \\ 8.7 \text{ db}}]{102} (103) \quad 2A_{\perp} = \frac{943\sqrt{i_b^3 P_b}}{I_{sp}^3\sqrt{1 - 10.7 i_b/I_{sp}}} .$$

The net attenuation through a perpendicular path within the ion exhaust beam for the case of the Jupiter orbiter example is given by

$$\xrightarrow[2\text{-}3]{103} (104) \quad 2A_{\perp} = 7.6 \times 10^{-4} \text{ db}$$

at the exit plane, which is the maximum value for this case and decreases with inverse second power of distance along the ion exhaust beam axis. While the attenuation through some diagonal path may be somewhat higher it is not expected to very much higher. Hence for the ion rocket engines contemplated for the next few years the losses due to attenuation in the ion exhaust beam interior appear to be negligible.

It should be noted that the specific impulse is very large for the above case and that the attenuation increases rapidly with decreasing specific impulse. Also, if the electron drift velocity relative to the ions were negligible, the attenuation would be substantially greater. Oscillations in the plasma may produce localized regions in which the collision cross section and hence attenuation is orders of magnitude larger than the average. Such circumstances require further investigation. Also, if much larger ion engines are required, if larger current densities are utilized and/or if lower signal frequencies are employed, the attenuation through the beam interior can be objectionably high.

APPENDIX H: SIGNAL REDUCTION DUE TO REFLECTION AT THE ION ROCKET EXHAUST BEAM SURFACE

H.1 Introduction

The signal strength is also decreased by reflections at the surface of the ion exhaust beam. The reflection losses are accounted for by the use of interface transmission factors. The analysis presented here is for the case of two reflections: one upon entering and one upon exiting the ion exhaust beam. A more extended analysis is required for cases where the ion exhaust beam is inhomogeneous over the cross section perpendicular to its symmetry axis. Because of the complexity of the general problem, this effort is limited to estimating the importance of the reflection losses under various extreme conditions. Losses for the case of normal incidence are considered first. The reflection loss becomes 100% as the incident ray approaches the critical angle. Hence, regardless of how tenuous the ion exhaust beam is, there will be a range of parameters over which the signal ray is totally blocked for the ion exhaust beam model used. Some bounds on this range are determined for the cases of reception and transmission.

H.2 Transmission Loss for Nearly Normal Incidence

For nearly normal incidence,

$$\xrightarrow{\text{condition}} (1) \quad i << 1$$

Snell's law

$$\xrightarrow{\text{D-12, D-14}} (2) \quad n = \begin{cases} \dfrac{\sin i}{\sin r} \\ \\ \dfrac{\sin r}{\sin i} \end{cases} \text{ at the } \begin{cases} \text{input} \\ \\ \text{output} \end{cases} \text{ surface}$$

gives, if the refractive index does not differ too greatly from unity,

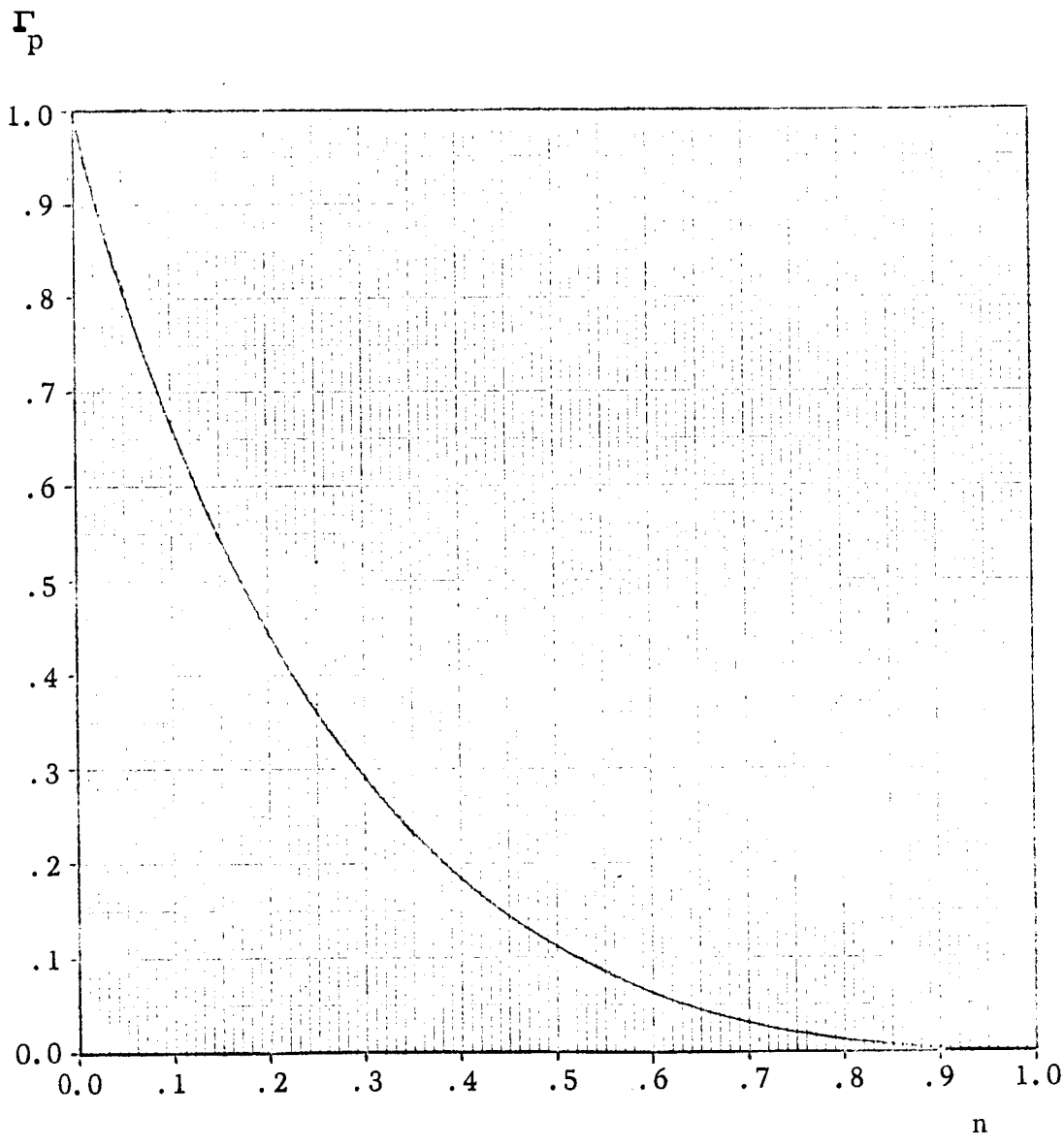

Fig. H.1 Power Reflection Coefficient Versus Index of Refraction

$\xrightarrow[1]{2}$ (3) $r << 1$.

In this case Snell's law simplifies to

$$\xrightarrow[1,3]{2} (4) \quad n = \begin{cases} \frac{i}{r} \\ \\ \frac{r}{i} \end{cases} \text{ at the } \begin{cases} \text{input} \\ \\ \text{output} \end{cases} \text{ surface,}$$

and the reflection coefficients for both E and H-waves reduce to the same thing,

$$\xrightarrow[1,3]{D\text{-}59,\ D\text{-}60} (5) \quad \Gamma_E = \Gamma_E^E = \Gamma_E^H = \frac{i - r}{i + r} \ .$$

Consequently

$$\xrightarrow[3]{5} (6) \quad \Gamma_E = \Gamma_E^E = \Gamma_E^H = \begin{cases} \frac{n - 1}{n + 1} \\ \\ \frac{1 - n}{1 + n} \end{cases} \text{ at the } \begin{cases} \text{input} \\ \\ \text{output} \end{cases} \text{ surface.}$$

The power transmission loss factor is thus

$$\xrightarrow[6]{D\text{-}85} (7) \quad \Gamma_P = \left(\frac{n - 1}{n + 1}\right)^2 \ .$$

For refractive indices near zero and unity this simplifies to

$$\xrightarrow{7} (8) \quad \Gamma_P = \begin{cases} 1 - 4n & n << 1 \\ \\ \left(\frac{n - 1}{2}\right)^2 & n - 1 << 1 \end{cases} \ .$$

The power reflection coefficient is graphed in Fig. H.1.

The index of refraction for a plasma is given by

$$\xrightarrow{\text{E-125}} (9) \quad n_p = \begin{cases} \sqrt{1 - \dfrac{\omega_p^2}{\omega^2}} & \omega < \omega_p \\ \dfrac{\nu \omega_p}{2\omega^2} \Big/ \sqrt{1 - \dfrac{\omega^2}{\omega_p^2}} & \omega < \omega_p \end{cases}$$

if the collision frequency is sufficiently small compared to the signal frequency.

For small values of the plasma resonant frequency

$$\xrightarrow{\text{restriction}} (10) \quad \frac{f_p}{f} = \frac{\omega_p}{\omega} < \frac{1}{3}$$

the expression for the refractive index simplifies to

$$\xrightarrow[10]{9} (11) \quad n_p \approx 1 - \frac{\omega_p^2}{2\omega^2} \qquad \omega > 3\omega_p \quad .$$

Consequently the power reflection coefficient expression simplifies to

$$\xrightarrow[10,11]{7} (12) \quad \Gamma_p = \frac{\omega_p^4}{16\omega^4} = \frac{f_p^4}{16 f^4} \qquad \omega > 3\omega_p \quad .$$

For the case of the center frequency

$$\xrightarrow[f=2.2\,GHz]{\text{E-56}} (13) \quad \frac{\omega_p}{\omega} = 4.08 \times 10^{-9} \sqrt{n_e} \quad .$$

Expressing the normalized plasma frequency in terms of ion beam parameters gives

$$\xrightarrow[B-55]{13} (14) \quad \frac{\omega_p}{\omega} = 3.26 \sqrt{\frac{i_b}{I_{sp}}} \quad .$$

Consequently the plasma refractive index can be expressed in the form,

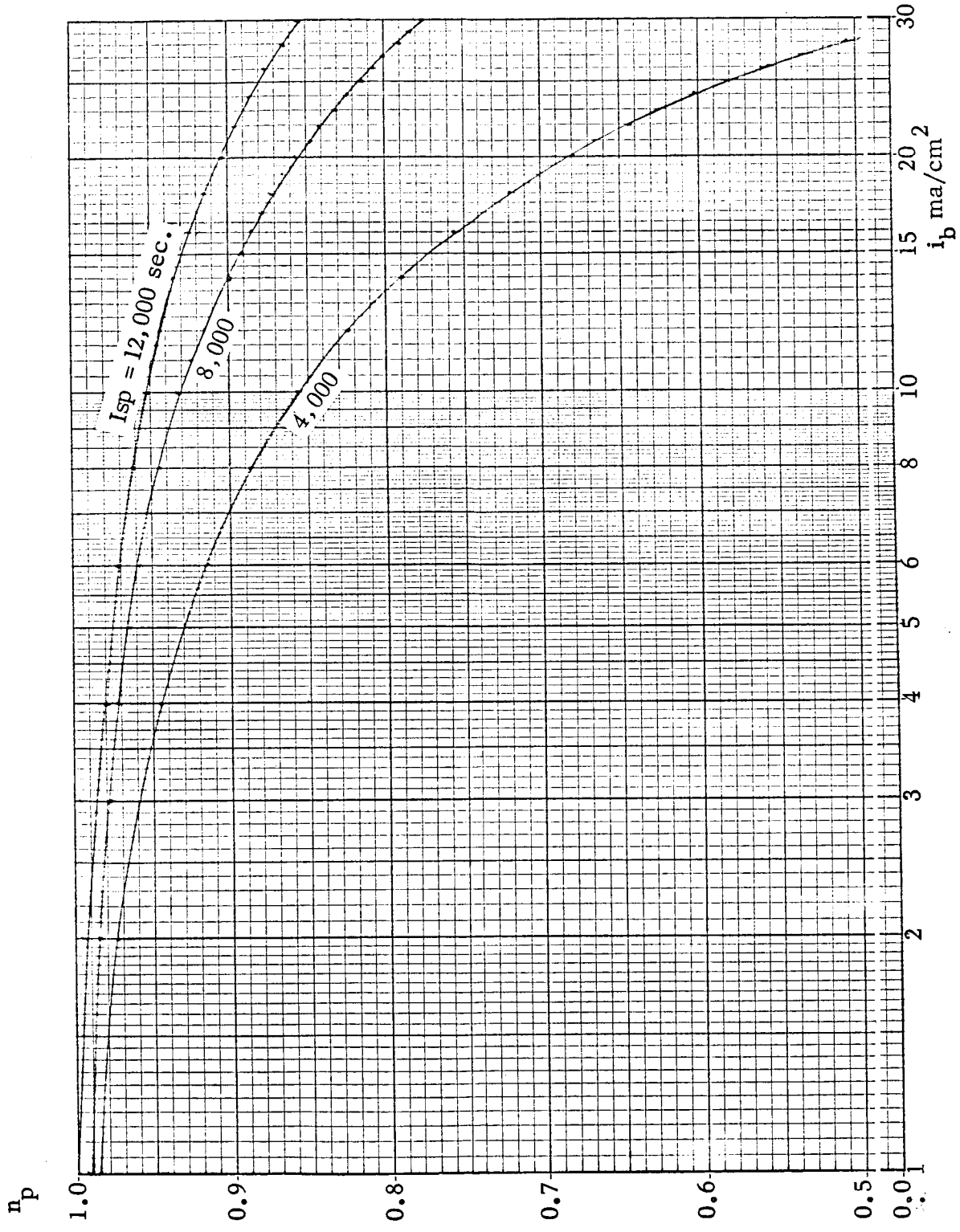

Fig. H.2 Refractive index vs current density for various specific impulses.

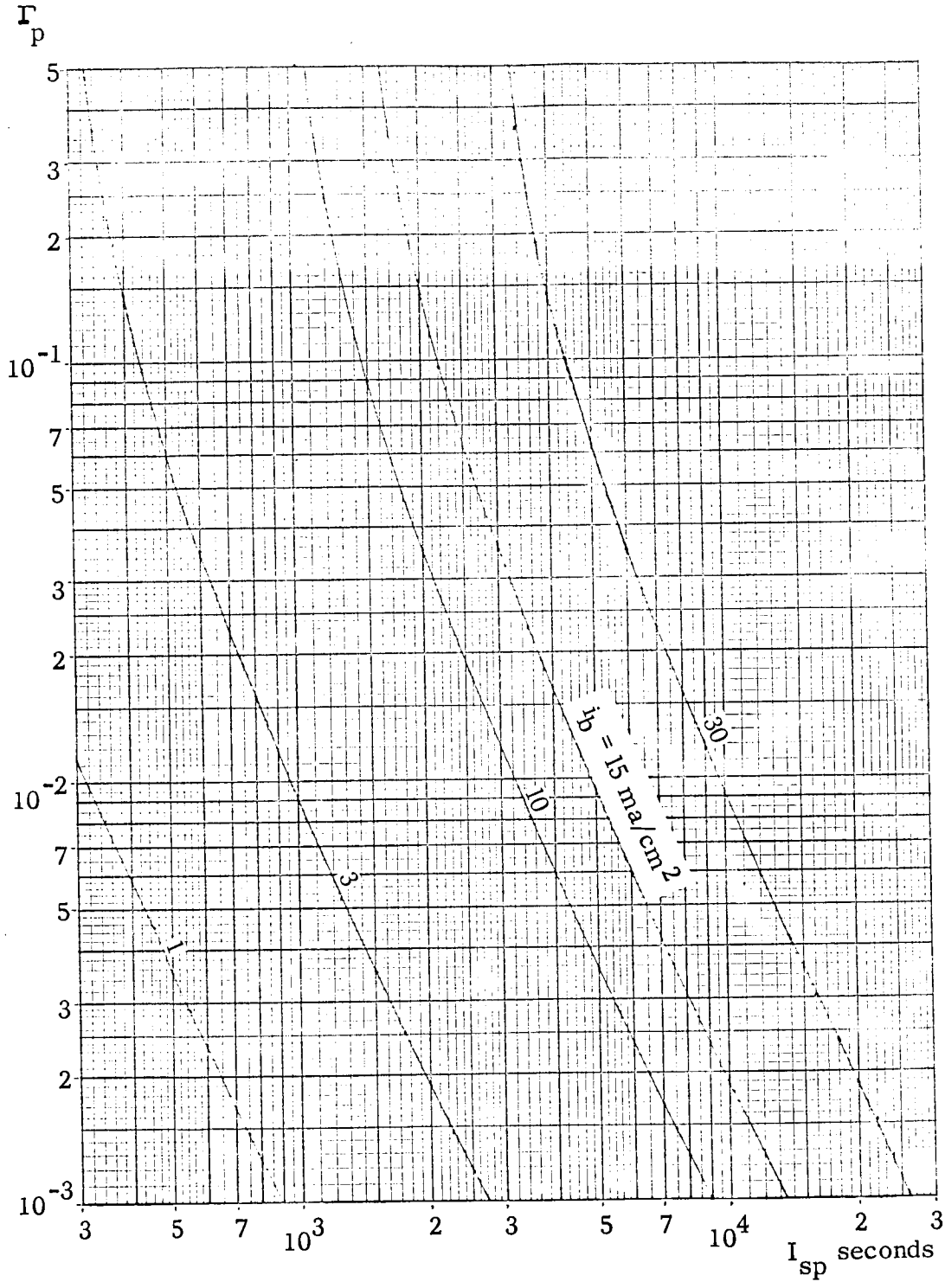

Fig. H.3 Power reflection coeeficient, Γ_p, versus specific impulse, I_{sp}, for various current densities.

$$\xrightarrow[14]{9,12} (15) \quad n_p = \sqrt{1 - 10.62 \frac{i_b}{I_{sp}}}$$

$$= 1 - 5.31 \frac{i_b}{I_{sp}}, \qquad I_{sp} > 10.62\, i_b \quad .$$

In this case, the reflection factor takes the particularly simple form

$$\xrightarrow[14]{12} (16) \quad \Gamma_p = 7.08 \frac{i_b^2}{I_{sp}^2}, \qquad \frac{1}{3} I_{sp} > 10.62\, i_b \quad .$$

The refractive index as a function of the specific impulse and ion current density is depicted in Fig. H.2. The power reflection coefficient as a function of the specific impulse and current density is depicted in Fig. H.3.

Interpretation of these curves is as follows. For refractive indices near unity, the reflection coefficient is negligible, but as the refraction index goes to zero, the reflection coefficient goes to unity as depicted in Fig. H.1. Unity reflection coefficient means total signal loss. Fig. H.2 depicts how the refractive index varies with the ion exhaust beam parameters; the smaller the specific impulse and/or the higher the ion emission current density the smaller the refractive index. Fig. H.3 gives the composite information of the previous two figures. For example, the ion emission current density of 30 ma/cm^2 curve, for a specific impulse of 12,000 seconds, gives a power reflection coefficient 0.0044. Hence, for the next generation of ion rockets anticipated, nearly normal incidence of signal rays in the chosen frequency band will not experience appreciable reflection. However, it should be noted that the power reflection coefficient becomes very large as the specific impulse drops and may become objectionally large for specific impulses in the low thousands of seconds.

H.3 Reflection Loss Considerations for Arbitrary Incidence Angle

The interface power transmission factor is

$$\xrightarrow{\text{D-88}}(17) \quad T_P = T_E^2 \sqrt{\frac{n^{\pm 2} - \sin^2 i}{1 - \sin^2 i}} \begin{Bmatrix} + \\ - \end{Bmatrix} \text{ at the } \begin{Bmatrix} \text{input} \\ \text{output} \end{Bmatrix} \text{ surface.}$$

The field transmission factors are polarization dependent; hence, each polarization has a different transmission factor.

$$\xrightarrow{\text{D-59}_2, \text{D-60}_2}(18) \quad \begin{vmatrix} \Gamma_E^E \\ \\ \Gamma_E^H \end{vmatrix} = \frac{2 \sin r \cos i}{\sin(i+r)} \begin{vmatrix} \sqrt{\frac{1}{\cos(i-r)}} \\ \\ 1 \end{vmatrix} .$$

The interface power transmission factors are plotted as functions of the incidence angles for various values of the refractive index in Fig. D.3 and D.4.

A considerable amount of labor is required to determine the reduction in signal power received by use of the above formulae. Fig. D.3 and D.4 show that a substantial reflection loss only occurs near and beyond the critical incidence angle for any value of refractive index, n, which is substantially greater than zero. Consequently, the seriousness of the reflection loss is primarily represented by the fraction of the total received or transmitted signal which is completely blocked by the ion exhaust beam. For the received signal, the area blockage is the important factor. For the transmitted signal, the solid angle blockage is the important factor. This appendix considers the blocking planar angles in the principal planes. These could be used for estimating partial bounds on the blocked solid angle and the blocked area.

The transmission coefficient dependence on the incident ray entrance position into the ion exhaust beam is of prime interest. The position is specified by a peripheral coordinate around the ion exhaust beam and longitudinal coordinate along the ion exhaust beam. The geometry for the general case is quite involved. Two special cases considered are:

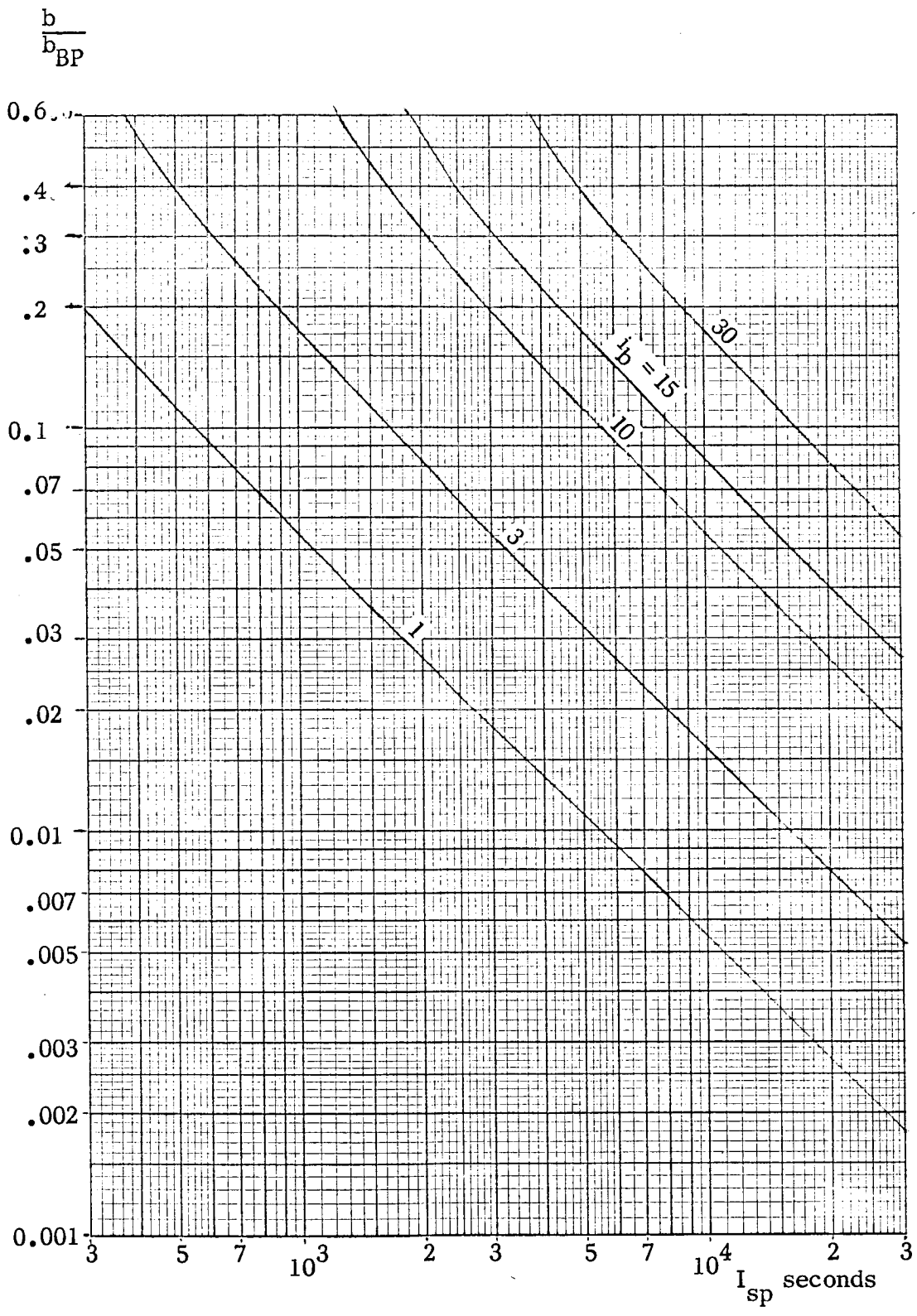

Fig. H.4 Fraction of ion exhaust beam which completely blocks plane wave perpendicular to axis of symmetry.

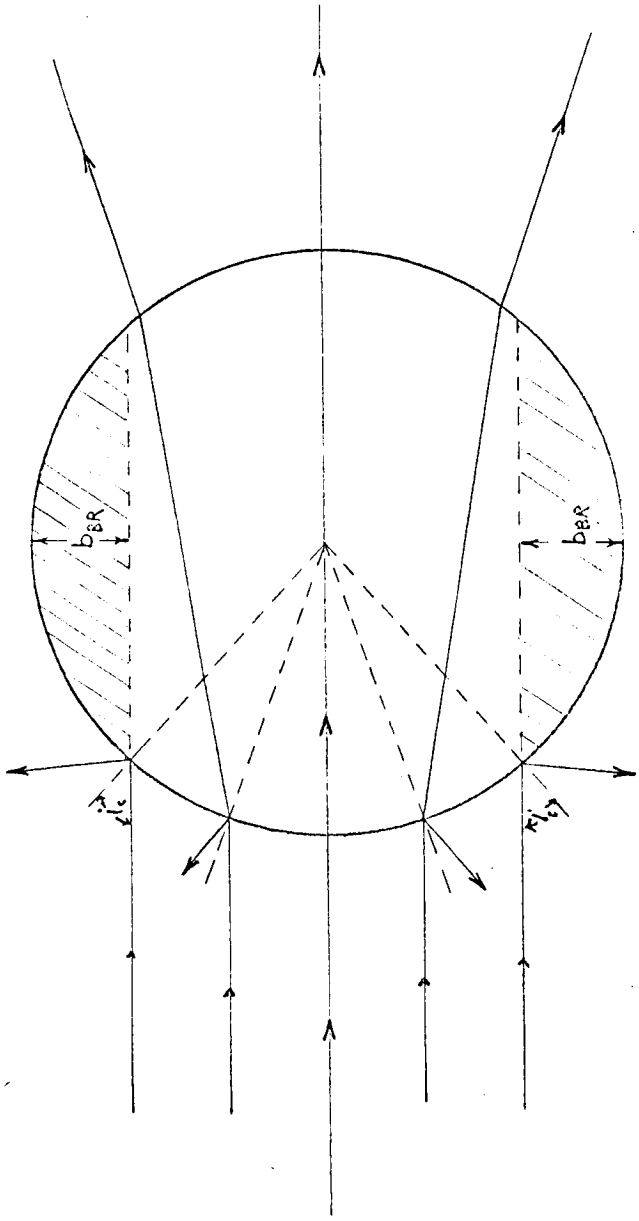

Fig. H.5 Parallel rays in the transverse plane incident on ion exhaust beam.

1. variation along the surface in the longitudinal cross section containing the axis of symmetry.
2. variation around the surface in a cross section perpendicular to the axis of symmetry.

H.4 Minimum Transverse Blockage Factor for Reception

Signal rays incident on the ion exhaust beam surface at angles equal to or greater than the critical angle are completely blocked. Fig. H.5 depicts the case for parallel rays in a plane perpendicular to the ion exhaust beam axis. For this case, the portion of the ion exhaust beam radius which completely blocks the incident ray is

$$\xrightarrow{\text{Fig. H.4}} (19) \quad b_{BR} = b(1 - \sin i_c) \quad .$$

Using the relation between the critical angle and the refractive index

$$\xrightarrow[r = \frac{1}{2}\pi]{\text{D-14}} (20) \quad n = \sin i_c \quad ,$$

gives

$$\xrightarrow[20]{19} (21) \quad \frac{b_{BR}}{b} = 1 - n \quad ,$$

and hence

$$\xrightarrow[9]{21} (22) \quad \frac{b_{BR}}{b} = 1 - \sqrt{1 - \frac{\omega_p^2}{\omega^2}} \qquad \omega > \omega_p \quad .$$

Expressing the fractional blockage in terms of specific impulse and current density gives

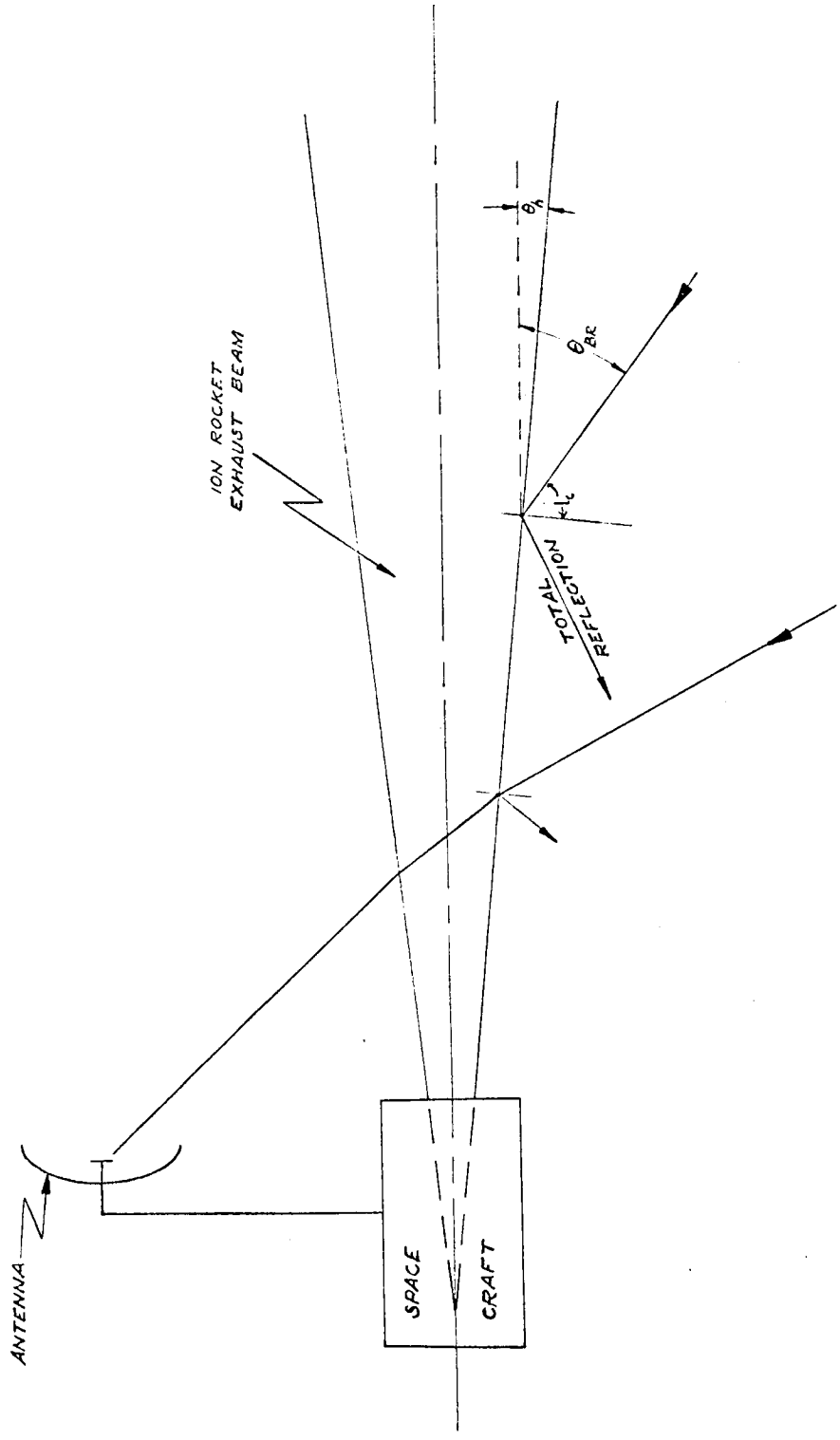

Fig. H.6 Received signal rays in the plane of the ion exhaust beam axis.

$$\xrightarrow[15]{22} (23) \quad \frac{b_{BR}}{b} = 1 - \sqrt{1 - 10.62 \frac{i_b}{I_{sp}}} \quad .$$

For large ratios of specific impulse to ion emission current density this reduces to

$$\xrightarrow{23} (24) \quad \frac{b_{BR}}{b} = 5.31 \frac{i_b}{I_{sp}} \quad .$$

The blockage ratio is plotted in Fig. H.4. For the Jupiter orbiter spacecraft example, the 15ma/cm^2 ion emission curve, for a specific impulse of 12,000 seconds gives a blockage of 0.066, i.e. 6.6 percent of the ion exhaust beam diameter completly blocks transmission of signal rays. As the incidence angle becomes more oblique to the surface, the fractional beam diameter which completely blocks signal rays increases until the entire ion exhaust beam diameter blocks the signal transmission.

H.5 Minimum Longitudinal Blockage Angle for Reception

The geometry for this case is depicted in Fig. H.6. The angular range, measured from the z-axis, for which the incoming ray will not penetrate the ion exhaust beam is given by

$$\xrightarrow{\text{Fig. H.6}} (25) \quad \theta_{BR} = \tfrac{1}{2}\pi - i_c + \theta_h \quad .$$

The refractive index as a function of position along the ion exhaust beam is given by

$$\xrightarrow[G\text{-}20]{9} (26) \quad n_p = \sqrt{1 - \left(\frac{\omega_{pr}}{\omega} \frac{z_r}{z}\right)^2} \quad .$$

A more appropriate quantity to normalize z to,is the beam radius at the exit plane,

$$\xrightarrow[G\text{-}19]{26} (27) \quad n_p = \sqrt{1 - \left(\frac{\omega_{pr}}{\omega} \frac{b_r \cot \theta_h}{z}\right)^2} \quad .$$

In terms of distance normalized with respect to wavelength

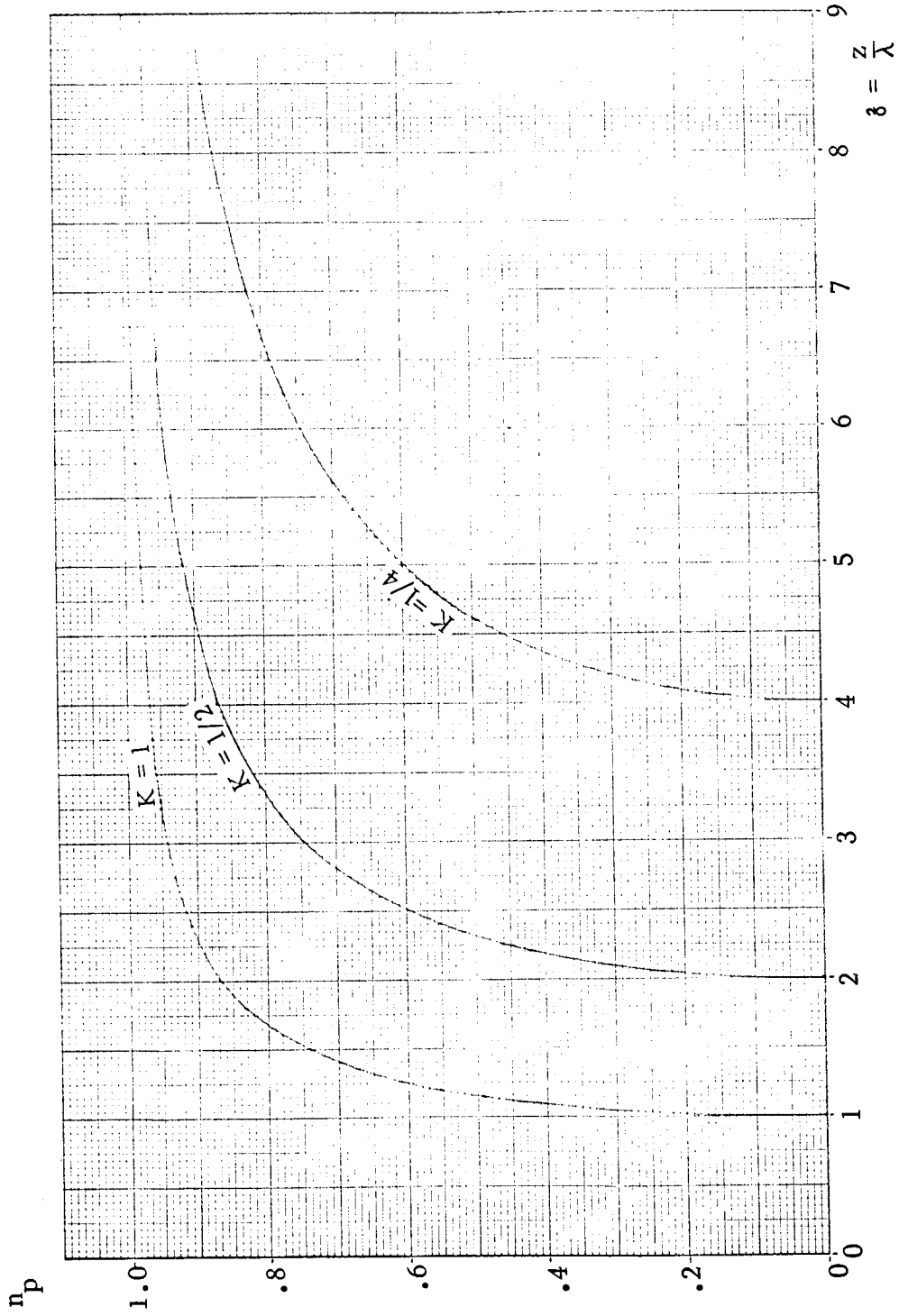

Fig. H.7 Refractive index variation along the ion exhaust beam axis for various ion beam $\left(K = \frac{c \tan \theta_h}{f_{pr} b_r}\right)$ parameter values.

$$\xrightarrow[G\text{-}73]{27} (28) \quad n_p = \sqrt{1 - \left(\frac{\omega_{pr}}{\omega} \frac{b_r}{\lambda} \frac{\cot \theta_h}{\delta}\right)^2} \quad .$$

Using the parameter K to designate the beam properties gives

$$\xrightarrow[G\text{-}77]{28} (29) \quad n_p = \sqrt{1 - \frac{1}{K^2 \delta^2}} \quad .$$

This refractive index is plotted against δ for various values of K in Fig. H.7. For refractive index values near unity, it is more convenient to use

$$\xrightarrow{20} (30) \quad n = \cos\left(\tfrac{1}{2}\pi - i_c\right)$$

to give

$$\xrightarrow[30]{29} (31) \quad \cos\left(\tfrac{1}{2}\pi - i_c\right) = \sqrt{1 - \frac{1}{K^2 \delta^2}} \quad .$$

For a plasma frequency small compared to the signal frequency,

$$\xrightarrow{\omega_p^2 \ll \omega^2} (32) \quad K^2 \delta^2 \gg 1 \quad .$$

The refractive index is near unity and the critical angle is near 90°. For this case

$$\xrightarrow[32]{31} (33) \quad 1 - \frac{1}{2}\left(\frac{\pi}{2} - i_c\right)^2 + \cdots = 1 - \frac{1}{2K^2 \delta^2} + \cdots$$

hence

$$\xrightarrow{33} (34) \quad i_c = \frac{\pi}{2} - \frac{1}{K\delta} \quad .$$

Therefore the incoming ray blocking angle range is given by

$$\xrightarrow[34]{25} (35) \quad \theta_{BR} = \frac{1}{K\delta} + \theta_h \quad .$$

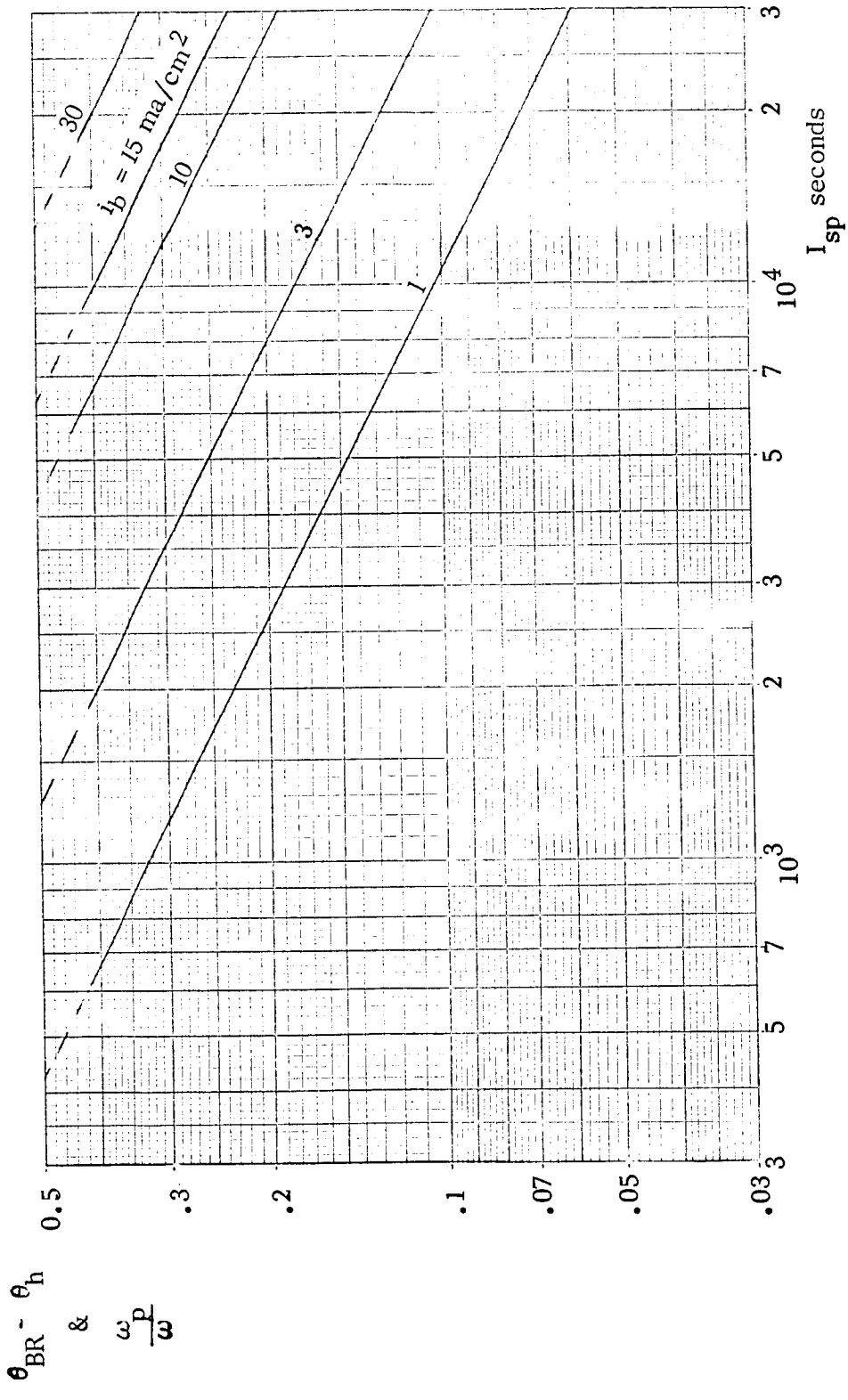

Fig. H.8 Angular plasma frequency and $\theta_{BR} - \theta_h$ versus I_{sp} and i_b.

The maximum blocking angle range is given by the minimum δ ; consequently

$$\xrightarrow[\delta = \delta_r]{35} (36) \quad \theta_{BR} = \frac{1}{K \delta_r} + \theta_h \quad .$$

Hence

$$\xrightarrow[\text{G-73/G-19, G-76}]{36} (37) \quad \theta_{BR} = \theta_h + \frac{\omega_{pr}}{\omega} \text{ radians.}$$

For this formula to be accurate, the blocking angle range must be small compared to one radian. If the blocking angle is not small compared to a radian, then (31) must be used instead of (34). One of the major unknowns that remains to be determined is the ion exhaust beam divergence angle. It is interesting to note that the normalized plasma frequency is equal to the difference between the blocking angle and the ion exhaust beam half angle

$$\xrightarrow{37} (38) \quad \frac{\omega_{pr}}{\omega} = \frac{f_{pr}}{f} = \theta_{BR} - \theta_h \quad .$$

Expressing this in terms of specific impulse and ion current density gives

$$\xrightarrow[14]{38} (39) \quad \theta_{BR} - \theta_h = \frac{\omega_{pr}}{\omega} = 3.26 \sqrt{\frac{i_b}{I_{sp}}} \quad .$$

This is graphed in Fig. H.8. The dashed portions of the curve represent the regions where the plasma frequency is not sufficiently smaller than the signal frequency for the approximation to be accurate. As an example, consider the Jupiter orbiter spacecraft design parameters, $i_b = 15 \text{ma/cm}^2$ and $I_{sp} = 12,000$ seconds which gives a blockage angle of 0.37 radians i.e. 21.1^o. This is a fairly significant blockage angle.

H.6 Blocking Angles for Transmission

The blocking angles for transmission are different from those for reception

because of the difference in the geometry between a parallel bundle of rays and a diverging bundle of rays. The overall effect on the receiver beam power and the transmitted power which is received by a distant station is the same because of reciprocity; however, the effect on an individual ray is not.

APPENDIX I: SIGNAL STRENGTH REDUCTION DUE TO SIGNAL BEAM DIVERGENCE

I.1 Introduction

The ion exhaust beam acts as a divergent lens on the signal rays passing through it as illustrated in Figs. I.1, I.2, I.3, and I.4. Figs. I.1 and I.2 depict the case for signal rays in the plane perpendicular to the ion exhaust beam axis for the cases of reception and transmission respectively. Figs. I.3 and I.4 depict the signal rays in the plane containing the ion exhaust beam axis for the cases of reception and transmission respectively.

The power-intensity-divergence transmission factor (reciprocal spreading factor) is given by

$$\xrightarrow{\text{F-20}} (1) \quad T_S = \frac{d\Omega_i}{d\Omega_o} \quad .$$

It is more convenient to think in terms of

$$\xrightarrow{\text{sym def}} (2) \quad S_\Omega = \text{the solid angle spreading (magnification) factor}$$

$$\xrightarrow{\text{geom def}} (3) \quad S_\Omega = \frac{d\Omega_o}{d\Omega_i}$$

than in terms of the power-intensity-divergence transmission factor in the formulational stage. The spreading factor varies with direction. It is convenient to divide a signal beam into differential signal beams by means of constant-coordinate surfaces which are separated by a differential coordinate change. Using φ-plane and θ-cone coordinate surfaces allows the solid-angle-spreading factor to be expressed in terms of the product of two plane-angle-spreading factors

$$\xrightarrow{\text{geometry}} (4) \quad S_\Omega = S_\varphi S_\theta$$

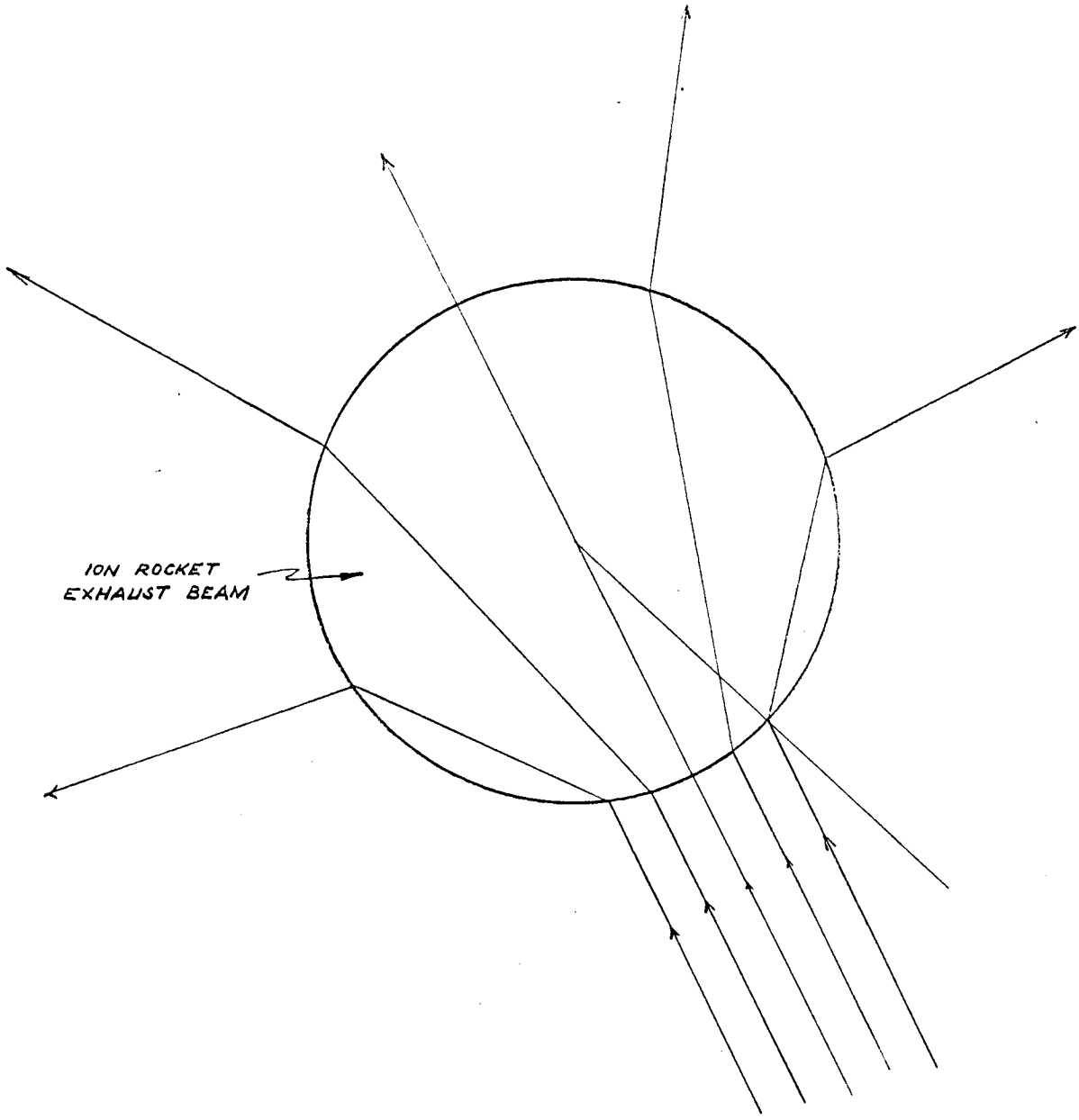

Fig. I.1. Divergence of a parallel bundle of signal rays through an ion exhaust beam cross section perpendicular to the axis of symmetry.

where

$\xrightarrow{\text{sym def}}$(5) S_φ = the azimuth angle spreading factor

and

$\xrightarrow{\text{sym def}}$(6) S_θ = the polar angle spreading factor.

The azimuth angle spreading factor is given by

$$\xrightarrow{\text{geom def}}(7) \quad S_\varphi = \frac{d\varphi_o}{d\varphi_i}$$

for the case in which the ray lies in a plane perpendicular to the z-axis. The polar spreading factor is given by

$$\xrightarrow{\text{geom def}}(8) \quad S_\theta = \frac{d\theta_o}{d\theta_i}$$

for the case in which the ray passes through the z-axis. This preliminary analysis is restricted to the cases depicted in Fig. I.1 and I.2. To obtain the spreading factors it is necessary to determine the functional relationship between the differential angles. Development of the general cases may be made in a subsequent effort if the preliminary results obtained here indicate that it is warranted. Since Fig. I.1 can be obtained as a special case of I.2, the latter is considered first.

I.2 Signal Rays in Plane Perpendicular to Symmetry Axis

The signal beam spreading in the plane perpendicular to the ion beam symmetry axis is depicted in Figs. I.1 and I.2. The azimuth angle φ, about the ion beam symmetry axis is taken as the independent variable. The incidence angle is related to φ by

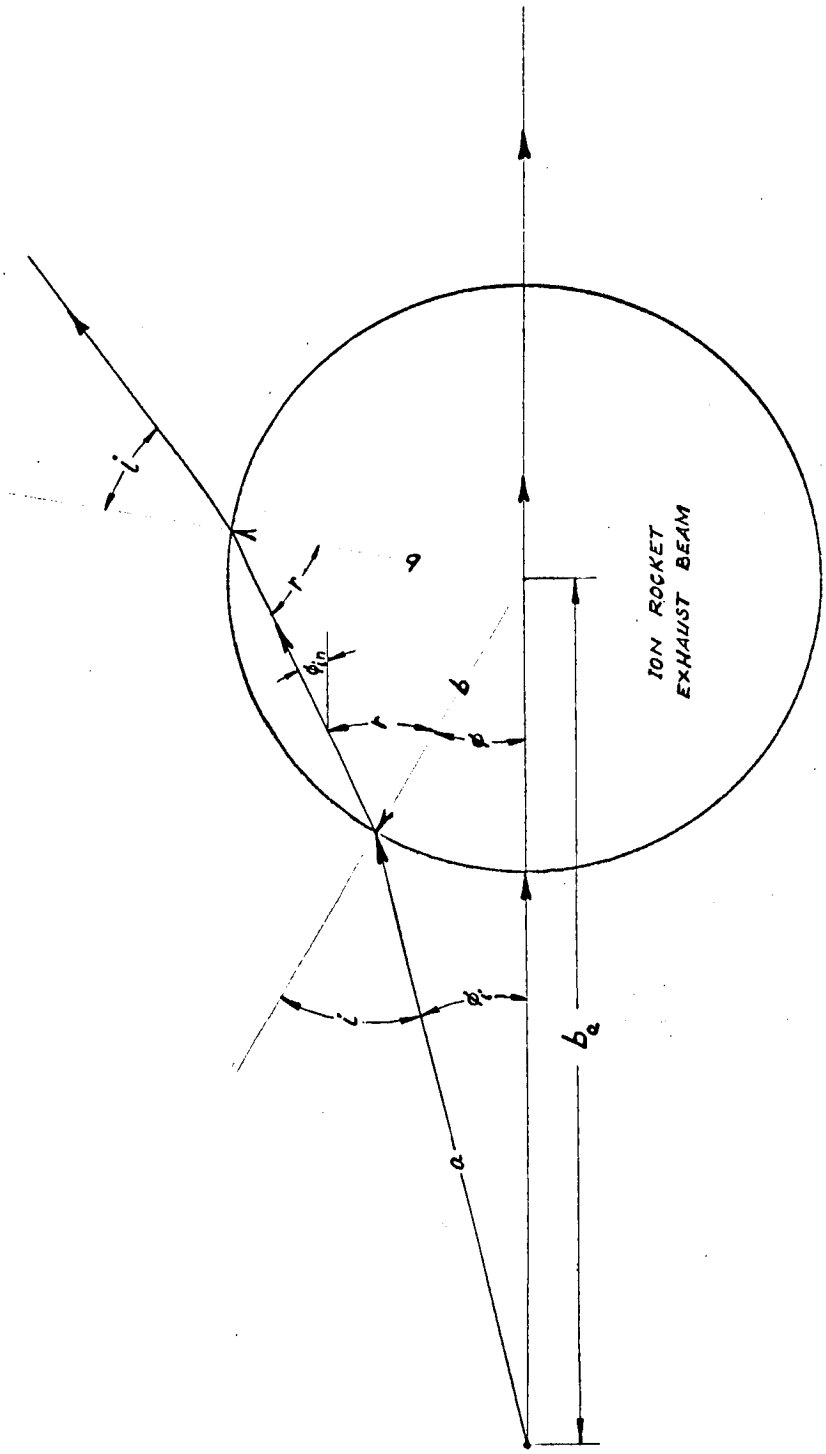

Fig. I.2 Divergence of a non parallel bundle of signal rays in a plane perpendicular to the ion exhaust beam axis of symmetry.

$$\xrightarrow{\text{Fig. I.2}} (9) \quad \frac{b_a}{\sin(\pi - i)} = \frac{b}{\sin(i - \varphi)} = \frac{a}{\sin \varphi} \quad .$$

Consequently,

$$\xrightarrow{9_1} (10) \quad \sin i \cos \varphi - \cos i \sin \varphi = \frac{b}{b_a} \sin i \quad .$$

Hence

$$\xrightarrow{10} (11) \quad \tan i = \tan \varphi + \frac{b}{b_a} \frac{\tan i}{\cos \varphi} \quad .$$

For the case of a parallel incoming bundle of rays

$$\xrightarrow[b_a \to \infty]{11} (12) \quad i = \varphi \quad .$$

The angle of the various ray segments are represented by

$$\xrightarrow[\text{(Fig. I.2)}]{\text{sym def}} (13) \quad \left\{ \begin{matrix} \varphi_i \\ \varphi_{in} \\ \varphi_o \end{matrix} \right\} = \text{angle between} \left\{ \begin{matrix} \text{input} \\ \text{interior} \\ \text{output} \end{matrix} \right\} \text{ ray segment and x-axis.}$$

A ray entering the ion exhaust beam interior, in the plane shown, undergoes a bending through the angle r - i, consequently,

$$\xrightarrow{\text{Fig. I.2}} (14) \quad \varphi_{in} = \varphi_i + r - i \quad .$$

The ray exciting the ion exhaust beam undergoes a bending through the same angle, consequently

$$\xrightarrow{\text{Fig. I.2}} (15) \quad \varphi_o = \varphi_{in} + r - i \quad .$$

The output beam direction is consequently related to the input beam direction by

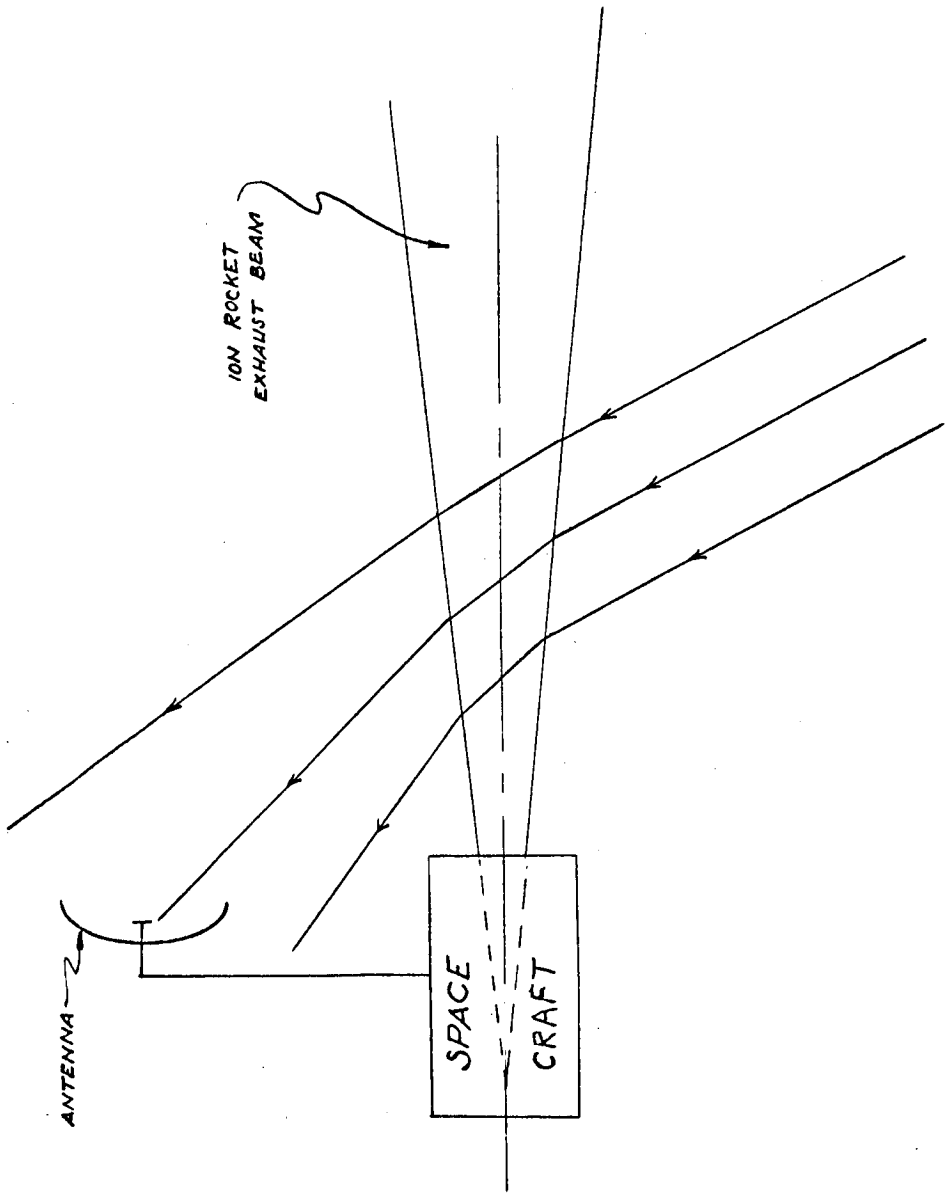

Fig. I.3. Divergence of a parallel bundle of signal rays through the ion exhaust beam symmetry axis.

$$\xrightarrow[14]{15} (16) \quad \varphi_o = \varphi_i + 2(r - i) \quad .$$

The angles are functionally related by

$$\xrightarrow{\text{Fig. I.2}} (17) \quad \varphi_i = i - \varphi$$

and

$$\xrightarrow{\text{D-14}} (18) \quad \sin i = n \sin r \quad .$$

It is convenient to take φ as the independent variable and to take φ_i, φ_o, i and r as dependent variables. Then

$$\xrightarrow{7} (19) \quad S_\varphi = \frac{d\varphi_o}{d\varphi} \Big/ \frac{d\varphi_i}{d\varphi} \quad .$$

Using

$$\xrightarrow{16} (20) \quad \frac{d\varphi_o}{d\varphi} = \frac{d\varphi_i}{d\varphi} + 2\left(\frac{dr}{d\varphi} - \frac{di}{d\varphi}\right)$$

and

$$\xrightarrow{17} (21) \quad \frac{d\varphi_i}{d\varphi} = \frac{di}{d\varphi} - 1$$

gives

$$\xrightarrow[20,21]{19} (22) \quad S_\varphi = 1 + 2\,\frac{\frac{dr}{d\varphi} - \frac{di}{d\varphi}}{\frac{di}{d\varphi} - 1} \quad .$$

Simplifying gives

$$\xrightarrow{22} (23) \quad S_\varphi = 1 + 2\,\frac{\frac{dr}{di} - 1}{1 - \frac{d\varphi}{di}} \quad .$$

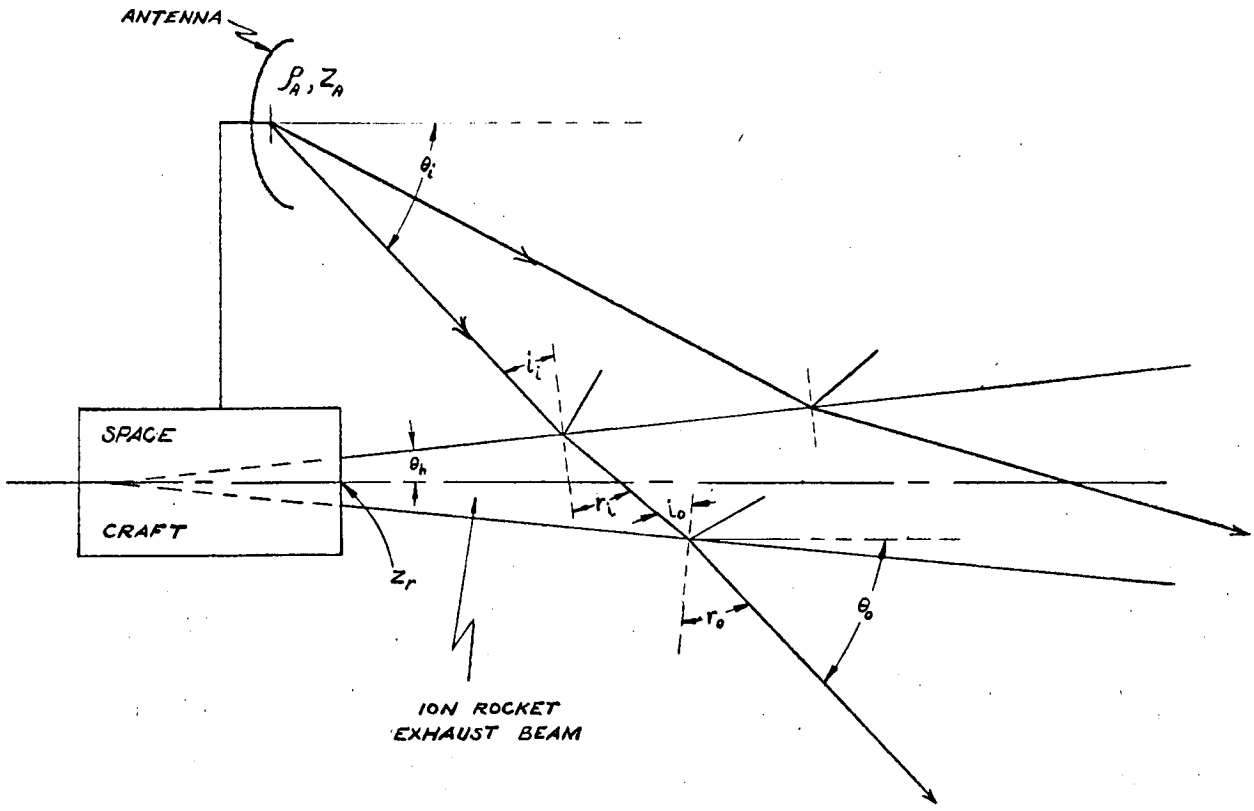

Fig. I.4 Divergence of a non parallel bundle of rays through the ion exhaust beam symmetry axis.

Using the antenna distance normalized with respect to the ion exhaust beam radius

$$\xrightarrow{\text{sym def}} (24) \quad B = \frac{b}{a}$$

gives

$$\xrightarrow[24]{11} (25) \quad \tan i = \frac{\tan \varphi}{1 - \frac{1}{B \cos \varphi}}$$

or

$$\xrightarrow{25} (26) \quad \tan i = \frac{B \sin \varphi}{B \cos \varphi - 1} \quad .$$

Differentiating gives

$$\xrightarrow{26} (27) \quad \sec^2 i = \frac{B (B \cos \varphi - 1) \cos \varphi + B \sin^2 \varphi}{(B \cos \varphi - 1)^2} \frac{d\varphi}{di} \quad .$$

Consequently

$$\xrightarrow{S7} (28) \quad \frac{d\varphi}{di} = \frac{(B \cos \varphi - 1)^2}{B (B - \cos \varphi)} \sec^2 i \quad .$$

Using

$$\xrightarrow{18} (29) \quad \cos r \frac{dr}{di} = \frac{1}{n} \cos i$$

gives

$$\xrightarrow{29} (30) \quad \frac{dr}{di} = \frac{1}{n} \frac{\cos i}{\cos r} \quad .$$

Using

$$\xrightarrow{18} (31) \quad \cos r = \sqrt{1 - n^{-2} \sin^2 i}$$

gives

$$\xrightarrow[31]{30} (32) \quad \frac{dr}{di} = \frac{\cos i}{\sqrt{n^2 - \sin^2 i}} \quad .$$

Using

$$\xrightarrow{26} (33) \quad \begin{vmatrix} \sin i \\ \\ \cos i \end{vmatrix} = \frac{1}{\sqrt{B^2 - 2B \cos \varphi + 1}} \cdot \begin{vmatrix} B \sin \varphi \\ \\ B \cos \varphi - 1 \end{vmatrix}$$

gives

$$\xrightarrow[33]{32} (34) \quad \frac{dr}{di} = \frac{B \cos \varphi - 1}{\sqrt{n^2(B^2 - 2B \cos \varphi + 1) - B^2 \sin^2 \varphi}}$$

and

$$\xrightarrow[36_2]{28} (35) \quad \frac{d\varphi}{di} = \frac{B^2 - 2B \cos \varphi + 1}{B(B - \cos \varphi)} \quad .$$

The azimuth spreading factor can now be written as

$$\xrightarrow[34,35]{23} (36) \quad S_\varphi = 1 + 2 \frac{\dfrac{B \cos \varphi - 1}{\sqrt{n^2(B^2 - 2B \cos \varphi + 1) - B^2 \sin^2 \varphi}} - 1}{1 - \dfrac{B^2 - 2B \cos \varphi + 1}{B(B - \cos \varphi)}} \quad .$$

Simplifying gives

$$\xrightarrow{36} (37) \quad S_\varphi = 1 + 2B \frac{B - \cos \varphi}{\sqrt{n^2(B^2 - 2B \cos \varphi + 1) - B^2 \sin^2 \varphi}} = 2B \frac{B - \cos \varphi}{B \cos \varphi - 1} \quad .$$

It would be of interest to plot S_φ against φ for various B. At the critical angle the spreading factor becomes infinite. The spreading factor is a minimum for a signal

ray directly through the axis of symmetry, for which case

$$\xrightarrow[\varphi = 0]{37} (38) \quad S_{\varphi}(0) = 1 + 2B\left(\frac{1}{n} - 1\right) \quad .$$

The expression for the minimum spreading factor is the simplest and, hence, it is examined first. Expressing the spreading factor in terms of ion exhaust beam properties gives

$$\xrightarrow[H\text{-}14_1]{38} (39) \quad S_{\varphi}(0) = 1 + 2B\left[\frac{1}{\sqrt{1 - 10.62\,\frac{i_b}{I_{sp}}}} - 1\right] \quad .$$

For large ratios of specific impulse to ion current density

$$\xrightarrow[n \approx 1]{39} (40) \quad S_{\varphi}(0) = 1 + 10.62\,B\,\frac{i_b}{I_{sp}} \quad .$$

This spreading factor is graphed in Fig. I.5 as a function of the antenna center (ray source approximation) distance from the ion exhaust beam axis for the case of an emission current density of 15 ma/cm^2 and a specific impulse of 12,000 seconds which was chosen for the Jupiter-orbiter example,

$$\xrightarrow[J\text{-example}]{40} (41) \quad S_{\varphi}(0) = 1 + 0.1328\,B \quad .$$

Considering that this is the minimum case, makes the signal beam spreading problem serious for signal beams passing through the ion exhaust beam.

The larger the antenna distance, the greater the spreading factor for the signal rays passing through the ion exhaust beam, however, the smaller the solid angle subtended by the ion exhaust beam. This tradeoff should be examined to determine an optimum or least objectionable compromise.

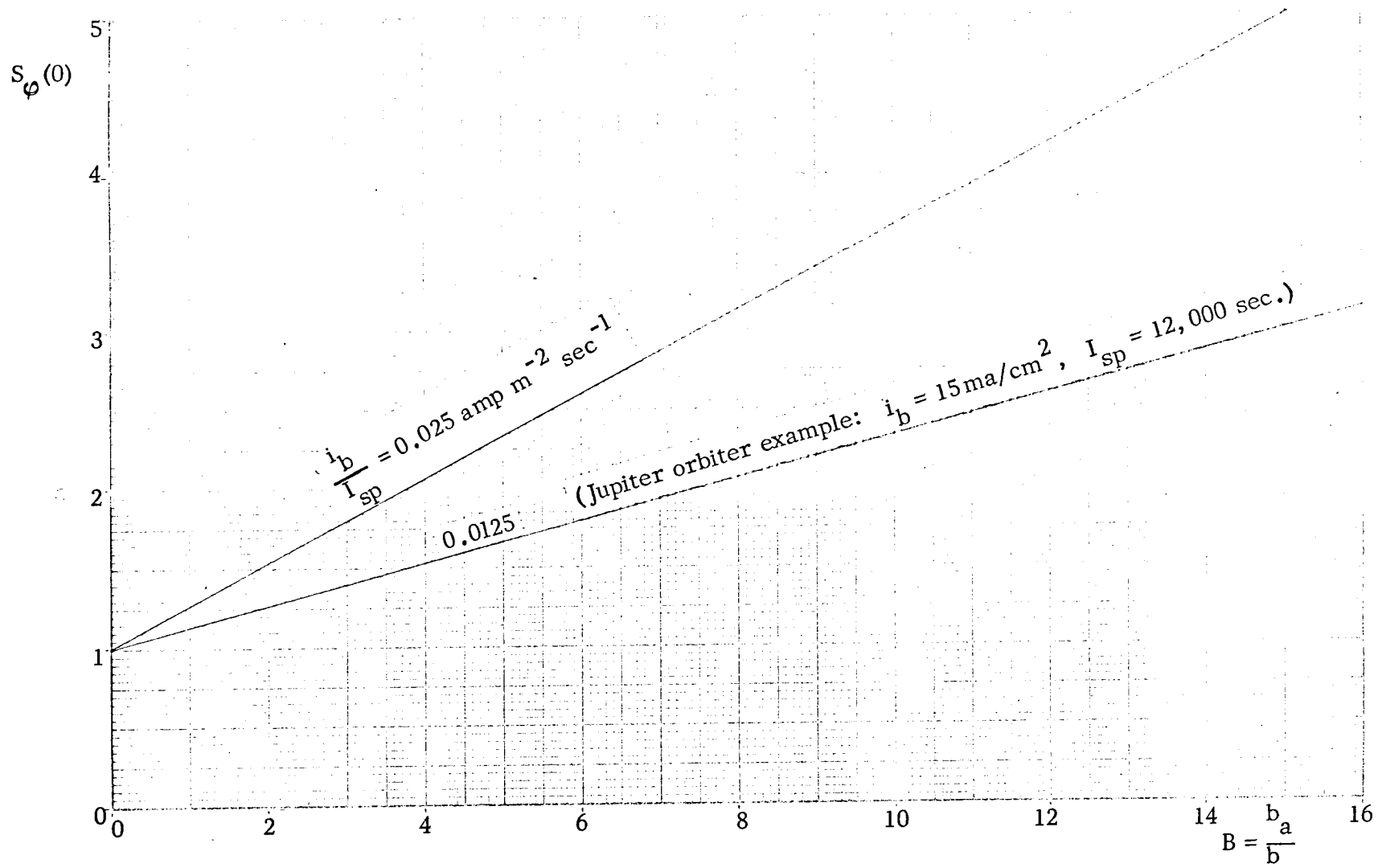

Fig. I.5 Minimum transverse spreading factor for signal rays in a plane perpendicular to the ion exhaust beam axis

APPENDIX J: SIGNAL DISTORTION

J.1 Introduction

Exact signal distortion analysis can be accomplished by Fourier resolution of a signal into its component frequencies, determination of the transmission channel affect on each frequency component and then Fourier integration of all the output frequency components to obtain the output signal. Distortion analysis can also be accomplished via Laplace transformation theory, or other appropriate resolution methods. Detailed examination of distortion requires specification of the signal (or class of signals) as well as specification of the transmission channel characteristics. Such analysis requires a relatively large amount of effort. In addition the desired signals have not yet been specified. It would be desirable to have a general rule-of-the-thumb for assessing the seriousness of the distortion, which could be applied to the broad class of signals.

J.2 Fourier Transform Theory

A rule-of-the-thumb criterion can be provided as follows. Fourier transform theory relates

$$\xrightarrow{\text{sym def}} (1) \left\{ \begin{matrix} f_i(t) \\ f_o(t) \end{matrix} \right\} = \text{the} \left\{ \begin{matrix} \text{input} \\ \text{output} \end{matrix} \right\} \text{time signal}$$

and

$$\xrightarrow{\text{sym def}} (2) \left\{ \begin{matrix} \overline{f}_i(\omega) \\ \overline{f}_o(\omega) \end{matrix} \right\} = \text{the} \left\{ \begin{matrix} \text{input} \\ \text{output} \end{matrix} \right\} \text{spectral signal}$$

via

sym def → (3) $T(\omega)$ = the transmission channel transfer function.

The spectral input signal is related to the time input signal by

Fourier Transform → (4) $$\overline{f}_i(\omega) = \frac{1}{2\pi}\int_{-\infty}^{\infty} f_i(\tau)\, e^{-j\omega\tau} d\tau \quad .$$

The spectral output signal is related to the spectral input signal via the transfer function by

causality → (5) $$\overline{f}_o(\omega) = \overline{f}_i(\omega)\ T(\omega) \quad .$$

The output time signal is related to the output spectral signal by

Fourier Integral → (6) $$f_o(t) = \int_{-\infty}^{\infty} \overline{f}_o(\omega)\, e^{-j\omega t} d\omega \quad .$$

Consequently, the output time signal is related to the input spectral signal by

$\frac{6}{5}$ → (7) $$f_o(t) = \int_{-\infty}^{\infty} \overline{f}_i(\omega)\ T(\omega)\, e^{-j\omega t} d\omega \quad .$$

Expressing the transfer function in terms of magnitude and angle

identity → (8) $$T(\omega) = |T(\omega)|\, e^{j\angle T(\omega)}$$

gives

$\frac{7}{8}$ → (9) $$f_o(t) = \int_{-\infty}^{\infty} \overline{f}_i(\omega)\ |T(\omega)|\, e^{-j\left[\omega t - \angle T(\omega)\right]} d\omega \quad .$$

J.3 Complex Fourier Integral

The development is simplified by using the complex function given by the one

sided integral

$$\xrightarrow{\text{sym def}} (10) \quad \check{f}(t) = 2 \int_0^{\infty} \overline{f}(\omega) e^{j\omega t} d\omega \quad .$$

This transform type is advantageous because the signal frequency band occupies a single contiguous range, whereas with the double sided integral, it occupies two ranges, which are mirror images with respect to the frequency origin. The real-signal function is related to the complex-signal function via

$$\xrightarrow[\text{Integral}]{\text{Fourier}} (11) \quad f(t) = \int_{-\infty}^{\infty} \overline{f}(\omega) e^{j\omega t} d\omega \quad .$$

Expressing the two sided integral as two one-sided integrals over the same range gives

$$\xrightarrow{11} (12) \quad f(t) = \int_0^{\infty} \overline{f}(\omega) e^{j\omega t} d\omega + \int_0^{\infty} \overline{f}(-\omega) e^{-j\omega t} d\omega \quad .$$

The second integral is the complex conjugate of the first,

$$\xrightarrow{12} (13) \quad f(t) = \int_0^{\infty} \overline{f}(\omega) e^{j\omega t} d\omega + \left[\int_0^{\infty} \overline{f}(\omega) e^{j\omega t} d\omega \right]^* \quad .$$

Hence, the imaginary parts cancel leaving

$$\xrightarrow{13} (14) \quad f(t) = 2\mathcal{R} \int_0^{\infty} \overline{f}(\omega) e^{j\omega t} d\omega \quad .$$

Consequently, the real time function is related to the complex time function by

$$\xrightarrow[10]{14} (15) \quad f(t) = \mathcal{R}\, \check{f}(t) \quad .$$

The complex output time signal is consequently given by

9, 10 (16) $f_o(t) = 2 \int_0^\infty \overline{f_i}(\omega) |T(\omega)| e^{-j[\omega t - /T(\omega)]} d\omega$.

J.4 Transfer Function Criteria for Small Distortion

If the signal frequency content lies in the frequency range

band def (17) $\omega_1 \leq \omega \leq \omega_2$

the complex output time signal can be expressed as

16, 17 (18) $\overset{\vee}{f}_o(t) = 2 \int_{\omega_1}^{\omega_2} \overline{f_i}(\omega) |T(\omega)| e^{-j[\omega t - /T(\omega)]} d\omega$.

The transfer function magnitude and angle can be expanded about

sym def (19) ω_o = a suitably chosen value

within the signal frequency spectrum

condition (20) $\omega_1 < \omega_o < \omega_2$.

Expanding the transfer function magnitude gives

Taylor Exp (21) $|T(\omega)| = |T(\omega_o)| + |T|_1 (\omega - \omega_o) + \frac{1}{2} |T|_2 (\omega - \omega_o)^2 + \cdots$

where

sym def (22) $|T|_n = \left. \frac{d^n |T(\omega)|}{d\omega^n} \right|_{\omega = \omega_o}$.

Expanding the transfer function phase gives

Taylor exp (23) $\angle T(\omega) = \angle T_o + \angle T_1(\omega - \omega_o) + \frac{1}{2} \angle T_2(\omega - \omega_o)^2 + \cdots$

where

sym def (24) $\angle T_n = \left. \frac{d^n \angle T(\omega)}{d\omega^n} \right|_{\omega = \omega_o}$.

It is convenient to introduce

sym def (25) $R_n f(x)$ = the remainder of the series expansion starting with the nth term.

Expressing the Taylor expansions in terms of remainders gives

21 (26) $|T(\omega)| = |T(\omega_o)| + R_1 |T(\omega)|$

and

23 (27) $\angle T(\omega) = \angle T_o + \angle T_1(\omega - \omega_o) + R_2 \angle T(\omega)$.

The complex output time function can now be expressed in the form

18, 26, 27 (28) $\overset{v}{f}_o(t) = 2 \int_{\omega_1}^{\omega_2} \overline{f}_i(\omega) \left[|T(\omega_o)| + R_1 |T(\omega)| \right] e^{-j\left[\omega t - \angle T_o - \angle T_1(\omega - \omega_o) - R_2 \angle T(\omega)\right]} d\omega$.

Taking constant factors outside the integral gives

28 (29) $\overset{v}{f}_o(t) = |T(\omega_o)| e^{-j(\omega \angle T_1 - \angle T_o)} \overset{v}{f}_S(t)$

where

$$\xrightarrow{28,29,\text{ sym def}} (30) \quad \check{f}_s(t) = 2\int_{\omega_1}^{\omega_2}\left[1+\frac{R_1|T(\omega)|}{|T(\omega_o)|}\right]e^{-j\left[\omega(t-\angle T_1)-R_2\angle T(\omega)\right]}d\omega$$

is the signal shape which is essentially the input signal distorted to the form it has in the output; differing from the output signal only in magnitude by the factor $|T(\omega_o)|$ and in phase by the amount $\omega\angle T_1 - \angle T_o$.

If the frequency band is sufficiently narrow for the magnitude of the transfer function to have a negligible variation over the band,

$$\xrightarrow{\text{restriction}} (31) \quad \frac{R_1|T(\omega)|}{|T(\omega_o)|} << 1 \qquad \text{for} \quad \omega_1 < \omega < \omega_2$$

a good approximation to the signal shape is given by

$$\xrightarrow{30,\ 31} (32) \quad \check{f}_S(t) = 2\int_{\omega_1}^{\omega_2} \bar{f}_i(\omega)e^{-j\left[\omega(t-\angle T_1)-R_2\angle T(\omega)\right]}\,d\omega \quad .$$

For this case the distortion is only due to the nonlinearity in the phase characteristic of the transfer function; such distortion is referred to as phase distortion. If the transfer function phase characteristic is sufficiently linear over the band of interest

$$\xrightarrow{\text{restriction}} (33) \quad R_2\angle T(\omega) << 1 \qquad \omega_1 < \omega < \omega_2$$

a good approximation to the signal shape is then given by

$$\xrightarrow{32,\ 33} (34) \quad \check{f}_S(t) = 2\int_{\omega_1}^{\omega_2} \bar{f}_i(\omega)\,e^{-j\omega(t-\angle T_1)}\,d\omega \quad .$$

For this case the output signal shape is exactly that of the input signal

$$\xrightarrow{34,\ 10} (35) \quad \check{f}_S(t) = \check{f}_i(t-\angle T_1) \quad .$$

For this case the output signal is given by

$$\xrightarrow[35]{29} (36) \quad f_o(t) = |T(\omega_o)| e^{-j(\omega \angle T_1 - \angle T_o)} f_i(t - \angle T_1) \quad ,$$

hence, there is no distortion, but

$$\xrightarrow{36, \text{sym def}} (37) \quad \tau_d = \text{the time by which the signal is delayed}$$

is given by

$$\xrightarrow{35} (38) \quad \tau_d = \angle T_1 = \left. \frac{d \angle T(\omega)}{d\omega} \right|_{\omega = \omega_o} \quad .$$

In addition to the delay the signal is also reduced in amplitude by the factor $|T(\omega_o)|$ and shifted in phase by tha amount $\omega \angle T_1 - \angle T_o$.

The distortion in the signal is only of interest when the signal is not attenuated excessively. Under these conditions the transfer function amplitude does not have a significant variation over the frequency band of interest, hence only phase distortion need be considered. The remainder, after the linear term in the Taylor expansion for the transfer function phase angle,

$$\xrightarrow[38]{27} (39) \quad R_2 \angle T(\omega) = \angle T(\omega) - \angle T_o - \tau_d (\omega - \omega_o)$$

is the cause of the signal phase distortion. In expanded form

$$\xrightarrow{27\text{-}23} (40) \quad R_2 \angle T(\omega) = \tfrac{1}{2} \angle T_2 (\omega - \omega_o)^2 + \cdots \quad .$$

Small phase distortion requires that

$$\xrightarrow{32} (41) \quad |R_2 \angle T(\omega)| \ll 1 \quad .$$

For those cases in which the first term in the expansion of the remainder adequately represents the remainder value, which is generally the case for small phase distortion, a relatively easy to use the rule of the thumb is

$$\xrightarrow{40,41} (42) \quad \left| \tfrac{1}{2} \angle T_2 (\omega - \omega_o)^2 \right| \ll 1 \quad .$$

The choice for ω_o, for reasonably well behaved signals, which on the average would give the best convergence, i.e., the value of ω_o for which the second derivative would give the best average approximation to the remainder is

$$\xrightarrow{\text{arithmetic mean}} (43) \quad \omega_o = \frac{\omega_1 + \omega_2}{2} \quad .$$

The largest value of the left hand side of (42) is for ω at the edge of the signal frequency band. The inequality in (42) will be satisfied for all cases if it is satisfied for the worse case. Hence, using

$$\xrightarrow{\text{sym def}} (44) \quad B = f_2 - f_1 = \text{signal bandwidth}$$

gives

$$\xrightarrow{43,44} (45) \quad \omega_2 - \omega_o = \pi B$$

and hence .

$$\xrightarrow[45]{40} (46) \quad K_2 \angle \Upsilon(\omega_2) = \tfrac{1}{2}\pi^2 B^2 \angle T_2 + \cdots \quad .$$

Consequently, small phase distortion requires that

$$\xrightarrow[46]{41} (47) \quad \tfrac{1}{2}\pi^2 B^2 \left| \angle T_2 \right| \ll 1$$

and hence

47 (48) $|\angle T_2| << \frac{2}{\pi^2 B^2}$.

For narrow bandwidth the derivative at any frequency within the band can be used. Consequently, if the inequality

48 (49) $\left|\frac{d^2 \angle T}{d\omega^2}\right| << \frac{2}{\pi^2 B^2}$

is satisfied the phase distortion is negligible.

J.5 Channel Phase Distortion Index

The signal distortion depends on the bandwidth of the signal as well as on the phase shift characteristics of the transmission media. It is desireable, where possible, to express the term responsible for phase distortion as the product of two terms, one depending on signal bandwidth alone and the other depending on the transmission channel properties alone. This can be done for the case in which the remainder of the phase characteristic expansion, after the linear term, can be adequately represented by the quadratic term. Since it is desireable to deal with normalized quantities the ratio of the bandwidth to the signal carrier frequency is used. Thus

sym def (50) Ψ_D = a phase distortion index

can be defined so that

phys def (51) $R_2 \angle T(\omega) = \frac{B^2}{f_o^2} \Psi_D$.

With these conditions

46, 51 (52) $\Psi_D \approx \frac{1}{2}\pi^2 f_o^2 \angle T_2 = \frac{1}{8}\omega_o^2 \angle T_2$

consequently, small phase distortion requires that

48 / 52 (53) $|\Psi_D| \ll \frac{f_o^2}{B^2}$.

J.6 Transfer Function Phase Angle for Ion Exhaust Beam

The transfer function phase angle for the ion exhaust beam is

C-70 (54) $\angle T = \int_0^L \beta \, d\ell$.

For small collision frequency the phase factor is given by

E-127 (55) $\beta = \beta_v \sqrt{1 - \frac{\omega_p^2}{\omega^2}} \qquad \omega_p < \omega$.

Using

E-55 (56) $\omega_p = \omega_{pr} \sqrt{\frac{n_e(\ell)}{n_{er}}}$

gives

55 / 56 (57) $\beta = \beta_v \sqrt{1 - \frac{\omega_{pr}^2}{\omega^2} \frac{n_e(\ell)}{n_{er}}}$.

Consequently, the transfer function phase angle is given by

54 / 57 (58) $\angle T = \beta_v \int_0^L \sqrt{1 - \frac{\omega_{pr}^2}{\omega^2} \frac{n_e(\ell)}{n_{er}}} \, d\ell$.

J.7 Transfer Function Phase Angle for Signal Ray Perpendicular to Ion Exhaust Beam

The simplest case is that for which a signal ray traverses the ion exhaust beam normal to its axis and it should be quite representative of the more general case. For this case the phase factor does not vary along the signal ray path, hence,

54 (59) $\angle T = \beta L$.

Using

55 C-122 (60) $\beta = \frac{1}{c}\sqrt{\omega^2 - \omega_p^2}$

gives

59 60 (61) $\angle T = \frac{L}{c}\sqrt{\omega^2 - \omega_p^2}$.

J.8 Distortion Factor for Ray Perpendicular to Ion Exhaust Beam Axis

Differentiating the transfer function phase angle gives

55 (62) $\frac{d\angle T}{d\omega} = \frac{L}{c}\frac{\omega}{\sqrt{\omega^2 - \omega_p^2}}$.

Differentiating again gives

62 (63) $\frac{d^2\angle T}{d\omega^2} = \frac{L}{c}\frac{-\omega_p^2}{\left(\omega^2 - \omega_p^2\right)^{3/2}}$.

The phase distortion index is consequently given by

52 63 (64) $\Psi_D = \frac{-\frac{L}{c}\omega_o^2\omega_p^2}{8\left(\omega_o^2 - \omega_p^2\right)^{3/2}}$

64 → (65) $\Psi_D = \dfrac{-\frac{\pi}{4}\frac{L}{\lambda_o}\omega_o^{-2}\omega_p^2}{\left(1 - \frac{\omega_p^2}{\omega_o^2}\right)^{3/2}}$.

For this case the path length in terms of the ion exhaust beam radius is given by

Fig. G.1 → (66) $L = 2b$.

For the Jupiter orbiter example

G-13 → (67) $\omega_p^2 << \omega^2$

consequently the distortion index reduces to

65 / 67, 66 → (68) $\Psi_D = \dfrac{\pi b}{2\lambda_o}\dfrac{f_p^2}{f_o^2}$.

Expressing the distortion index in terms of the ion exhaust beam current density, specific impulse and power gives

68 / B-56, B-66 → (69) $\Psi_D = \dfrac{1.82 \times 10^{12}}{f_o}\dfrac{\sqrt{P_b i_b}}{I_{sp}^2}$.

Using the center frequency for the band of interest gives

69 / $f_o = 2.2 \times 10^9$ → (70) $\Psi_D = 830\dfrac{\sqrt{P_b i_b}}{I_{sp}^2}$.

For the Jupiter orbiter example

70 / 2-3 → (71) $\Psi_D = 4.17 \times 10^{-3}\sqrt{i_b}$.

At the ion exhaust beam exit plane

$$\xrightarrow[i_b = 15\,ma/cm^2]{73} (72) \quad \Psi_D = 0.498 \quad .$$

The minimum center frequency to bandwidth ratio for the spcified case is

$$\xrightarrow{\text{specification}} (73) \quad \frac{f_o}{B} = 11 \quad .$$

Hence

$$\xrightarrow{73} (74) \quad \frac{f_o^2}{B^2} = 121 \quad .$$

The inequality

$$\xrightarrow[72,74]{53} (75) \quad 0.498 << 121 \quad .$$

is more than adequate for the distortion to be quite negligible for the Jupiter orbiter example and the frequency band chosen. The distortion factor is most sensitive to the specific impulse, which if reduced by an order of magnitude with the other parameters remaining the same, would lead to significant signal distortion. If the signal frequency decreases by a factor approaching 2.7 the denominator in (65) approaches zero and the phase distortion may become excessive. This case would have to be examined with an improved approximation that includes the effect of the collision frequency.

APPENDIX K: BREMSSTRAHLUNG

K.1 Introduction

Radiation from accelerating electrons during random collision processes is called bremsstrahlung. Since the collisions are random, the radiation generated by these collisions is incoherent. This type of process is the principal basic source of noise in the radio frequency portion of the electromagnetic spectrum.

There is a sizeable literature on the subject of bremsstrahlung, for example references K1, K2, K3, K4, K5. A large variety of formulae have been derived for bremsstrahlung which provide various types of approximations. Large discrepancies occur between numerical results provided by formulae from different sources. Some of these discrepancies are due to the assumptions (often jerry-built) employed. These discrepancies may also be due to an inadequate specification of the terms entering the formula and their dimensions, to typographical errors and to misunderstanding on the part of the reader which are not fairly attributable to the author. Derivation of the necessary expressions, using the literature as a check, appears necessary not only to obtain sufficient consistency for their proper use both with respect to the validity range of the approximations introduced and to units employed but also to facilitate obtaining the formulae in suitable form for the case of interest.

The objective of this appendix is to determine the spectral noise power per unit volume generated in the ion exhaust beam plasma.

K.2 Electron Trajectories

To determine the radiation from an electron deflected by an ion, it is necessary to know the acceleration of the electron as a function of time. This is obtained by

solving the equation of motion for the electrons. The forces in the equation of motion are the inverse square law attraction force due to the ion and the self radiation force. The radiation force is generally small in the cases of interest here and its effect on the electron trajectory is neglected in the approximation employed. With this approximation the electron's equation of motion is

Newton, Coulomb → (1) $\ddot{\mathbf{r}} = \frac{k}{r^3}\mathbf{r}$

where

sym def → (2) $k = \frac{Ze^-}{4\pi\epsilon_v m_e}$

which numerically is

2 → A-1, A-4, A-5 (3) $k = 253\ Z\ \text{meters}^3 - \text{sec}^{-2}$

and

sym def → (4) $Z =$ ion charge in units of e .

The ion acceleration is neglected in this development since its mass is more than four orders of magnitude larger than the electron mass.

The three dimensional vector equation of motion reduces to a two dimensional vector equation of motion. Using the vector cross product definition gives

identity → (5) $\mathbf{r} \times \mathbf{r} = 0$

consequently

$\xrightarrow{1,5}$ (6) $\mathbf{r} \times \ddot{\mathbf{r}} = 0$.

This can be re-expressed as a perfect derivative

$\xrightarrow{6,5}$ (7) $\frac{d}{dt} \mathbf{r} \times \dot{\mathbf{r}} = 0$.

Integrating gives

$\xrightarrow{7}$ (8) $\mathbf{r} \times \dot{\mathbf{r}} =$ constant vector .

The vectors $\mathbf{r}$ and $\dot{\mathbf{r}}$ determine a plane which is perpendicular to their cross product. Since the cross product $\mathbf{r} \times \dot{\mathbf{r}}$ does not vary with time, the orientation of the plane does not change with time. Consequently, the trajectory of an electron deflected by an ion lies in a fixed plane. By taking this plane to be the

$\xrightarrow{8,\text{choice}}$ (9) $z = 0$

plane, the spherical radial vector

$\xrightarrow{\text{vector identity}}$ (10) $\mathbf{r} = \boldsymbol{\rho} + 1_z z$

reduces to the cylindrical radial vector

$\xrightarrow{\frac{10}{9}}$ (11) $\mathbf{r} = \boldsymbol{\rho}$

and consequently the equation of motion reduces to

$\xrightarrow{\frac{1}{11}}$ (12) $\ddot{\boldsymbol{\rho}} = -\frac{k}{r^3} \boldsymbol{\rho}$.

The scalar radial equation of motion is consequently

$$\xrightarrow{11} (13) \quad \ddot{\rho} - \rho\dot{\varphi}^2 = -\frac{k}{\rho^2}$$

and the aximuth angle equation of motion is thus

$$\xrightarrow{11} (14) \quad \rho\ddot{\varphi} + 2\dot{\rho}\dot{\varphi} = 0 \ .$$

The azimuth equation of motion is a perfect derivative,

$$\xrightarrow{14} (15) \quad \frac{d}{dt}\rho^2\dot{\varphi} = 0 \ .$$

Integrating gives

$$\xrightarrow{15} (16) \quad \rho^2\dot{\varphi} = \text{constant} \ .$$

Hence

$$\xrightarrow{\text{sym def}} (17) \quad \ell = \text{the angular momentum}$$

which is given by

$$\xrightarrow{\text{phys def}} (18) \quad \ell = m_e\rho^2\dot{\varphi}$$

is a constant,

$$\xrightarrow[16]{18} (19) \quad \ell = \text{constant} \ .$$

The radial equation of motion can be converted to a differential equation for the trajectory by changing the independent variable from t to φ. Using

$$\xrightarrow{\text{identity}} (20) \quad \dot{\rho} = \frac{d\rho}{d\varphi}\dot{\varphi}$$

gives

$$\xrightarrow[18]{20} (21) \quad \dot{\rho} = \ell m_e^{-1} \rho^{-2} \frac{d\rho}{d\varphi} \ .$$

Simplifying gives

$$\xrightarrow{21} (22) \quad \dot{\rho} = -\frac{\ell}{m_e} \frac{d}{d\varphi} \frac{1}{\rho} \ .$$

Using

$$\xrightarrow{\text{identity}} (23) \quad \ddot{\rho} = \frac{d\dot{\rho}}{d\varphi} \dot{\varphi}$$

gives

$$\xrightarrow[18,22]{23} (24) \quad \ddot{\rho} = -\ell^2 m_e^{-2} \rho^{-2} \frac{d^2}{d\varphi^2} \frac{1}{\rho} \ .$$

The radial equation of motion thus reduces to the differential equation for the trajectory

$$\xrightarrow[18,34]{13} (25) \quad \frac{1}{\rho} + \frac{d^2}{d\varphi^2} \frac{1}{\rho} = k m_e^2 \ell^{-2} \ .$$

Integrating gives the trajectory equation

$$\xrightarrow{25} (26) \quad \frac{1}{\rho} = k m_e^2 \ell^{-2} + A \cos(\varphi + \varphi_o)$$

which is the polar coordinate equation of a hyperbola. Orienting the z-axis to bisect the hyperbola requires that

$$\xrightarrow{\text{symmetry}} (27) \quad \varphi_o = \left\{ \begin{matrix} 0 \\ \pi \end{matrix} \right\} \text{ for the force center on the } \left\{ \begin{matrix} \text{negative} \\ \text{positive} \end{matrix} \right\} \text{ x-axis .}$$

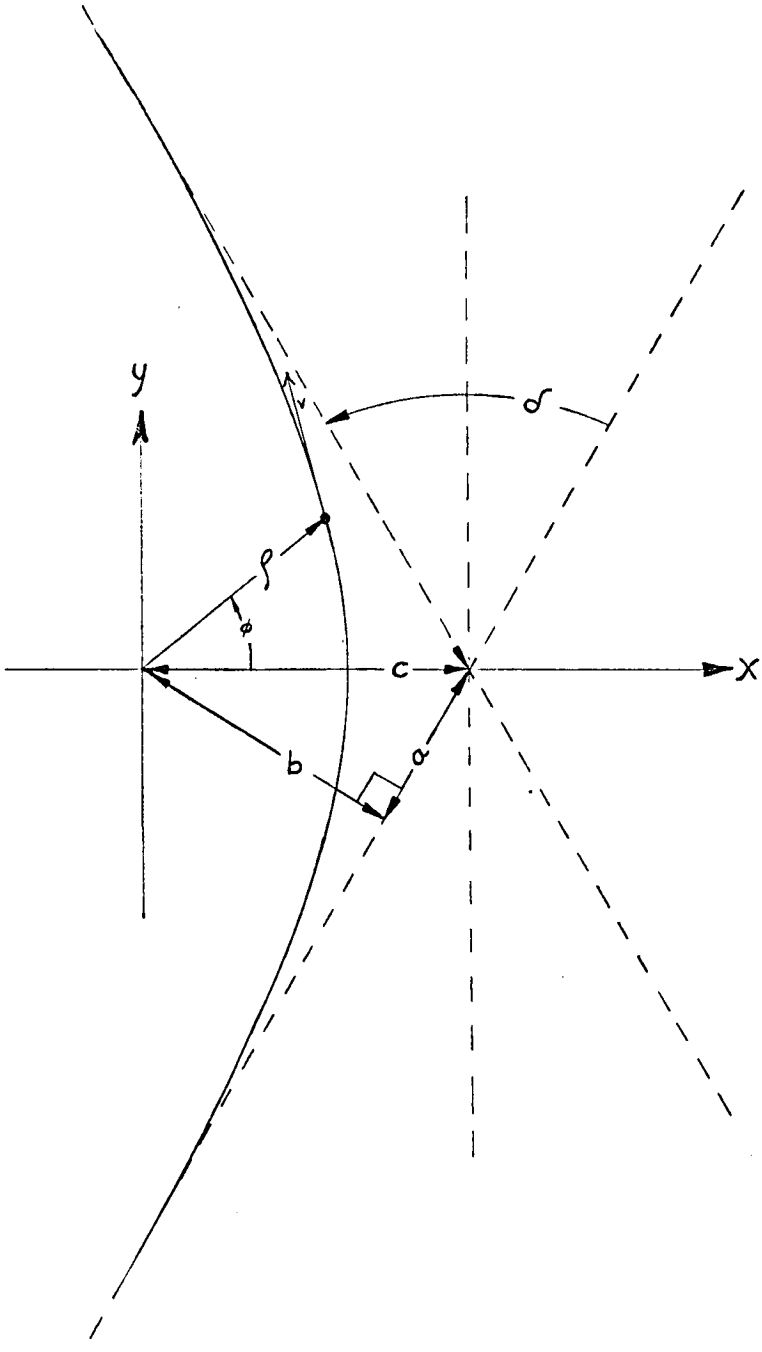

Fig. K.1 Hyperbolic Trajectory of a Charged Particle in an Attractive Inverse Square Law Field.

K.3 Deflection Angle

The attracted particle hyperbolic trajectory depicted in Fig. K.1, has the polar equation

analytic geometry $\longrightarrow$ (28) $\frac{b \cos \frac{1}{2}\delta}{\rho} = \sin \frac{1}{2}\delta + \cos \varphi$.

Expressing the dynamically derived trajectory in comparable form gives

$\xrightarrow[27_1]{26}$ (29) $\frac{1}{A\rho} = \frac{km_e^2}{A\ell^2} + \cos \varphi$.

Comparing the equations derived from mechanics and from geometry for the hyperbola gives the relationship between the deflection angle and the physical parameters.

$\xrightarrow{28,29}$ (30) $b \cot \frac{\delta}{2} = \frac{\ell^2}{km_e^2}$

It is convenient to have the constant angular momentum expressed in terms of

$\xrightarrow{\text{sym def}}$ (31) v_∞ = the electron speed at large distances from the ion

and

$\xrightarrow{\text{sym def}}$ (32) b = the collision parameter (perpendicular distance from ion to trajectory asymptote .

Using

$\xrightarrow{28}$ (33) $b \cos \frac{\delta}{2} \frac{\dot{\rho}}{\rho^2} = \sin \varphi \dot{\varphi}$

gives

$$\xrightarrow[33]{18} (34) \quad \ell = m_e b \frac{\cos\frac{1}{2}\delta}{\sin\varphi}\dot{\rho} \ .$$

Using

$$\xrightarrow{\text{Fig. K.1}} (35) \quad \dot{\rho} \xrightarrow[t\to\infty]{} v_\infty$$

and

$$\xrightarrow{\text{Fig. K.1}} (36) \quad \varphi \xrightarrow[t\to\infty]{} \frac{\pi+\delta}{2}$$

gives

$$\xrightarrow[35,36]{34} (37) \quad \ell = m_e b v_\infty \ .$$

Consequently

$$\xrightarrow[36]{18} (38) \quad \rho^2\dot{\varphi} = bv_\infty \ .$$

A more convenient formula for the deflection angle is thus

$$\xrightarrow[37]{30} (39) \quad \tan\frac{\delta}{2} = \frac{k}{bv_\infty^2} \ .$$

The complexity of many of the analytical developments required here make it expedient to use a number of approximations. To assess the validity of these approximations, it is necessary to know the range of parameter variations involved. This is facilitated by various graphical displays. Of particular interest is the range of deflection angles of importance because of the approximations which can be made for the case of small deflection angles.

It is more convenient to have expressions in terms of

$\xrightarrow{\text{sym def}}$ (40) V = the electron kinetic energy in electron volts

than the electron speed. The energy in electron volts is related to

$\xrightarrow{\text{sym def}}$ (41) W = the electron kinetic energy

by

$\xrightarrow{\text{phys def}}$ (42) $V = \frac{W}{e}$

where

$\xrightarrow{\text{phys def}}$ (43) $W = \frac{1}{2} m_e v^2$.

Hence the kinetic energy in volts in terms of the speed is given by

$\xrightarrow[43]{42}$ (44) $V = \frac{m_e v^2}{2e}$.

Consequently the deflection angle is related to the asymptotic kinetic energy in electron volts by

$\xrightarrow[44]{39}$ (45) $\tan \frac{\delta}{2} = \frac{m_e k}{2ebV_\infty}$.

Evaluating the constants for graphical representation gives

$\xrightarrow[3, Z=1, A=6]{45}$ (46) $\tan \frac{\delta}{2} = \frac{7.19 \times 10^{-10}}{bV_\infty}$.

Expressing the collision parameter in angstrom units gives

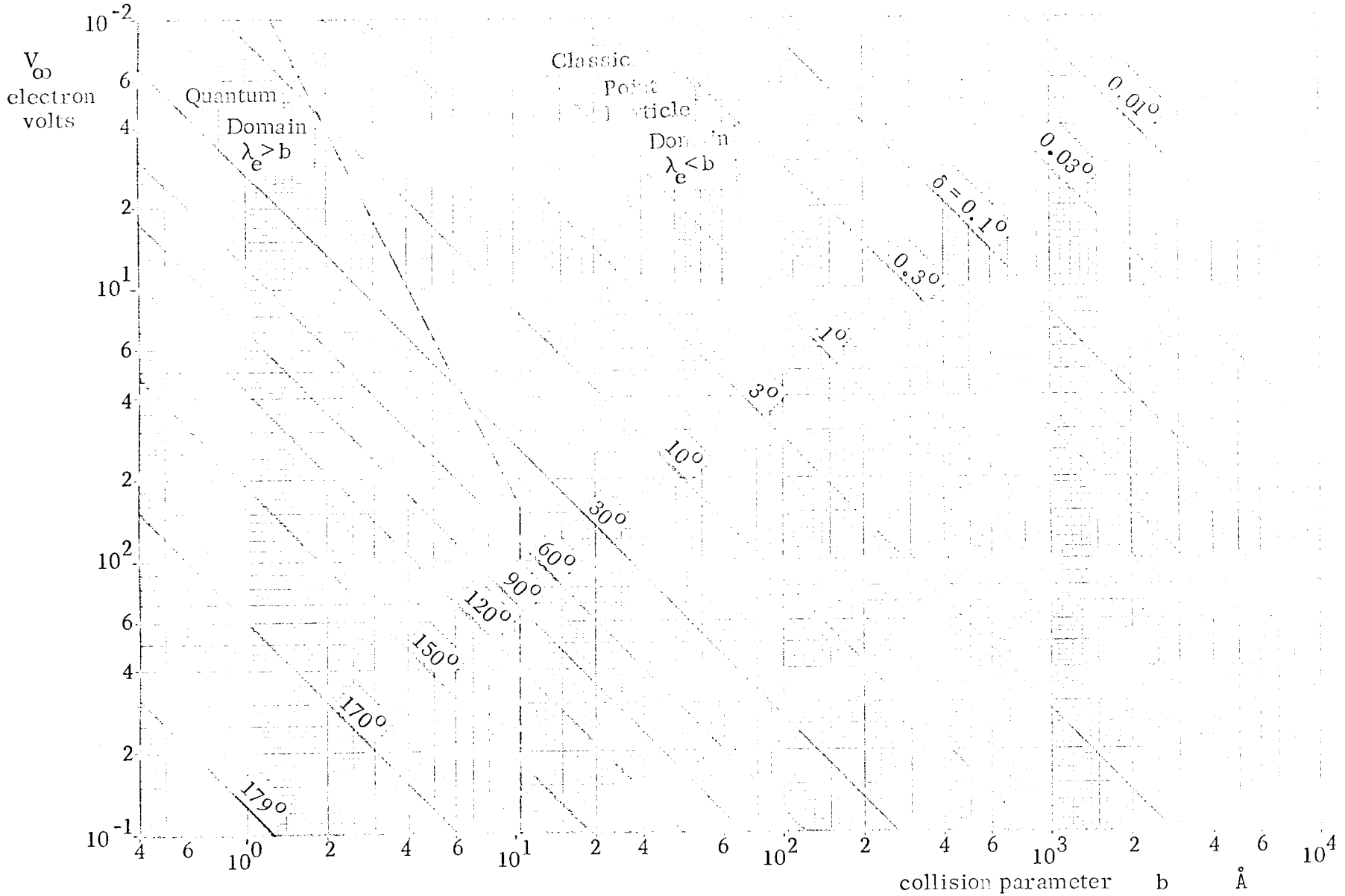

Fig. K.2 Deflection Angle in Terms of the Electron Energy and Collision Parameter

$$\xrightarrow[1\text{Å} = 10^{-10}\text{m}]{46} (47) \quad \tan\frac{\delta}{2} = \frac{7.19}{b_{\text{Å}} V_\infty}$$

For small angles

$$\xrightarrow[\frac{1}{2}\delta < 5^0]{47} (48) \quad \delta = \frac{14.38}{b_{\text{Å}} V_\infty} \text{ radians} = \frac{823}{b_{\text{Å}} V_\infty} \text{ degrees} .$$

The relationship between the deflection angle, collision parameter and the electron energy is graphically depicted in Fig. K. 2.

K.4 Quantum Considerations

The above analysis is based on treating the electron as a classical point particle. The uncertainty principle, in effect, provides the electron with an effective extended structure. This structure is described by a wave packet. The extension of the wave packet is approximately represented by

$$\xrightarrow{\text{sym def}} (49) \quad \lambda_e = \text{the deBroglie wavelength for the electron}$$

which is given by

$$\xrightarrow{\text{deBroglie}} (50) \quad \lambda_e = \frac{h}{m_e v} .$$

Evaluating the physical constants gives

$$\xrightarrow[\text{A-5, A-11}]{50} (51) \quad \lambda_e = \frac{7.27 \times 10^{-4}}{v} \text{ meters} .$$

If the closest approach distance is large compared to the deBroglie wavelength, the electron behaves as a point particle and the classical deflection angle is correct.

If the closest approach distance is of the order of,or shorter than the deBroglie wavelength, the electron does not appear as a point particle to the scattering ion and, hence, the classically derived deflection angle is incorrect. It is instructive to subdivide the (electron energy) - (collision parameter) domain in Fig. K.2 into a classical domain (where classical theory gives correct predictions), and a quantum mechanical domain (where classical theory does not give correct predictions). Using

$$\xrightarrow{44} (52) \quad v = \sqrt{\frac{2eV}{m_e}} = 5.93 \times 10^5 \sqrt{V} \text{ meters/sec}$$

gives the deBroglie relation in terms of energy (in electron volts)

$$\xrightarrow[52]{51} (53) \quad \lambda = \frac{h}{\sqrt{2m_e eV}} .$$

Evaluating the physical constants gives

$$\xrightarrow[A-4, A-5, A-11]{53} (54) \quad \lambda = \frac{1.226 \times 10^{-9}}{\sqrt{V}} \text{ meters} .$$

This relation provides the basis for dividing the $b - V_\infty$ domain of Fig. K.2 into a domain where the classical point particle approximation is valid and a domain where it is not. For small deflection angles the particle velocity and hence the deBroglie wavelength is nearly constant over the trajectory, hence

$$\xrightarrow{54} (55) \quad \lambda = \lambda_\infty = \frac{12.26}{\sqrt{V_\infty}} \text{ Å} .$$

This relationship is graphically depicted in Fig. K.2 by the heavy dashed negative sloping line.

For low values of the electrons asymptotic kinetic energy (less than 1 ev) and for small values of the collision parameters the electron kinetic energy gained from the potential energy may be almost the total electron kinetic energy when the electron is at the perigee. Under these conditions the electrons deBroglie wavelength at the perigee for the case of no asymptotic velocity is a lower bound on the collision parameter. The potential energy (in electron volts) which can be converted to kinetic energy is

$$\xrightarrow{\text{Coulomb}} (56) \quad V = \frac{Ze}{4\pi\epsilon_v \rho} .$$

Hence

$$\xrightarrow[A-1, A-4, Z\neq 1]{56} (57) \quad V = \frac{1.44 \times 10^{-9}}{\rho} \text{ volts} = \frac{14.4}{\rho_{\mathring{A}}} \text{ volts} .$$

The variation of deBroglie wavelength with radial distance is consequently given by

$$\xrightarrow[57]{54} (58) \quad \lambda_{\mathring{A}} = 3.23\sqrt{\rho_{\mathring{A}}} .$$

The deBroglie wavelength becomes equal to the radial distance at

$$\xrightarrow{58} (59) \quad \lambda_{\mathring{A}} = \rho_{\mathring{A}} = 10.43 \text{ Å} .$$

This value is shown as a heavy dashed vertical line in Fig. K.2 The two dashed curves are thus asymptotes for the high and low energy electron cases respectively; the upper dashed curve represents the case in which the contribution of the potential energy to the kinetic energy at the perigee is negligible and the lower dashed curve represents the curve for which the asymptotic kinetic energy contribution to the total kinetic energy at the perigee is negligible.

For large deflection angles the velocity and hence the deBroglie wavelength varies significantly over the trajectory. Consequently the division between classical and quantum mechanical cases must be made on the basis of

$\xrightarrow{\text{sym def}}$ (60) λ_o = the deBroglie wavelength of the electron at the point of closest approach

and hence requires further analysis to delineate it more accurately in the (V_∞, b) domain than already done by its two asymptotes.

Since the electron speed is a maximum at the point of closest approach, the deBroglie wavelength is a minimum at the point of closest approach. Consequently the range of collision parameters over which the classical approximation is valid extends to smaller values than given by the heavy dashed line in Fig. K.2, particularly at the corner where they join. The amount by which the range of b is extended increases as V_∞ decreases. In terms of

$\xrightarrow{\text{sym def}}$ (61) $\breve{\rho}$ = the minimum distance of approach (perigee distance)

the maximum velocity is given by

$\xrightarrow{18}$ (62) $v_o = \dfrac{\ell}{m_e \breve{\rho}}$,

and hence by

$\xrightarrow[37]{62}$ (63) $v_o = \dfrac{b}{\breve{\rho}} v_\infty$.

The hyperbolic trajectory equation gives for the perigee point

$$\xrightarrow[\varphi = 0]{28} (64) \quad \frac{b}{\rho} = \frac{1+\sin\frac{\delta}{2}}{\cos\frac{\delta}{2}} \; .$$

Consequently the perigee speed is given by

$$\xrightarrow[64]{63} (65) \quad v_o = v_\infty \frac{1+\sin\frac{\delta}{2}}{\cos\frac{\delta}{2}}$$

and perigee potential energy in electron volts by

$$\xrightarrow{44,65} (66) \quad V_o = V_\infty \left(\frac{1+\sin\frac{\delta}{2}}{\cos\frac{\delta}{2}}\right)^2 \; .$$

The deBroglie wavelengths are related to the energies by

$$\xrightarrow{53} (67) \quad \frac{\lambda_o}{\lambda_\infty} = \sqrt{\frac{V_\infty}{V_o}}$$

consequently

$$\xrightarrow[65]{67} (68) \quad \frac{\lambda_o}{\lambda_\infty} = \frac{\cos\frac{\delta}{2}}{1+\sin\frac{\delta}{2}}$$

The labor of computing these formulae for graphical representation is reduced by the use of asymptotic expressions for large deflection angles. For deflection angles approaching 180^o it is more convenient to express the deflection formula in the form

$$\xrightarrow{47} (69) \quad \cot\frac{\pi - \delta}{2} = \frac{7.19}{b_{\mathring{A}} V_\infty}$$

or

$$\xrightarrow{69} (70) \quad \tan\frac{\pi-\delta}{2} = 0.139\, b_{\mathring{A}}\, V_\infty \quad .$$

Using the inequality

large deflection constraint

$$\xrightarrow{} (71) \quad \pi - \delta << 1$$

gives

$$\xrightarrow{73,71} (72) \quad \pi - \delta = 0.278\, b_{\mathring{A}}\, V_\infty \quad .$$

For deflection angles approaching 180^o it is more convenient to express the perigee to asymptotic deBroglie wavelength ratio in the form

$$\xrightarrow{68} (73) \quad \frac{\lambda_o}{\lambda_\infty} = \frac{\sin\frac{\pi-\delta}{2}}{1+\cos\frac{\pi-\delta}{2}} \quad .$$

Using the large deflection constraint gives

$$\xrightarrow[71]{73} (74) \quad \frac{\lambda_o}{\lambda_\infty} = \frac{\pi-\delta}{4} \quad .$$

Consequently the perigee asymptotic deBroglie wavelength ratio becomes

$$\xrightarrow[72]{74} (75) \quad \frac{\lambda_o}{\lambda_\infty} = 0.0695\, b_{\mathring{A}}\, V_\infty \quad .$$

The perigee deBroglie wavelength is consequently given by

$$\xrightarrow[54]{75} (76) \quad \lambda_o = 0.852\, b_{\mathring{A}} \sqrt{V_\infty} \ \mathring{A} \quad .$$

While λ_∞ only depends on V_∞, (54), λ_o depends on both V_∞ and b.

For the large deflection parameter range the value of λ_o should be less than r for the classical formula to give reasonably accurate results. The perigee wavelength is related to the perigee distance by

$$\xrightarrow{67,68} (77) \quad \frac{\tilde{\rho}}{b} = \frac{\lambda_o}{\lambda_\infty} \ .$$

Consequently the perigee distance is related to the collision parameter by

$$\xrightarrow[54,76]{77} (78) \quad \rho_{\mathring{A}} = 0.0695 b_{\mathring{A}}^2 V_\infty \ .$$

Consequently the perigee deBroglie wavelength is related to the perigee distance by

$$\xrightarrow{76,78} (79) \quad \lambda_{o\mathring{A}} = 3.23 \sqrt{r_{\mathring{A}}} \ .$$

This relationship is just (58), thereby providing a somewhat circuitous but interesting cross check.

The locus of points for which the perigee deBroglie wavelength equals the collision parameter is just to the left of the bent dashed line in Fig. K. 2 and has the branches of the bent dashed line for asymptotes. For the classical results to apply the deBroglie wavelength must be less than the perigee distance which is less than the collision parameter. The radiated power is dependent on the lower limit of collision parameters. The effective or extended electron, as it approaches the deflection ion, envelopes the ion. As the separation decreases below a deBroglie wavelength the effective net charge of the electron on which the ion can exert a force decreases rapidly. In this region the force goes to zero as the separation goes to zero and hence the acceleration goes to zero. Hence the extended structure of the electron causes the acceleration, and hence, the radiation contributed by

approaches closer than the deBroglie wavelength to fall off sharply. Hence, the total radiation can be approximated by considering only those electrons whose closest approach is equal to or greater than the deBroglie wavelength at the perigee. The small contribution lost by neglecting closer approaches is partially offset by the slightly greater accelerations predicted by the classical point electron formula for separations slightly greater than the deBroglie wavelength.

K.5 Spectral Energy Radiated During a Collision

In terms of

$\xrightarrow{\text{sym def}}$ (80) P_r = the instantaneous power radiated by an electron

the energy radiated during a collision is given by

$\xrightarrow{\text{con def}}$ (81) $W_e = \int_{\infty}^{\infty} P_r(t)\, dt$.

This assumes that each collision is a distinct event, i.e. successive collisions are not overlapping. This is a reasonably good approximation for the plasma in the ion rocket exhaust beam under consideration. The electron energies in the ion rocket exhaust are nonrelativistic. In terms of

$\xrightarrow{\text{sym def}}$ (82) $\dot{v}$ = the electron acceleration

the power radiated by a nonrelativistic electron is given by

$\xrightarrow{\text{Larmor}}$ (83) $P_r = K\dot{v}\,\dot{v}$

where

RK6:301 → (84) $K = \dfrac{e^2}{6\pi\epsilon_v c^3}$

which numerically is given by

84, A1, A-3, A-4 → (85) $K = 5.69 \times 10^{-54}\ \text{watt-sec}^4\ \text{meters}^{-2}$.

The energy radiated during a collision is thus

81, 83 → (86) $W_e = K \int_{-\infty}^{\infty} |\dot{v}(t)|^2\ dt$.

The spectral distribution of the radiated energy is of prime interest to the communication engineer. The spectral distribution could be obtained by evaluating the integral in (86) and then taking the Fourier transform. However, it is simpler to obtain the Fourier transform more directly by use of

Parseval's Theorem → (87) $\int_{-\infty}^{\infty} f^2(r)\,dt = 2\pi \int_{-\infty}^{\infty} |\bar{f}(\omega)|^2\,d\omega$.

Thus the radiated energy can be expressed as an integral over frequency

86, 87 → (88) $W_e = 2\pi K \int_{-\infty}^{\infty} |\bar{v}(\omega)|^2\,d\omega$,

where the Fourier transform of the acceleration is given by

Fourier Resolution → (89) $\bar{v}(\omega) = \dfrac{1}{2\pi}\int_{-\infty}^{\infty} v(t)\,e^{-j\omega t}dt$.

Since the total energy can be expressed as the integral of the spectral energy function

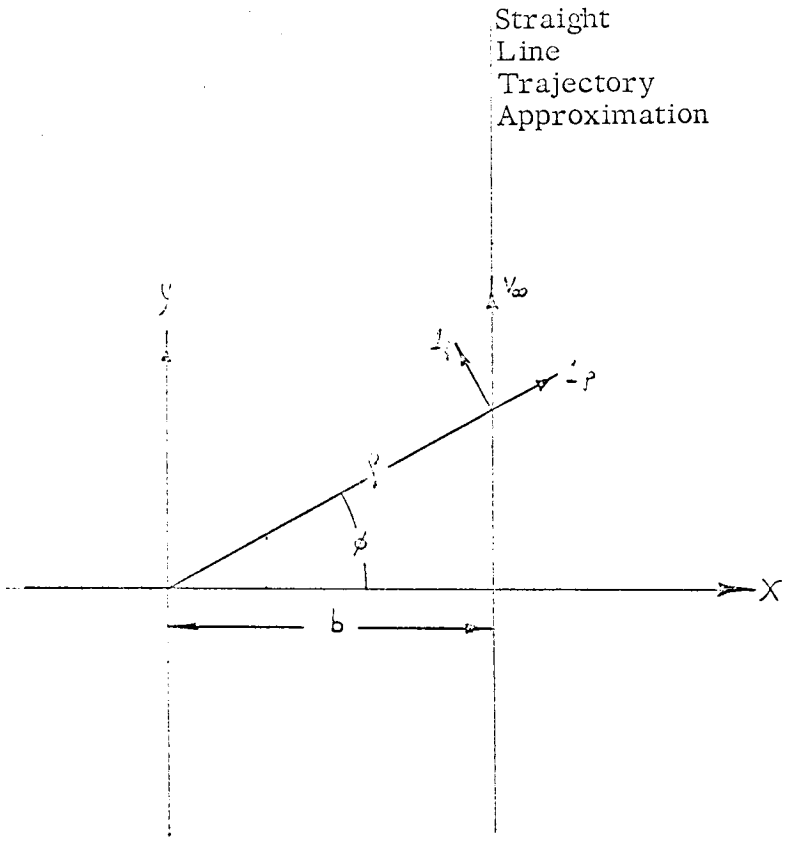

Fig. K.3 Straight Line Trajectory Approximation.

$$\xrightarrow{\text{super-position}} (90) \quad W_e = \int_{-\infty}^{\infty} w_e(\omega)\, d\omega \ ,$$

the energy spectrum radiated by the electron is given by

$$\xrightarrow{88,90} (91) \quad w_e(\omega) = 2\pi K \left|\bar{\dot{v}}(\omega)\right|^2 \ .$$

For very small deflection angles the electron trajectory is almost a straight line. Approximating the trajectory by a straight line greatly simplifies the analysis. The range over which this approximation does not introduce an appreciable error remains to be determined. With the orientation of the coordinate system employed this approximation gives a trajectory depicted in Fig. K.3. For this trajectory it is convenient to express the acceleration in terms of rectangular coordinate components

$$\xrightarrow{\text{resolution}} (92) \quad \dot{v} = 1_x \dot{v}_x + 1_y \dot{v}_y \ .$$

Consequently the spectral energy can be expressed by

$$\xrightarrow[92]{91} (93) \quad w_e(\omega) = 2\pi K \left[\left|\bar{\dot{v}}_x\right|^2 + \left|\bar{\dot{v}}_y\right|^2 \right]$$

where

$$\xrightarrow{89} (94) \quad \begin{Bmatrix} \bar{\dot{v}}_x(\omega) \\ \bar{\dot{v}}_y(\omega) \end{Bmatrix} = \frac{1}{2\pi} \int_{-\infty}^{\infty} \begin{Bmatrix} \dot{v}_x(t) \\ \dot{v}_y(t) \end{Bmatrix} e^{-j\omega t}\, dt \ .$$

The acceleration components are given by

$$\xrightarrow{1,\text{Fig. K.3}} (59) \quad \begin{vmatrix} \dot{v}_x \\ \dot{v}_y \end{vmatrix} = -\frac{k}{\rho^2} \begin{vmatrix} \cos\varphi \\ \sin\varphi \end{vmatrix}$$

Using the coordinate transformation

$$\xrightarrow{\text{coor. velocity}} (96) \quad \begin{vmatrix} \overline{x} \\ y \end{vmatrix} = \rho \begin{vmatrix} \overline{\cos\varphi} \\ \sin\varphi \end{vmatrix}$$

to express the acceleration components in terms of cylindrical coordinates, gives

$$\xrightarrow{95, \text{Fig. K.3}} (97) \quad \begin{vmatrix} \overline{\dot{v}_x} \\ \dot{v}_y \end{vmatrix} = \frac{-k}{(b^2+y^2)^{3/2}} \begin{vmatrix} \overline{b} \\ y \end{vmatrix} .$$

The acceleration component Fourier transforms are thus

$$\xrightarrow[97]{94} (98) \quad \begin{Bmatrix} \bar{v}_x(\omega) \\ \bar{v}_y(\omega) \end{Bmatrix} = \frac{-k}{2\pi} \int_{-\infty}^{\infty} \frac{e^{-j\omega t}}{(b^2+y^2)^{3/2}} \begin{Bmatrix} b \\ y \end{Bmatrix} dt .$$

To integrate these expressions it is necessary to know the y coordinate as a function of time. For the case of very small deflection angles

$$\xrightarrow[\delta << 1]{28} (99) \quad \frac{b}{\rho} = \cos\varphi .$$

Differentiating gives

$$\xrightarrow{99} (100) \quad \frac{b}{\rho^2}\dot{\rho} = \sin\varphi\,\dot{\varphi} .$$

The angular speed

$$\xrightarrow{\text{kinematics}} (101) \quad v_\varphi = \rho\dot{\varphi}$$

can be expressed by

$$\xrightarrow[38]{101} (102) \quad v_\varphi = \frac{bv_\infty}{\rho} .$$

Hence, the velocity components in polar coordinates can be expressed by

$$\xrightarrow[38;99]{100;102} (103) \quad \begin{vmatrix} v_\rho \\ v_\varphi \end{vmatrix} = v_\infty \begin{vmatrix} \sin\varphi \\ \cos\varphi \end{vmatrix} .$$

The rectangular velocity components in terms of the polar velocity components are given by

$$\xrightarrow{\text{geometry}} (104) \quad \begin{vmatrix} v_x \\ v_y \end{vmatrix} = \begin{vmatrix} \cos\varphi & -\sin\varphi \\ \sin\varphi & \cos\varphi \end{vmatrix} \begin{vmatrix} v_\rho \\ v_\varphi \end{vmatrix}$$

hence

$$\xrightarrow[101]{102} (105) \quad \begin{vmatrix} v_x \\ v_y \end{vmatrix} = v_\infty \begin{vmatrix} \cos\varphi & -\sin\varphi \\ \sin\varphi & \cos\varphi \end{vmatrix} \begin{vmatrix} \sin\varphi \\ \cos\varphi \end{vmatrix} .$$

This simplifies to

$$\xrightarrow{105} (106) \quad \begin{vmatrix} v_x \\ v_y \end{vmatrix} = \begin{vmatrix} 0 \\ v_\infty \end{vmatrix} .$$

Thus, the velocity turning out to be constant, is a direct consequence of the straight line trajectory approximation rather than being an additional independent approximation as indicated in some publications. This increases the self consistency of the straight line approximation. The straight line approximation appears to introduce

a logical inconsistency because:

1. the straight line approximation gives a constant particle velocity (106)
2. a constant particle velocity means no acceleration ($v = o$)

and thus, is in contradiction with

3. the constant velocity gives a variable position
4. the variable position gives a variable acceleration via the equation of motion (1).

This inconsistency is removed by noting that the straight line approximation is a first approximation which gives a constant velocity with zero acceleration and variable position (1, 2, 3) which comprise a first approximation. Substituting this variable position first approximation, back into the equation of motion (reiteration) gives a second approximation for the acceleration which is not zero.

Taking the time origin at the instant when $y = 0$ gives

$\xrightarrow{106}$ (107) $\quad y = v_\infty t \quad .$

Consequently the expressions for the spectral acceleration components is given by

$$\xrightarrow[107]{98} (108) \quad \begin{Bmatrix} \bar{\dot{v}}_x(\omega) \\ \bar{\dot{v}}_y(\omega) \end{Bmatrix} = \frac{-k}{2\pi} \int_{-\infty}^{\infty} \frac{1}{(b^2 + v_\infty^2 t^2)^{3/2}} \begin{Bmatrix} b \\ v_\infty t \end{Bmatrix} dt \quad .$$

The time interval over which significant acceleration takes place determines to a large extent the frequency range containing the major portion of the radiation. Using

$\xrightarrow{\text{RF3(408.04)}}$ (109) $\quad e^{-j\omega t} = \cos \omega t - j \sin \omega t$

and the odd and even function symmetry gives

$$\xrightarrow[109]{108} (110)\quad \begin{Bmatrix} \bar{v}_x(\omega) \\ \bar{v}_y(\omega) \end{Bmatrix} = \frac{k}{\pi}\int_0^\infty \frac{1}{(b^2+v_\infty^2 t^2)^{3/2}} \begin{Bmatrix} -b\cos\omega t \\ jv_\infty t\sin\omega t \end{Bmatrix} dt \quad .$$

Introducing the parameters

$$\xrightarrow{\text{sym def}} (111)\quad \begin{vmatrix} u \\ \xi \end{vmatrix} = \omega \begin{vmatrix} t \\ \frac{b}{v_\infty} \end{vmatrix}$$

to simplify integration gives

$$\xrightarrow[111]{110} (112)\quad \begin{Bmatrix} \bar{v}_x(\omega) \\ \bar{v}_y(\omega) \end{Bmatrix} = \frac{k\omega}{\pi v_\infty^2}\int_o^\infty \frac{1}{(\xi^2+u^2)^{3/2}} \begin{Bmatrix} -\xi\cos u \\ ju\sin u \end{Bmatrix} du \quad .$$

These integrals can be evaluated by using

$$\xrightarrow{\text{RK7:203}} (113)\quad K_o(\xi) = \int_o^\infty \frac{\cos u}{\sqrt{\xi^2+u^2}}\, du$$

and

$$\xrightarrow{\text{RK7:204}} (114)\quad K'_\nu(\xi) = \frac{\nu}{\xi}K_\nu(\xi) - K_{\nu+1}(\xi) \quad .$$

Using

$$\xrightarrow{113} (115)\quad K'_0(\xi) = -\xi\int_0^\infty \frac{\cos u}{(\xi^2+u^2)^{3/2}}\, du$$

and

$$\xrightarrow{114} (116)\quad K'_0(\xi) = -K_1(\xi)$$

gives

$$\xrightarrow[115]{116} (117) \quad \int_0^\infty \frac{\cos u}{(\xi^2+u^2)^{3/2}}\,du = \frac{1}{\xi}K_1(\xi) \quad .$$

Using integration by parts

$$\xrightarrow{\text{identity}} (118) \quad \int z\,dv = zv - \int v\,dz$$

with

$$\xrightarrow{\text{comparison}} (119) \quad \begin{vmatrix} z \\ \\ dv \end{vmatrix} = \begin{vmatrix} (\xi^2+u^2)^{-\frac{1}{2}} \\ \\ \cos u\,du \end{vmatrix} .$$

gives

$$\xrightarrow{119} (120) \quad \begin{vmatrix} dz \\ \\ v \end{vmatrix} = \begin{vmatrix} \dfrac{-u\,du}{(\xi^2+u^2)^{3/2}} \\ \\ \sin u \end{vmatrix} ,$$

and consequently

$$\xrightarrow[119,120]{113,118} (121) \quad K_0(\xi) = \frac{\sin u}{\sqrt{\xi^2+u^2}}\Bigg|_0^\infty + \int_0^\infty \frac{u \sin u}{(\xi^2+u^2)^{3/2}}\,du \quad .$$

Hence

$$\xrightarrow{121} (122) \quad \int_0^\infty \frac{u \sin u}{(\xi^2+u^2)^{3/2}}\,du = K_0(\xi) \quad .$$

Therefore the spectral acceleration components can be expressed in the form

$$\xrightarrow[117]{112} (123) \quad \begin{vmatrix} \bar{v}_x(\omega) \\ \bar{v}_y(\omega) \end{vmatrix} = \frac{k\omega}{\pi v_\infty^2} \begin{vmatrix} -K_1\left(\frac{\omega b}{v_\infty}\right) \\ jK_o\left(\frac{\omega b}{v_\infty}\right) \end{vmatrix} .$$

The modified Bessel function of the second kind diverge as the argument goes to zero, however, they occur in a combination multiplied by the argument

$$\xrightarrow{123} (124) \quad \begin{vmatrix} \bar{v}_x(\omega) \\ \bar{v}_y(\omega) \end{vmatrix} = \frac{k}{\pi b v_\infty} \begin{vmatrix} -\frac{\omega b}{v_\infty} K_1\left(\frac{\omega b}{v_\infty}\right) \\ j\frac{\omega b}{v_\infty} K_o\left(\frac{\omega b}{v_\infty}\right) \end{vmatrix}$$

The function $\xi K_0(\xi)$ and $\xi K_1(\xi)$ are plotted for handy reference in Fig. K.4. The total spectral energy can now be expressed as

$$\xrightarrow[124]{93} (125) \quad w_e(\omega) = 2\pi K \left(\frac{k}{\pi b v_\infty} \frac{\omega b}{v_\infty}\right) \left[K_1^2\left(\frac{\omega b}{v_\infty}\right) + K_0^2\left(\frac{\omega b}{v_\infty}\right)\right] .$$

The normalized ratio

$$\xrightarrow{125} (126) \quad \frac{w_e \pi b^2 v_\infty^2}{2k^2 K} = \left(\frac{\omega b}{v_\infty}\right)^2 \left[K_1^2\left(\frac{\omega b}{v_\infty}\right)^2 + K_0^2\left(\frac{\omega b}{v_\infty}\right)\right]$$

is also graphed in Fig. K.4 against $\omega b/v_\infty$. It should be noted that this is the total spectral energy radiated and does not give angle or polarization distribution information. The polar pattern for the radiation due to the x-component of acceleration is different from the polar pattern of the z-component of acceleration and hence, in general the addition as made in (125) may be misleading. However (126) is correct for a large collection of the accelerating particles with an isotropic velocity distribution since averaging over the particle collection provides spherically symmetric radiation. Particles in thermal equilibrium have the necessary spherical velocity distribution for isotropic radiation from each small spherical volume element,

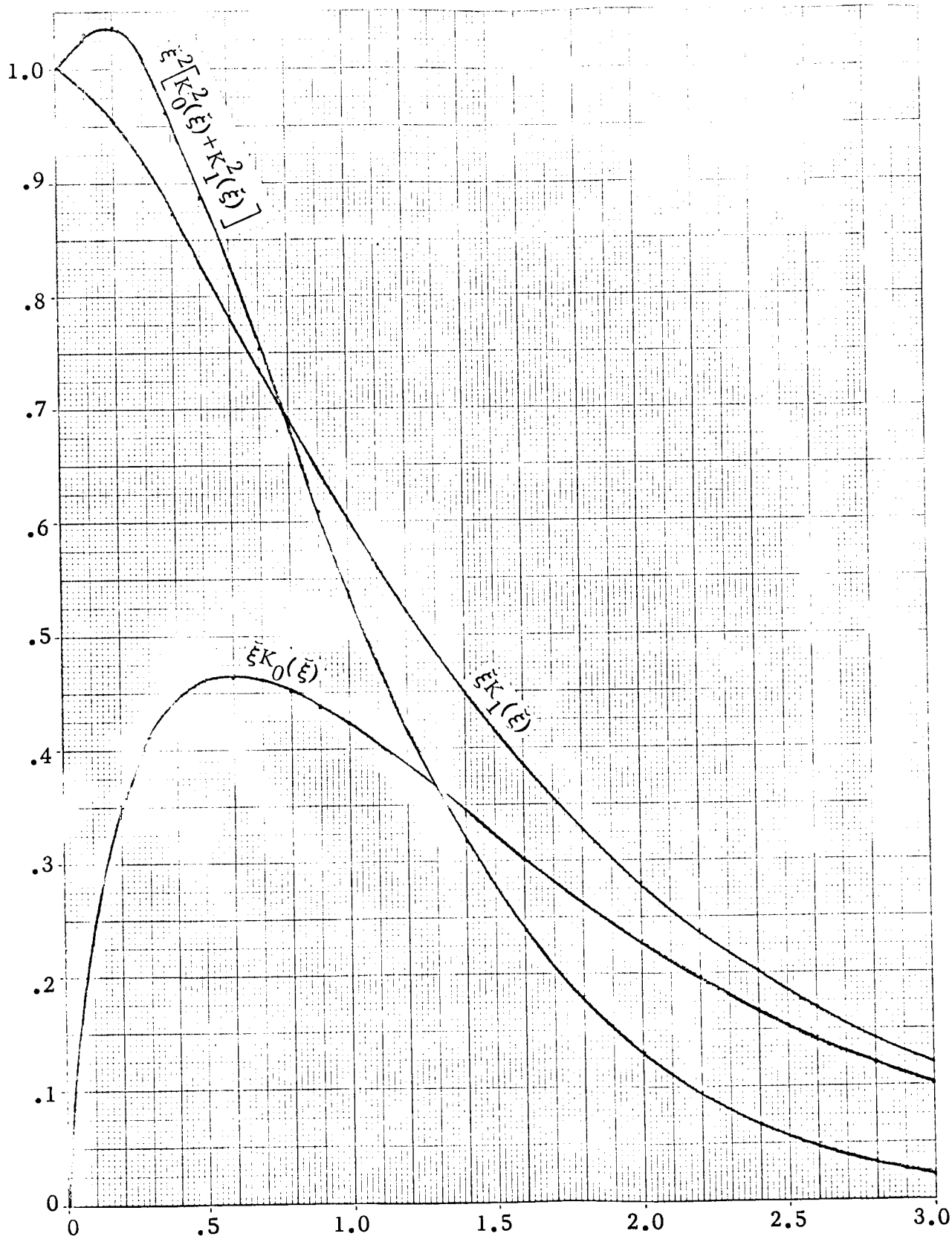

Fig. K.4 Modified Bessel Functions, $\xi K_o(\xi)$, $\xi K_1(\xi)$, and $\xi^2\left[K_0^2(\xi)+K_1^2(\xi)\right]$ vs. ξ.

however this condition does not prevail for the electron motions with respect to the ions in the ion rocket exhaust beam. The angle and polarization distribution of radiation, which should be considered, is left for subsequent consideration. Here the isotropic approximation is pursued to obtain an estimate of the importance of the bremsstrahlung radiation.

K.6 Radiated Spectral Power per Electron

If the average spectral energy radiated per collision were known together with the collision frequency, the spectral power radiated per electron would simply be their product. However, the radiation varies strongly with the collision parameter in addition to which the elementary collision frequency is only logically definable for each collision parameter. All of the electrons having the same collision parameter have the same radiated spectral power. Thus using

$\xrightarrow{\text{sym def}}$ (127) $dP_{e\omega}$ = the spectral power radiated per electron for encounters with the collision parameter in the range of b to b+db

and

$\xrightarrow{\text{sym def}}$ (128) $d\nu$ = the electron collision frequency with the collision parameter in the range b to b+db

gives

$\xrightarrow{\text{addition}}$ (129) $dP_{e\omega} = w_e(\omega)d\nu$.

This differential collision frequency is the velocity times

$\xrightarrow{\text{sym def}}$ (130) dn_c = the number of electron collision per unit length with the collision parameter in the range b to b+db

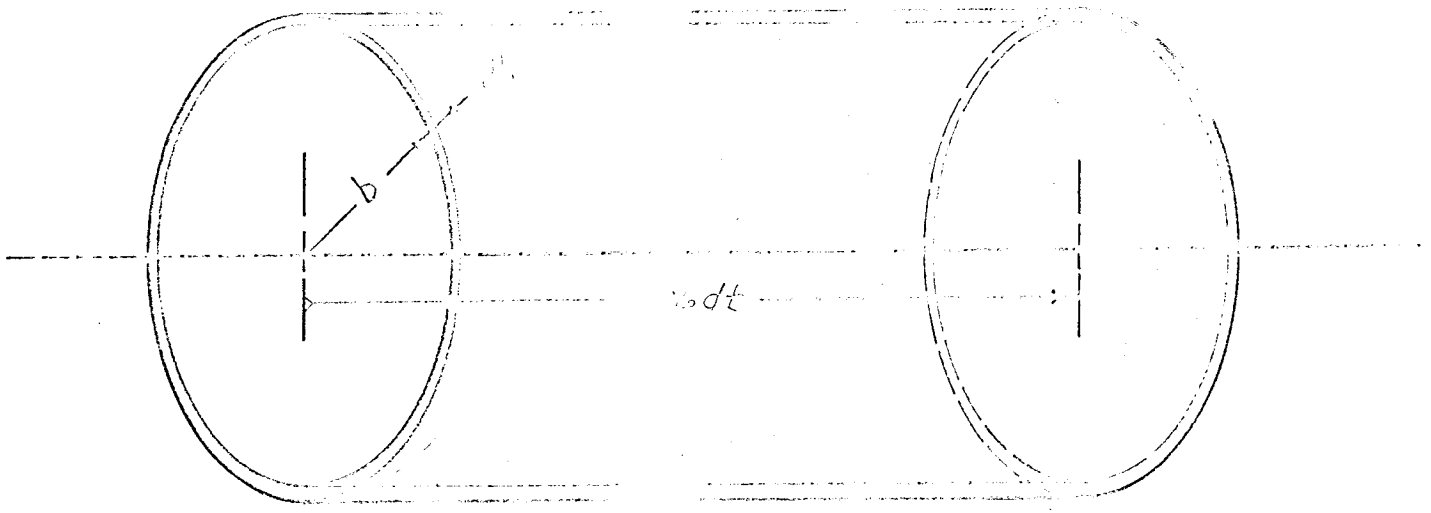

Fig. K.5 Cylindrical Shell Containing Ions for which the Collision Parameters are in the Range b to b+db.

thus

$$\xrightarrow{\text{addition}} (131) \quad d\nu = v_\infty dn_c \ .$$

The differential number of collision per unit length with the collision parameter in the range b to b+db is simply the number of ions in a cylindrical shell volume of inner radius b, outer radius b+db and at unit length as depicted in Fig. K.5. Thus

$$\xrightarrow{130,\ \text{Fig. K.5}} (132) \quad dn_c = n_i 2\pi b db \ .$$

The differential collision frequency is consequently given by

$$\xrightarrow[132]{131} (133) \quad d\nu = v_\infty n_i 2\pi b db$$

and the differential spectral power is hence given by

$$\xrightarrow[133]{129} (134) \quad dP_{e\omega} = v_\infty n_i w_e(\omega) 2\pi b db$$

The total spectral power per electron is consequently

$$\xrightarrow{134} (135) \quad P_{e\omega} = 2\pi n_i v_\infty \int_0^\infty w_e(\omega, v_\infty, b)\, b db \ .$$

Expressing the spectral energy in terms of the collision parameter gives

$$\xrightarrow{135} (136) \quad P_{e\omega} = 4n_i K k^2 \frac{\omega^2}{v_\infty^3} \int_b^\infty \left[K_1^2\left(\frac{\omega b}{v_\infty}\right) + K_0^2\left(\frac{\omega b}{v_\infty}\right)\right] b db$$

This integral is singular if the lower limit is zero. As shown in section K.4 the smallest collision parameter of significance is the deBroglie wavelength at the perigee. For small deflection angles the perigee deBroglie wavelength differs little from the asymptotic deBroglie wavelength. To evaluate the integral it is

convenient to use the previous integration parameter, giving

$$\xrightarrow[111_2]{136} (137) \quad P_{e\omega} = \frac{4n_1 Kk^2}{v_\infty} \int_{\frac{\omega b}{v_\infty}}^{\infty} \left[K_1^2(\xi)+K_0^2(\xi)\right] \xi d\xi$$

Using

$$\xrightarrow{\text{RK7:206}} (138) \quad \int_{\breve{\xi}}^{\infty} K_\nu^2(\xi)\xi d\xi = \tfrac{1}{2}\xi^2\left[K'^2_\nu(\breve{\xi}) - \left(1+\frac{\nu^2}{\breve{\xi}^2}\right)K_\nu^2(\breve{\xi})\right] \qquad \breve{\xi} > 0$$

gives

$$\xrightarrow{137,138} (139) \quad P_{e\omega} = \frac{2n_1 Kk^2 \breve{\xi}^2}{v_\infty}\left[K'^2_1(\breve{\xi}) - \left(1+\frac{1}{\breve{\xi}^2}\right)K_1^2(\breve{\xi})+K_1'^2(\breve{\xi}) - K_0^2(\breve{\xi})\right]$$

Using

$$\xrightarrow{\text{RK7:204}} (140) \quad K'_\nu(\xi) = -\frac{\nu}{\xi}K_\nu(\xi) - K_{\nu-1}(\xi)$$

gives

$$\xrightarrow{140} (141) \quad K'_1(\xi) = -\frac{1}{\xi}K_1(\xi) - K_0(\xi) \ .$$

Eliminating the derivative from the expression for the spectral power per electron gives

$$\xrightarrow[116,141]{139} (142) \quad P_{e\omega} = \frac{2n_1 Kk^2 \breve{\xi}^2}{v_\infty}\left[\left\{\frac{1}{\breve{\xi}}K_1(\breve{\xi})+K_0(\breve{\xi})\right\}^2 - \left(1+\frac{1}{\breve{\xi}^2}\right)K_1^2(\breve{\xi})+K_1^2(\breve{\xi}) - K_0^2(\breve{\xi})\right]$$

Simplifying gives

$$\xrightarrow{142} (143) \quad P_{e\omega} = \frac{4n_1 Kk_2 \breve{\xi}}{v_\infty} K_1(\breve{\xi}) K_0(\breve{\xi})$$

where

$$\xrightarrow{111_2} (144) \quad \breve{\xi} = \frac{\omega \breve{b}}{v_\infty}$$

K.7 Spectral Power Generated per Unit Volume

The spectral power generated per unit volume is that generated per electron times the density of electrons

$$\xrightarrow[\text{addition}]{\text{incoherent}} (145) \quad p_\omega = n_e P_{e\omega} \ .$$

The spectral power generated per unit volume is thus

$$\xrightarrow[143/144]{145} (146) \quad p_\omega = \frac{4 n_i n_e K k^2 \omega \breve{b}}{v_\infty^2} k_1\left(\frac{\omega \breve{b}}{v_\infty}\right) K_0\left(\frac{\omega \breve{b}}{v_\infty}\right) \ .$$

For the case of interest the ions are singly charged

$$\xrightarrow{\text{ion exhaust beam}} (147) \quad Z = 1$$

and macroscopically the beam is approximately neutral

$$\xrightarrow{\text{neutrality}} (148) \quad n_i = n_e \ .$$

Using

$$\xrightarrow[A\text{-}4]{84} (149) \quad K = \frac{e^2 \mu_v}{6\pi c} = 5.69 \times 10^{-54} \quad \text{watt sec}^4 \text{m}^{-2}$$

and

$$\xrightarrow[160]{2,3} (150) \quad k = \frac{e^2}{4\pi\epsilon_v m} = 253$$

gives

$$\xrightarrow[149,150]{146} (151) \quad p_\omega = 1.46 \times 10^{-48} \left(\frac{n\omega\breve{b}}{v_\infty}\right)^2 K_0\left(\frac{\omega\breve{b}}{v_\infty}\right) K_1\left(\frac{\omega\breve{b}}{v_\infty}\right)$$

Expressing the spectral power in terms of power per cycle instead of power per radian gives

$$\xrightarrow{151} (152) \quad p_f = 9.16 \times 10^{-48} \left(\frac{n\omega\breve{b}}{v_\infty}\right)^2 K_0\left(\frac{\omega\breve{b}}{v_\infty}\right) K_1\left(\frac{\omega\breve{b}}{v_\infty}\right) \frac{\text{watts}}{\text{Hz m}^3}$$

Before graphing it is necessary to specify the minimum collision parameter. Using

$$\xrightarrow{\text{section K.4}} (153) \quad \breve{b} = \lambda_\infty$$

which is given by

$$\xrightarrow{153} (154) \quad \breve{b} = \frac{12.26 \times 10^{-10}}{\sqrt{V_\infty}}$$

gives

$$\xrightarrow{154 \div 52} (155) \quad \frac{\breve{b}}{v_\infty} = \frac{2.06 \times 10^{-15}}{V_\infty} .$$

Consequently

$$\xrightarrow{155} (156) \quad \frac{\omega\breve{b}}{v_\infty} = 1.3 \times 10^{-14} \frac{f}{V_\infty}$$

Expressing the signal in terms of giga Hertz gives

$$\xrightarrow{156} (157) \quad \frac{\omega\breve{b}}{v_\infty} = 1.3 \times 10^{-5} \frac{f_{Ghz}}{V_\infty} \quad .$$

Consequently, for frequencies of interest

$$\xrightarrow{157} (158) \quad \frac{\omega\breve{b}}{v_\infty} << 1 \qquad \text{for} \qquad V_\infty > 10^{-3} \text{ electron volts} \quad .$$

With such small argument values the modified Bessel functions can be adequately represented by

$$\xrightarrow[\nu = 1]{RK8(9.6.8)} (159) \quad K_0(\xi) = \ell n \frac{1}{\xi}$$

and

$$\xrightarrow{RK8(9.6.9)} (160) \quad K_1(\xi) = \frac{1}{\xi} \quad .$$

Therefore the modified Bessel function product can be approximated by

$$\xrightarrow{159,160} (161) \quad \xi^2 K_0(\xi) K_1(\xi) = \xi \ell n \frac{1}{\xi} \quad .$$

Consequently

$$\xrightarrow[161]{152} (162) \quad p_f = 9.16 \times 10^{-48} n^2 \frac{\omega\breve{b}}{v_\infty} \ell n \frac{v_\infty}{\omega b}$$

and hence

$$\xrightarrow[157]{172} (163) \quad p_f = 1.29 \times 10^{-52} \frac{f_{GHz} n^2}{V_\infty} \ell n \frac{7.7 \times 10^3 V_\infty}{f_{GHz}}$$

Using the center frequency in the band of interest gives

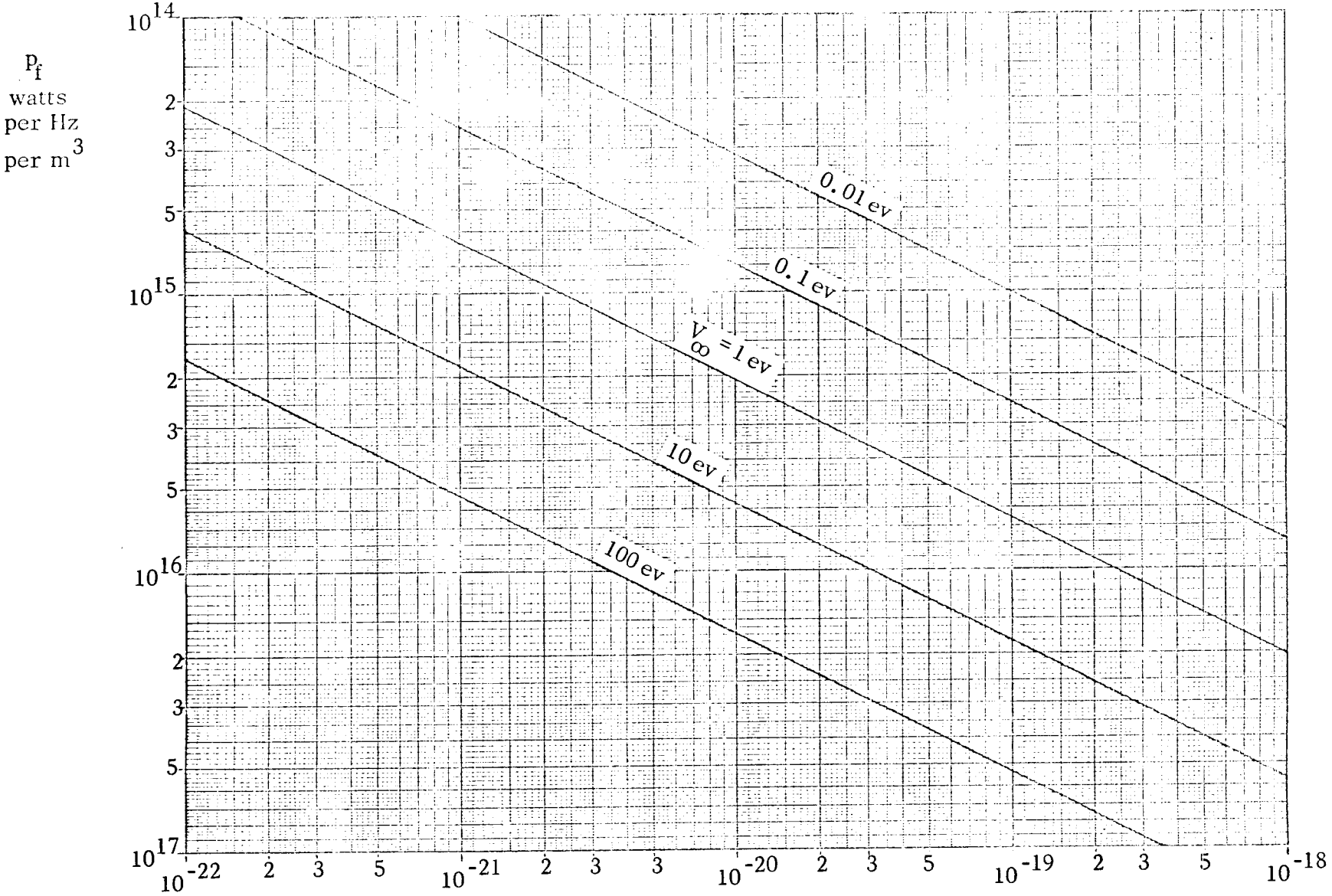

Fig. K.6 Spectral Power Generated per Unit Volume in the Ion Exhaust Bean by Bremsstrahlung in the Frequency Band 2.1 to 2.3 GHz

$$\xrightarrow[f_{GHz}=2.2]{163} (164) \quad p_f = 2.84 \times 10^{-52} \frac{n^2}{V_\infty} \ell n\, 3.5 \times 10^3 V_\infty$$

For various electron energies

$$V_\infty$$

$$\xrightarrow{164} (165) \quad p_f = \left\{ \begin{matrix} 101 \\ 16.1 \\ 2.32 \\ 0.297 \\ 0.0352 \end{matrix} \right\} \times 10^{-51} n^2 \left\{ \begin{matrix} 10^{-2} \\ 10^{-1} \\ 10^{0} \\ 10^{1} \\ 10^{2} \end{matrix} \right. \quad \text{watts/Hz/m}^3 \ .$$

This is graphed in Fig. K.6

In general a single velocity or electron energy, V_∞ is not appropriate since the electron aggregate has a distribution of velocities. Hence, the power per electron should be integrated over the velocity distribution in order to obtain a correct value of p_f. However, for a thermal distribution the speeds are distributed about the most probable speed

$$\xrightarrow{RB4:30} (166) \quad u_o = \sqrt{\frac{2kT}{m_e}}$$

or the most probable energy in electron volts

$$\xrightarrow{16} (167) \quad V_o = \frac{k}{e} T = 8.62 \times 10^{-5} \quad \text{ev} \ ,$$

which is superimposed upon the electron drift velocity with respect to the ions. Such an integration changes the result by an amount which is probably less than an order of magnitude. The effect of this distribution is expected to increase the noise generated because of the relatively greater contributions made by the electrons with relatively lower velocities. The expression in (164) is more appropriate for an ion exhaust beam than for a thermal distribution because it consists essentially of a thermal distribution superimposed on the average exhaust velocity where the

mean thermal speed is small compared to the average relative drift speed.

The straight line trajectory approximation requires the introduction of a lower limit on the allowable collision parameter range in order to make the integrals involved in the approximation convergent. Less exact approaches than the one followed here even require an upper limit to be inserted in order to avoid a divergent integral. The upper limit is usually set either by the Debye shielding distance or the plasma dimensions, whichever is smaller. The lower limit may be set by quantum mechanical deviations from classical causality or by the charged particle's equivalent structure.

Examination of (164) indicates p_f goes to infinity as V_∞ goes to zero. This clearly violates conservation of energy. However, the straight line trajectory approximation does not apply in this case since the smaller the electron energy the greater the deflection angle. Examination of Fig. K.2 gives a rough indication of the range of electron energies and collision parameters for which the straight line trajectory is valid. The deflection angles, for the lower allowable parameter range, are too large for the straight line trajectory to apply. Since the result is so sensitive to the lower bound of collision parameters the effect of the significant deviation from a straight line trajectory should be more accurately considered.

APPENDIX L: LIST OF REFERENCES

1.1 Kaufman, Harold R., "An Ion Rocket With an Electron-Bombardment Ion Source", NASA Technical Note 0-585, pp.38, January 1961, Lewis Research Center, Cleveland, Ohio.

1.2 Kerrish, D. J., "Arc-Type Ion Sources for Electrical Propulsion", ASD Technical Note 61-4, pp. 56, Rocketdyne, Contract AF33 616-5927, Project 3141, May 26, 1961.

1.3 Kerrish, Daniel J., "Potentialities of Electron Bombardment Ion Engines for Electric Propulsion", IRE Trans. on Space Electronics and Telemetry, June 1962, pp. 188-193.

1.4 Strickfaders, Wm. B., and Kenneth L. Gieler, "Probe Measurement of the Discharge in an Operating Electron Bombardment Engine", AIAA Journal Vol. I, No. 8, August 1963, pp. 1815-1823.

1.5 Kemp, Robert F., Sellen, J. M., Sr.(STL-Canoga Park, California) and Eugene V. Pawlik (NASA Lewis Res. Center, Cleveland) American Rocket Society Preprint Nov. 13-18, 1962. Also NASA Technical Note D-1733 of july 1963.

1.6 Clouties, G. G. and T. W. Johnston (RCA Victor E. Std. Montreal, Canada), "Charge Neutralization in an Ionic Rocket".

1.7 Perlstein, L. D., Rosenbluth, M. N. and G. W. Stuart, 16 August 1962, Final Report under NASA Contract 8-1690, Project 225 "The Theory of Ion Beam Neutralizations", General Atomic GA-3291, General Atomic Division, General Dynamics, San Diego, September 30, 1963.

1.8 Perlstein, L. D., Rosenbluth, M. N. and G. W. Stuart, "The Theory of Ion Beam Neutralization II", NASA Contract NAS 3-2507 - NASA Program Manager Warren H. Rayle.

4.1 "Frequency Analysis, Modulation and Noise" by S. Goldman, McGraw-Hill, 1948, p. 254.

A.1 "American Institute of Physics Handbook" 2^{d} Ed. McGraw-Hill, 1963.

A.2 "Static and Dynamic Electricity" 2^{d} Ed., by W. R. Smyth McGraw-Hill, 1950.

A.3 "Handbook of Chemistry and Physics" 45th Ed. 1964-65, The Chemical Rubber Co.

B.1 Speiser, Evelyn W., "Performance of Nuclear-Electric Propulsion Systems in Space Exploration", JPL Technical Report No. 32-159, Dec. 15, 1961.

B.2 Beale, R. J., Womack, J. R. et al JPL Report dated November 1963, "A Nuclear-Electric Propulsion System Providing Capabilities For The Comprehensive Unmaned Explorations of The Solar System".

B.3 "Plasmas and Controlled Fusion", by D. J. Rose and M. Clark, Jr., John Wiley & Sons, 1961.

B.4 "Introduction To The Theory of Ionized Gases", by J. L. Delcroix, Interscience Publication, 1960.

E.1 "Magnetosonic Waves", George I. Cohn, Space Program Summary No. 37-30, Vol. IV., pp. 56-64.

E.2 "Research Towards an AC Plasma Diode", George I. Cohn, JPL Space Program Summary No. 38-28, Vol. IV., pp. 31-39.

E.3 "Tables of Integrals and Other Mathematical Data", 4th Ed., H. B. Dwight, Macmillan Co., 1964.

K.1 "On The Theory of X-Ray Absorption and of The Continuous X-Ray Spectrums", by H. A. Kramers, Phil. Mag. 46, 1923 (836-871).

K.2 "Emission of Radio-Frequency Waves From Plasmas", by G. Bekefi and S. C. Brown, American Jr. of Physics, Vol. 29, No. 7, July 1961, (404-428).

K.3 "Emissions, Absorption, and Conductivity of a Fully Ionized Gas at Radio Frequencies", by L. Ostes Reveiw of Modern Physics, Vol. 33, No. 4, October 1961, (525-543).

K.4 "Radiation Processes in Plasmas", by T. Birmingham, J. Dawson, and C. Oberman, The Physics of Fluids, Vol. 8, No. 2, February 1965, (297-307).

K.5 "Plasma Dynamics", Summer Session, 1959, MIT, Section 4.

K.6 "Classical Electricity and Magnetism", Panofsky and Phillips, Addision-Wesley 1955, p. 325.

K.7 "Bessel Functions for Engineers", by N. W. McLachlan, 2 Ed. Oxford 1955, p. 203, 204.

K.8 "Handbook of Mathematical Functions With Formulas, Graphs, and Mathematical Tables", Edited by M. Abramowitz and I. A. Stegrn, National Bureau of Standards, Applied Mathematics, Series 55, June 1964.